

**FINAL PROJECT**

**ANALYSIS OF SLOPE STABILITY WITH SOIL  
NAILING REINFORCEMENT USING PLAXIS  
PROGRAM**

**(STUDY CASE: STA 7+300 OF TAWANG-NGALANG  
SEGMENT IV ROAD AND BRIDGE PROJECT)**



**ALIIFAH BIANCA NURADRINA  
19511155**

**CIVIL ENGINEERING STUDY PROGRAM  
FACULTY OF CIVIL ENGINEERING AND PLANNING  
UNIVERSITAS ISLAM INDONESIA  
2024**

## PLAGIARISM STATEMENT

I declare that the Final Project report I prepared as a requirement for completing the Bachelor's degree program in the Civil Engineering Undergraduate Program, Faculty of Civil Engineering and Planning, Universitas Islam Indonesia is the result of my work. Certain parts of writing the Final Project report that I quoted from other people's work have been written in the source clearly in accordance with the norms, rules, and ethics of writing scientific papers. If in the future it is discovered that all or part of this Final Project report is not my own work or there is plagiarism in certain parts, I am willing to accept sanctions, including revocation of the academic title I hold in accordance with applicable laws and regulations.

Yogyakarta, 27 February 2024

Declaring the statement,



Aliifah Bianca Nuradrina

(19511155)

**FINAL PROJECT**

**ANALYSIS OF SLOPE STABILITY WITH SOIL  
NAILING REINFORCEMENT USING PLAXIS  
PROGRAM**

**(STUDY CASE: STA 7+300 OF TAWANG-NGALANG  
SEGMENT IV ROAD AND BRIDGE PROJECT)**

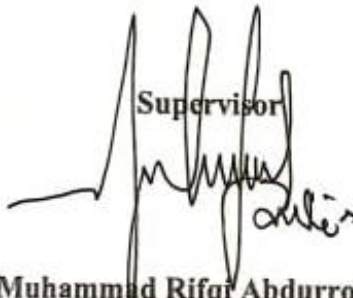
Arranged by

**Aliifah Bianca Nuradrina  
19511155**

Has been accepted as one of the requirements  
for obtaining a Bachelor's degree in Civil Engineering

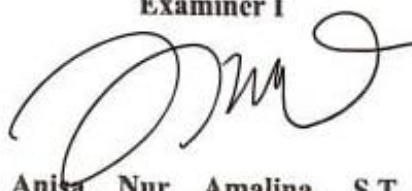
Tested on 27 February 2024  
By the Board of Examiners

Supervisor



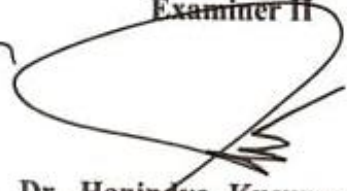
Muhammad Rifqi Abdurrozak,  
ST., M.Eng.  
NIK: 135111101

Examiner I



Anisa Nur Amalina, S.T.,  
M.Eng.  
NIK: 215111305

Examiner II

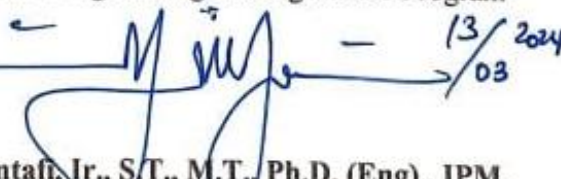


Dr. Hanindya Kusuma Artati,  
S.T., M.T.  
NIK: 045110407



Approving,

Head of the Civil Engineering Undergraduate Program



13/03/2024

Yunalia Muntafi, Ir., S.T., M.T., Ph.D. (Eng.), IPM.  
NIK: 09511010

## ABSTRACT

Retaining walls can be designed using soil nailing as reinforcement according to the soil characteristics and seismic profile of the site. This research explores the Factor of Safety (FS) and the displacement of roadside soil nailing retaining wall of different configurations located in Yogyakarta, Indonesia.

This research analyzes the effect of static loading representing a building atop the slope and dynamic loading of local earthquake ground acceleration value on the roadside retaining wall in clay soil to obtain the FS and displacement values. These values are obtained by modeling the variations of soil nail length, soil nail inclination, and soil nail vertical spacing, which is processed using Finite Element Method programmed into a software. After deciding the appropriate configurations according to preceding studies, the analysis is carried out, which observes the impact of different configurations on several reinforced slope features.

The result of the analysis shows that across all models, the 20° nail inclination yields the highest FS, the same goes to 1,5 meters of vertical spacing. Soil nail length difference does not have notable impact towards the FS. The maximum value of displacement is the lowest at 20° nail inclination, with the lowest values for 2,5 meters vertical spacing. Earthquake loading brings down the FS about 0,4 points for all models with consistent results for both static and dynamic loading.

**Keywords:** Retaining Wall, Soil Nailing, Factor of Safety, Displacement, Earthquake Loading



## FOREWORD

The author would like to thank Allah SWT for His guidance to complete the Final Project titled “Analysis of Slope Stability with Soil Nailing Reinforcement Using PLAXIS Program (Study Case: Sta 7+300 Of Tawang-Ngalang Segment Iv Road And Bridge Project)”. This Final Project is one of the academic requirements for completing the Civil Engineering Undergraduate Program, Faculty of Civil Engineering and Planning, Universitas Islam Indonesia, Yogyakarta.

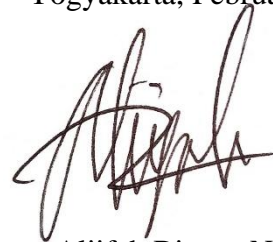
In preparing this Final Project, the author faced several obstacles, but thanks to suggestions, criticism, and encouragement from various people, this Final Project was completed. In this regard, the author would like to express gratitude towards:

1. Mr. Muhammad Rifqi Abdurrozak, ST., M.Eng. as the Supervisor,
2. Ms. Anisa Nur Amalina, S.T., M.Eng. as the Examiner I,
3. Dr. Mrs. Hanindya Kusuma Artati, S.T., M.T. as the Examiner II,
4. Mrs. Yunalia Muntafi, Ir., S.T., M.T., Ph.D. (Eng)., IPM. as the Head of Civil Engineering Undergraduate Program,
5. Irine Seri Palupi, S.T. and Mohammad Septariadi, S.T., the author’s parents who have loved and prayed for the author, whom deserve the world and more,
6. Friends who affect the author’s lives in various ways these college years.

Finally, the author hopes that this Final Project may educate and help the readers. There are errors and limitations in this research, but the author hopes that the content may open more meaningful and nuanced discussions that contribute to the field of Geotechnics in civil engineering.

Yogyakarta, February 2024

Author,



Aliifah Bianca Nuradrina

(19511155)

## TABLE OF CONTENT

TITLE PAGE	i
PLAGIARISM STATEMENT	ii
VALIDATION SHEET	iii
ABSTRACT	iv
FOREWORD	v
TABLE OF CONTENT	vi
TABLE LIST	x
FIGURE LIST	xii
ATTACHMENT LIST	xv
CHAPTER I PRELIMINARY	1
1.1 Background	1
1.2 Problem Formulation	4
1.3 Purpose	4
1.4 Advantage	5
1.5 Limit	5
CHAPTER II LITERATURE REVIEW	6
2.1 General Review	6
2.2 Soil Nailed Retaining Wall	6
2.2.1 Stability of Soil Nailed Retaining Wall	7
2.2.2 Preceding Report of Study Case for Soil Nailed Retaining Wall	17
CHAPTER III THEORETICAL BASIS	19
3.1 Soil	19

3.1.1	Soil Components	20
3.1.2	Soil Classification	23
3.1.3	Soil Properties	24
3.2	Soil Shear Strength	26
3.2.1	Soil Shear Strength Definition	26
3.2.2	Soil Shear Strength Theory	27
3.3	Soil Elastic Properties	28
3.4	Soil Investigation	29
3.5	Slope Stability	30
3.5.1	Slope Stability Definition	30
3.5.2	Factors Affecting Slope Stability	30
3.5.3	Landslide	31
3.6	Slope Stability Analysis	34
3.6.1	Slope Stability Analysis Theory	34
3.6.2	Simplified Bishop Method	35
3.7	Soil Nailing	36
3.7.1	Soil Nailing Basic Elements	37
3.7.2	Soil Nailing Basic Construction	41
3.7.3	Slope Stability Analysis with Soil Nailing Reinforcement	46
3.8	Slope Stability Analysis Using PLAXIS V20	52
<b>CHAPTER IV METHODOLOGY</b>		<b>54</b>
4.1	Research Method	54
4.2	Research Location	54
4.3	Data Collection	55
4.4	Research Stages	56

4.5	Proposed Soil Nailing Reinforced Design Slope	57
4.5.1	Modelling Variation	57
4.5.2	Loading Variation	58
4.6	Flowchart	61
CHAPTER V ANALYSIS AND DISCUSSION		64
5.1	Prerequisite Data	64
5.2	Non-Reinforced Slope Stability Analysis	66
5.2.1	Modelling using PLAXIS V20	66
5.2.2	Manual Calculation using Fellenius Method	68
5.3	Reinforced Slope Stability Analysis	71
5.3.1	Manual Calculation using Wedge Method	72
5.3.2	Modelling Variations for PLAXIS V20	81
5.3.3	Modelling Results for PLAXIS V20	87
	1) Model a	87
	2) Model b	89
	3) Model c	92
	4) Model d	94
	5) Model e	97
	6) Model f	99
	7) Model g	102
	8) Model h	104
5.3.4	Recapitulation of Modelling Results using PLAXIS V20	107
5.3.5	Analysis of Variable Comparison	108
CHAPTER VI CONCLUSIONS AND SUGGESTIONS		120
6.1	Conclusions	120

6.2 Suggestions	121
BIBLIOGRAPHY	123
ATTACHMENT	127

## TABLE LIST

2.1	Former and Current Research Comparison	13
3.1	Soil Specific Gravity	23
3.2	Soil Internal Shear Angle	25
3.3	Soil Granular Material Young's Modulus in MPa	28
3.4	Soil Cohesive Material Young's Modulus in MPa	28
3.5	Relation between Factor of Safety Number and Slope Condition	35
3.6	Properties of Grade 60 Solid-Threaded Bars	38
3.7	Properties of Grade 75 Solid-Threaded Bars	38
3.8	Shear Lateral Reaction Modulus	48
3.9	Soil Nailing Shear Bearing Capacity for Sandy Soils	50
5.1	Existing Slope Material Input Data	64
5.2	Recapitulation of Soil Nail Safety Factor using Fellenius Method	71
5.3	Soil Nail Material Input Data	71
5.4	Coefficients for Sandy Soil	74
5.5	Slope Modelling Variations in PLAXIS V20	81
5.6	Group 1 of Inclination Variable at 5 Meters Length and 2,5 Meters Vertical Spacing	86
5.7	Group 2 of Inclination Variable at 5 Meters Length and 1,5 Meters Vertical Spacing	86
5.8	Group 3 of Length Variable at 20° Inclination and 2,5 Meters Vertical Spacing	86
5.9	Group 4 of Length Variable at 20° Inclination and 1,5 Meters Vertical Spacing	87

5.10	Recapitulation of Modelling Results for Factor of Safety using PLAXIS V20	107
5.11	Recapitulation of Modelling Results for Displacement using PLAXIS V20	107
5.12	Factor of Safety of Group 1	108
5.13	Displacement of Group 1	109
5.14	Factor of Safety of Group 2	110
5.15	Displacement of Group 2	111
5.16	Factor of Safety Comparison between Group 1 and Group 2	112
5.17	Displacement Comparison between Group 1 and Group 2	113
5.18	Factor of Safety of Group 3	114
5.19	Displacement of Group 3	115
5.20	Factor of Safety of Group 4	116
5.21	Displacement of Group 4	117
5.22	Comparison of Factor of Safety between Group 3 and Group 4	118
5.23	Comparison of Displacement between Group 3 and Group 4	119



## FIGURE LIST

1.1	Location of Project	2
1.2	Site of Project	2
2.1	Reinforcement Stability Condition of STA 7+300 with Existing Slope	17
2.2	Reinforcement Stability Condition of STA 7+300 with Soil Nail of 5 Meters Length and 10 Millimeters Diameter	18
3.1	Soil Phase Diagram	20
3.2	Mohr and Coulomb Failure Criterion	27
3.3	Various Landslide Types	34
3.4	Assumed Slice	36
3.5	Shotcrete Installation	40
3.6	Drainage System	41
3.7	Soil Excavation	42
3.8	Nail Holes Drilling	43
3.9	Nail Bar Installation	43
3.10	Shotcrete Reinforcement	45
3.11	External Failure Modes	46
3.12	Working Forces in Wedge Method	47
3.13	Correlation Graphic for API Sandy Soil	49
4.1	Research Location	55
4.2	Proposed Design Scheme	57
4.3	Modelling Variation	58
4.4	Traffic Loading for Stability Analysis	59
4.5	Earthquake Ground Acceleration Map for Gunung Kidul	60

4.6	Final Project Research Flowchart	62
5.1	Existing Slope	66
5.2	Non-Loaded Static Existing Slope Potential Failure Area Output	67
5.3	Non-Loaded Dynamic Existing Slope Potential Failure Area Output	67
5.4	Loaded Static Existing Slope Potential Failure Area Output	68
5.5	Loaded Dynamic Existing Slope Potential Failure Area Output	68
5.6	Illustration of Slope for Fellenius Method Calculation	69
5.7	Current Reinforcement	72
5.8	Illustration of Slope for Wedge Method	73
5.9	Illustration of Slope for Wedge Method with Three Nails	77
5.10	Model a	82
5.11	Model b	82
5.12	Model c	83
5.13	Model d	83
5.14	Model e	84
5.15	Model f	84
5.16	Model g	85
5.17	Model h	85
5.18	Model a Non-Loaded Static Potential Failure Area Output	87
5.19	Model a Non-Loaded Dynamic Potential Failure Area Output	88
5.20	Model a Loaded Static Potential Failure Area Output	88
5.21	Model a Loaded Dynamic Potential Failure Area Output	89
5.22	Model b Non-Loaded Static Potential Failure Area Output	90
5.23	Model b Non-Loaded Dynamic Potential Failure Area Output	90
5.24	Model b Loaded Static Potential Failure Area Output	91

5.25	Model b Loaded Dynamic Potential Failure Area Output	91
5.26	Model c Non-Loaded Static Potential Failure Area Output	92
5.27	Model c Non-Loaded Static Potential Failure Area Output	93
5.28	Model c Loaded Static Potential Failure Area Output	93
5.29	Model c Loaded Dynamic Potential Failure Area Output	94
5.30	Model d Non-Loaded Static Potential Failure Area Output	95
5.31	Model d Non-Loaded Dynamic Potential Failure Area Output	95
5.32	Model d Loaded Static Potential Failure Area Output	96
5.33	Model d Loaded Dynamic Potential Failure Area Output	96
5.34	Model e Non-Loaded Static Potential Failure Area Output	97
5.35	Model e Non-Loaded Dynamic Potential Failure Area Output	98
5.36	Model e Loaded Static Potential Failure Area Output	98
5.37	Model e Loaded Dynamic Potential Failure Area Output	99
5.38	Model f Non-Loaded Static Potential Failure Area Output	100
5.39	Model f Non-Loaded Dynamic Potential Failure Area Output	100
5.40	Model f Loaded Static Potential Failure Area Output	101
5.41	Model f Loaded Dynamic Potential Failure Area Output	101
5.42	Model g Non-Loaded Static Potential Failure Area Output	102
5.43	Model g Non-Loaded Dynamic Potential Failure Area Output	103
5.44	Model g Loaded Static Potential Failure Area Output	103
5.45	Model g Loaded Dynamic Potential Failure Area Output	104
5.46	Model h Non-Loaded Static Potential Failure Area Output	105
5.47	Model h Non-Loaded Dynamic Potential Failure Area Output	105
5.48	Model h Loaded Static Potential Failure Area Output	106
5.49	Model h Loaded Dynamic Potential Failure Area Output	106

5.50	Factor of Safety of Group 1	108
5.51	Displacement of Group 1	109
5.52	Factor of Safety of Group 2	110
5.53	Displacement of Group 2	111
5.54	Factor of Safety Comparison between Group 1 and Group 2	112
5.55	Displacement Comparison between Group 1 and Group 2	113
5.56	Factor of Safety of Group 3	114
5.57	Displacement of Group 3	115
5.58	Factor of Safety of Group 4	116
5.59	Displacement of Group 4	117
5.60	Comparison of Factor of Safety between Group 3 and Group 4	118
5.61	Comparison of Displacement between Group 3 and Group 4	119

## **ATTACHMENT LIST**

- Attachment 1 Bore Log
- Attachment 2 Soil Laboratory Test Results
- Attachment 3 Non-Loaded Static Existing Slope Effective Stress Output
- Attachment 4 Non-Loaded Static Existing Slope Deformed Mesh Output
- Attachment 5 Non-Loaded Static Existing Slope Direction of Movement Output
- Attachment 6 Non-Loaded Static Existing Slope Displacement Output
- Attachment 7 Non-Loaded Dynamic Existing Slope Effective Stress Output
- Attachment 8 Non-Loaded Dynamic Existing Slope Deformed Mesh Output
- Attachment 9 Non-Loaded Dynamic Existing Slope Direction of Movement Output
- Attachment 10 Non-Loaded Dynamic Existing Slope Displacement Output
- Attachment 11 Loaded Static Existing Slope Effective Stress Output
- Attachment 12 Loaded Static Existing Slope Deformed Mesh Output
- Attachment 13 Loaded Static Existing Slope Direction of Movement Output
- Attachment 14 Loaded Static Existing Slope Displacement Output
- Attachment 15 Loaded Dynamic Existing Slope Effective Stress Output
- Attachment 16 Loaded Dynamic Existing Slope Deformed Mesh Output
- Attachment 17 Loaded Dynamic Existing Slope Direction of Movement Output
- Attachment 18 Loaded Dynamic Existing Slope Displacement Output
- Attachment 19 Model a Non-Loaded Static Effective Stress Output
- Attachment 20 Model a Non-Loaded Static Deformed Mesh Output
- Attachment 21 Model a Non-Loaded Static Direction of Movement Output
- Attachment 22 Model a Non-Loaded Static Displacement Output
- Attachment 23 Model a Non-Loaded Dynamic Effective Stress Output

Attachment 24 Model a Non-Loaded Dynamic Deformed Mesh Output

Attachment 25 Model a Non-Loaded Dynamic Direction of Movement Output

Attachment 26 Model a Non-Loaded Dynamic Displacement Output

Attachment 27 Model a Loaded Static Effective Stress Output

Attachment 28 Model a Loaded Static Deformed Mesh Output

Attachment 29 Model a Loaded Static Direction of Movement Output

Attachment 30 Model a Loaded Static Displacement Output

Attachment 31 Model a Loaded Dynamic Effective Stress Output

Attachment 32 Model a Loaded Dynamic Deformed Mesh Output

Attachment 33 Model a Loaded Dynamic Direction of Movement Output

Attachment 34 Model a Loaded Dynamic Displacement Output

Attachment 35 Model b Non-Loaded Static Effective Stress Output

Attachment 36 Model b Non-Loaded Static Deformed Mesh Output

Attachment 37 Model b Non-Loaded Static Direction of Movement Output

Attachment 38 Model b Non-Loaded Static Displacement Output

Attachment 39 Model b Non-Loaded Dynamic Effective Stress Output

Attachment 40 Model b Non-Loaded Dynamic Deformed Mesh Output

Attachment 41 Model b Non-Loaded Dynamic Direction of Movement Output

Attachment 42 Model b Non-Loaded Dynamic Displacement Output

Attachment 43 Model b Loaded Static Effective Stress Output

Attachment 44 Model b Loaded Static Deformed Mesh Output

Attachment 45 Model b Loaded Static Direction of Movement Output

Attachment 46 Model b Loaded Static Displacement Output

Attachment 47 Model b Loaded Dynamic Effective Stress Output

Attachment 48 Model b Loaded Dynamic Deformed Mesh Output

Attachment 49 Model b Loaded Dynamic Direction of Movement Output

Attachment 50 Model b Loaded Dynamic Displacement Output

Attachment 51 Model c Non-Loaded Static Effective Stress Output

Attachment 52 Model c Non-Loaded Static Deformed Mesh Output

Attachment 53 Model c Non-Loaded Static Direction of Movement Output

Attachment 54 Model c Non-Loaded Static Displacement Output

Attachment 55 Model c Non-Loaded Dynamic Effective Stress Output

Attachment 56 Model c Non-Loaded Dynamic Deformed Mesh Output

Attachment 57 Model c Non-Loaded Dynamic Direction of Movement Output

Attachment 58 Model c Non-Loaded Dynamic Displacement Output

Attachment 59 Model c Loaded Static Effective Stress Output

Attachment 60 Model c Loaded Static Deformed Mesh Output

Attachment 61 Model c Loaded Static Direction of Movement Output

Attachment 62 Model c Loaded Static Displacement Output

Attachment 63 Model c Loaded Dynamic Effective Stress Output

Attachment 64 Model c Loaded Dynamic Deformed Mesh Output

Attachment 65 Model c Loaded Dynamic Direction of Movement Output

Attachment 66 Model c Loaded Dynamic Displacement Output

Attachment 67 Model d Non-Loaded Static Effective Stress Output

Attachment 68 Model d Non-Loaded Static Deformed Mesh Output

Attachment 69 Model d Non-Loaded Static Direction of Movement Output

Attachment 70 Model d Non-Loaded Static Displacement Output

Attachment 71 Model d Non-Loaded Dynamic Effective Stress Output

Attachment 72 Model d Non-Loaded Dynamic Deformed Mesh Output

Attachment 73 Model d Non-Loaded Dynamic Direction of Movement Output



Attachment 74 Model d Non-Loaded Dynamic Displacement Output

Attachment 75 Model d Loaded Static Effective Stress Output

Attachment 76 Model d Loaded Static Deformed Mesh Output

Attachment 77 Model d Loaded Static Direction of Movement Output

Attachment 78 Model d Loaded Static Displacement Output

Attachment 79 Model d Loaded Dynamic Effective Stress Output

Attachment 80 Model d Loaded Dynamic Deformed Mesh Output

Attachment 81 Model d Loaded Dynamic Direction of Movement Output

Attachment 82 Model d Loaded Dynamic Displacement Output

Attachment 83 Model e Non-Loaded Static Effective Stress Output

Attachment 84 Model e Non-Loaded Static Deformed Mesh Output

Attachment 85 Model e Non-Loaded Static Direction of Movement Output

Attachment 86 Model e Non-Loaded Static Displacement Output

Attachment 87 Model e Non-Loaded Dynamic Effective Stress Output

Attachment 88 Model e Non-Loaded Dynamic Deformed Mesh Output

Attachment 89 Model e Non-Loaded Dynamic Direction of Movement Output

Attachment 90 Model e Non-Loaded Dynamic Displacement Output

Attachment 91 Model e Loaded Static Effective Stress Output

Attachment 92 Model e Loaded Static Deformed Mesh Output

Attachment 93 Model e Loaded Static Direction of Movement Output

Attachment 94 Model e Loaded Static Displacement Output

Attachment 95 Model e Loaded Dynamic Effective Stress Output

Attachment 96 Model e Loaded Dynamic Deformed Mesh Output

Attachment 97 Model e Loaded Dynamic Direction of Movement Output

Attachment 98 Model e Loaded Dynamic Displacement Output

Attachment 99 Model f Non-Loaded Static Effective Stress Output

Attachment 100 Model f Non-Loaded Static Deformed Mesh Output

Attachment 101 Model f Non-Loaded Static Direction of Movement Output

Attachment 102 Model f Non-Loaded Static Displacement Output

Attachment 103 Model f Non-Loaded Dynamic Effective Stress Output

Attachment 104 Model f Non-Loaded Dynamic Deformed Mesh Output

Attachment 105 Model f Non-Loaded Dynamic Direction of Movement Output

Attachment 106 Model f Non-Loaded Dynamic Displacement Output

Attachment 107 Model f Loaded Static Effective Stress Output

Attachment 108 Model f Loaded Static Deformed Mesh Output

Attachment 109 Model f Loaded Static Direction of Movement Output

Attachment 110 Model f Loaded Static Displacement Output

Attachment 111 Model f Loaded Dynamic Effective Stress Output

Attachment 112 Model f Loaded Dynamic Deformed Mesh Output

Attachment 113 Model f Loaded Dynamic Direction of Movement Output

Attachment 114 Model f Loaded Dynamic Displacement Output

Attachment 115 Model g Non-Loaded Static Effective Stress Output

Attachment 116 Model g Non-Loaded Static Deformed Mesh Output

Attachment 117 Model g Non-Loaded Static Direction of Movement Output

Attachment 118 Model g Non-Loaded Static Displacement Output

Attachment 119 Model g Non-Loaded Dynamic Effective Stress Output

Attachment 120 Model g Non-Loaded Dynamic Deformed Mesh Output

Attachment 121 Model g Non-Loaded Dynamic Direction of Movement Output

Attachment 122 Model g Non-Loaded Dynamic Displacement Output

Attachment 123 Model g Loaded Static Effective Stress Output

Attachment 124 Model g Loaded Static Deformed Mesh Output

Attachment 125 Model g Loaded Static Direction of Movement Output

Attachment 126 Model g Loaded Static Displacement Output

Attachment 127 Model g Loaded Dynamic Effective Stress Output

Attachment 128 Model g Loaded Dynamic Deformed Mesh Output

Attachment 129 Model g Loaded Dynamic Direction of Movement Output

Attachment 130 Model g Loaded Dynamic Displacement Output

Attachment 131 Model h Non-Loaded Static Effective Stress Output

Attachment 132 Model h Non-Loaded Static Deformed Mesh Output

Attachment 133 Model h Non-Loaded Static Direction of Movement Output

Attachment 134 Model h Non-Loaded Static Displacement Output

Attachment 135 Model h Non-Loaded Dynamic Effective Stress Output

Attachment 136 Model h Non-Loaded Dynamic Deformed Mesh Output

Attachment 137 Model h Non-Loaded Dynamic Direction of Movement Output

Attachment 138 Model h Non-Loaded Dynamic Displacement Output

Attachment 139 Model h Loaded Static Effective Stress Output

Attachment 140 Model h Loaded Static Deformed Mesh Output

Attachment 141 Model h Loaded Static Direction of Movement Output

Attachment 142 Model h Loaded Static Displacement Output

Attachment 143 Model h Loaded Dynamic Effective Stress Output

Attachment 144 Model h Loaded Dynamic Deformed Mesh Output

Attachment 145 Model h Loaded Dynamic Direction of Movement Output

Attachment 146 Model h Loaded Dynamic Displacement Output

# CHAPTER I

## PRELIMINARY

### 1.1 Background

Indonesia, as a developing country with an abundance of potential, is projected to be one with the biggest economic growth compared to other countries in Asia (World Bank, 2023). Several attempts are made to support the progress, one of them being the intense infrastructure development rush happening all over Indonesia, what with the establishment of road networks such as *Transjawa*, the utilization of inter-island bridges, the betterment of public transportation, the list is endless. Java, being the center of growth, has gone through a lot of changes for the purpose of better connectivity, which in turn encourages regional growth away from Jakarta to east and west reach.

Yogyakarta becomes one of the regions that is hugely impacted by the plan for economic growth, with the biggest course of action being infrastructure projects that are rooted in the idea of connecting the main city to the potential regions. The province relies on tourism as well as trade, and the reach is currently expanded to outskirts regions along the southern path, starting from Prambanan region and including touristic regions such as Gunung Kidul. Realizing this plan, the Department of Public Works, Housing, and Mineral Resources Energy D.I Yogyakarta hatches the Tawang-Ngalang road project in Gunung Kidul and divides it into five construction packages, comprising five road segments of different length. This project is carried out to support the tourism goals in the Gunung Kidul area, and to ease the access for farming and industrial transport through the mountainous region. All is done with the hope of livelihood improvement from increased traffic and activity in the area that branches out from the more prominent Prambanan touristic region.

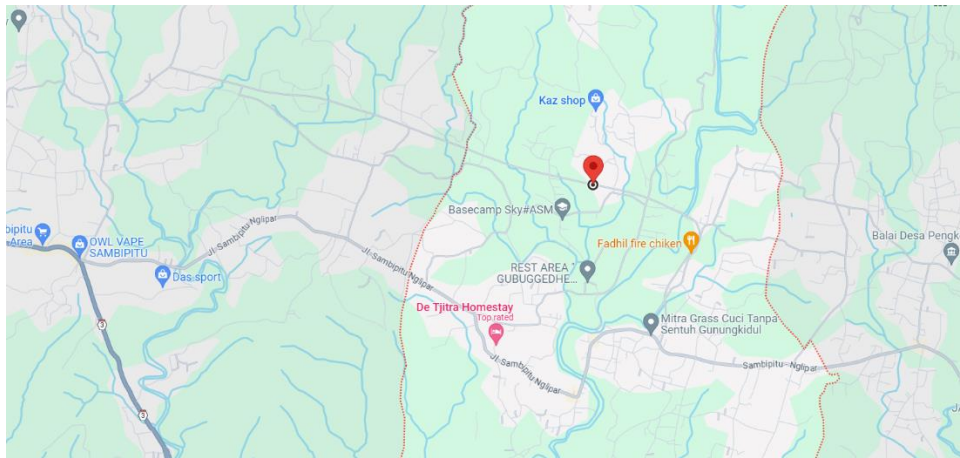


**Figure 1.1 Location of Project**

(Source: Google Maps, 2023)

This final project takes on the study case of Tawang-Ngalang Segment IV Road and Bridge Construction Project, which takes place in Nglegi Village, Gunung Kidul, and is made up of 3.5 km-long road and 0.8 km-long bridge. The location of the project can be seen in Figure 1.1 above. The surrounding area is touristic and has quite dense traffic flow. The site was originally a series of hills that required vegetation cleansing and soil conditioning, as shown in Figure 1.2 below. The site conditioning takes up a big portion of the preparation work and involves various heavy equipment.



**Figure 1.2 Site of Project**

Due to the project site contour, the attempts at constructing a flat freeway requires kilometers of roadside retaining walls. Roadside retaining walls have been used to support road safety over the last few centuries along the rapid development of road networks passing through unfavorable geological features. Roadside retaining walls are utilized to secure bodies of soil on higher levels compared to the road, securing the slope on either or both sides of the road.

In relation to the study case, the specific branch of geotechnics becomes the main focus, as it is a civil engineering concentration that deals with problems regarding soil properties such as stability, deformation, integrity, and so on. These mechanical properties of soil are integral especially in regions like Indonesia with its active plates, meaning the soil and rock which support the structures above are more dynamic and thus require more careful planning in the construction stage. Having been mentioned briefly in the previous paragraph, slopes are especially common in road construction projects, be it naturally-formed or human-made. In both cases, adequate safety measures are needed if the space is used for transport, living space, and other purposes. This affects the measurements of the main structure, which, in this case is the road, but also affects the safety measures of roadside retaining walls and drainage. More considerations should be taken if the infrastructure cuts the existing structures in the region, for example, if there were local residences around the road project, as the safety of the locals may be compromised from construction to utilization stage.

These retaining walls experience varieties of loads and pressures due to static or moving happenings. The project site at Tawang-Ngalang Segment IV is prone to instability due to its soil profile. During its construction, specifically on July 23, 2022, a landslide happened, breaking a section of the roadside retaining wall between STA 7+300 and STA 7+325. The section was constructed using gabion and shotcrete, and was very close to a local residence, causing a part of the residence front porch to break off and slide down. Having been treated with a different method of soil retaining, and with the precedent of landslide already happening to one section of the roadside retaining wall, there needs to be an analysis of how the factors affect the structure's stability. For the specific condition of roadside

retaining walls, the slope stability and deformation as a metric of safety are analyzed to figure out the integrity of the structure, comparing between different methodologies that are implemented pre and post landslide.

## **1.2 Problem Formulation**

The problem formulation is as follows.

1. How is the stability of the non-reinforced slope at STA 7+300 of the Tawang-Ngalang Segment IV Road and Bridge Construction Project?
2. How is the stability and displacement of the current soil nailing-reinforced slope at STA 7+300 of the Tawang-Ngalang Segment IV Road and Bridge Construction Project?
3. How is the stability and displacement of the soil nailing-reinforced slope impacted by different soil nailing variables at STA 7+300 of the Tawang-Ngalang Segment IV Road and Bridge Construction Project?
4. How does earthquake impact the stability and displacement of the soil nailing-reinforced slope with different soil nailing variables at STA 7+300 of the Tawang-Ngalang Segment IV Road and Bridge Construction Project?

## **1.3 Purpose**

The purpose of this final project is as follows.

1. Determining the stability of the non-reinforced slope at STA 7+300 of the Tawang-Ngalang Segment IV Road and Bridge Construction Project.
2. Determining the stability and displacement of soil nailing-reinforced slope at STA 7+300 of the Tawang-Ngalang Segment IV Road and Bridge Construction Project.
3. Determining the stability and displacement of the soil nailing-reinforced slope impacted by different soil nailing variables at STA 7+300 of the Tawang-Ngalang Segment IV Road and Bridge Construction Project.
4. Determining the impact of earthquake on the stability and displacement of the soil nailing-reinforced slope with different soil nailing variables at STA 7+300 of the Tawang-Ngalang Segment IV Road and Bridge Construction Project?



#### **1.4 Advantages**

The advantages of this final project are as follows.

1. Finding out the stability of roadside retaining wall in the specific project with one reinforcement method.
2. Finding out the performance of roadside retaining wall with the same type of reinforcement and different variables.

#### **1.5 Limit**

For the writing of the final project proposal to be structured, the following observation limits are made.

1. The analysis is based on the data from Tawang-Ngalang Segment IV Road and Bridge Project, which was carried out in Nglegi, Gunung Kidul, D.I. Yogyakarta Province in 2022,
2. The analysis is only focused on analyzing slope stability and displacement with earthquake loading impact,
3. The type of roadside retaining wall is limited to soil nailed wall,
4. The project site analyzed is represented as tiered slope after cutting and conditioning,
5. The building load input is based on field observation,
6. In the process of analysis, the factor of safety in static loading and dynamic loading of roadside retaining wall is determined by computation using the PLAXIS program.

## **CHAPTER II**

### **LITERATURE REVIEW**

#### **2.1 General Review**

Retaining wall is a structure that is designed to retain soil in place and prevent erosion, effectively preventing happenings such as landslides. There are several types of retaining wall, namely gravity retaining wall which is made from heavy material and relies on its own weight to resist soil pressure, cantilever retaining wall which uses reinforced concrete slab extending below ground as support, counterfort retaining wall with vertical concrete webs on the back side of the wall to distribute load and resist overturning, anchored retaining wall which is supported by cables or rods anchored to the soil or rock behind the wall for soil of poor condition, sheet pile retaining wall made of steel, vinyl, or wood sheet piles driven vertically and creating a barrier, and lastly gabion retaining wall made of wire mesh being filled with rocks for proper drainage and erosion prevention. Retaining wall can be defined as a structure that can help stabilize an earthen mass that is unstable due to its natural slope (Gandomi et al., 2015).

#### **2.2 Soil Nailed Retaining Wall**

The choice of retaining walls is influenced by a number of variables, including the use and objective, outer requirements, and the building specifications. There are various retaining wall designs, each one with certain qualities and capabilities. The material weight that is retained may also affect the selection criterion for retaining walls. As a result, retaining walls require being thoroughly examined for each unique situation in order to choose the best type depending on the specifications and circumstances of the project. Soil nailing is a practical technique utilized to support excavations in soil or soft, weathered rock, the sidewalls of subway access roads, the construction of tunnel gates, the construction of highways and railways, the abutments of bridges, etc., it is an innovative and

incredibly cost-effective reinforcement technique that uses passive elements drilled and grouted sub-horizontally into the ground (Benayoun et al., 2021).

### 2.2.1 Stability of Soil Nailed Retaining Wall

Fauzi (2012) conducted a study of soil nailed retaining wall stability in three conditions. The modeling is done using PLAXIS 8.2, and the method used is the finite element method (FEM), while the Mohr-Coulomb modeling is utilized to show the failure point. The data collection is done by summarizing past analysis data of soil type, slope inclination, nail inclination, and nail length. All variations in the analysis data for soil type A ( $c \approx 0$ ,  $\alpha = 30^\circ$ ,  $i = 10^\circ$ , nail length 20 m) experienced a collapse, according to the analysis's findings. The highest factor of safety (FS) value is 4,433, which is higher than the safe requirement of 1,5. occurs on a slope of  $30^\circ$ , a nail slope of  $30^\circ$ , a nail length of 30 meters, and soil type C ( $\phi \approx 0$ ,  $\alpha = 60^\circ$ ,  $i = 30^\circ$ , nail length 30 m) with  $c = 0$  and  $\rho = 48,67$  values. In every combination of analysis variables, soil type B ( $c$  &  $\phi$ ,  $\alpha = 45^\circ$ ,  $i = 20^\circ$ , nail length 25 m) is the most stable soil type when compared to other soil types.

Hanif (2016) carried out research on slope stability of soil nailed walls by utilizing GEOSLOPE and manual calculation of the Fellenius method. According to the findings, the factor of safety will drop by 52,6% when the slope angle increases from  $60^\circ$  to  $90^\circ$ . The factor of safety will increase by roughly 14,8% when the nail length is increased from 8 m to 10 m, and by 11,3% when it is increased from 10 m to 12 m. The factor of safety will rise by about 27,9% as nail length is increased from 8 to 12 meters. The factor of safety will increase by 23,2% when the slope is transformed into a bench with a width of 4 m at half the slope's overall height. This change in slope shape also widens the crucial slip surface beneath the slope and reduces the nail bar's internal stability.

Hermawan (2016) conducted a study to analyze slope stability using soil nailing through limit equilibrium method (LEM) in GEOSLOPE with variations on nail distance and nail uniform length. The slopes are 14 meters high, have a considerable angle of  $60^\circ$ , and are steep enough to be dangerous for people driving on the slope's side. The data is collected from a previous study in 2015 in the form

of soil properties and topography. In order to increase the factor of safety's value, this study intends to first assess the slope's factor of safety (FS) value before applying reinforcement. Variations were examined in this investigation at distances of 1,3 nails, 1,5 meters, and 1,8 meters. The distance has been modified to the FHWA standard, which is used as a guide when planning the placement of soil nails. Variations are also carried out at uniformly spaced nails and on a cross-section resembling nails. Based on these findings, the factor of safety (FS) before amplification has a calculated value of 1,196. After installing soil nails, factor of safety values increased from 1,565 to 2,313. Extra nail distances of 1,3, 1,5, and 1,8 meters cause a factor of safety in nail uniform length to be compromised by 5,79% and 13,54%, while the length of the nail varies by 2,09% and 1,88%. When compared to uniform nail length, the value of the factor of safety that causes nail length variations also dropped. A factor of safety of 29,57%, 26,80%, and 16,93% is generated for distances of 1,3 nails, 1,5 meters, and 1,8 meters, respectively.

Rahmanta (2018) conducted research to determine the stability of soil nailed retaining walls through various methods. The modeling is done using GEOSLOPE, and the results are compared with calculation using Fellenius method and Taylor method for non-retained wall, as well as with wedge analysis. The internal stability is tested against reinforcement that is cut off and extracted, while the external stability is tested against shifting. The Fellenius method yields an FS value of  $0,76 < 1,5$ ; the Taylor method yields an FS value of  $0,88 < 1,5$ ; and the GEOSLOPE software yields an FS value of  $0,86 < 1,5$ . For slope reinforcement analysis using the wedge method, a height of 14 meters and a nail distance of 2 meters results in an FS value of 1,6, a height of 14 meters and a nail distance of 1 meter produces an FS value of 2,1, a height of 19 meters and a nail distance of 1 meter produces an FS value of 2,44, and a height of 25 meters results in an FS value of 2,5. FS values of  $0,793 < 1,5$  and  $1,6 > 1,5$  are obtained using the GEOSLOPE program for installation heights of 14 meters and nail spacing of 2 meters, FS owing to and without earthquake loads of  $6,166 > 1,5$  and  $1,2 < 1,5$ , FS for an installation height of 19 meters and a nail distance of 1 meter due to and without earthquake loads of  $5,928 > 1,5$  and  $1,813 > 1,5$ , FS for an installation height of 14 meters and a nail

distance of 1 meter due to and without earthquake loads of  $6,166 > 1,5$  and  $1,2 < 1,5$ , FS owing to earthquake loads of  $8,025 > 1,5$  and  $2,002 > 1,5$  for mounting at a height of 25 meters and a nail spacing of 1 meter. The investigation's findings revealed FS discrepancies between manual analysis (metered wedge) and analysis conducted with the use of the GEOSLOPE application. This is due to the fact that the GEOSLOPE program employs a circular landslide slip field for analysis, but the Baji (wedge) approach uses the Planas landslide slip plane, and the difference is the consequence of manually or automatically analyzing unreinforced slope calculations. Because determining the slip plane is comparable to determining the GEOSLOPE, the results are not much different.

Utomo (2019) conducted research to determine the stability of a soil nailed retaining wall with varieties of nail inclinations. The calculation is done using the Fellenius method and Bishop method with earthquake and non-earthquake considerations, while the modeling is done using GEOSLOPE. From the study, the results attained are that the Fellenius method yields FS of  $0,9292 < 1,3$  while the Bishop method yields FS of  $1,125 < 1,3$ . Utilizing GEOSLOPE, FS of  $0,933 < 1,3$  is obtained from Fellenius method analysis, while FS of  $1,125 < 1,3$  is obtained from Bishop method analysis. Through the manual wedge method analysis at three nail inclination, the results are as such; nail inclination of  $10^\circ$  resulted in FS of  $1,5391 > 1,3$ , the GEOSLOPE program obtained FS without earthquake load of  $2,294 > 1,3$  and FS with earthquake load of  $1,278 > 1,1$ . For nail inclination  $20^\circ$ , FS is  $1,5977 > 1,3$ , the GEOSLOPE program resulted in FS without earthquake load of  $2,944 > 1,3$  and FS with earthquake load of  $1,503 > 1,3$ . For nail inclination of  $30^\circ$ , the FS is  $1,6051 > 1,3$ , through GEOSLOPE FS without earthquake load is  $3,253 > 1,3$  while FS with earthquake load is  $1,653 > 1,3$ . According to the findings, the wedge method and GEOSLOPE differing FS values were caused by the former's use of planar landslide fields and the latter's use of a circle landslide slip plane.

Nalgire et al. (2020) conducted a study of the stability of dump slope with differing parameters of soil nail diameter, spacing, and nail length. The calculation of finite slope stability analysis is done using Morgenstren-Price Method, Spencer Method, Bishop Method, Janbu Method, Ordinary Slices Method, and Sarma

Method. The modeling is done using GEOSLOPE, with wall height of 17,5 meters and width of 40 meters. Meanwhile, the slope inclination ranges from 25° to 45°. The non-reinforced wall shows average for factor of safety (FS) of 1,023 for 45° inclination and increasing up to average of 1.573 for 25° with consistent interval for each inclination across six methods. Upon being reinforced using soil nailing, the nail diameter of 16 millimeters to 30 millimeters with 2 millimeters interval shows little effect on the FS, as proven by the inconsistent intervals and values across all six methods and all varieties of soil diameter. For the parameter of nail spacing, the 1 meter spacing yields the highest FS across all methods with an average of 3.433, and with an increased interval of 0,25 meters, the 3 meters spacing yields an average FS of 1,747. Lastly, soil nail length starting from 0,25 meters with 0,25 meters intervals up to 3 meters shows an increase in FS beyond the failure plane, with FS across all methods constant for 2,75 meter and 3 meters nail length, and this is due to resistance development in the passive zone.

Pham et al. (2020) carried out a study to determine the stability of soil nailed retaining wall based on the parameters of nail inclination and length. The soil nail wall is modeled to be 6 meters high. The nail inclination  $\alpha$  is set to be 0°, 5°, 10°, 15°, 20°, and 25° with nail length varying from 5 to 11 meters. The calculation is done using the Limit Equilibrium Method, while the modeling is carried out through PLAXIS 8.6. There are three patterns in modeling; (1) is soil nail length decreasing with depth starting from 11 meters to 5 meters with 2 meters interval, (2) is constant soil nail length at 8 meters for two nails, and (3) is increasing soil nail length with depth using the same lengths and interval as pattern (1). Through the modeling, the results show that the factor of safety (FS) stays around 1,5 for the 0° to 20° nail inclinations. Meanwhile, for the 20° to 25° nail inclination, the FS drops drastically from to 0. This means that at such a large value of inclination, there is no significant effect to the wall stability itself, and that the optimum FS for this model is at inclination of 10°. In addition to that, pattern (3) is proven to undergo the smallest deformation while maintaining FS of above 1,5.

Villalobos and Villalobos (2020) conducted research to determine the stability of a soil nailed retaining wall with different nail spacing combinations. The

retaining wall is designed with variations of wall inclination  $\beta$  from  $50^\circ$  to  $90^\circ$ , while the nail spacing  $S$  starts from 1 m, increases by 0,25 m up to 2,5 m, while other design parameters of  $L$ ,  $H$ ,  $\alpha$ ,  $D$ ,  $r_s$ ,  $\gamma$ ,  $c'$ ,  $\phi'$ ,  $\psi$ ,  $E$ ,  $\nu$  are constant. The calculation is done using the limit equilibrium method (LEM) which is the more popular method in current geotechnics works and finite element method (FEM). From the results obtained, it is apparent that FEM attains a considerable improvement of wall stability compared to LEM, through the FSG- $\beta$ - $S$  plot that follows logical trend, as well as the consideration of  $L$ ,  $\alpha$ ,  $d$ ,  $r_s$ ,  $c'$  and  $\phi'$  parameters. Further nail spacing, for example  $S$  value of above 2 m can threaten soil nailed wall stability of FSG below 1,1. The FEM should be utilized compared to LEM, and that in utilization of LEM there should be careful assessment in the case of steep walls and close nail spacing.

Nowroozi et al. (2021) carried out research to determine the stability of a soil nailed retaining wall that varies dimensionally. The retaining wall is designed through Model 1 of 13,5 meters depth with 2 of each 13 m, 14 m, and 12 m nails, 12 degrees angle downward, and 1,5 m vertical distance. Meanwhile, Model 2 has 21 meters of depth with 2 nails of 14 m and 6 nails of 12 m, 10 degrees angle downward, and 1,5 m vertical distance. The nails are flexible yet plastic cables, and there is shotcrete. Using FLAC3D finite difference software, a comparison is done for the factor of safety, horizontal displacement, and lateral pressure behind the wall between the two models. The calculation is done using the Mohr-Coulomb model. Through the linear elements, the shotcrete is modeled. It demonstrates that the most effective depth is around the midpoint of the completed wall height. Taking into account the number of reinforcing nails with the same lengths, installing two rows of nails as opposed to three or five rows of nails significantly lowered the maximum wall displacement. This redesign attains a higher factor of safety.

Arvin et al. (2022) conducted a study to determine the optimal nail inclination angle in soil nailed walls based on the limit equilibrium method (LEM). The calculation is done using LEM with nail inclination angle  $\eta$  being the main variable affecting the factor of safety (FS). Other considered factors are nail dimensions, soil friction, slope and back slope angle, and nails layout. The

conclusion is that nail diameter increase means higher FS and  $\eta_{opt}$ . It is also found that  $1,875H$  increase of nail length resulted in slope stability undergoing the most notable improvement. Additionally, an improvement in FS and a modest rise in  $\eta_{opt}$  are produced by an increase in soil friction. Steeper nail walls require more  $\eta_{opt}$ , a linear function of slope orientation ( $\alpha$ ), and are less sturdy. It was discovered that a greater back slope angle reduced FS. Additionally, it was discovered that the most effective placement for the nails is in the lower third of the slope, and that they have no effect on the stability of short walls or slopes with a high degree of cohesiveness.



**Table 2.1 Former and Current Research Comparison**

Former Research						Current Research
Researcher	Fauzi (2012)	Hanif (2016)	Hermawan (2016)	Rahmanta (2018)	Utomo (2019)	Nuradrina (2023)
Title	<i>Analisis Tegangan-Perpindahan dan Faktor Keamanan (FS) Pada Lereng Miring Dengan Perkuatan Soil Nailing Menggunakan Program PLAXIS 8.2</i>	<i>Analisis Perkuatan Soil Nailing sebagai Metode Perbaikan Stabilitas Lereng</i>	<i>Analisis Stabilitas Lereng dengan Perkuatan Soil Nailing Menggunakan Program Komputer (Studi Kasus: Desa Tambakmerang, Kecamatan Girimarto, Kabupaten Wonogiri)</i>	<i>Analisis Stabilitas Lereng dengan Perkuatan Soil Nailing Menggunakan Metode Perhitungan Fellenius dan Taylor serta Program GEOSLOPE Studi Kasus Desa Srimartan, Kecamatan Piyungan, Kabupaten Bantul</i>	<i>Analisis Stabilitas Lereng dengan Perkuatan Soil Nailing dengan Menggunakan Program GEOSLOPE</i>	Analysis of Slope Stability with Soil Nailing Reinforcement Using PLAXIS Program  (Study Case: STA 7+300 of Tawang-Ngalang Segment IV Road and Bridge Project)
Researcher	Nalgire et al. (2020)	Pham et al. (2020)	Villalobos and Villalobos (2020)	Nowroozi et al. (2021)	Arvin et al. (2022)	
Title	Slope Stability Analysis by GeoSlope	Study on The Effect of some Parameters of Soil Nails on The Stability of Vertical Slopes	Effect of nail spacing on the global stability of soil nailed walls using limit equilibrium and finite element methods	Optimum Design for Soil Nailing to Stabilize Retaining Walls Using FLAC3D	Optimization of Nail Inclination Angle in Soil Nail Walls Based on a Prevalent Limit Equilibrium Method	

**Continuation of Table 2.1 Former and Current Research Comparison**

Former Research						Current Research
Researcher	Fauzi (2012)	Hanif (2016)	Hermawan (2016)	Rahmanta (2018)	Utomo (2019)	Nuradrina (2023)
Purpose	Determining factor of safety (FS) of soil nailed retaining wall in three conditions with variability on soil type, slope inclination, nail inclination, and nail length.	Determining factor of safety (FS) of soil nailed retaining wall with variability on slope angle, nail length, and slope width-height particular ratio.	Determining factor of safety (FS) of soil nailed retaining wall with variability on nail distance and nail uniform length.	Determining the factor of safety (FS) of soil nailed retaining wall through several methods with variability of three wall heights and two nail spacing for each height.	Determining the factor of safety (FS) of soil nailed retaining wall with variability of nail inclinations of three angles as well as earthquake and non-earthquake analysis.	Determining the factor of safety (FS) and displacement of soil nailed retaining wall with variability of nail vertical spacing, nail length, and nail inclination in comparison to the current model, while keeping parameters such as wall height, wall inclination, soil type, and slope inclination the same.
Researcher	Nalgire et al. (2020)	Pham et al. (2020)	Villalobos and Villalobos (2020)	Nowroozi et al. (2021)	Arvin et al. (2022)	
Purpose	Determining the factor of safety (FS) of dump slope with differing parameters of soil nail diameter, spacing, and nail length	Determining the factor of safety (FS) of soil nailed retaining wall based on the parameters of nail inclination and length.	Determining the factor of safety (FS) of soil nailed retaining wall with variability of wall inclination and nail spacing.	Determining factor of safety (FS) of soil nailed retaining wall with variability of two wall heights combined with three nail lengths, one nail inclination, and one vertical nail distance for each height.	Determining the factor of safety (FS) with main variability of nail inclination angle and considering nail dimensions, soil friction, slope and back slope angle, and nail layout.	

**Continuation Table 2.1 Former and Current Research Comparison**

Former Research						Current Research
Researcher	Fauzi (2012)	Hanif (2016)	Hermawan (2016)	Rahmanta (2018)	Utomo (2019)	Nuradrina (2023)
Method	Finite element method (FEM), PLAXIS 8.2, Mohr-Coulomb	Fellenius Method, GEOSLOPE	Limit Equilibrium Method (LEM), GEOSLOPE	GEOSLOPE, Fellenius Method, Taylor Method for non-retained wall, Wedge Analysis	Fellenius Method, Bishop Method, GEOSLOPE, Wedge Method Analysis	Limit Equilibrium Method (LEM), Fellenius Method, PLAXIS V20
Researcher	Nalgire et al. (2020)	Pham et al. (2020)	Villalobos and Villalobos (2020)	Nowroozi et al. (2021)	Arvin et al. (2022)	
Method	Morgenstren-Price Method, Spencer Method, Bishop Method, Janbu Method, Ordinary Slices Method, and Sarma Method, GEOSLOPE	Limit Equilibrium Method, PLAXIS 8.6	Limit Equilibrium Method (LEM), Finite Element Method (FEM)	FLAC3D, Mohr-Coulomb Model	Limit Equilibrium Method (LEM)	

**Continuation of Table 2.1 Former and Current Research Comparison**

Former Research						Current Research
Researcher	Fauzi (2012)	Hanif (2016)	Hermawan (2016)	Rahmanta (2018)	Utomo (2019)	Nuradrina (2023)
Result	Condition B (c & Ø, α = 45°, i = 20°, nail length 25 m) is the most stable.	The factor of safety (FS) decreases as slope angle increases, increases as nail length increases proportional to the length difference, and increases when there is bench transformation at half the slope's total height.	The factor of safety (FS) increases with the installment of soil nails, bigger nail distance compromises FS further, and the uniform nail length results in higher FS compared to varied nail lengths.	The factor of safety (FS) from Fellenius Method, Taylor Method, and GEOSLOPE is below standard of 1,5, while Wedge Analysis resulted in varieties of FS below and above standard. Shorter nail spacing increases FS at its given height. GEOSLOPE earthquake analysis resulted in FS above standard at four given conditions, while the non-earthquake has FS below & above standard for two conditions each.	The factor of safety (FS) for Fellenius Method and Bishop Method are below standard of 1,3, the same goes for modeling using GEOSLOPE for both methods, meanwhile the Wedge Method at three angles for earthquake and non-earthquake load yields FS higher than standard for nine conditions.	FS is most optimal at 20° soil nailing inclination for static and dynamic loading compared to 35° and 50°. 1,5 meters of nail vertical spacing yields higher FS compared to the 2,5 meters under static loading, meanwhile for dynamic loading, 2,5 meters yields higher FS except for one case. 4,5 meters nail length achieves the same results as the original 5 meters, with 1,5 meters and 2,5 meters nail spacings both yields equally optimal FS in both lengths. The most optimal model is Model h with the length of 4,5 meters, nail inclination of 20°, and vertical spacing of 1,5 meters, which is also more cost-effective.
Researcher	Nalgire et al. (2020)	Pham et al. (2020)	Villalobos and Villalobos (2020)	Nowroozi et al. (2021)	Arvin et al. (2022)	
Result	The factor of safety (FS) for 1 meter nail spacing yields the highest FS across all methods with an average of 3.433, while an increase in nail length creates an increase in FS beyond failure plane up to 3 meters length.	The FS is not significantly affected by nail inclination around 20°, while the optimum FS is 10° inclination, and increasing nail length with depth results in smallest deformation and maintaining above 1,5 FS.	The overall stability of the wall is improved significantly using FEM compared to LEM, which is the more common method, meanwhile further nail spacing decreases stability.	The FS is the most optimum at effective depth of around the midpoint of finished wall height, and two rows of nails are better compared to three or five rows of the same lengths in lowering the maximum wall displacement.	The FS increases with increase of nail diameter and nail inclination, as well as soil friction increase, it is also found that an increase in back slope angle decreases FS, while the optimal nail placement is in the lower third of the slope with little effect on stability in some cases.	

## 2.2.2 Preceding Report of Study Case for Soil Nailed Retaining Wall

The soil reporting for Tawang-Ngalang Segment IV Road and Bridge Construction Project is carried out by PT. Geomine Bara Studio. The data obtained is classified as secondary data, and the features of the particular STA are the benchmark for the modeling that will be undertaken in this final project. The secondary data includes soil characteristics and the modeling of current soil nailed retaining wall.

The existing slope at STA 7+300 of Tawang-Ngalang Segment IV Road and Bridge Construction Project needs stability analysis as it has the tendency to have the condition in which the slope angle is equal to or bigger than the shear strength of the material. The slope soil profile is assumed to be the same in the modeling, and the STA is excavated or cut. In the report it is also pointed out that weather can affect stability, that saturated layer decreases material shear strength, and that the more saturated the material, the lower the Poisson's Ratio is.

The non-reinforced design slope of STA 7+300 has the Factor of Safety of 1,38, as shown below.

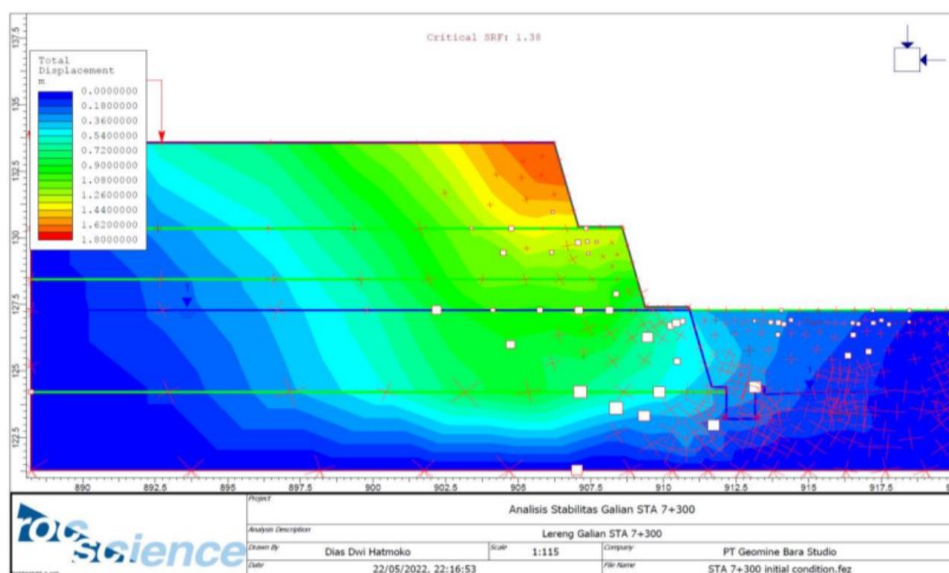


**Figure 2.1 Reinforcement Stability Condition of STA 7+300 with Existing Slope**

(Source: PT Geomine Bara Studio, 2022)

According to the modeling, the direction of the stress is problematic as it is moving to the excavated slope. In certain conditions the material will be in elastic condition, so that the slope is able to maintain resisting force against collapse. The figure above shows that material elasticity increases in value and amount as it gets closer to the slope convex corner, which may be caused by the elasticity of the material that is yet surpassed. Compared to other STA, the convex corner of this section has the most critical presence and intensity of strain.

The current soil nailing reinforced design slope is modeled below, where the obtained factor of safety is 1,27 that charts below the standard of 1,5 as is the benchmark for the researches mentioned in Chapter II. Some features of the reinforcement are uniform length of 5 meters and diameter of 10 millimeters for the nails, uniform inclination of  $35^\circ$ , and nail spacing of 2,5 meters. Meanwhile Figure 4.4 also shows the shotcrete reinforcement of 10 centimeters thickness.

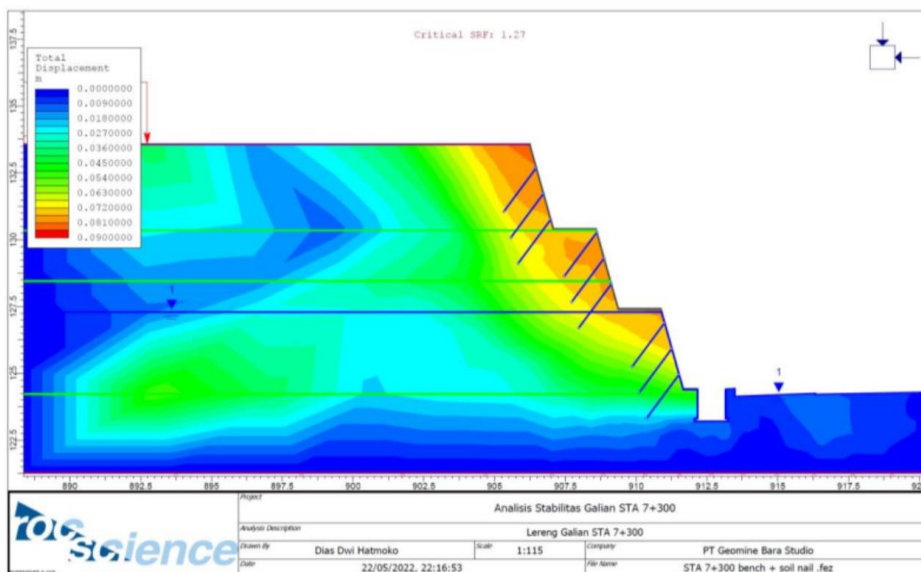


**Figure 2.2 Reinforcement Stability Condition of STA 7+300 with Soil Nail of 5 Meters Length and 10 Millimeters Diameter**

(Source: PT Geomine Bara Studio, 2022)

## **CHAPTER III**

### **THEORETICAL BASIS**

#### **3.1 Soil**

Organic material, minerals, gasses, liquids, and living things all coexist in soil to support life as we know it. It is a dynamic ecosystem that supports a wide range of microorganisms, aids in the cycling of nutrients and carbon, and gives plants nutrition and water. It takes thousands of years for soil to form, and throughout that time, it slowly changes over time according to biotic, climatic, and topographical influences as well as parent material. The ratios of sand, silt, and clay as well as the amount of organic matter present determine the type of soil that is created. Based on diverse characteristics, including texture, structure, color, and pH, soil is divided into various categories. Sandy loamy, clayey, and peaty soils are some examples of typical soil types. The success of farming and agriculture can also be influenced by the soil's characteristics, which vary according to the needs of different plants. Because soil takes a long time to produce and is susceptible to erosion, pollution, and degradation, it is also a non-renewable resource. For the soil ecosystem to remain healthy and sustainable, proper soil conservation and management measures are crucial. In a more comprehensive view, a human society that is always evolving and in which the push for continuing economic expansion and rapid technical advancement, along with the continual rise of information, frequently results in significant and unanticipated changes, benefits from soil (Dazzi & Papa, 2021).

The complicated process of soil creation takes place over thousands of years and involves the interaction of a number of variables, such as terrain, parent material, organisms, and time. The five steps that make up the fundamental process of soil formation are as follows; first is the disintegration of rocks and minerals into smaller particles as a result of physical, chemical, and biological processes known as weathering, second is soil accumulation which is the buildup of weathered materials to create the foundational soil layers, third is the creation of various soil layers is the result of the weathered components being changed by physical,

chemical, and biological processes, fourth is soil transfer when soil is moved from one place to another as a result of erosive, accumulative, or other processes, fifth is soil development where over time, the soil continues to change and develop, giving rise to distinctive soil features and traits. Depending on the particulars of the environment, these steps may take place concurrently or in order. The resulting soil is an intricate blend of minerals, organic matter, water, and air that offers the critical nutrients and support for plant growth as well as serving as a key resource for people and other living things.

### 3.1.1 Soil Components

Three things make up soil: water, air, and solid stuff (granules). Air is thought to have no technical impact, whereas water has a significant technical impact on soil. Void between grains that may be partially or entirely filled with water or air. The soil becomes partially saturated when the voids are filled with water and air. A body of soil with no water content, or dry soil, is completely devoid of water. Below, the illustration showing soil phase and components can be seen in Figure 3.1 with Figure 3.1a showing homogenous soil layer and its volume relative to its weight, while Figure 3.1b shows the layers or ratio of air, water, and granules as well as each component's volume and weight respectively.

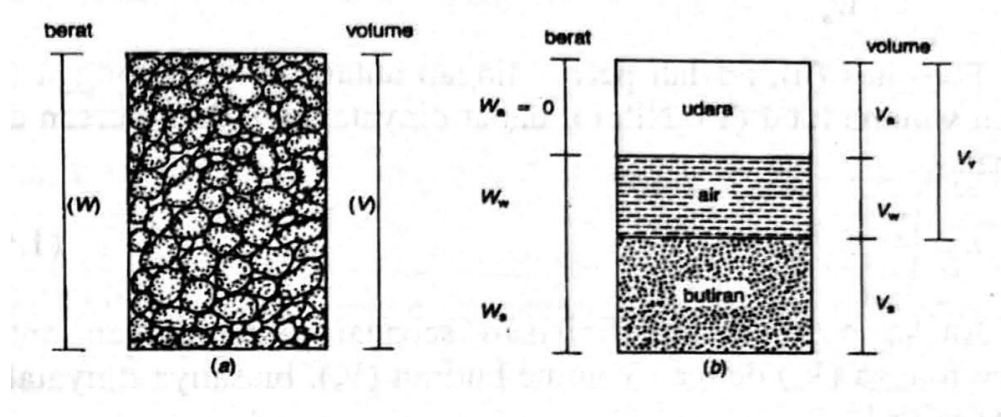


**Figure 3.1 Soil Phase Diagram**

(Source: Hardiyatmo, 2012)

Several formulas can be generated from the illustration above:



## 1. Soil Weight (gr)

$$W = W_s + W_w$$

2. Volume/content (cm<sup>3</sup>)

$$V = V_s + V_w + V_a$$

3. Volume/void (cm<sup>3</sup>)

$$V_v = V_w + V_a$$

with:

$W_s$  = granule weight

$W_w$  = water weight

$V_s$  = granule volume

$V_w$  = water volume

$V_a$  = air volume

From Figure 3.1 above, the resulting weight and volume equations are as follows:

## 1. Moisture Content/Water Content

Moisture content ( $w$ ) is the ratio between the weight of water ( $W_w$ ) and the weight of the granules solid ( $W_s$ ), the water content is expressed in Equation 3.1 below.

$$w(\%) = \frac{W_w}{W_s} \times 100 \quad (3.1)$$

## 2. Porosity

Porosity ( $n$ ) is the ratio between void volume ( $V_v$ ) with total volume ( $V$ ).  $n$  Value can be expressed in percentage or decimal such as in Equation 3.2.

$$n = \frac{V_v}{V} \quad (3.2)$$

## 3. Void Number

Void number ( $e$ ) is the ratio between void volume ( $V_v$ ) with granule volume ( $V_s$ ), typically expressed in decimal. It is displayed in the following Equation 3.3.

$$e = \frac{V_v}{V_s} \quad (3.3)$$

#### 4. Damp or Wet Volume Weight (Damp or Wet Density)

Wet unit weight ( $\gamma$ ), is the ratio between the weight of the soil particles including water and air ( $W$ ) to the volume of soil ( $V_v$ ), wet unit weight expressed in Equation 3.4 as follows.

$$\gamma_b = \frac{W}{V} \quad (3.4)$$

with  $W = W_w + W_s + W_a$  with  $W_a = 0$ . If the void is completely filled with water ( $V_a = 0$ ), the soil becomes saturated.

#### 5. Dry Volume Weight (Dry Density)

Dry unit weight ( $\gamma_d$ ), is the ratio between the weight of the soil particles including water and air ( $W$ ) to the total volume of soil ( $V$ ). Dry unit weight is stated in the following Equation 3.5.

$$\gamma_d = \frac{W_s}{V} \quad (3.5)$$

#### 6. Granule Volume Weight

Granule volume weight ( $\gamma_s$ ) is the ratio between granule weight ( $W_s$ ) and granule volume ( $V_s$ ) as presented in the following Equation 3.6.

$$\gamma_s = \frac{W_s}{V_s} \quad (3.6)$$

#### 7. Specific Gravity

Specific gravity ( $G_s$ ) is the ratio between the volume weight of solid granules ( $\gamma_s$ ), with the volume weight of water ( $\gamma_w$ ), the measured temperature 4°C. The specific gravity is expressed in Equation 3.5 below.

$$G_s = \frac{\gamma_s}{\gamma_w} \quad (3.7)$$

$G_s$  is dimensionless. The specific gravity of different types of soil ranges from 2,65 to 2,75. The  $G_s = 2,67$  value of specific gravity is typically used for cohesionless soils. Meanwhile, for non-organic cohesive soils, the value ranges from 2,68 to 2,72. The specific gravity values of different soils are presented in Table 3.1.

**Table 3.1 Soil Specific Gravity**

Soil Type	Specific Gravity (Gs)
Gravel	2,65 - 2,68
Sand	2,65 - 2,68
Inorganic Silt	2,62 - 2,68
Organic Clay	2,58 - 2,65
Inorganic Clay	2,68 - 2,75
Humus	1,37
Peat	1,25 - 1,80

(Source: Hardiyatmo, 2012)

### 3.1.2 Soil Classification

The process of classifying soils according to their physical, chemical, and biological characteristics is known as soil classification. Depending on the categorization's objective, such as in engineering or agricultural applications, a different classification system may be employed. The Soil Taxonomy, which was created by the United States Department of Agriculture (USDA), is one widely used system for classifying soil. A hierarchical system of categories based on the qualities and properties of the soil is used in soil taxonomy. The categories are as follows, increasing in specificity: Order, Suborder, Great Group, Subgroup, Family, and Series. Each category is based on particular soil characteristics, such as soil horizon depth, mineralogy, organic matter content, and texture. The Unified Soil Classification System (USCS), which is largely used in engineering applications, is another widely used soil classification system. Based on the particle size distribution and plasticity index, the USCS categorizes soils. The USCS's classifications are;

1. soils with a coarse texture, such as sand and gravel,
2. fine-grained soils, such as clay and silt,
3. extremely organic soils, such as peat, and

4. different soils, such as expansive soils.

Application areas for soil categorization include engineering, environmental management, and agriculture. Scientists and professionals who are knowledgeable about the characteristics of various soils can choose the best methods for managing and utilizing them. Historically, the unified classification was first pioneered by Cassagrande in the mid 1900's, and then was revised and perfected by the United States Bureau of Reclamation (Hardiyatmo, 2012).

### 3.1.3 Soil Properties

Among the various physical and non-physical soil properties, the main focus of this research are wet volume weight ( $\gamma$ ), internal friction angle ( $\phi$ ), and cohesion ( $c$ ).

#### 1. Wet volume weight ( $\gamma$ )

The weight of soil per unit volume when the soil is in its natural, damp state is measured using the term "wet volume weight of soil," also known as "wet unit weight." It is a crucial factor in the design and study of many different kinds of structures, including embankments, retaining walls, foundations, and pavements. Numerous variables, such as the soil type, moisture content, compaction effort, and void ratio, have an impact on the wet unit weight of soil. In general, as moisture content and compaction effort rise, so does a soil's wet unit weight. By weighing a known volume of damp soil, dividing the weight by the volume, and repeating this process several times, it is possible to empirically calculate the wet unit weight of soil. By measuring the dimensions of a known container and the volume of soil it holds, or by utilizing a soil sample ring, the volume can be calculated. The soil's moisture content can also be calculated by weighing it before and after it has been dried in an oven, then dividing the difference in weight by the original weight.

The units used to represent the moist unit weight of soil are commonly kilograms per cubic meter ( $\text{kg/m}^3$ ) or pounds per cubic foot (pcf). A soil with a moist unit weight of  $20 \text{ kN/m}^3$ , for instance, is weighed at 20 kilograms per cubic meter in its natural, damp state.

## 2. Internal Shear Angle ( $\phi$ )

The soil internal shear angle, sometimes referred to as the internal friction angle or the shearing resistance angle, is an indicator of how well a soil can withstand sliding or deformation when a load is applied. The maximum slope that the soil can retain without collapsing or shearing is measured as the angle between the horizontal plane and that line. The type of soil, the distribution of grain sizes, the amount of porosity, the moisture content, and the presence of cementing agents are some of the variables that affect the value of the soil internal shear angle. The internal shear angles of cohesive soils, such as clays, are often lower than those of non-cohesive soils, like sands and gravels. The stability of slopes, retaining walls, and foundations is affected by the soil internal shear angle, which is a crucial parameter in geotechnical engineering. It can be discovered using field testing like the Standard Penetration Test (SPT) or Cone Penetration Test (CPT), as well as laboratory tests like direct shear tests or triaxial compression tests. Below is Table 3.2 which presents the different types of soil internal shear angle.

**Table 3.2 Soil Internal Shear Angle**

Soil Type	Internal Shear Angle
Sandy Gravel	35° - 40°
Boulder Gravel	35° - 40°
Solid Sand	35° - 40°
Loose Sand	30°
Silty Clay	25° - 30°
Clay	20° - 25°

(Source: Das, 1985)

## 3. Cohesion ( $c$ )

The ability of a soil to withstand shear pressures is known as soil cohesiveness. Surface tension, electrostatic forces, chemical bonds, and other factors of

attraction interact with soil particles to produce this strength. The soil's shear strength, or the maximum force it can bear before failing and beginning to deform, is a common way to quantify cohesion. Numerous elements, including soil type, moisture content, particle size distribution, and the presence of organic matter or minerals, can affect the cohesiveness of soil. While soil with low cohesiveness may be vulnerable to landslides and other types of instability, soil with high cohesion tends to be more stable and less prone to erosion.

## **3.2 Soil Shear Strength**

### **3.2.1 Soil Shear Strength Definition**

The capacity of a soil to withstand sliding or shearing along a failure plane is known as soil shear strength. In order to construct and assess geotechnical structures like foundations, retaining walls, slopes, and tunnels, it is essential for soils to have this attribute. Typically, laboratory techniques like the direct shear test, triaxial compression test, or unconfined compression test are used to assess the shear strength of soil. In these experiments, a soil sample is subjected to a shear stress, and the subsequent deformation or failure is measured. The mineral composition, particle size distribution, soil structure, moisture content, and stress history are some of the variables that affect a soil's shear strength. Because clay minerals can link together and withstand shear deformation, cohesive soils like clays have a higher shear strength. Due to the absence of this cohesive link, granular soils such as sand and gravel have a lower shear strength. A shear strength parameter, such as the shear strength coefficient or angle of internal friction, is commonly used to express the shear strength of a soil. When designing buildings to withstand applied loads, geotechnical engineers use these factors to determine the shear resistance of the soils. Hardiyatmo (2012) emphasizes on the importance of soil shear strength parameters in analyzing soil bearing capacity, slope stability, and thrust for soil retaining walls.

### 3.2.2 Soil Shear Strength Theory

A prominent theory regarding the soil shear strength was proposed by Mohr in 1910, where it is synthesized that the combination of critical conditions between normal stress and shear stress causes material failure, which is expressed in Equation 3.8 below.

$$\tau = f(\sigma) \quad (3.8)$$

where  $\tau$  is the shear stress at failure, and  $\sigma$  is the normal stress at failure as well.

Meanwhile, the  $f(\sigma)$  according to Coulomb can be expressed as such in Equation 3.9 below.

$$\tau = c + \sigma \operatorname{tg} \phi \quad (3.9)$$

where  $c$  is soil cohesion and  $\phi$  is internal friction angle of soil.

The relation between Mohr Theory and Coulomb Theory is presented in Figure 3.2.

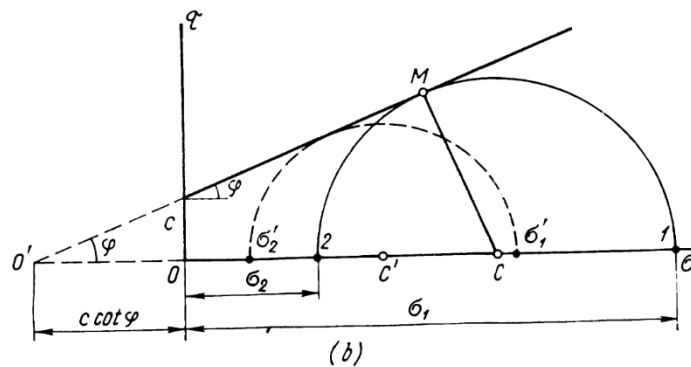


Fig. 22. Diagram of ultimate stresses of soils at shearing  
(a) for loose soils; (b) for cohesive soils

### Figure 3.2 Mohr and Coulomb Failure Criterion

(Source: Tsytovich, 1976)

The understanding derived from the figure is that new stresses will not cause soil failure due to shear at point P, but soil failure will happen if the stresses reach

point Q, which is the failure envelope. All the while, it is impossible for the stresses to reach point R, because before then, the soil will have collapsed already.

### 3.3 Soil Elastic Property

There is one main elastic property of soil that is used in this research, which is Soil Young's modulus (E). Often known as soil elastic modulus, this is a soil characteristic that measures soil stiffness. In the context of elastic soil behavior, it refers to the ratio of stress to strain along an axis. The elastic modulus is frequently utilized in soil settlement estimation and elastic deformation analysis. Soil elastic modulus can be calculated via laboratory or in-situ testing, or by comparing it to other soil parameters. It can be determined in the laboratory with a triaxial test or indirectly using an oedometer test. It can be estimated in the field using a standard penetration test, a cone penetration test, a pressuremeter, or an indirect dilatometer test. Based on Obrzud & Truty (2012), the typical values of Young's Modulus in granular and cohesive material in MPa are presented below.

**Table 3.3 Soil Granular Material Young's Modulus in MPa**

USCS	Description	Loose	Medium	Dense
GW, SW	Gravels/Sand well-graded	30-80	80-160	160-320
SP	Sand, uniform	10-30	30-501	50-80
SM, GM	Sand/Gravel silty	7-12	12-20	20-30

(Source: Obrzud & Truty, 2012)

**Table 3.4 Soil Cohesive Material Young's Modulus in MPa**

USCS	Description	Very soft to soft	Medium	Stiff to very stiff	Hard
ML	Silts with slight plasticity	2,5 – 8	10 – 15	15 – 40	40 – 80



ML, CL	Silts with low plasticity	1,5 – 6	6 – 10	10 – 30	30 – 60
CL	Clays with low-medium plasticity	0,5 – 5	5 – 8	8 – 30	30 – 70
CH	Clays with high plasticity	0,35 – 4	4 – 7	7 – 20	20 – 32
OL	Organic silts	-	0,5 – 5	-	-
OH	Organic clays	-	0,5 – 4	-	-

### 3.4 Soil Investigation

In order to ascertain whether a particular soil is suitable for specific engineering and construction projects, it is necessary to examine and test its physical, chemical, and mechanical qualities. Numerous methods, including drilling, sampling, testing, and analysis of soil samples, are used. Soil investigation's main goal is to learn more about the properties and behavior of the soil at a construction site in order to assure that the foundation design and construction will be risk-free, long-lasting, and economical. Engineers and geologists can establish the type of foundation needed, the soil's bearing capability, the depth of the foundation, and other crucial design factors with the use of soil study. Environmental and geotechnical assessments also depend heavily on the results of soil investigations. It aids in locating possible dangers like sinkholes, landslides, and contaminated soil. The outcomes of a soil inquiry are utilized to create slope stabilization, erosion control, and soil remediation solutions. Typically, soil investigation is divided into steps such as boring, extraction of specimen, and specimen testing. Examples of soil investigation as presented by Hardiyatmo (2012) are Direct Shear Test, Triaxial Test, and Unconfined Compression Test.

## **3.5 Slope Stability**

### **3.5.1 Slope Stability Definition**

Slope stability describes a slope's or embankment's capacity to withstand the pull of gravity and preserve its shape without falling or collapsing. Since slopes and embankments must be safe and stable in a variety of building projects, slope stability analysis is an essential component of geotechnical engineering. The stability of a slope can be impacted by a number of variables, including the type of soil, groundwater level, slope geometry, and external loads. Assessing the soil's shear strength and calculating the factor of safety, or the ratio of driving forces to resisting forces, are two common steps in a slope stability analysis. Slope stability analysis can be done using a variety of techniques, such as limit equilibrium analysis, finite element analysis, and numerical modeling. The method chosen will depend on how complicated the slope is and how accurate you need it to be. There are a number of steps that may be done to prevent slope instability and assure safety, such as enhancing soil strength through stabilization techniques, constructing drainage systems to lower water pressure, altering slope geometry, and putting monitoring systems in place to find unstable slopes early on. In order to assure the security and durability of building projects as well as to lessen the risks related to natural hazards like landslides and erosion, slope stability analysis is crucial in geotechnical engineering.

### **3.5.2 Factors Affecting Slope Stability**

The stability of a slope or embankment can be impacted by a number of things. The following are some of the key elements that geotechnical engineers take into account when evaluating slope stability.

1. Soil characteristics: The type, content, and strength of the soil all have a significant role in slope stability. Compared to non-cohesive soils like sand, cohesive soils, like clay, often have higher shear strengths and are more stable.
2. Water content: The soil's water content has a big impact on the stability of the slope. The strength, weight, and water pressure of the soil can all rise with an increase in water content, which can cause the slope to fail.

3. **Slope geometry:** The stability of the slope can be impacted by the slope's angle, height, and form. Concave slopes are more stable than convex slopes, whereas steeper slopes are typically less stable than kinder slopes.
4. **Vegetation:** By strengthening the soil and limiting erosion, vegetation can stabilize slopes. However, removing vegetation could endanger the slope's stability.
5. **External loading:** The slope may experience additional loads from structures outside of it, such as buildings, roads, or other structures, which could increase the forces pushing on it and decrease its stability.
6. **Geological conditions:** The stability of the slope may be impacted by the geological conditions, such as the presence of faults, fractures, or other geological features.
7. **Climatic:** By affecting soil characteristics and the amount of water in the soil, climatic factors including rainfall, temperature, and freeze-thaw cycles can also have an impact on slope stability.

Slope stability is a complicated problem that calls for careful consideration of numerous elements. Geotechnical engineers examine slope stability using a variety of approaches to decide what steps should be taken to assure stability and safety.

Meanwhile, Cruikshank (2002) stated that slope stability hinges on three soil mechanics parameters; the first one is concerned with soil strength which includes cohesion, friction, grains interlocking, and other factors, the second one is soil geometry including ground surface shape, slide surface shape, soil layering pattern, and the existence of joints or shear zones, lastly the third is pore-water pressure including seepage forces.

### **3.5.3 Landslide**

A form of mass wasting event known as a landslide is when rocks, dirt, or other materials slide down a slope as a result of gravity. Based on the type of movement, the material involved, and other variables, there are various types of landslides. Here are a few typical landslide types:

A. Rotation Slide

This type of slide has a concave upward surface of rupture, and it moves roughly in a rotation about an axis that is parallel to the ground and runs transverse to the slide.

B. Translational Slide

Sliding down a surface that is roughly planar, with little twisting or tilting to the rear, is known as a translational slide.

C. Block Slide

A block slide is a translational slide in which the mass that is traveling downslope is made up of just one unit or a small group of closely linked units.

D. Rockfall

Falls are sudden movements of geologic material masses, such as rocks and boulders, that separate from cliffs or steep slopes. Movement involves falling freely, bouncing, and rolling, and separation happens along discontinuities like fractures, joints, and bedding planes. Gravity, mechanical weathering, and the presence of interstitial water all have a significant impact on falls.

E. Topple

Toppling failures are distinguished by the forward rotation of a unit or units about a pivot point that is below or low in the unit, under the influence of gravity, forces from neighboring units, or fluids in fissures.

F. Debris flow

In a debris flow, a slurry of loose soil, rock, organic matter, air, and water mobilizes and flows downslope at a high rate (fig. 3F). About 50% of debris flows are fines. Debris flows are frequently created by high surface-water flow that erodes and mobilizes loose soil or rock on steep slopes as a result of heavy precipitation or quick snowmelt. Other forms of landslides that happen on steep slopes, are almost saturated, and contain a significant amount of silt- and sand-sized material frequently mobilize debris flows as well. Steep gullies are frequently found near debris-flow source locations, and the presence of debris fans at gully mouths typically indicates the existence of debris-flow deposits. mudflow. Debris flows are frequently swift-moving and capable of serious

harm. Slopes that have been burned down become more vulnerable to debris flows because the vegetation has been destroyed.

G. Debris Avalanche

This is a type of highly quick to very quick debris flow.

H. Earthflow

Earthflow has the "hourglass" shape of earthflows as a defining feature. A bowl-shaped dip or runout from the slope material creates the slope's head. It typically happens in fine-grained materials or rocks that contain clay, on moderate slopes, and in saturated conditions. The flow itself is elongate. Granular material flows can, however, also occur dry.

I. Creep

The gradual, steady descent of slope-forming soil or rock is known as creep. Shear stress that is large enough to create permanent deformation but not enough to cause shear collapse is what causes movement. In general, there are three different kinds of creep: (1) seasonal, where movement occurs within the depth of the soil and is influenced by seasonal variations in soil moisture and soil temperature; (2) continuous, where shear stress continuously exceeds the material's strength; and (3) progressive, where slopes are approaching the point of failure along with other types of mass movements. Curved tree trunks, twisted fences or retaining walls, tilted poles or fences, and minor soil ripples or ridges are all signs of creep.

J. Lateral Spreads

Because they typically occur on flat terrain or relatively gentle slopes, lateral spreads stand out. With shear or tensile fractures, lateral extension is the predominant mechanism of movement. Liquefaction, the process by which saturated, loose, cohesionless sediments (often sands and silts) are changed from a solid to a liquefied condition, is what led to the failure. Failure can be purposely generated but is typically brought on by sudden ground motion, such as that encountered during an earthquake. The top units may fracture and extend, subside, translate, rotate, disintegrate, or liquefy and flow when cohesive material, such as bedrock or soil, rests on materials that liquefy.

Progressive lateral spreading typically occurs in fine-grained materials on shallow slopes.

It is essential to comprehend the type of landslide in order to evaluate its potential effects and create effective mitigation strategies. The type of landslide and the potential risk to infrastructure and human lives are determined by geotechnical engineers using a variety of approaches. The illustrations of various landslide types are displayed in Figure 3.4 below.

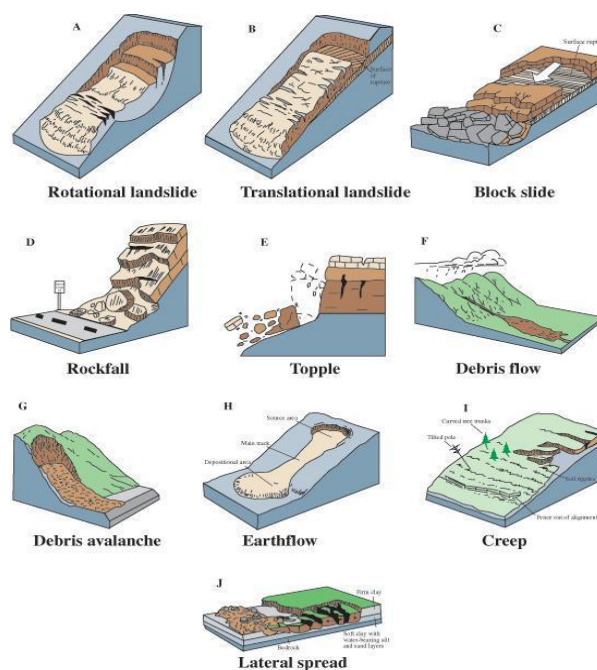


**Figure 3.3 Various Landslide Types**

(Source: U.S. Department of the Interior, 2004)

## 3.6 Slope Stability Analysis

### 3.6.1 Slope Stability Analysis Theory

Slope stability analysis is a procedure for assessing a slope's stability and safety in the face of potential failure brought on by forces acting on it. The analysis entails evaluating the soil's shear strength and calculating the factor of safety, or the ratio of driving forces to resisting forces on a potential slip surface. The driving forces include the soil's weight, water pressure, and any external loading, while the resisting forces are the soil's shear strength and any additional strengthening

measures. The analysis is based on different conditions such as slope angle, soil type, slope height, etc. factor of safety is expressed in Equation 3.11 below.

$$FS = \frac{\tau}{\tau_d} \quad (3.11)$$

where:

$\tau$  = Shear strength performed by soil

$\tau_d$  = Shear stress from collapsing soil weight

FS = Factor of safety

Typically, the acceptable estimation for factor of safety against soil shear strength is 1,2 - 1,5. Meanwhile, the relation between factor of safety number and slope condition is presented in Table 3.6 below.

**Table 3.5 Relation between Factor of Safety Number and Slope Condition**

factor of safety Number	Slope Condition
FS < 1,07	Unstable
1,07 < FS < 1,25	Critical
FS > 1,25	Stable

(Source: Bowles, 1984)

The most common method used by geotechnical engineers is the Limit Equilibrium Method (LEM) which assumes that soil mass is in equilibrium state, thus the factor of safety is determined directly through the comparison of resisting and driving forces. The other method is Finite Element Method (FEM) where the soil is simulated behaviorally through numerical modeling, to then compute the factor of safety. FEM is seen to be more accurate than LEM, however, it requires more computational processes and is thus less practical.

### 3.6.2 Fellenius Method

Slope stability analysis, which involves figuring out the factor of safety against slope failure, can also be done using the Ordinary Method of Slices or also known as Fellenius Method which was coined by Fellenius in 1936. The Fellenius method for analyzing slope stability is carried out by dividing the total of driving

force over the total of resisting force that are summed up from the slices of the slope on the upper end and the slip surface on the bottom.

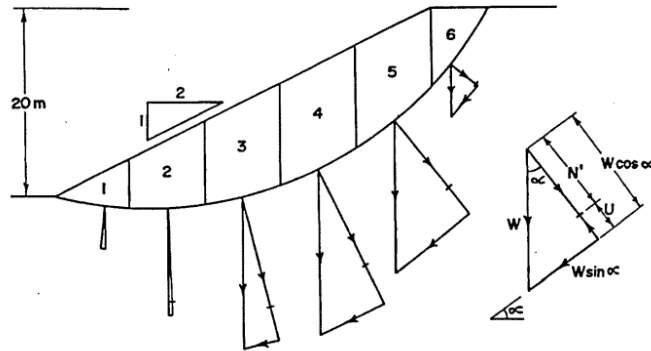


**Figure 3.4 Assumed Slice**

(Source: Styles & Yuen, 2009)

From the illustration above, the mathematical formula is presented in Equation 3.14 as follows.

$$FS = \frac{\sum_{i=1}^n (c\alpha + n_i \tan \varphi)}{\sum_{i=1}^n (W_i \sin \theta_i)} \quad (3.14)$$

Where :

- n = Number of slices
- c = Cohesion (kN/m<sup>2</sup>)
- α = Slip arc length (m)
- φ = Internal friction angle (°)
- W = Slice weight (kN/m)
- θ = Slip surface inclination (°)

### 3.7 Soil Nailing

Soil nailing process involves inserting steel bars (nails) into the ground and grouting them with cement or another type of grout to strengthen soil slopes, excavations, or retaining walls.

Soil nailing has several advantages as a soil retaining wall reinforcement. The first one is that soil nailing is the most cost-effective stabilizer compared to alternative methods like shotcrete, soil anchors, or ground improvement techniques.



The second one is its simple and rapid installation that only needs a small crew of employees and very little equipment. The third is how it is versatile to be used in a variety of soil types and situations. The fourth is how soil nailing causes little disruption to the surrounding area and can be utilized in locations with restricted access or where vibration or noise is prohibited. The last advantage is that soil nailing is sturdy, as it is composed of high-strength steel, which gives the retaining wall long-term sturdiness.

However, there are also several disadvantages to soil nailing. The first one is limited load capacity, and soil characteristics including soil type, cohesiveness, and angle of internal friction might affect how well they work. The second one is its weather-sensitivity, since the installation process for soil nails might be impacted by rain or other unfavorable weather conditions. The third one is design complexity, since a soil-nailed retaining wall's design can be intricate, and it calls for a high level of knowledge in both geotechnical engineering and soil mechanics. The fourth one is the need for routine maintenance to ensure their long-term performance. Lastly, soil nailing has limited aesthetic appeal, since they may not be visually appealing, and their design places more emphasis on functionality than aesthetics.

### **3.7.1 Soil Nailing Basic Elements**

Below are the elements needed for soil-nailing retaining walls.

#### **1. Nail Bar**

Nail bar in the form of threaded tendon is used for dirt nails. The threads may be cut into bare reinforcing bars or may form a continuous, spirally-deformed ribbing (continuous thread bars). To properly attach the bearing plate and nut, bars must have a minimum of 6 in. or 15,24 cm of threading on the cut face. The reduction in steel area in the threaded portion of the bar must be taken into account during design if threads are cut into a non-threaded bar. Normal tendon tensile strengths range from 60 ksi (Grade 60) to 75 ksi (Grade 75). Steel tendons of grade 60 or 75 should adhere to ASTM A615. There are various diameters ranging from 19 - 43 mm, with length up to 18 m. The specifics of these bar properties are presented in Table 3.7 and Table 3.8 below.

**Table 3.6 Properties of Grade 60 Solid-Threaded Bars**

Bar Designation	Maximum Diameter (w/ threads)	Minimum Cross-Sectional Area	Unit Weight	ASTM Grade	Yield Stress	Yield Load
Conventional	inch	inch <sup>2</sup>	lb/ft	Conventional	ksi	kip
#6	0.86	0.44	1.50	60	60	26
#7	0.99	0.60	2.04	60	60	36
#8	1.12	0.79	2.67	60	60	47
#9	1.26	1.00	3.40	60	60	60
#10	1.43	1.27	4.30	60	60	76
#11	1.61	1.56	5.31	60	60	93
#14	1.86	2.25	7.65	60	60	135

(Source: Dywidag, Williams and Contech in US Federal Highway Administration, 2015)

**Table 3.7 Properties of Grade 75 Solid-Threaded Bars**

Bar Designation	Maximum Diameter (w/ threads)	Minimum Cross-Sectional Area	Unit Weight	ASTM Grade	Yield Stress	Yield Load
Conventional	inch	inch <sup>2</sup>	lb/ft	Conventional	ksi	kip
#6	0.86	0.44	1.50	75	75	33
#7	0.99	0.60	2.04	75	75	45
#8	1.12	0.79	2.67	75	75	59
#9	1.26	1.00	3.40	75	75	75
#10	1.43	1.27	4.30	75	75	95
#11	1.61	1.56	5.31	75	75	117
#14	1.86	2.25	7.65	75	75	168

(Source: Dywidag, Williams and Contech in US Federal Highway Administration, 2015)

According to US Federal Highway Administration (2015), lower diameter bars below No.8 are frequently avoided because they may tend to bend significantly when handled and installed, and because they may cause the spacing of the nails to be too close and ineffective. The maximum tensile load of bars No. 14 and bigger may not be effective due to geotechnical pullout and facing strength limitations.

## 2. Nail Head

The portion of the steel that sticks out from the wall's cross section or view is known as the nail head. A bearing or retaining plate, hex nut, washer or ring composed of rubber or metal, and headed stud make up this component. The

nuts and washers that are utilized must have the same melting strength as the steel bars, and bearing plates are typically square with sides lengths of 200-250 mm, 19 mm thick, and 250 MPa yield strength (ASTM A36).

3. Grout

To cover the gap between the steel bars and the surrounding earth, grout is employed. The most popular kind of grout used in soil nailing retaining walls is cementitious grout. The grout mix may contain cement Types I, II, III, V, or Type I/II that complies with AASHTO M85/ASTM C150. For the majority of applications, Type I (common or general purpose) cement is advised.

4. Geotextile fabric

By keeping the soil from eroding and enhancing the stability of the retaining wall overall, geotextile fabric can be used to separate the soil from the grout.

5. Reinforcing Mesh

The soil can be further reinforced by using reinforcing mesh or fabric. Usually, steel or high-strength synthetic fibers are used to create the mesh or fabric.

6. Centralizer

Each solid bar has centralizers fitted at various points along its length to guarantee that the tendon is entirely covered by a minimum layer of grout. They are positioned at regular intervals, not more than 10 feet or 3 m apart down the length of the nail and roughly 1.5 feet or 0,5 m apart from each end. In order to position the tendon within an inch of the drill hole's center, introduce a tremie pipe to the bottom of the hole, and allow grout to freely flow up the drill hole, centralizers must be securely fastened to the tendons.

7. Wall Facing

At the excavation face or slope surface, tendon connections to a facing system are made. The two types of facings that are most frequently used are an initial facing made of shotcrete and a final facing made of CIP or shotcrete. The initial facing serves to establish initial connection between nails, support the exposed soil between them during nail installation, and give protection against soil erosion and sloughing at the excavation face. The final face serves the same purposes as the original facing and offers the chance to satisfy the project's

aesthetic needs. Long-term corrosion and climate changes must be taken into account in the final facing design as needed.

To add stability and support, shotcrete is a type of concrete that is sprayed onto the soil's surface. It can be used in conjunction with soil nailing to increase the retaining wall's strength and durability. Shotcrete is pneumatically blasted onto the exposed soil surface as it shoots out of the feed hose at a high rate of speed. Mortar or small-aggregate concrete must be used for shotcrete. The concrete is solidified as a result of the material's impact energy. Both wet and dry application methods are available for shotcrete. The installation of wall facing, specifically shotcrete, can be seen in Figure 3.8 below.



**Figure 3.5 Shotcrete Installation**

#### 8. Drainage System

Vertical geocomposite strip drains, also known as strip drains, are put behind the first facing and along the excavation face to prevent water pressure buildup behind the wall. A drainage core and a filtration geotextile are the two main components of geocomposite strip drains. The strip drains are equipped with drainage components that enable water to depart the strips and reach the exterior of the wall. Additionally, strip drains can be configured to drain into a pipe drain that runs along the base of the wall or through weepholes that discharge through the facing and to the toe of the wall. A snap-on cap or grate and an exit PVC pipe connected to the underdrain system make up the majority

of PVC drainage elements. The underdrain system typically consists of a drainage pipe embedded in a trench filled with gravel that runs parallel to the excavation's bottom. An example of a drainage system for a soil nailed retaining wall is displayed in Figure 3.9.



**Figure 3.6 Drainage System**

(Source: Schnabel Engineering in US Federal Highway Administration, 2015)

#### 9. Coupler or Connector

Connectors come in the forms of bearing plates, beveled washers, hexagonal nuts, washers, and headed studs are the steel parts that join soil nails to the facing. The headed studs link the nail end to the final face, while the bearing plate, hex nuts, and washers connect the nail to the initial facing. The bearing plate's function is to disperse the force imparted at the nail end onto the initial face of shotcrete and the soil behind the facing.

### 3.7.2 Soil Nailing Construction

Construction steps of soil nailing are explained in the following points.

#### 1. Soil Excavation

Surface water controls should be constructed along the top of the wall prior to any excavation to stop surface water from flowing into the excavation. If this happens, construction will be negatively impacted and the excavated face will become unstable. Surface water is captured and directed via collector tunnels

behind the excavation's perimeter. The final trimming of the excavation face can be done with a backhoe or excavator from this platform after performing soil excavation with conventional mass excavation or earth-moving equipment. Initially, the cut is frequently 0,9 to 1,55 m high. To avoid using too much shotcrete, the excavated face profile should be moderately smooth and not too irregular. The lowest margins of safety may occur for the lower excavation lifts when the open cut is momentarily unsupported, or before nails and shotcrete are applied at these levels. During construction, it's crucial to keep an eye out for early indications of instability, such as bulging, sloughing, and excessive deformation of the exposed soil face. It is crucial to backfill the exposed face with a temporary berm right once if early indications of wall instability are seen. The length of an excavation that can be stabilized and covered with shotcrete in a single working shift should be the maximum exposed length. Excavation step is presented in Figure 3.10 below.



**Figure 3.7 Soil Excavation**

## 2. Nail Holes Drilling

Nail holes drilling can be done using several methods such as rotary, auger, percussion, and rotary-percussion drilling. In many cases, uncased auger equipment is utilized as it is more efficient and less expensive. However, the use of cased auger is more recommended for drilling bigger nail diameters into unstable bodies of soil to prevent collapse. Nail holes drilling step is shown in Figure 3.11 below.



**Figure 3.8 Nail Holes Drilling**

(Source: US Federal Highway Administration, 2015)

### 3. Nail Bar Installation and Grouting

A tremie pipe is used to fill the drill hole with grout once the tendon has been placed into it. The grout pipe is put into the drill hole's bottom, and grout is pumped through it until the hole is filled. The grout adheres to the tendon and the surrounding soil as it hardens. Gravity grouting offers bond strengths that are frequently enough to make soil nailing practical and affordable. Higher bond strengths might be needed in instances of poor soil conditions, nevertheless, to maintain reasonable soil nail lengths. The construction process is illustrated in Figure 3.12 below.



**Figure 3.9 Nail Bar Installation**

(Source: Schnabel Engineering in US Federal Highway Administration, 2015)

### 4. Strip Drain Installation

Strip drains are positioned with the geotextile filter side facing the ground and against the excavation face. Shotcrete must be placed to each lift before being rolled down to provide a continuous surface if the strip drain is packaged in rolls. If the strip drains are of the panel variety, they must be joined at the base

of each excavation lift and typically need a minimum 30,48 cm. overlap between the core and the geotextile filter to ensure that the water flow and filtering are not hampered. The strip drains are connected to the bottom drainage cap and exit pipe, which are fastened to the facing's reinforcing steel. To stop shotcrete from seeping into the system during shotcrete placement, the exit pipe must be sufficiently covered. If necessary, the exit pipe can be linked to the underdrain system once the shotcrete procedure is finished.

#### 5. Initial Wall Facing Installation

Shotcrete is used to create the first facing for soil nail wall installations, with a thickness that is typically between 7,5 to 10,2 cm. Wet mix and dry mix shotcrete techniques are both used. The aggregate and cement are mixed dry and fed into the shotcrete gun while the mix water is added at the nozzle in the dry mix method. Admixtures can be inserted at the mix plant or with the water, depending on their characteristics. Accelerators are the most popular admixtures used in shotcrete construction on vertical surfaces. The flexibility of the shotcrete can be altered at the nozzle, if necessary, by adding water there. In the wet mix method, the cement, water, admixtures, and aggregate are combined in a batch plant before being pumped to the nozzle. When using the wet method, compressed air is used to apply the plastic mix at a faster rate than when using the dry method. Cement content or ratio and in situ density are some of the most integral factors that determine shotcrete quality and durability. Cement content impacts the ease of pumping and shooting, while in situ density of the mixture is affected by air level entering the mixture and simply put, more air means lower strength.

Welded wire mesh is frequently used as initial facing reinforcement. On rare occasions, final facing may also be done with it. The wire mesh cross-sectional area and mesh opening are chosen to satisfy structural criteria such as punching and flexural shear capacities as well as constructability restrictions. The chosen welded wire mesh panel needs to be at least one full mesh cell wider than the excavated lift height (which is comparable to the vertical nail spacing). As part



of the soil nail wall design, the welded wire mesh wire diameter and mesh aperture dimensions are examined. Around nail heads, extra reinforcement such as walers and vertical bars is positioned to increase flexural resistance. Typically, two horizontal walers and two vertical bars—one on either side of the nail—are inserted. Figure 3.13 displays the shotcrete reinforcement.



**Figure 3.10 Shotcrete Reinforcement**

(Source: Ryan R. Berg & Associates, Inc. in US Federal Highway Administration, 2015)

#### 6. Construction of Subsequent Levels

In this part, step number 1 to 4 is repeated until the lowest level. At the lowest excavation the collecting toe drain becomes the anchor for the geo-composite.

#### 7. Permanent Wall Facing Installation

A reinforced shotcrete final face typically has a total thickness between 15,24 cm to 30,48 cm, omitting the thickness of the first facing. To join the final facing to the earth nails, headed studs that were welded to the bearing plates are employed. Shotcrete is applied in successive layers to achieve the final facing's thickness. Usually, but not always, the deepest lift of the initial facing is finished before the final facing is applied, and it is advanced in stages from the bottom up. The entire final facing thickness can also be built as excavation proceeds, but care must be given to sustain the face's heavy weight during successive excavation lifts properly. Using welded wire mesh or rebar, the shotcrete facing is reinforced.

### 3.7.3 Slope Stability Analysis with Soil Nailing Reinforcement

Internal and external forces affect soil retaining wall performance, and thus, it is of highest importance to design stable and safe walls. With that being said, there are two analyses of wall stability, which are internal stability and external stability, as is displayed in Figure 3.14 below.

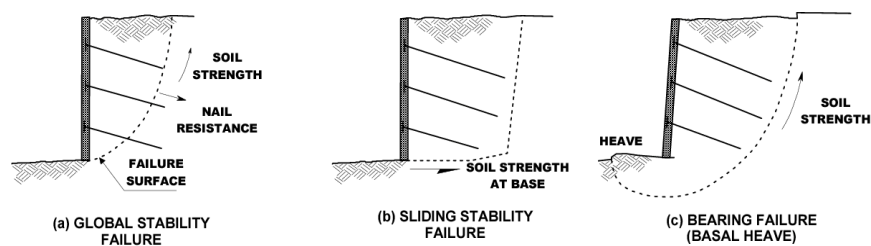


FIGURE 1: EXTERNAL FAILURE MODES

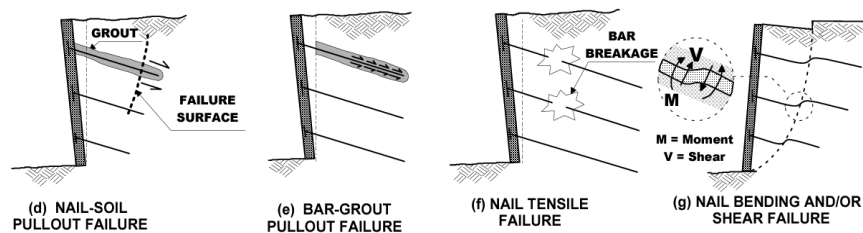


FIGURE 2: INTERNAL FAILURE MODES

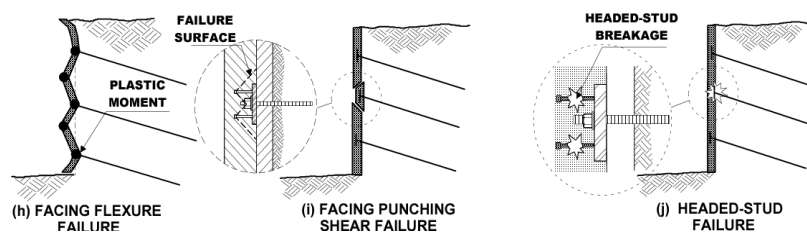


Figure 3.11 External Failure Modes

(Source: Lazarte et al., 2012)

#### 1. External Stability Analysis

External stability analysis is done to determine the safety factor against slope collapse from external forces.

##### a. Global Stability Failure Safety Factor

In determining the safety value against global collapse, an analysis of global slope failure is carried out. The method of wedge with planar slip plane is

utilized in this calculation. The working forces are as shown in Figure 3.15 below.

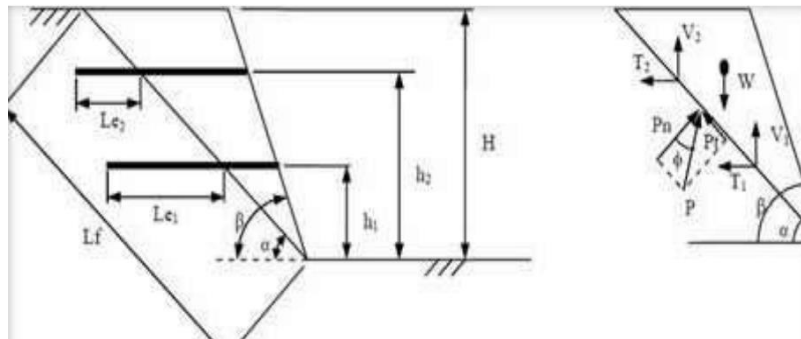


**Figure 3.12 Working Forces in Wedge Method**

(Source: Juran & Elias, 1999)

According to Figure 3.15, the analysis using wedge method is done through Equation 3.15 and 3.16 as follows.

$$\sum T_i - P_n \sin \alpha + P_t \cos \alpha = 0 \quad (3.15)$$

$$W - P_n \cos \alpha - P_t \sin \alpha - \sum v_i = 0 \quad (3.16)$$

The shear safety factor can be calculated using formula as shown in Equation 3.17.

$$FS = \frac{c \cdot L_f + W \cos \alpha \cdot \tan \phi + (\sum T_i \sin(\alpha + i) - \sum V_i \cos(\alpha + i)) \tan \phi}{W \sin \alpha - \sum T_i \cos(\alpha + i) - \sum V_i \sin(\alpha + i)} \quad (3.17)$$

Where:

FS = Factor of safety,

c = Soil cohesion (kN/m<sup>2</sup>),

$\phi$  = Soil internal friction angle (°),

$\alpha$  = Slip surface angle against horizontal line,

W = Soil slice weight number-n (kN/m),

Q = Dead weight on top of the slope (kN/m),

L<sub>f</sub> = Circle length at slice number-n (m),

L<sub>e</sub> = Nail bar length behind slip surface (m),

B = Slope angle (°),

i = Nail installation inclination angle (°),

$\sum T_i$  = Amount of resisting forces against driving forces (kN/m), and

$\sum V_i$  = Amount of shear force supporting forces (kN/m).

## 1) Global shear force and allowable tensile force

The nail bar shear force and tensile force to calculate slope stability against global reinforcement, which is calculated through Equation 3.18 and 3.19.

$$V = \frac{R_n}{2\sqrt{1+4\tan^2(90^\circ-\alpha)}} \quad (3.18)$$

$$T = 4V \tan(90^\circ - \alpha) \quad (3.19)$$

Where:

V = Nail bar allowable shear force

T = Nail bar tensile force

R<sub>n</sub> = Nail bar pulling supporting forces

Soil allowable shear force is calculated using Equation 3.20 as follows.

$$V = P_{max} = \frac{D}{2} L_o \quad (3.20)$$

Where:

V = Soil passive allowable shear forces

D = Nail bar + grouting diameter

L<sub>o</sub> =  $\sqrt[4]{\frac{4Ei}{K_s D}}$  = Distribution length

E<sub>i</sub> = Nail bar stiffness, with nail bar without grouting, and

K<sub>s</sub> = Soil lateral reaction modulus

The soil lateral reaction modulus K<sub>s</sub> is obtained based on Table 3.9 below.

**Table 3.8 Soil Lateral Reaction Modulus**

Soil Type	K <sub>s</sub> (kN/m <sup>3</sup> )
Loose sand	4800 – 16000
Medium dense sand	9600 – 80000
Dense sand	64000 – 80000
Clayey medium dense sand	32000 – 80000
Silty medium dense sand	24000 – 48000
Clayey soil:	
q <sub>a</sub> ≤ 200 kPa	12000 – 24000
200 kPa < q <sub>a</sub> ≤ 800 kPa	24000 – 48000
q <sub>a</sub> > 800 kPa	> 48000

(source: Bowles, 1996)

Meanwhile, the coefficients  $c_1$ ,  $c_2$ , and  $c_3$  can be obtained from the following Figure 3.13.

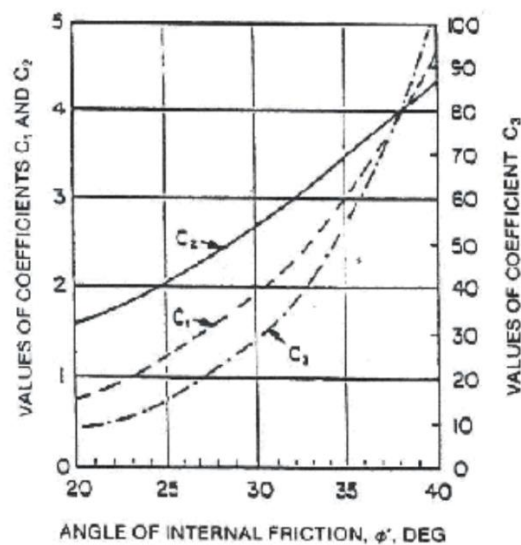


**Figure 3.13 Correlation Graphic for API Sandy Soil**

(Source: API, 1987)

After obtaining the smallest allowable shear force between the nail bar and the soil, there should be a limitation put into the allowable tensile force of the nail bar, which is determined from Equation 3.21 below.

$$\frac{V_{max}^2}{RC^2} + \frac{T_{max}^2}{RC^2} = 1 \quad (3.21)$$

Where:

$V_{max}$  = Global allowable shear force

$T_{max}$  = Global allowable tensile force

$Rc = \frac{Rn}{2}$  = Nail bar shear supporting forces

## 2) Soil nailing reinforcement allowable tensile force

The maximum allowable force for the tensile force is chosen to be applied, and if that value is less than the global acceptable force, the global allowable force is applied instead. The tensile force can be determined from Equation 3.22 as follows.

$$T_i = \frac{\pi D L e f_{max}}{Fos} \quad (3.22)$$

Shear supporting force  $F_{max}$  applies to soil and nail bar surface connection. It is better to do field testing to obtain the value. The typical value of  $f_{max}$  for sandy soils can be seen in Table 3.10 below.

**Table 3.9 Soil Nailing Shear Bearing Capacity for Sandy Soils**

Soil Type	$\tau$ (kN/m <sup>3</sup> )
Silty clay	35 – 50
Clayey silt	90 – 140
Loess	25 – 75
Soft clay	20 – 30
Stiff clay	40 – 60
Stiff clayey silt	40 – 100
Calcareous sandy clay	90 – 140

(source: Elias and Juran, 1991)

b. Shear Analysis

This analysis is key in figuring out the factor of safety for slope reinforcement against soil shear failure, the consideration used in the calculation is the weight of reinforcement alone. The analysis is presented in equation 3.23.

$$FS = \frac{cb \times BL + (W + Q + PAx \sin \delta) \tan \phi}{PA \cos \delta} \quad (3.23)$$

The calculations for active lateral pressure are displayed in Equation 3.24 and 3.25 as follows.

$$PA = \frac{CH12}{2} \cdot Ka \quad (3.24)$$

$$Ka = tg^2(45^\circ - \frac{\phi}{2}) \quad (3.25)$$

Where:

- FS = Factor of Safety
- Cb = Soil cohesion (kN/m)
- BL = Structure width (m)
- W = Soil slice weight (kN/m)
- Q = Dead weight atop slope (kN/m)
- $\phi$  = Soil internal friction angle (o )
- H = Soil wall height (m)
- $\gamma$  = Soil content structure (kN/m)

$\delta$  = Friction angle between foundation soil and structural base (with the assumption of very rough concrete foundation  $\text{tg } \delta = \text{tg } \varphi$ )

## 2. Internal Stability Analysis

This analysis is carried out to determine the factor of safety for slope reinforcement of soil nailing against internal factors such as reinforcement measures, including reinforcement strength and the possibility of the reinforcement being cut or pulled out.

### a. Analysis of cut reinforcing bar

The ratio between reinforcing bar distance from each other and soil pressure that will be received by rebar is calculated in this analysis.

The calculation is carried out through Equation 3.26 and 3.27 below.

$$Fr = \frac{0,25 \times \pi \times d^2 \times fy}{1000 \times \sigma_h \cdot Sv \cdot Sh} \quad (3.26)$$

$$\sigma_h = Ka \gamma z \quad (3.27)$$

Where:

Fr = Factor of Safety against cut reinforcing bar

Sv = Vertical rebar distance (m),

Sh = Horizontal rebar distance (m),

fy = Steel tensile supporting force (MPa),

d = Rebar diameter (mm),

$\sigma_h$  = Horizontal soil pressure at analyzed depth (kN/m<sup>2</sup>),

$\gamma$  = Soil content weight (kN/m),

z = Analyzed soil depth (m),

Ka = Lateral active pressure coefficient for Equation 3.24

### b. Analysis of plugged reinforcing bar

This analysis is done to determine the strength of rebar from plugging forces. It is integral to ensure that no structure failure occurs due to such forces by undermining rebar length, for example.

The calculation is carried out using Equation 3.28.

$$Fp = \frac{\pi qu D dh Lp}{\sigma_h \cdot Sv \cdot Sh} \quad (3.28)$$

Where:

$F_p$	= Factor of Safety against pulled out reinforcing bar
$S_v$	= Vertical rebar distance (m),
$q_u$	= ultimate bond strength (kN/m <sup>2</sup> ),
$\sigma_h$	= Horizontal soil pressure at analyzed depth (kN/m <sup>2</sup> ),
$L_p$	= Rebar length at passive zone (m),
$\phi$	= Soil internal friction angle (°),
$D_{dh}$	= Bore hole diameter (m)

### 3.8 Slope Stability Analysis Using PLAXIS V20 Program

A finite element analysis program specifically made for geotechnical engineering applications is called PLAXIS V20. It is employed to examine how soil and rock structures respond to various loading scenarios. Numerous geotechnical issues, such as foundation design, excavation support, tunneling, embankments, and slope stability analysis, can be simulated using the software. In addition to comprehensive modeling features for complicated soil and rock behavior, such as consolidation analysis, dynamic analysis, and soil-structure interaction, PLAXIS V20 has a user-friendly interface. The program is a common choice for both academic and business applications, and it is widely utilized in the geotechnical engineering sector. Bentley Systems, a leader in software for infrastructure design, building, and operations, created and sells PLAXIS V20.

A feature to use in PLAXIS V20 for slope stability analysis is the phi/c reduction method, in which the factor  $\sum M_{sf}$  is utilized to define the reduction of soil materials strength until two conditions occur; the first one is if the stable value of  $\sum M_{sf}$  condition has reached failure, the second one is if the number of calculation steps has maxed out. A change in excess pore pressures in the model could result from a drop in strength if a project has one or more material sets designated as Undrained A or Undrained B. By choosing the "Ignore undrained behaviour" option during the Safety analysis phase, this shift in excess pore pressures can be avoided. In this scenario, the extra pore pressures that were already



present at the start of the safety analysis phase will persist and won't alter during the Safety analysis. In this case, there are two aspects to consider, as follows.

1. For embankments and other loading problems, considering the excess pore pressures change more often results in an increase of excess pore pressures, which means lower factor of safety compared to if no change is considered.
2. For excavations and other unloading problems, considering the excess pore pressures change more often results in a decrease of excess pore pressures and sometimes even suction or pore tensions. This means a higher factor of safety compared to if no change is considered.

Based on the considerations above, the “Ignore undrained behavior” option could be utilized or ignored as long as the lowest factor of safety is achieved. Another viewpoint points out that excess pore pressures should never be changed since the factor of safety should always be determined from a particular circumstance with a fixed excess pore pressure. In other words, the safety factor should be assessed from a segmental scenario during the design and analysis processes, and as a result, the excess pore pressures from the project analysis should be maintained throughout the safety analysis.

## **CHAPTER IV**

### **METHODOLOGY**

#### **4.1 Research Method**

The research methodology applied in this final project is quantitative research. The research will investigate the occurrence of the specified condition through quantitative data collection and analyzing the data using engineering approaches. The method is the Finite Element Method (FEM) as the method employed by PLAXIS V20, as well as manual calculation using Fellenius Method for non-reinforced slope and Wedge Method for reinforced slope. The equipment used in this project includes Ms. Excel, PLAXIS V20, and AutoCAD. The modeling is carried out with modifications on nail vertical spacing, nail length, and nail inclination compared to the current retaining wall design. The research utilizes the material model of Mohr-Coulomb, as this model is the initial approach for all types of soil. This model displays the failure point. Soil parameters are obtained from the soil data compiled before and during the construction project, and should there be incomplete data, there will be assumed values and approximation according to the existing soil data. The parameter variations will yield stress-strain relations at the STA, as well as the graph of FS value. The FS value is obtained from the last analysis results run by PLAXIS at each new parameter of the nail features.

#### **4.2 Research Location**

Research location is in Nglegi, Gunung Kidul, Daerah Istimewa Yogyakarta, displayed below as Figure 4.1.

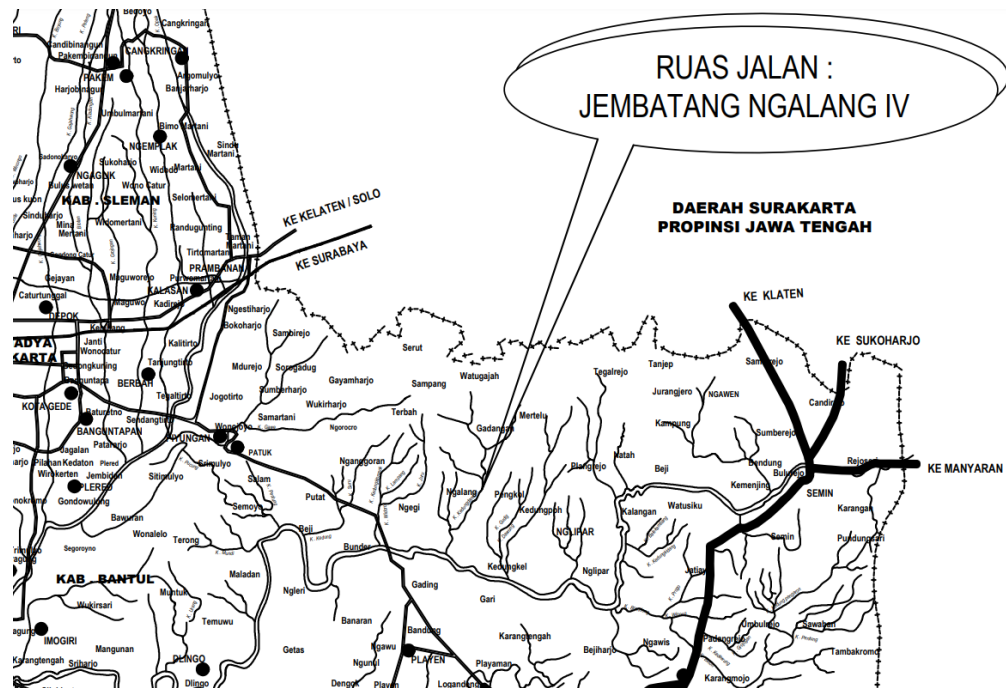


**Figure 4.1 Research Location**

(Source: Dinas Pekerjaan Umum, Perumahan dan Energi Sumber Daya Mineral Daerah Istimewa Yogyakarta, 2022)

### 4.3 Data Collection

In this final project research, the data is obtained from the Tawang-Ngalang Segment IV Road and Bridge Project. The data collection is carried out in steps as follows:

#### 1. Secondary Data

Secondary data includes technical drawings of STA 7+300 of Tawang-Ngalang Segment IV Road and Bridge Project, soil profile data of STA 7+300 of Tawang-Ngalang Segment IV Road and Bridge Project, soil investigation data using standard penetration test method (SPT), laboratory data of soil investigation.

#### 2. Observation

Observation is an integral part of a research project. The objective is to obtain legitimate data of condition of the analyzed object.

#### 4.4 Research Stages

There are several stages that must be completed before obtaining the desired results, and so the stages of this research are as such.

1. Literature Review is a critical assessment and study of the scholarly literature and current research on a particular subject. It entails searching material, reading it, and combining it from a range of resources, including academic journals, books, and other works. A literature review's objectives are to present a thorough grasp of the current state of knowledge on a particular subject, to spot any gaps or contradictions in the literature, and to offer recommendations for further research. Research projects, dissertations, and academic articles frequently include literature reviews.

In this final project, the literature review spans across ten years and includes eight independent researches of similar themes and objectives, five of which were carried out by Indonesian researchers, and the last three coming from international researchers. All of the researchers aim to determine the factor of safety (FS) of existing soil nailed retaining walls, which are then redesigned, modeled, compared, and calculated according to different formulas to ultimately achieve the optimum FS value. Common processes involved in the previous researches were employing Limit Equilibrium Method (LEM) through GEOSLOPE and Finite Element Method (FEM) through PLAXIS, and then to achieve more legitimate results, manual calculations were carried out. The variation of the wall feature typically revolves around slope inclination, wall height, wall inclination, as well as nail length, diameter, vertical spacing, and angle. The past researches serve as the guideline of variables to be considered, approach to take, the extent of steps needed, and the standards of results for this final project, which takes a specific study case.

2. Data Collection is a stage carried out to support the research analysis which includes collecting primary and secondary data.
3. Modeling the existing slope, design slope, current slope reinforcement, and proposed slope reinforcement design.

4. Calculation of factor of safety (FS) through Finite Element Method (FEM) using the PLAXIS program.
5. Analysis of the results obtained from calculation and modeling.
6. Conclusion and Suggestion.

#### 4.5 Proposed Soil Nailing Reinforced Design Slope

The proposed design focuses on several variables. The first one is non-loaded and loaded condition, with the loading consisting of building and traffic loads. The next variable is non-reinforced and reinforced, with soil nailing as the method of reinforcement. Lastly, the variable is static and dynamic condition, where earthquake loading will be applied to each model to see the changes in FS. The illustration of the proposed design models is as seen in Figure 4.2 below.

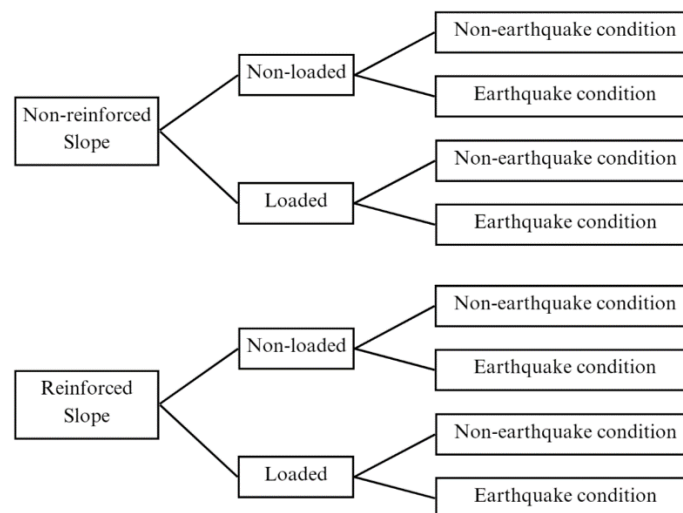


**Figure 4.2 Proposed Design Scheme**

Then, the details of the variables are as follows.

##### 4.5.1 Modelling Variation

In this research, the proposed soil nailing reinforced design slope modeling in PLAXIS V20 has several features. Based on the preceding research and considerations of slope condition, there are three main variables of proposed changes to the soil nail reinforcement for STA 7+300. The first one is the nail inclination tried at 20° and 50°, having 15° interval from the current 35° with the

understanding that across the research in former chapter, around  $5^\circ$  interval holds no effect on the factor of safety. The second one is the decrease in vertical spacing of 1,5 meters from the current 2,5 meters, as in the precedent, its effect towards the factor of safety varied. The third is the nail length which will be modeled and analyzed at 4,5 meters to understand the effect compared to the current 5 meters length, as shorter nails are more cost effective with minimal effect on the factor of safety. All other factors such as slope inclination, slope height, and nail material are maintained. The method for analysis is Finite Element Method (FEM) for its main usage in the PLAXIS program. All in all, there are 8 modeling combinations based on the three variables.

The illustration of the modelling variation is as seen in Figure 4.3.

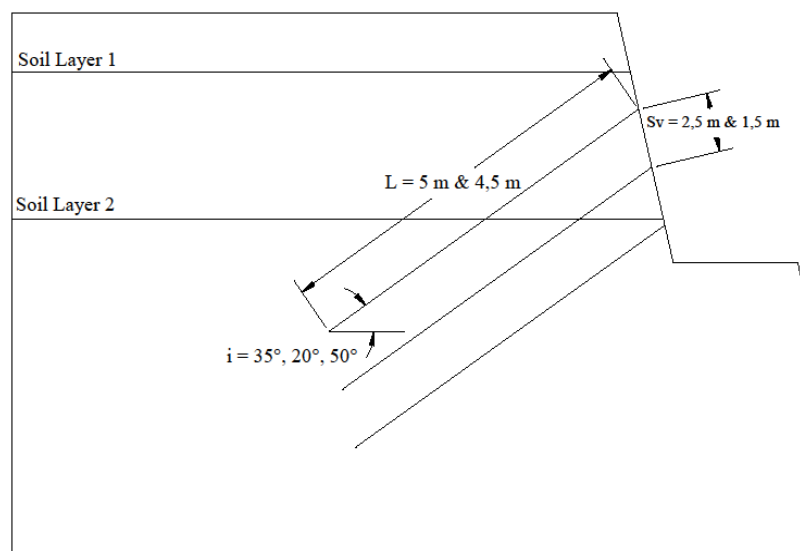


**Figure 4.3 Modelling Variation**

#### 4.5.2 Loading Variation

Meanwhile, the loading variation for the models in PLAXIS V20 is as follows.

##### 1. Internal Load

The loading for this research is applied in vertical and horizontal directions. The considerations include soil weight, cohesion, material makeup, angle of internal friction, and so on. The main takeaway is to understand the slope angle

and how the internal load affects stability when faced with a slip surface. As it happens, the STA 7+300 went through slope failure despite being reinforced already. The data for internal loading is obtained from site observation and testing by PT. Geomine Bara Studio in their soil investigation report. In PLAXIS V20, loading input will be done in relation to load combination, weight, slope geometry, pore pressure, etc.

## 2. Traffic Load

This type of loading is considered for geotechnical analysis not only for the safety of the structure, but also for the amount of investment. The values for traffic loading are different regionally based on the experience and design practice of the particular region. Some examples would be 12 kPa of applied traffic load in the USA, 20 kPa for China, and 10 kPa for initial construction in Australia. The assumption for modeling is that the value of traffic loading is applied uniformly across the road portion to ensure the stability of the surrounding structure is sound. The traffic loading that is considered in this study is based on the standards by Dinas Pekerjaan Umum for traffic loading of road body, which is 15 kN/m<sup>2</sup> for road class I, with the classification below.

**Tabel 5-6** Beban Lalu Lintas untuk Analisis Stabilitas

<b>Kelas Jalan</b>	<b>Beban Lalu Lintas (kPa)</b>
I	15
II	12
III	12

**Figure 4.4** Traffic Loading for Stability Analysis

(Source: Departemen Perumahan dan Prasarana Wilayah, 2002)

Then, the dynamic loading variation for PLAXIS V20 modeling is as follows.

### 1. Without Earthquake

The dynamic analysis is done using dynamic multipliers, either in structures or stage construction mode. The reference value for load dynamic components is needed, and the dynamic components are time-dependent, able to show the rate of deformation at the initial stage of slope reinforcement versus around 10 years of being in use. This is not considering the earthquake loading factor, which means the analysis depends on the loading configuration that affects the slope dynamically, be it through vibration of an equipment or others.

### 2. With Earthquake

According to the research by Jacob and Venkataramana (2020), through PLAXIS modeling it is determined that 0,2 g difference of earthquake loading can have roughly 20% - 40% impact on the factor of safety of a slope depending on the initial height of the slope and the ratio of vertical to horizontal sides. This proves true across three slope heights of 3, 6, and 9 meters. Meanwhile, Sari (2016) conducted an onsite observation to identify ground vibration acceleration in earthquake conditions for Gunung Kidul region which amounts to 232,6 - 361,1 cm/s<sup>2</sup> or 0,2 g - 0,4 g. Below is the Bina Marga earthquake zonation map for Gunung Kidul, showing that the region is within the 0,3 to 0,4 g of Peak Ground Acceleration (PGA).

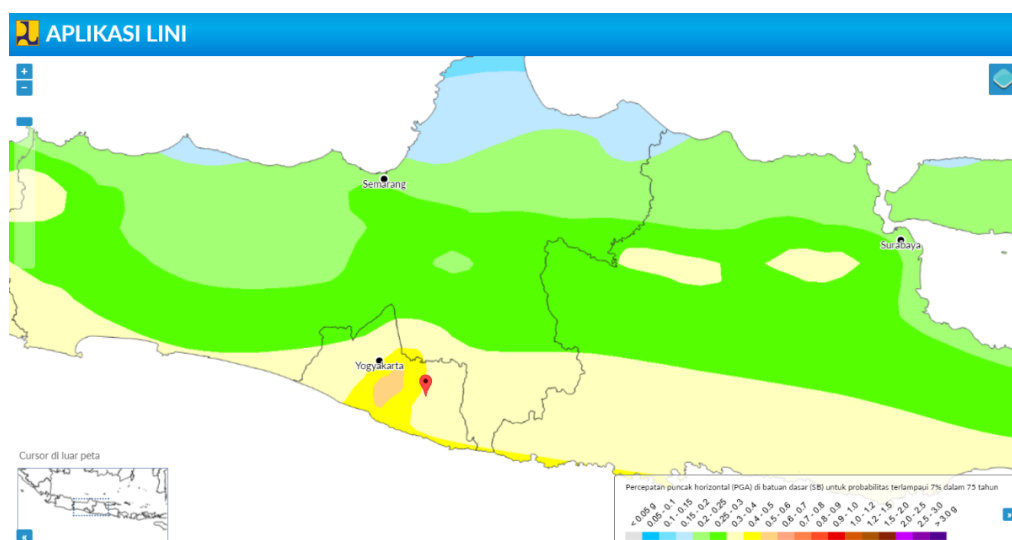


**Figure 4.5 Earthquake Ground Acceleration Map for Gunung Kidul**

(Source: Bina Marga, 2022)

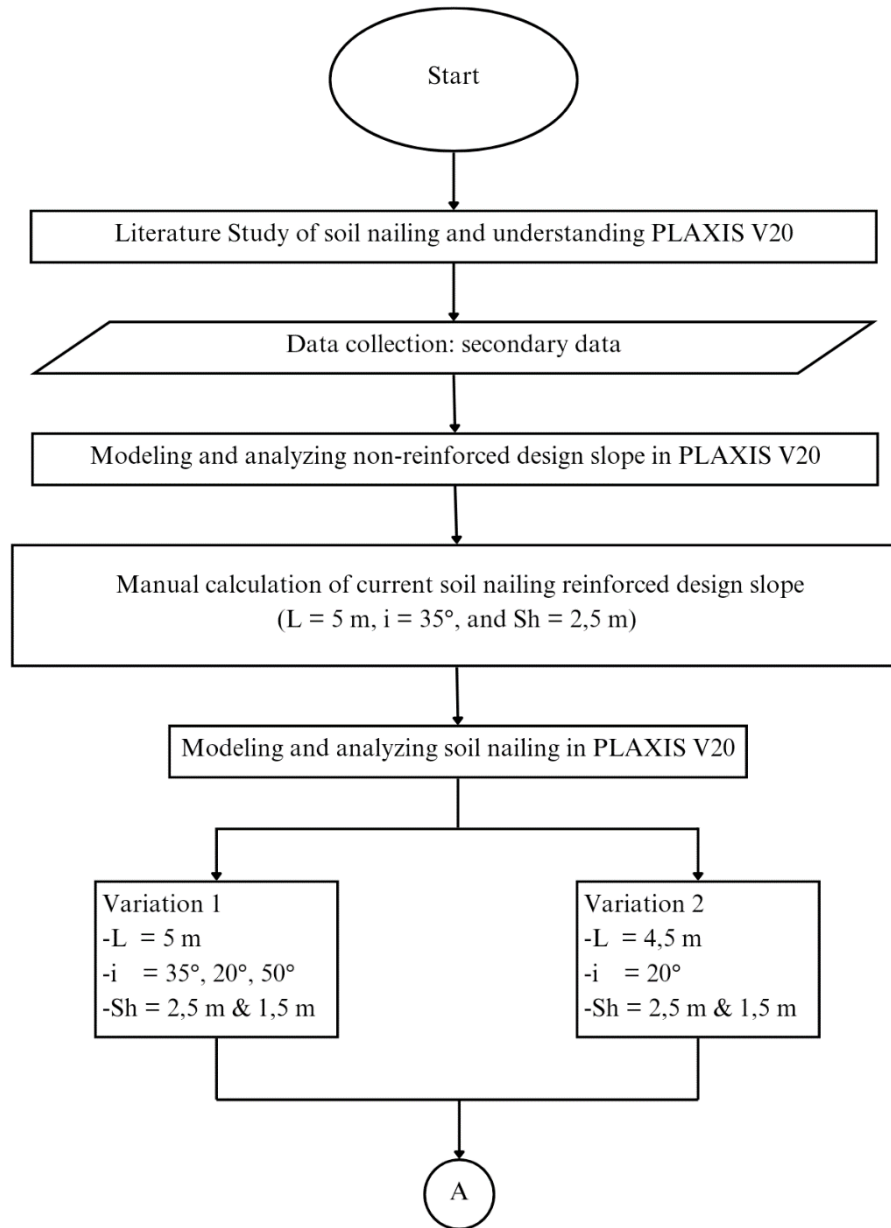


Based on SNI 8460:2017, Article 12.2.5 on *Persyaratan gempa untuk dinding penahan*, point b of Mononabe-Okabe approach with soil cohesion consideration subpoint 3, it is said that 50% reduction from horizontal seismic coefficient can be applied to the calculation. In this research, the earthquake load modelling is carried out using static equivalent, in which  $\pm 0,2$  g will be considered for calculation, deriving from the PGA of 0,4 g from the sources above, with 50% reduction due to earthquake loading impact that spreads and lessen from bed rock to the soil retaining wall atop the soil body.

#### **4.6 Flowchart**

A flowchart for research is a graphic representation of a procedure, system, or algorithm. The process phases and decisions that must be made at each step are represented by standardized symbols. A process or system can be managed, designed, documented, or analyzed using flowcharts, which can also be used to explain it to others. They give the steps in a process a clear and succinct representation, making it simpler to grasp and follow. In many different industries, including engineering, computer programming, business, and education, flowcharts are frequently utilized.

In this final project the flowchart is as follows.



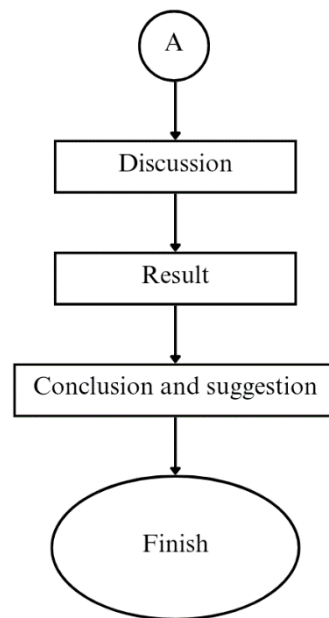


**Figure 4.6 Final Project Research Flowchart**

## CHAPTER V

### ANALYSIS AND DISCUSSION

#### 5.1 Prerequisite Data

The prerequisites pertain to input parameters that are obtained from typical parameters of soil according to soil profile on project site, and then back analysis is carried out. There are two main parameters being considered in this step onward for the non-reinforced as well as reinforced slope analysis and modelling; the first one being soil parameters, and the second one being building load on top of the slope. Below are the details of the parameters.

##### 1. Soil Parameters Data

Soil parameters data utilized in this analysis is based on project site soil profile.

The recapitulation of the input parameters can be seen in Table 5.1 below.

**Table 5.1 Existing Slope Material Input Data**

Soil Layers (from the top)	Soil Properties				Shear Parameter		Elastic Parameter
	Soil Model	Material Type	Wet Volume Weight ( $\gamma_w$ )	Dry Volume Weight ( $\gamma_d$ )	c	$\theta$	E
			(kN/m <sup>3</sup> )	(kN/m <sup>3</sup> )	(kN/m <sup>2</sup> )	°	(kN/m <sup>2</sup> )
Soft Clay (0 – 0,77) m	Mohr-Coulomb	Drained	16,66	12,18	6	1	255
Hard Clay (0,77 – 2,67) m	Mohr-Coulomb	Drained	20,41	14,88	11	6	603
Claystone (2,67 – 7,89) m	Mohr-Coulomb	Drained	26,65	19,65	100	30	4636
Lapilli (7,89 – 10) m	Mohr-Coulomb	Drained	35,54	26,63	100	30	7418

(Source: PT. Geomine Bara Studio, 2022)

The data above are obtained as secondary data from PT. Geomine Bara Studio soil investigation report, especially the soil layer profile and the topmost layer properties, shear parameter, and elastic parameter. However, due to incomplete laboratory data for the soil properties, shear parameter, and elastic parameter

of the three bottom layers, back analysis was carried out with reference to typical soil parameters data that are commonly utilized in soil studies. The soil layers explanations are as follows:

- a) Soft clay soil is highly moldable due to its fine texture and great flexibility when saturated. Because the particles are microscopic and compacted tightly, it has a tendency to retain water and has poor drainage. It is prone to erosion, with low load-bearing capacity.
- b) Hard clay soil is a soil type with a firm, compacted texture and a high concentration of clay particles. Hard clay soil is non-pliable and resistant to deformation. Clay soil's fine particle close packing is frequently cited as the reason for its hardness. This particle compactness may result in sluggish water infiltration and inadequate drainage.
- c) Claystone, classifying as a sedimentary rock, is made up mostly of clay-sized particles with a fine-grained texture. One of claystone's main qualities is that it is impervious to water due to its low porosity and permeability. Because of this, claystone functions as a strong barrier to fluid flow and is frequently linked to the sealing layers that keep water from migrating into sedimentary basins.
- d) Lapilli, a small-sized and angular to spherical pieces of volcanic rock are released during a volcanic eruption. Usually, when molten or semi-molten lava is thrown into the air, these pieces are created. Lapilli are formed when the material that is expelled cools quickly and hardens into tiny volcanic particles. Lapilli can be made of several kinds of lava rock, pumice, and volcanic glass, among other materials. One kind of volcanic deposit known as a layer of lapilli can occur on the ground around a volcanic vent when these volcanic pieces end up in.

## 2. Building Load

On top of the slope there is a building, which is modeled as a uniform load of  $10 \text{ kN/m}^2$  for one-story, single-family house. This load is placed 5 meters away from slope edge and with load length of 9 meters inward based on field

observation of house features. This load is modeled in static condition as well as dynamic condition.

The existing slope is illustrated in Figure 5.1 below.

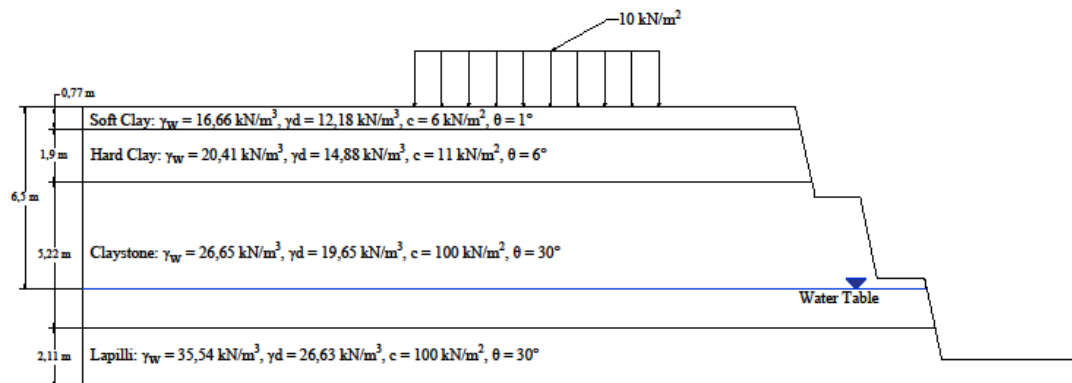


**Figure 5.1 Existing Slope**

(Source: PT. Geomine Bara Studio, 2022)

## 5.2 Non-Reinforced Slope Stability Analysis

Non-reinforced slope stability analysis is done using PLAXIS V20 to determine the initial factor of safety and slip surface. Then manual calculation is carried out to compare the results, based on the obtained factor of safety and slip surface from PLAXIS V20.

### 5.2.1 Modelling using PLAXIS V20

Based on the existing slope features and loading as detailed in the subchapter 5.1, the existing slope PLAXIS V20 modeling yields results of 1,360 for static condition in both non-loaded and loaded condition. Meanwhile, for dynamic condition, the FS is 1,059 for both loaded and non-loaded condition. The displacements vary; for non-loaded static condition the displacement is  $0,3010 \times 10^{-3}$  m, the non-loaded dynamic condition is 0,6413 m, the loaded static condition is 0,01497 m, and the loaded dynamic condition is 0,6402 m. The existing slope modelling output for non-loaded static condition are is shown in Figure 5.2 below.

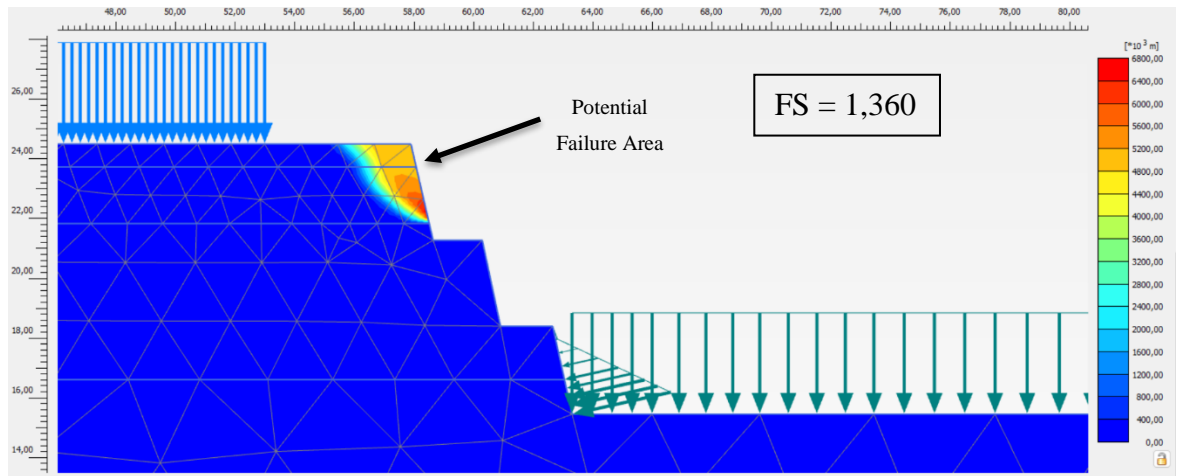


**Figure 5.2 Non-Loaded Static Existing Slope Potential Failure Area Output**

The existing slope modelling outputs for non-loaded dynamic condition is as shown in Figure 5.3 below.

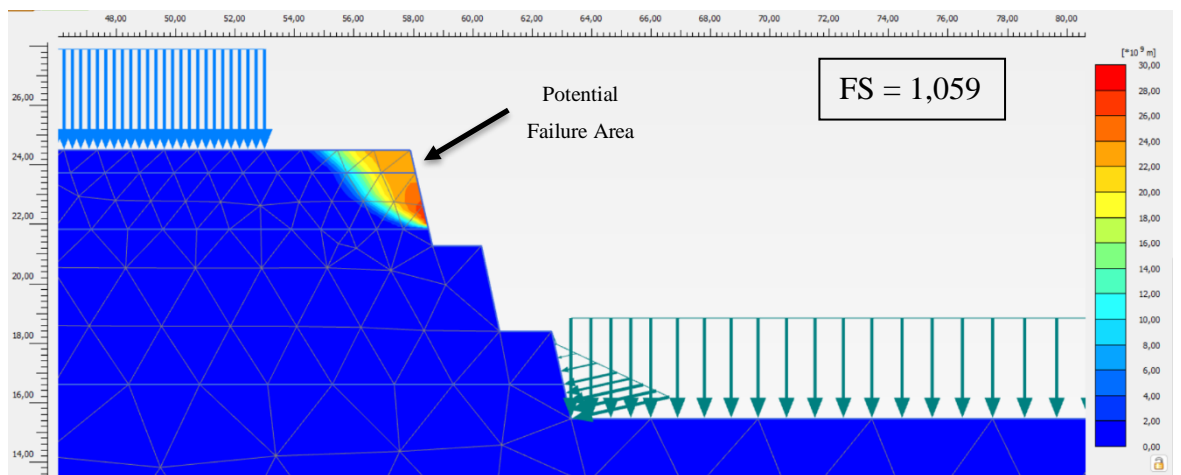


**Figure 5.3 Non-Loaded Dynamic Existing Slope Potential Failure Area Output**

The existing slope modelling outputs for loaded static condition is as shown in Figure 5.4 below.

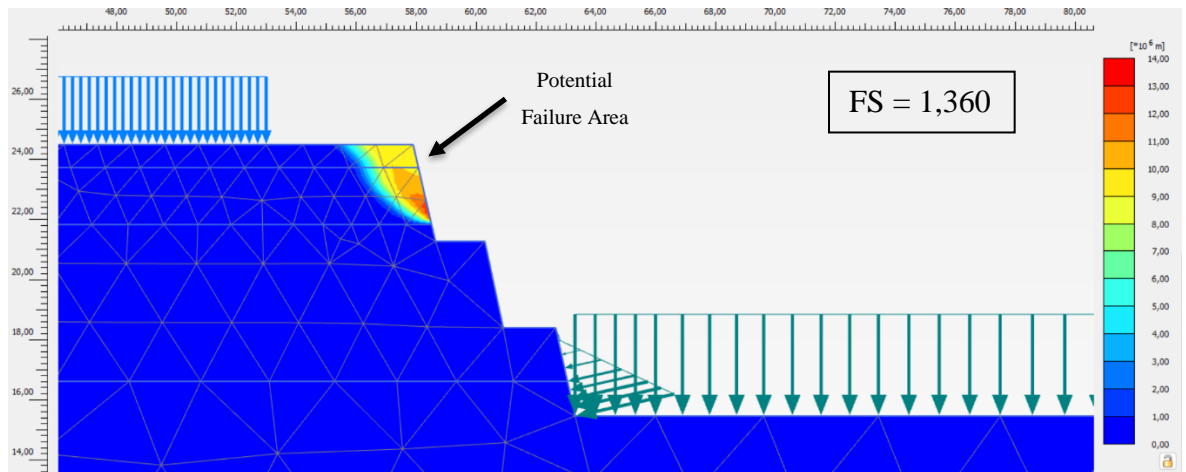


**Figure 5.4 Loaded Static Existing Slope Potential Failure Area Output**

The existing slope modelling outputs for loaded dynamic condition is as shown in Figure 5.5 below.

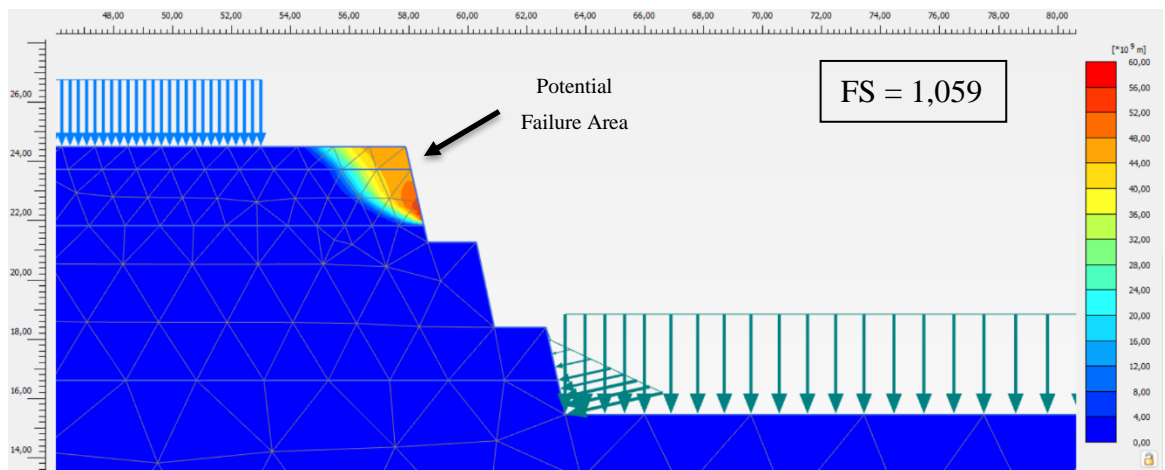


**Figure 5.5 Loaded Dynamic Existing Slope Potential Failure Area Output**

## 5.2.2 Manual Calculation using Fellenius Method

Before getting into the PLAXIS modelling of the reinforced slope, the manual calculations are carried out.



### 1. Slip Surface Failure Analysis

The existing slope Safety Factor calculation using Fellenius Method is carried out.

The calculation follows the formula below.

$$FS = \frac{\sum_{i=1}^{i=n}(c\alpha + n_i \text{tg}\varphi)}{\sum_{i=1}^{i=n}(W_i \sin\theta_i)}$$

Where :

n = Number of slices

c = Cohesion

$\alpha$  = Slip arc length

$\varphi$  = Internal shear angle

W = Slice weight

$\theta$  = Slip surface inclination

The calculation is based on the obtained slip surface dimensions from PLAXIS as show above. The slip surface is illustrated in Figure 5.6 as follows.

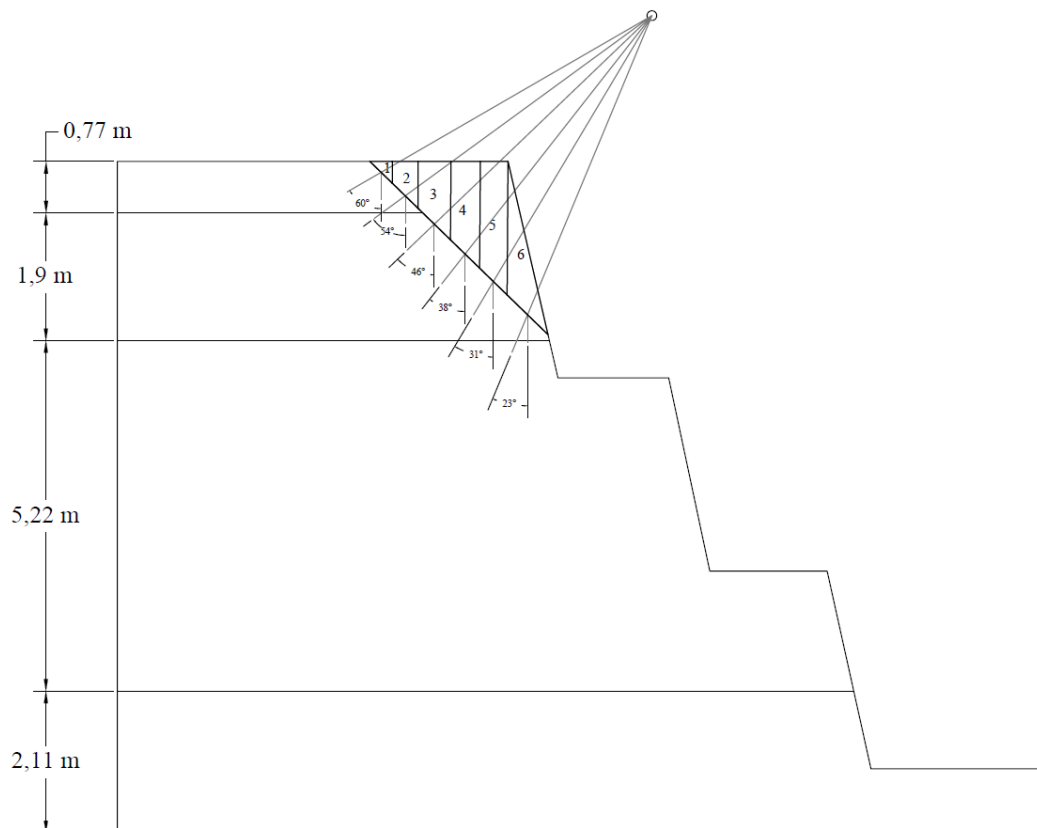


**Figure 5.6 Illustration of Slope for Fellenius Method Calculation**

An example can be taken from slice number 1 above. The following data is known:

$$A = 0,054 \text{ m}^2$$

$$\gamma = 16,66 \text{ kN/m}^3$$

$$\theta = 60^\circ$$

$$c = 6 \text{ kN/m}^2$$

$$\alpha = 0,466 \text{ m}$$

$$\varphi = 1^\circ$$

The steps are as follows.

a. Soil Slice Weight

$$\begin{aligned} W_1 &= \gamma \times A_1 \\ &= 16,66 \times 0,054 \\ &= 0,9 \text{ kN/m} \end{aligned}$$

b. Driving Force

$$\begin{aligned} \sin \theta &= 0,866 \\ W_1 \times \sin \theta &= 0,9 \times 0,866 \\ &= 0,78 \text{ kN} \end{aligned}$$

c. Resisting Force

$$\begin{aligned} \cos \theta &= 0,5 \\ n_i &= W_i \times \cos \theta \\ &= 0,9 \times 0,5 \\ &= 0,45 \text{ kN} \\ \tan \varphi &= 0,017 \\ c\alpha + n_i \tan \varphi &= 6 \times 0,466 + 0,45 \times 0,017 \\ &= 2,8 \text{ kN} \end{aligned}$$

The calculation steps are repeated for the other 5 slices, and then the total of resisting force is divided by the total of driving force, resulting in Safety Factor. The results are presented in Table 5.2.

**Table 5.2 Recapitulation of Soil Nail Safety Factor using Fellenius Method**

n	A (m <sup>2</sup> )	Y (kN/ m <sup>3</sup> )	W <sub>i</sub> (kN/m)	θ (°)	c (kN/ m <sup>2</sup> )	α (m)	c x α (kN)	W <sub>i</sub> sinθ (kN)	n <sub>i</sub> = W <sub>i</sub> cos θ (kN)	φ	cα + n <sub>i</sub> tanφ (kN)	FS
1	0,054	16,66	0,90	60	6	0,466	2,797	0,78	0,45	1	2,80	
2	0,197	16,66	3,29	54	6	0,537	3,224	2,66	1,93	1	3,26	
3	0,455	20,41	9,28	46	11	0,672	7,391	6,67	6,44	6	8,07	
4	0,604	20,41	12,32	38	11	0,606	6,668	7,58	9,71	6	7,69	
5	0,737	20,41	15,05	31	11	0,571	6,280	7,75	12,90	6	7,64	
6	0,610	20,41	12,45	23	11	0,850	9,350	4,86	11,46	6	10,55	
Σ								30,32			40,01	1,32

From the table, the FS is 1,32 which is deemed unsafe as it is below the required 1,5. Compared to the PLAXIS FS result for static loading, which is 1,361, this manual calculation yields similar FS. In conclusion, both results mean that soil nails are needed for reinforcement.

### 5.3 Reinforced Slope Stability Analysis

The reinforced slope stability analysis is done manually for one sample, as well as in PLAXIS V20. Both methods employ the same soil parameters and geometry as explained in subchapter 5.1.

The additional input data are the soil nail parameters. The soil nail diameter is obtained from PT. Geomine Bara Studio final investigation report, while the other parameters are obtained from typical parameters used in similar researches, and are cross-checked against SNI 2052:2014 guideline on concrete reinforcing steel as well as marketplace research for its availability and characteristics.

**Table 5.3 Soil Nail Material Input Data**

Parameters	Values
Material Type	Elastic
Young's Modulus (kN/m <sup>2</sup> )	210000000
Density (kN/m <sup>3</sup> )	60
Diameter (m)	0,01
Axial Skin Resistance for Start & End (kN/m)	1000

(Source: PT. Geomine Bara Studio, 2022)

### 5.3.1 Manual Calculation using Wedge Method

Reinforcement calculations are carried out by assuming two soil nails embedded cutting the slip surface, which is modelled in planar or straight trajectory. The features of the soil nails used in this calculation are based on Model a, which is the current reinforcement on the field with soil nail length of 5 meters, inclination of  $35^\circ$  and vertical spacing of 2,5 meters as shown in Figure 5.7 below.

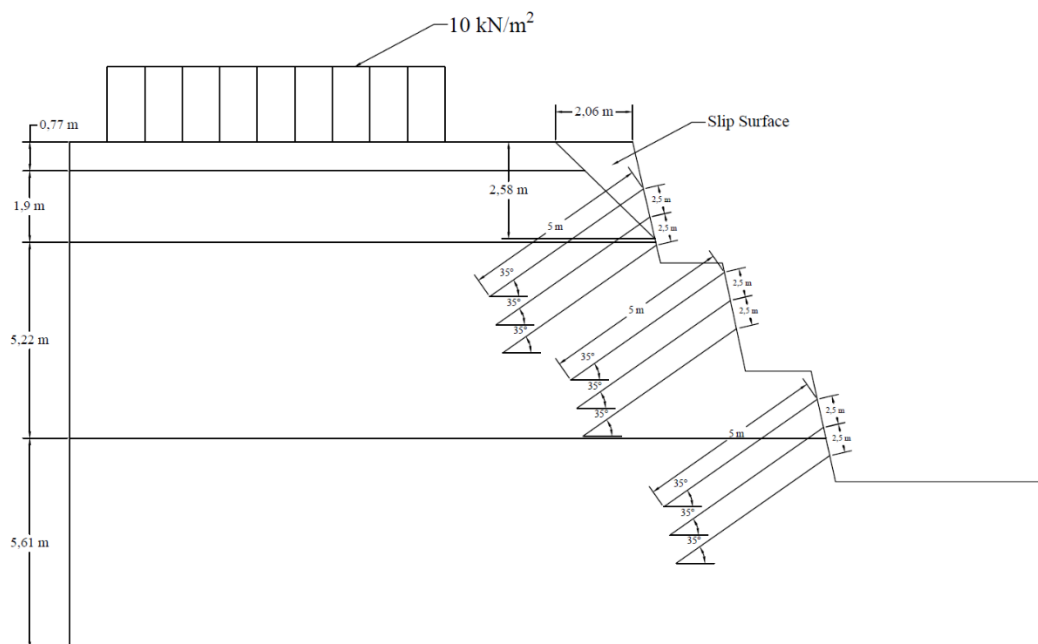


**Figure 5.7 Current Reinforcement**

(Source: PT. Geomine Bara Studio, 2022)

The difference in the calculation is the number of soil nails that is fewer than the current design used by PT. Geomine Bara Studio of three soil nails in vertical direction on the topmost tier of slope. This consideration is due to the placement of the third soil nail that doesn't touch the slip surface. Then, the method of wedge is used to calculate the FS and other factors relevant to the soil nail reinforcement design. The illustration is as follows in Figure 5.8.

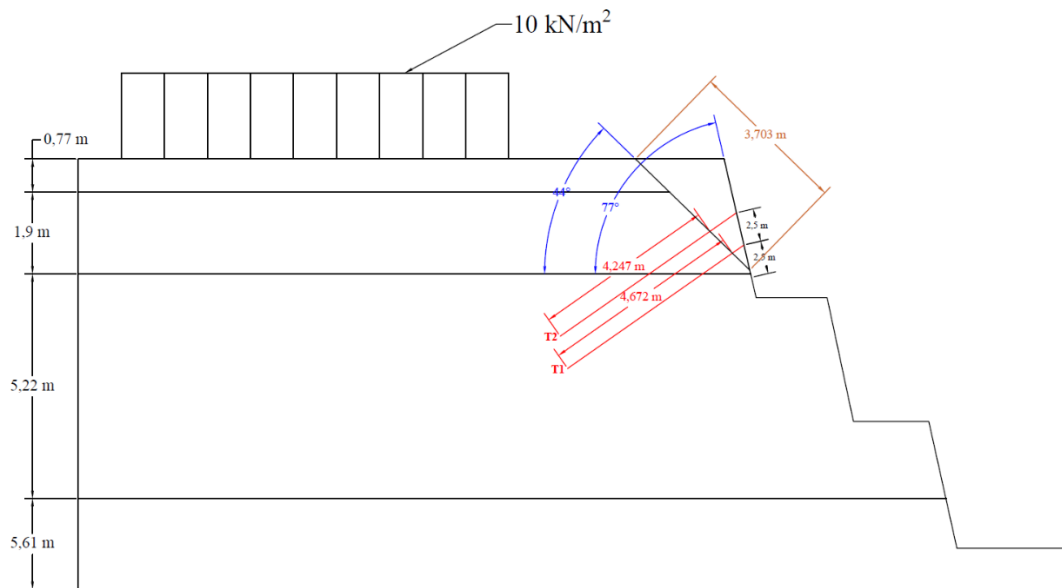


**Figure 5.8 Illustration of Slope for Wedge Method**

From the illustration, here is the known data:

$$\begin{aligned} \alpha &= 44^\circ \\ \beta &= 77^\circ \\ L_f &= 3,703 \text{ m} \\ L_{e1} &= 4,672 \text{ m} \\ L_{e2} &= 4,247 \text{ m} \\ \varphi &= 6^\circ \\ c &= 11 \text{ kN/m}^2 \\ i &= 35^\circ \\ W &= 54,236 \text{ m}^2 \end{aligned}$$

The following calculations are based on Formula 3.17 to Formula 3.28 as explained in Chapter III of this study. The calculation steps are as follows.

#### 1. Slip Surface Failure Analysis

With the known data of:

$$\begin{aligned} D &= 0,01 \text{ m} \\ K_s &= 24000 \text{ kN/m}^3 \text{ (based on Table 3.9)} \\ E &= 210000000 \text{ kN/m}^2 \\ I &= 1,55 \times 10^{-10} \text{ kg.m}^2 \end{aligned}$$

$$S_v = 2,5 \text{ m}$$

$$F_y = 420 \text{ MPa}$$

a. Check against tension force and allowable shear force

1) Reinforcement tension supporting for

$$R_n = F_y \times A_s \text{ Reinforcement}$$

$$= 420 \times \left(\frac{1}{4} \times \pi \times 10^2\right)$$

$$= 32970 \text{ kN}$$

$$R_c = \frac{1}{2} \times R_n$$

$$= \frac{1}{2} \times 32970$$

$$= 16485 \text{ kN}$$

2) Reinforcement allowable shear force

$$V_n = \frac{R_n}{2\sqrt{1+4\tan^2(90^\circ-(\alpha+i))}}$$

$$= \frac{32970}{2\sqrt{1+4\tan^2(90^\circ-79^\circ)}}$$

$$= 30729,53 \text{ kN}$$

3) Reinforcement tension allowable force

$$T = 4 \times V_n \times \tan(90^\circ - (\alpha + i))$$

$$= 4 \times 30729,53 \times \tan(11^\circ)$$

$$= 23892,86 \text{ kN}$$

4) Soil allowable shear force

The values of  $c_1$ ,  $c_2$ , and  $c_3$  are known from the relational graphic between internal friction angle to  $c_1$ ,  $c_2$ , and  $c_3$  on Figure 3.13.

The known values are as follows in Table 5.4.

**Table 5.4 Coefficients for Sandy Soil**

	Layer 1	Layer 2
$c_1$	0,75	0,75
$c_2$	1,6	1,6
$c_3$	10	10

Pu Value calculation

Possibility 1:

$$P_u = (c_1 \times H_i + c_2 \times d) \times \gamma \times H_i$$

$$\begin{aligned}
 P_{u1} &= (c_1 \times H_1 + c_2 \times d) \times \gamma \times H_1 \\
 &= (0,75 \times 0,77 + 1,6 \times 0,01) \times 16,66 \times 0,77 \\
 &= 7,614 \text{ kN}
 \end{aligned}$$

$$\begin{aligned}
 P_{u2} &= (c_1 \times H_2 + c_2 \times d) \times \gamma \times H_2 \\
 &= (0,75 \times 1,9 + 1,6 \times 0,01) \times 20,41 \times 1,9 \\
 &= 55,881 \text{ kN}
 \end{aligned}$$

$$\begin{aligned}
 P_u &= P_{u1} + P_{u2} \\
 &= 63,495 \text{ kN}
 \end{aligned}$$

Possibility 2:

$$P_u = c_3 \times D \times \gamma \times H_1$$

$$\begin{aligned}
 P_{u1} &= c_3 \times D \times \gamma \times H_1 \\
 &= 10 \times 0,01 \times 16,66 \times 0,77 \\
 &= 1,283 \text{ kN}
 \end{aligned}$$

$$\begin{aligned}
 P_{u2} &= c_3 \times D \times \gamma \times H_2 \\
 &= 10 \times 0,01 \times 20,41 \times 1,9 \\
 &= 3,878 \text{ kN}
 \end{aligned}$$

$$\begin{aligned}
 P_u &= P_{u1} + P_{u2} \\
 &= 5,161 \text{ kN}
 \end{aligned}$$

From both possibilities, lower  $P_u$  value is taken, which is 5,161 kN for the next calculation.

$$\begin{aligned}
 P_p &= \frac{P_u}{2} \\
 &= \frac{5,161}{2} \\
 &= 2,5805 \text{ kN}
 \end{aligned}$$

$$\begin{aligned}
 V_s &= P_p \times \frac{D}{2} \times L_o \\
 &= P_p \times \frac{D}{2} \times \sqrt[4]{\frac{4Ei}{KsD}} \\
 &= 2,5805 \times \frac{0,01}{2} \times \sqrt[4]{\frac{4 \times 210000000 \times 1,55 \times 10^{-10}}{24000 \times 0,01}} \\
 &= 0,00197 \text{ kN}
 \end{aligned}$$

Since  $V_s < V_n$ , the global allowable shear force ( $V_{max}$ ) used is 0,0026 kN.

Due to the limitation of allowable shear force, the nail bar allowable tension force has to be corrected to:

$$\frac{V_{max}^2}{Rc^2} + \frac{T_{max}^2}{Rn^2} = 1$$

$$\frac{0,00197^2}{16485^2} + \frac{T_{max}^2}{32970^2} = 1, \text{ so } T_{max} = 32970 \text{ kN}$$

#### b. Nail Bar Allowable Tension Force

Below is the added known data:

$$f_{max} = 25 \text{ kN/m}^2 \text{ (from Table 3.10)}$$

$$FS = 1,5$$

$$T = \frac{\pi \cdot D \cdot L \cdot e \cdot f_{max}}{FS}$$

$$T_1 = \frac{3,14 \times 0,01 \times 4,672 \times 25}{1,5}$$

$$= 2,445 \text{ kN}$$

$$T_2 = \frac{3,14 \times 0,01 \times 4,247 \times 25}{1,5}$$

$$= 2,223 \text{ kN}$$

$$\sum T_i = \frac{T_1 + T_2}{S_v}$$

$$= \frac{2,445 + 2,223}{2,5}$$

$$= 1,867 \text{ kN}$$

#### c. Safety Factor

$$FS = \frac{c \cdot L_f + W \cos \alpha \cdot \tan \phi + (\sum T_i \sin(\alpha + i) - \sum V_i \cos(\alpha + i)) \tan \phi}{W \sin \alpha - \sum T_i \cos(\alpha + i) - \sum V_i \sin(\alpha + i)}$$

$$FS = \frac{11 \times 3,703 + 54,236 \times \cos 44^\circ \times \tan 6^\circ + (1,867 \times \sin(44^\circ + 35^\circ) - 0,0018 \times \cos(44^\circ + 35^\circ)) \times \tan 6^\circ}{54,236 \times \sin 44^\circ - 1,867 \times \cos(44^\circ + 35^\circ) - 0,0018 \times \sin(44^\circ + 35^\circ)}$$

$$FS = 1,207$$

From the calculation, for first and second nails that cut through the slip surface, the final FS is  $1,207 < 1,5$  so the soil nails are not adequate. This notable gap with the desired FS may be due to inaccuracies in soil and nail properties due to incomplete data from laboratory testing and specification. However, looking at the design from PT. Geomine Bara Studio, there is a third nail, as illustrated in Figure 5.9.



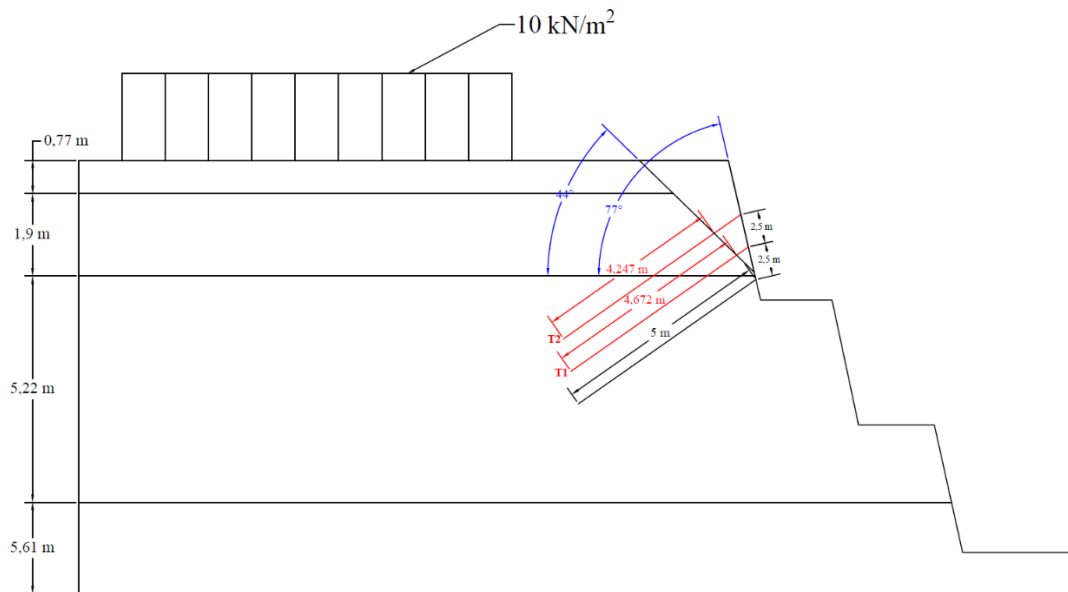


**Figure 5.9 Illustration of Slope for Wedge Method with Three Nails**

The FS for the third nail can be calculated using the same formula, with the following data known.

$$\alpha = 44^\circ$$

$$L_f = 3,8503 \text{ m,}$$

$$L_{e3} = 5 \text{ m, full soil nail length as it lies beyond the slip surface}$$

$$\varphi = 30^\circ$$

$$c = 100 \text{ kN/m}^2$$

$$i = 35^\circ$$

$$W = 70,817 \text{ m}^2 \text{ with } A = 2,6573 \text{ m}^2 \text{ and } \gamma = 26,65 \text{ kN/m}^3$$

$$FS = \frac{c \cdot L_f + W \cos \alpha \cdot \tan \varphi + (\sum T_i \sin(\alpha + i) - \sum V_i \cos(\alpha + i)) \tan \varphi}{W \sin \alpha - \sum T_i \cos(\alpha + i) - \sum V_i \sin(\alpha + i)}$$

$$FS = \frac{100 \times 3,8503 + 70,817 \times \cos 44^\circ \times \tan 30^\circ + (0,2355 \times \sin(44^\circ + 35^\circ) - 0,066 \times \cos(44^\circ + 35^\circ)) \times \tan 30^\circ}{70,817 \times \sin 44^\circ - 0,2355 \times \cos(44^\circ + 35^\circ) - 0,066 \times \sin(44^\circ + 35^\circ)}$$

$$FS = 7,95$$

For the third nail, the obtained FS is  $7,96 > 1,5$ . This means that the support in the third nail is enough, which is due to the soil characteristics that are firmer and the nail placement outside of the slip surface.

## 2. Slope Stability against Shear Force Analysis

The FS calculation follows the following formula.

$$FS = \frac{cb \times BL + (W + Q + P \sin \delta) \tan \phi}{P \cos \delta}$$

With the known data below.

$$I = 35^\circ$$

$$\beta = 77^\circ$$

$$L_{\text{nail}} = 5 \text{ meter}$$

$$T_{\text{nail}} = 0,5 \text{ meter}$$

$$H = 7,89 \text{ meter}$$

$$\text{a. Slope inclination length} = \frac{7,89}{\sin(77^\circ)}$$

$$= 8,098 \text{ meter}$$

$$\text{b. } X_i = \cos(77^\circ) \times \text{slope inclination length}$$

$$= 0,225 \times 8,098$$

$$= 1,822 \text{ kN/m}^2$$

c. Building Load (Q)

$$K_{a1} = \tan^2 \left( 45 - \frac{\phi}{2} \right)$$

$$= \tan^2 \left( 45 - \frac{1}{2} \right)$$

$$= 0,966$$

$$K_{a2} = \tan^2 \left( 45 - \frac{\phi}{2} \right)$$

$$= \tan^2 \left( 45 - \frac{6}{2} \right)$$

$$= 0,755$$

d. Cohesion Effect

$$\text{Layer 1} = -2 \times c \times \sqrt{K_{a1}}$$

$$= -2 \times 6 \times \sqrt{0,966}$$

$$= -11,794 \text{ kN/m}^2$$

$$\text{Layer 2} = -2 \times c \times \sqrt{K_{a2}}$$

$$= -2 \times 11 \times \sqrt{0,755}$$

$$= -19,116 \text{ kN/m}^2$$

e. Total Active Soil Pressure behind Reinforcement Zone per Layer

Based on distributed load:

$$\begin{aligned} Pa_1 &= \frac{\gamma \times H_1^2}{2} \times Ka_1 \\ &= \frac{16,66 \times 0,77^2}{2} \times 0,966 \\ &= 4,771 \text{ kN/m} \end{aligned}$$

$$\begin{aligned} Pa_2 &= \frac{\gamma \times H_2^2}{2} \times Ka_2 \\ &= \frac{20,41 \times 1,9^2}{2} \times 0,755 \\ &= 27,814 \text{ kN/m} \end{aligned}$$

$$\begin{aligned} Pa &= Pa_1 + Pa_2 \\ &= 32,585 \text{ kN/m} \end{aligned}$$

f. Safety Factor against Shear

$$\begin{aligned} Lx &= L_{\text{nail}} \times \cos i - t \times \tan \alpha \\ &= 5 \times \cos(35^\circ) - 0,5 \times \tan(44^\circ) \\ &= 3,613 \text{ meter} \end{aligned}$$

$$\begin{aligned} BL &= X_i + Lx \\ &= 1,822 + 3,613 \\ &= 5,435 \text{ meter} \end{aligned}$$

$$\begin{aligned} W &= A_i \times \gamma \\ &= 1,5237 \times 16,66 + 2,1914 \times 20,41 \\ &= 70,111 \text{ kN} \end{aligned}$$

Safety Factor is calculated below.

$$\begin{aligned} FS &= \frac{cb \times BL + (W + Q + Pa \sin \delta) \tan \phi}{Pa \cos \delta} \\ &= \frac{20,41 \times 5,435 + (70,111 + 32,585 \times \sin 6^\circ) \tan 6^\circ}{32,585 \times \cos 6^\circ} \\ &= \frac{118,655}{32,407} \\ &= 3,66 > 1,5, \text{ then it is safe.} \end{aligned}$$

Based on the calculation, the shear safety factor against the reinforced slope of 3,66 (FS > 1,5), the slope is safe against the shear force.

### 3. Internal Stability Analysis against Broken and Pulled Out Reinforcement

These calculations are done on each nail. The following data is known.

$$L_{\text{nail}} = 5 \text{ meter}$$

$$S_v = 2,5 \text{ meter}$$

$$q_u = 25 \text{ kN/m}^2$$

a. Active Lateral Soil Pressure Coefficient

$$\begin{aligned} K_{a1} &= \tan^2 \left( 45 - \frac{\varphi}{2} \right) \\ &= \tan^2 \left( 45 - \frac{1}{2} \right) \\ &= 0,966 \end{aligned}$$

$$\begin{aligned} K_{a2} &= \tan^2 \left( 45 - \frac{\varphi}{2} \right) \\ &= \tan^2 \left( 45 - \frac{6}{2} \right) \\ &= 0,755 \end{aligned}$$

b. Horizontal Stress

$$\begin{aligned} \sigma_{h1} &= ((q \times K_{a2}) - 2 \times c \times \sqrt{K_{a2}}) + (\gamma_2 \times z_1 \times K_{a2}) \\ &= ((10 \times 0,755) - 2 \times 11 \times \sqrt{0,755}) + (20,41 \times 2 \times 0,755) \\ &= 19,253 \text{ kN/m}^2 \end{aligned}$$

$$\begin{aligned} \sigma_{h2} &= ((q \times K_{a2}) - 2 \times c \times \sqrt{K_{a2}}) + (\gamma_2 \times z_2 \times K_{a2}) \\ &= ((10 \times 0,755) - 2 \times 11 \times \sqrt{0,755}) + (20,41 \times 1,25 \times 0,755) \\ &= 7,696 \text{ kN/m}^2 \end{aligned}$$

c. Safety Factor against Each Nail Broken Reinforcement

$$\begin{aligned} Fr_1 &= \frac{\left( \frac{0,25 \times \pi \times d^2 \times f_y}{1000} \right)}{\sigma_{h1} \times S_v \times S_h} \\ &= \frac{\left( \frac{0,25 \times \pi \times 0,01^2 \times 420}{1000} \right)}{19,253 \times 2,5 \times 1} \\ &= 0,685 \end{aligned}$$

$$\begin{aligned} Fr_2 &= \frac{\left( \frac{0,25 \times \pi \times d^2 \times f_y}{1000} \right)}{\sigma_{h1} \times S_v \times S_h} \\ &= \frac{\left( \frac{0,25 \times \pi \times 0,01^2 \times 420}{1000} \right)}{7,696 \times 2,5 \times 1} \\ &= 1,714 \end{aligned}$$

d. Safety Factor against Pulled Out Reinforcement

$$\begin{aligned}
 Fp_1 &= \frac{\pi \times qu \times Ddh \times Le_1}{\sigma h_1 \times Sv \times Sh} \\
 &= \frac{\pi \times 25 \times 0,02 \times 4,672}{19,253 \times 2,5 \times 1} \\
 &= 0,152 \\
 Fp_2 &= \frac{\pi \times qu \times Ddh \times Le_2}{\sigma h_2 \times Sv \times Sh} \\
 &= \frac{\pi \times 25 \times 0,02 \times 4,247}{7,696 \times 2,5 \times 1} \\
 &= 0,347
 \end{aligned}$$

Based on the FS for broken and pulled out reinforcement, it is determined that the current reinforcement is not the safest as the values are far from the standard of 1,5. This means that in the modelling there should be variations of nail configuration such as vertical spacing.

### 5.3.2 Modelling Variations for PLAXIS V20

Below are the variations of the modelling in PLAXIS V20, which hinges on the soil nail length, inclination, and vertical spacing, presented in Table 5.5.

**Table 5.5 Slope Modelling Variations in PLAXIS V20**

Model Name	Soil Nail		
	Length (m)	Inclination (°)	Vertical Spacing (m)
a	5	35	2,5
b	5	35	1,5
c	5	20	2,5
d	5	20	1,5
e	5	50	2,5
f	5	50	1,5
g	4,5	20	2,5
h	4,5	20	1,5

The number and configuration of soil nail is modeled exactly the same as the design by PT. Geomine Bara Studio, meaning, in addition to the three soil nails atop the slope, there are 6 more soil nails, 3 on the second tier of slope, and 3 on the lowest tier of slope. The second and third tiers of slope are made up of rocky layers, and the nails are used to anchor the whole retaining wall and to prevent rock

layer sliding or breakage. The modelling variations are illustrated in Figure 5.10 to Figure 5.17 below.

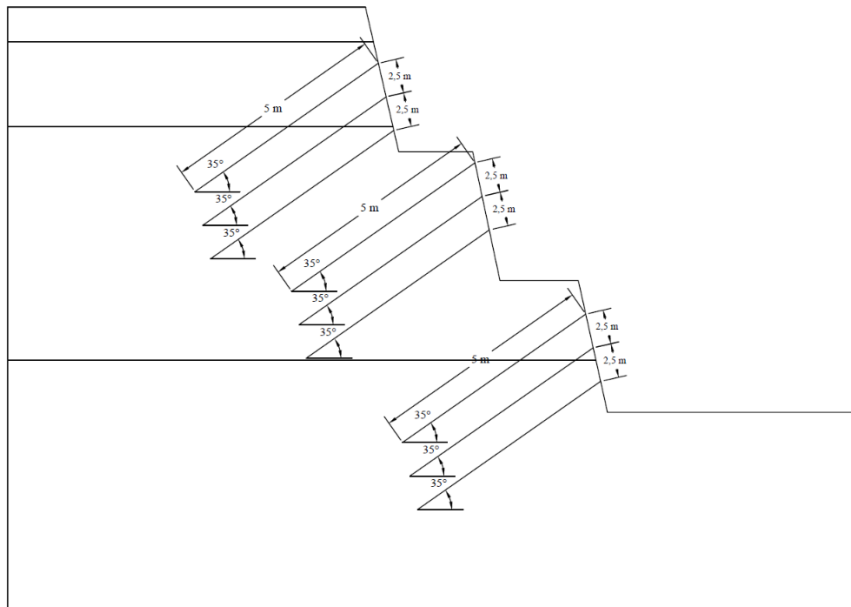


**Figure 5.10 Model a**

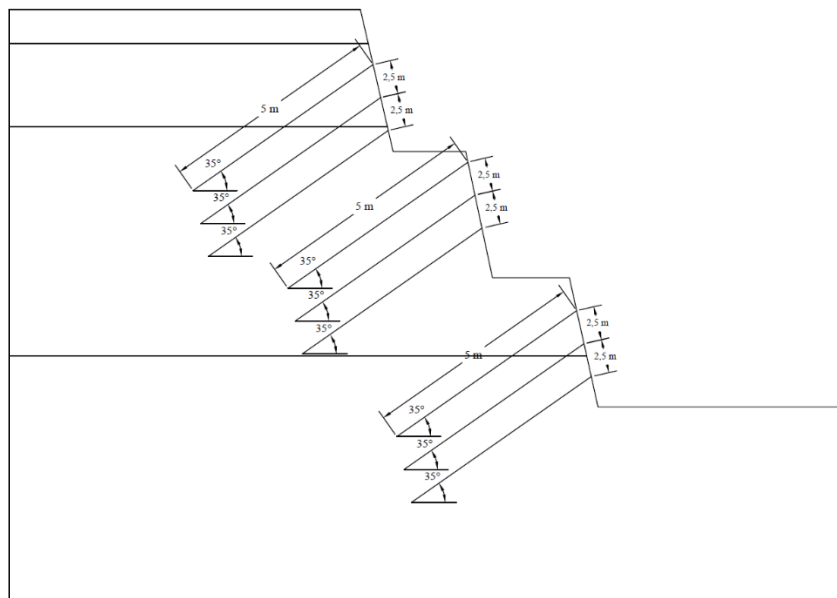


**Figure 5.11 Model b**

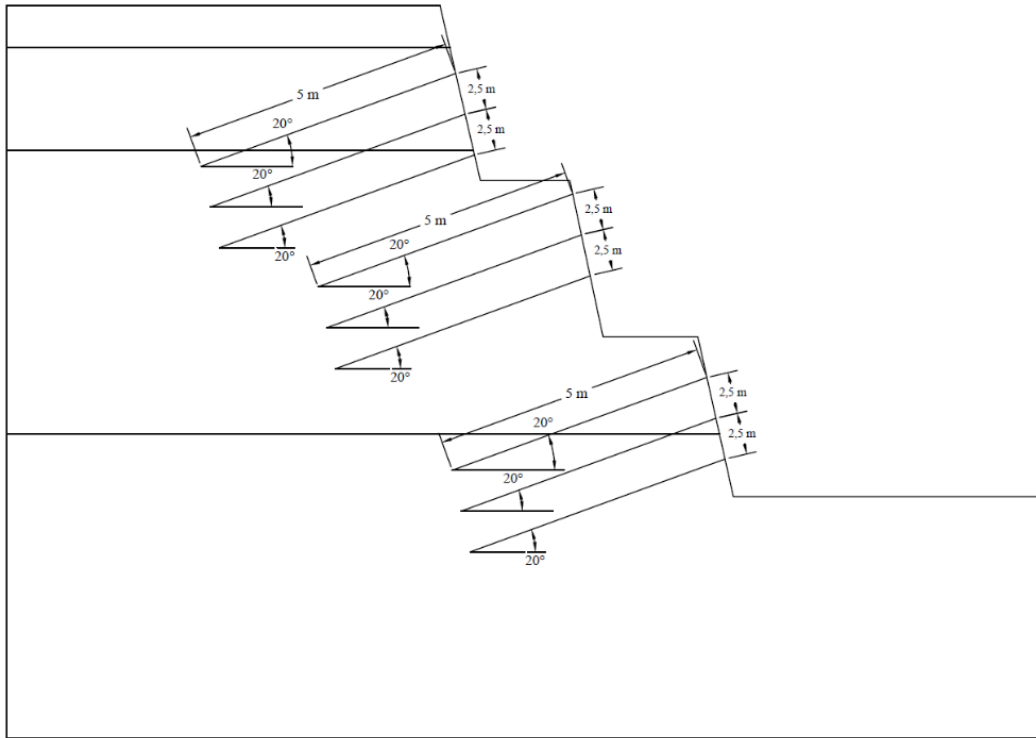


Figure 5.12 Model c

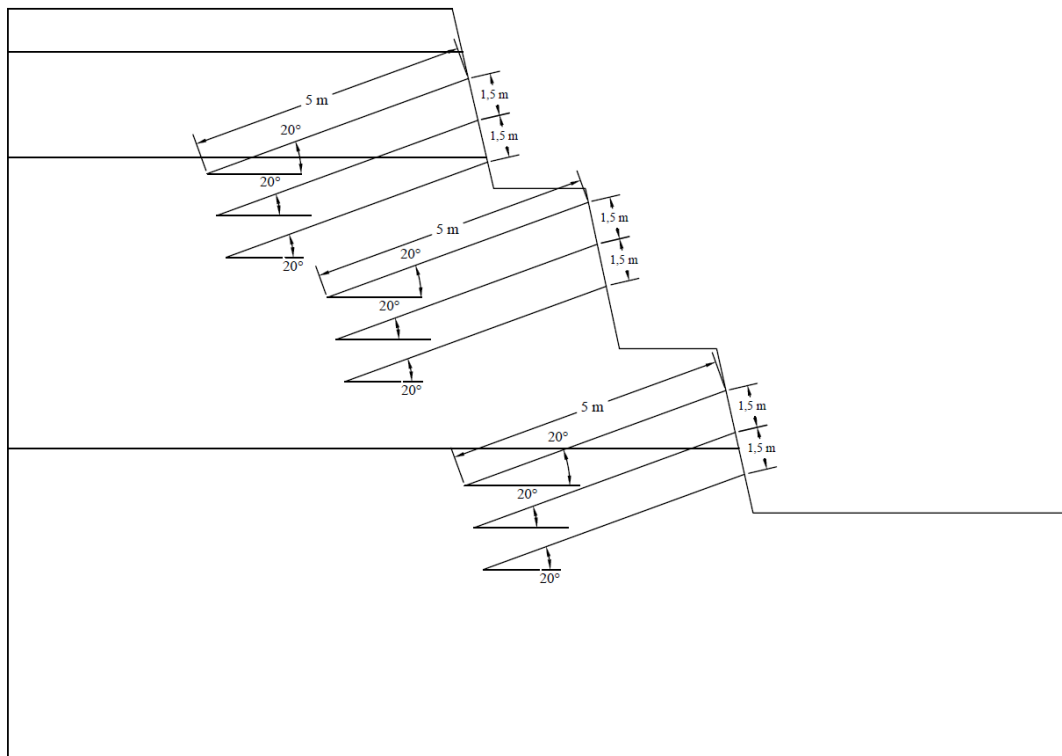
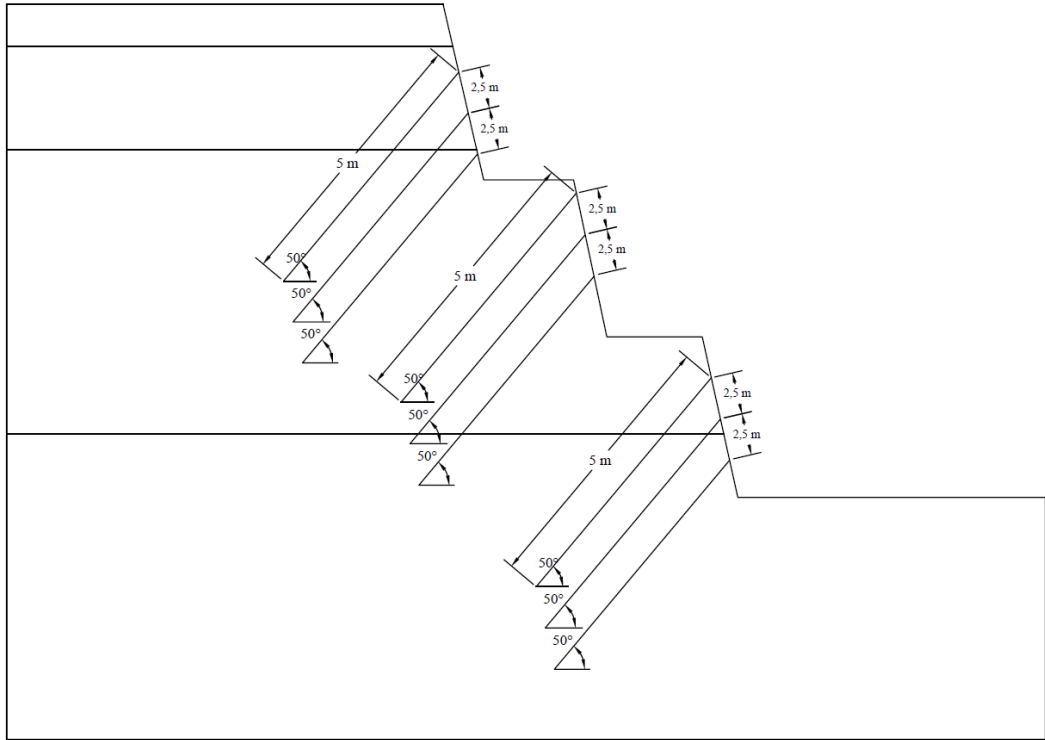
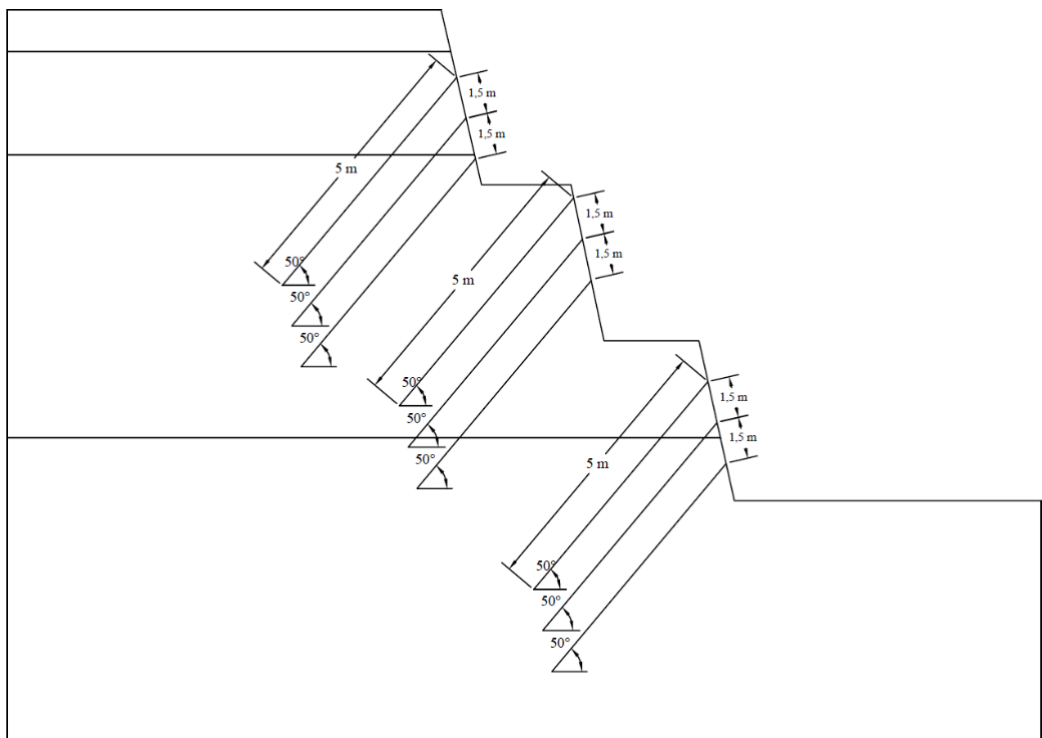


Figure 5.13 Model d



**Figure 5.14 Model e**



**Figure 5.15 Model f**



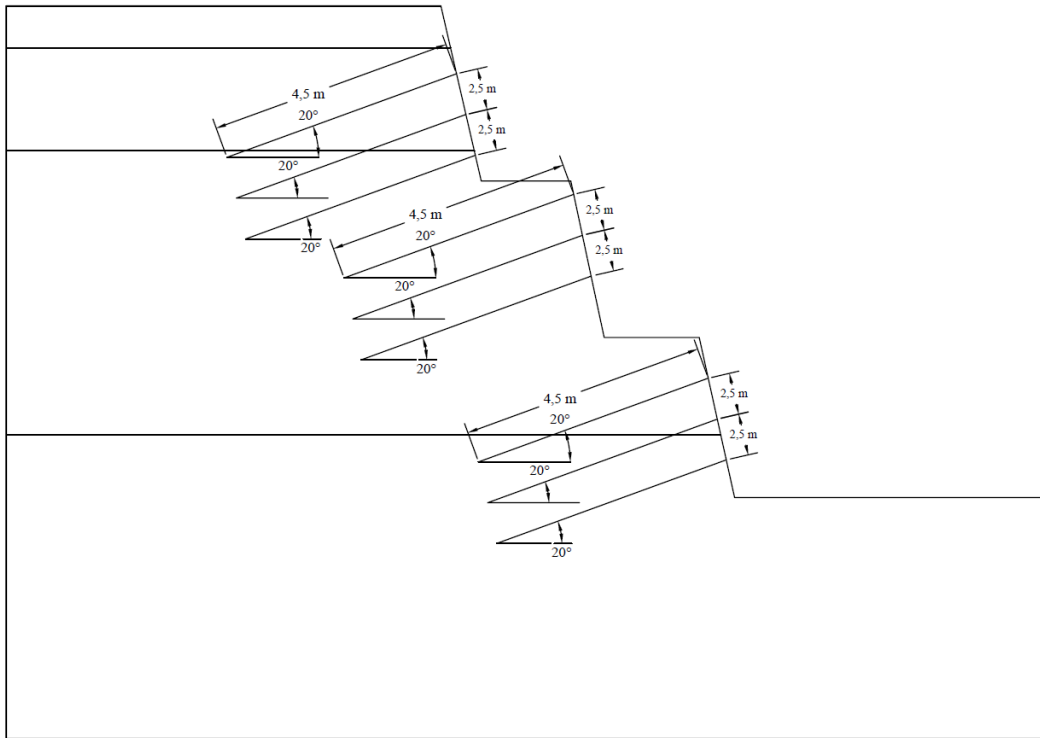


**Figure 5.16 Model g**

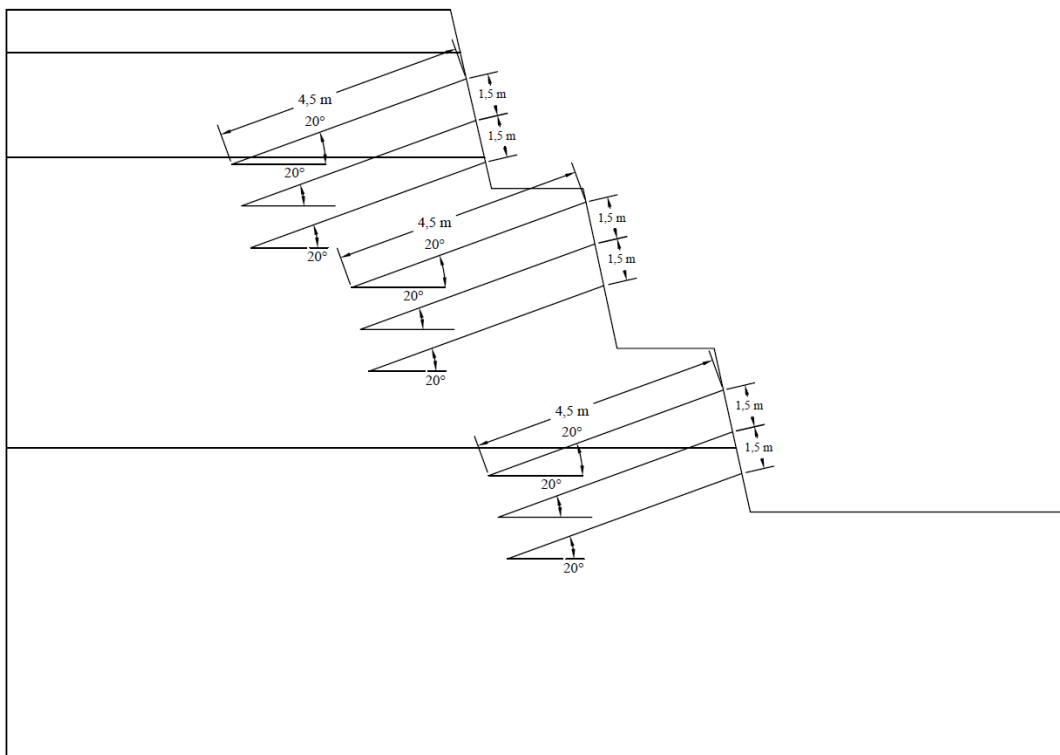


**Figure 5.17 Model h**

The soil nailing variations are group based on the investigated variable, and will be discussed in 5.3.5, this is carried out to produce more comprehensive conclusions in the next chapter.

The first group based on 5 meters length and inclination of 2,5 meters vertical spacing is as follows in Table 5.6.

**Table 5.6 Group 1 of Inclination Variable at 5 Meters Length and 2,5 Meters Vertical Spacing**

Model Name	Soil Nail		
	Length (m)	Inclination (°)	Vertical Spacing (m)
a	5	35	2,5
c	5	20	2,5
e	5	50	2,5

Then, the same variable of inclination is grouped at 5 meters length and 1,5 meters vertical spacing, as shown in Table 5.7 below.

**Table 5.7 Group 2 of Inclination Variable at 5 Meters Length and 1,5 Meters Vertical Spacing**

Model Name	Soil Nail		
	Length (m)	Inclination (°)	Vertical Spacing (m)
b	5	35	1,5
d	5	20	1,5
f	5	50	1,5

The next group compares the length of the nail at 20° inclination and 2,5 meters vertical spacing, as shown in Table 5.8 below.

**Table 5.8 Group 3 of Length Variable at 20° Inclination and 2,5 Meters Vertical Spacing**

Model Name	Soil Nail		
	Length (m)	Inclination (°)	Vertical Spacing (m)
c	5	20	2,5
g	4,5	20	2,5

The next group compares the length of the nail at 20° inclination and 1,5 meters vertical spacing, as shown in Table 5.9 below.

**Table 5.9 Group 4 of Length Variable at 20° Inclination and 1,5 Meters Vertical Spacing**

Model Name	Soil Nail		
	Length (m)	Inclination (°)	Vertical Spacing (m)
d	5	20	1,5
h	4,5	20	1,5

### 5.3.3 Modelling Results using PLAXIS V20

#### 1) Model a

The current slope reinforcement at STA 7+300 of Tawang-Ngalang Road and Bridge Project is soil nailing with the length of 5 meters, nail inclination of 35°, and vertical spacing of 2,5 meters. The FS for non-loaded condition is 1,603 in static condition and 1,426 in dynamic condition. Meanwhile, for loaded condition, the FS is 1,600 in static condition and 1,386 in dynamic condition. The displacements vary; for non-loaded static condition the displacement is  $2,078 \times 10^{-3}$  m, the non-loaded dynamic condition is 0,6742 m, the loaded static condition is 0,01496 m, and the loaded dynamic condition is 0,6726 m. The Model a modelling output for non-loaded static condition is as shown in Figure 5.18 below.

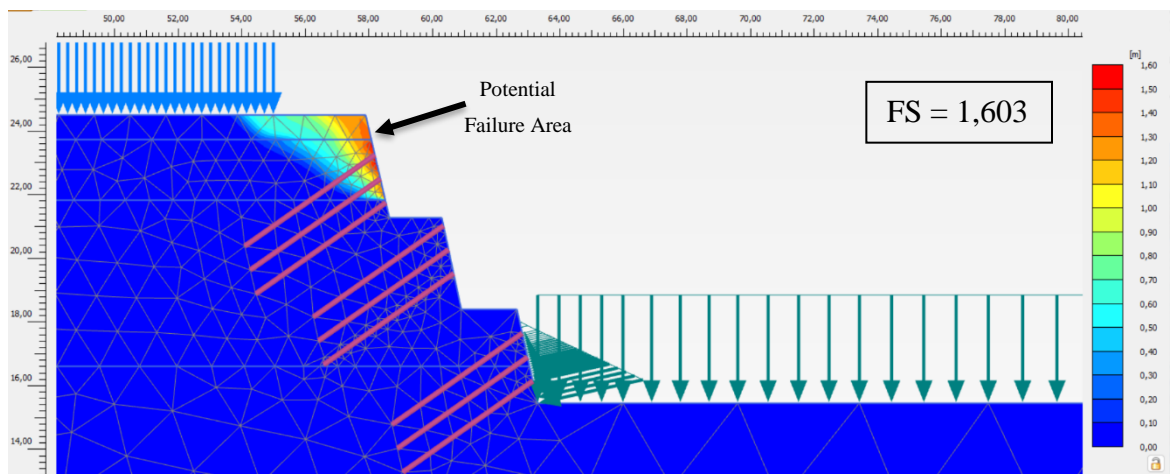


**Figure 5.18 Model a Non-Loaded Static Potential Failure Area Output**

The Model a modelling output for non-loaded dynamic condition is as shown in Figure 5.19.

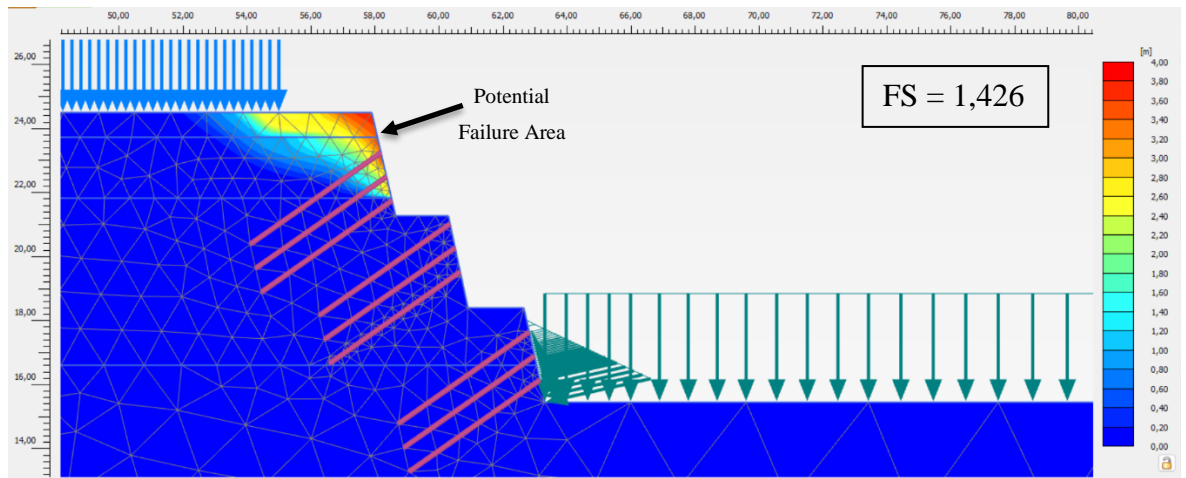


**Figure 5.19 Model a Non-Loaded Dynamic Potential Failure Area Output**

The Model a modelling output for loaded static condition is as shown in Figure 5.20.

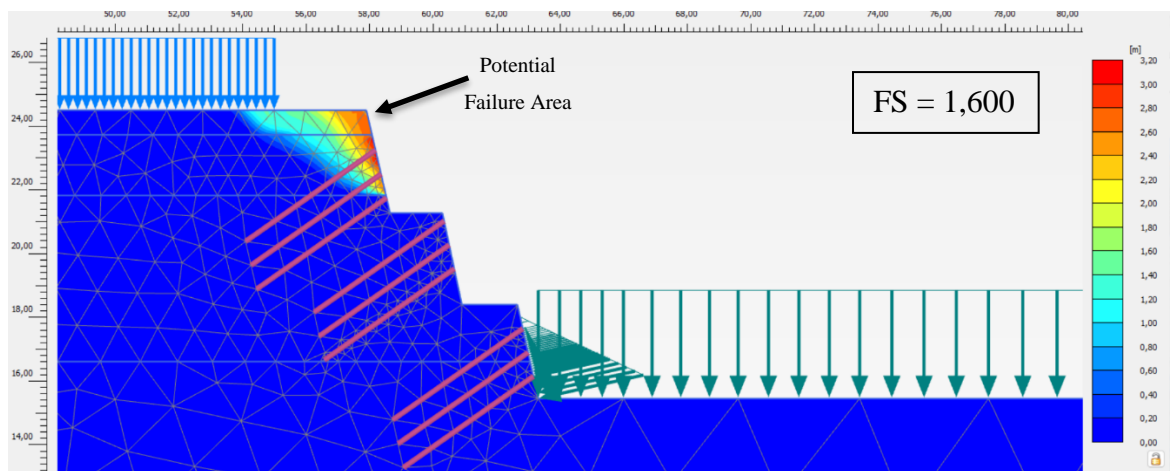


**Figure 5.20 Model a Loaded Static Potential Failure Area Output**

The Model a modelling output for loaded dynamic condition is as shown in Figure 5.21.

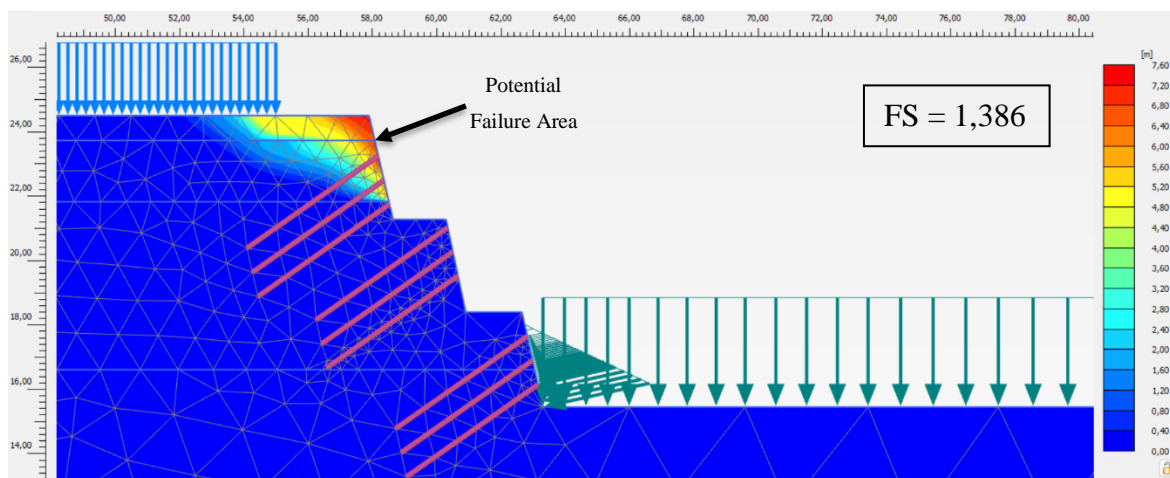


**Figure 5.21 Model a Loaded Dynamic Potential Failure Area Output**

The illustrations indicate slight differences between phases. The non-loaded static and non-loaded dynamic experience slight drop in FS from 1,603 to 1,426, meaning the earthquake load impact of 0,2 g is not significant. Meanwhile, the drop of FS from loaded static to loaded dynamic is slightly bigger from 1,600 to 1,386, meaning the traffic load combined with earthquake load has bigger impact towards FS. The FS between non-loaded and loaded static only drops by 0,003, indicating that traffic loading alone is not significant. However, with earthquake loading, traffic loading becomes more significant as shown in the difference between non-loaded and loaded dynamic FS condition.

## 2) Model b

The first modification for slope reinforcement at STA 7+300 of Tawang-Ngalang Road and Bridge Project is soil nailing with the length of 5 meters, nail inclination of 35°, and vertical spacing of 1,5 meters. The FS for non-loaded condition is 1,809 in static condition and 1,664 in dynamic condition. Meanwhile, for loaded condition, the FS is 1,789 in static condition and 1,680 in dynamic condition. The displacements vary; for non-loaded static condition the displacement is  $1,965 \times 10^{-3}$  m, the non-loaded dynamic condition is 0,6561 m, the loaded static condition is 0,01497 m, and the loaded dynamic condition is 0,6540 m. The Model b modelling output for non-loaded static condition is as shown in Figure 5.22 below.

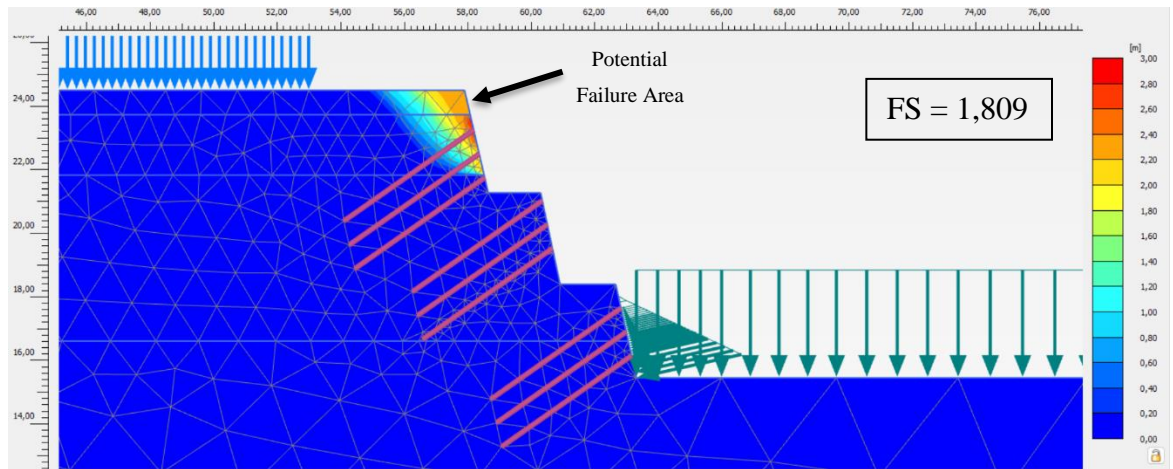


**Figure 5.22 Model b Non-Loaded Static Potential Failure Area Output**

The Model b modelling output for non-loaded dynamic condition is shown in Figure 5.24.

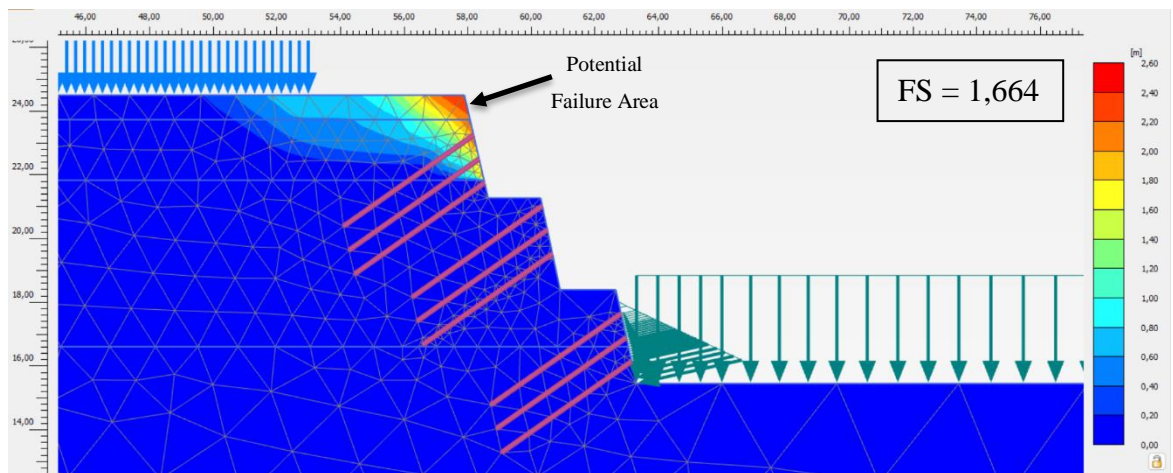


**Figure 5.23 Model b Non-Loaded Dynamic Potential Failure Area Output**



The Model b modelling output for loaded static condition is as shown in Figure 5.24 below.

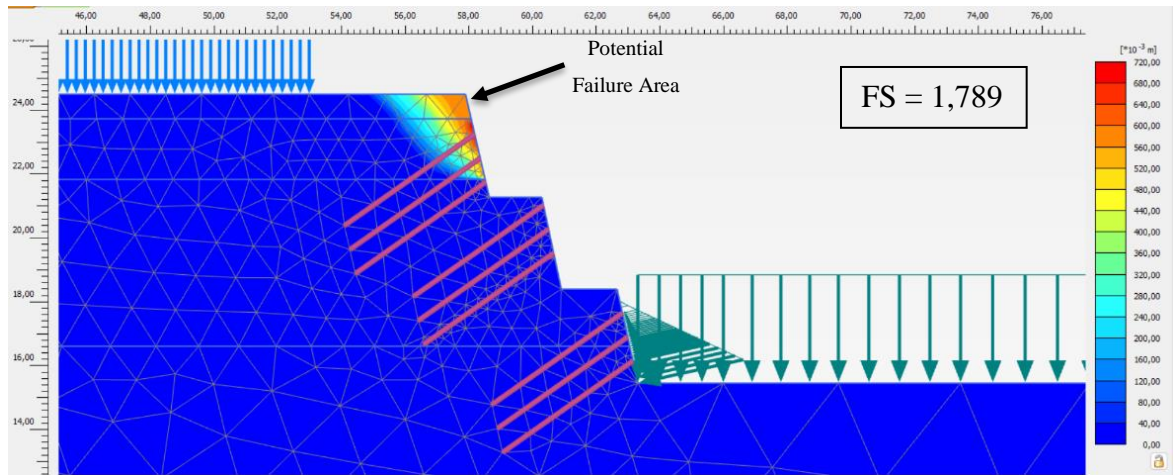


**Figure 5.24 Model b Loaded Static Potential Failure Area Output**

The Model b modelling output for loaded dynamic condition is as shown in Figure 5.25 below.

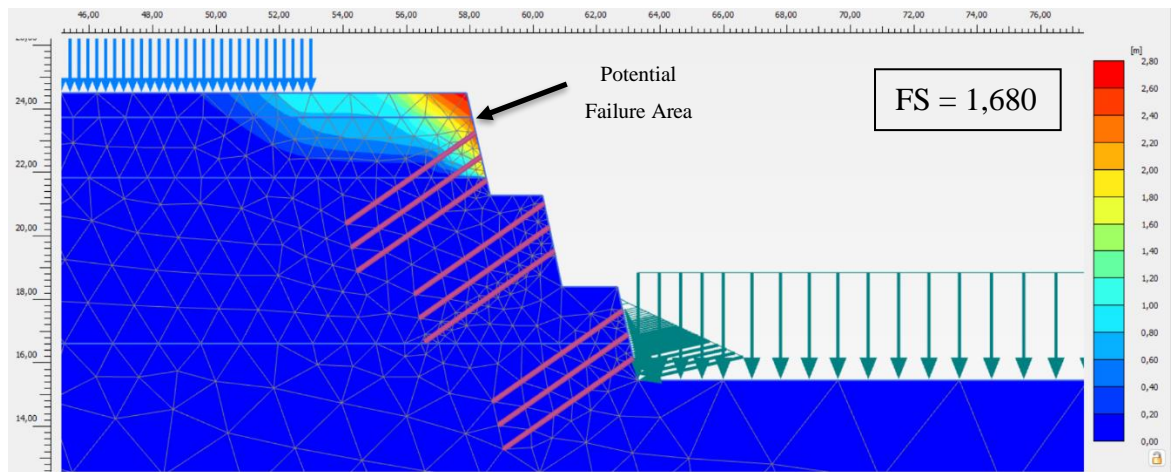


**Figure 5.25 Model b Loaded Dynamic Potential Failure Area Output**

The illustrations indicate a significant increase of FS across all phases. The non-loaded static and non-loaded dynamic experience a significant drop in FS from 1,809 to 1,664, meaning the earthquake load is quite impactful. Meanwhile, the

drop of FS from loaded static to loaded dynamic is smaller from 1,789 to 1,680, meaning the traffic load combined with earthquake load has smaller impact towards FS. The FS between non-loaded and loaded static only drops by 0,002, indicating that traffic loading alone is not significant. However, the FS oddly improves from non-loaded to loaded dynamic conditions.

### 3) Model c

The second modification for slope reinforcement at STA 7+300 of Tawang-Ngalang Road and Bridge Project is soil nailing with the length of 5 meters, nail inclination of  $20^\circ$ , and vertical spacing of 2,5 meters. The FS for non-loaded condition is 1,802 in static condition and 1,654 in dynamic condition. Meanwhile, for loaded condition, the FS is 1,807 in static condition and 1,642 in dynamic condition. The displacements vary; for non-loaded static condition the displacement is  $2,215 \times 10^{-3}$  m, the non-loaded dynamic condition is 0,6680 m, the loaded static condition is 0,01497 m, and the loaded dynamic condition is 0,6689 m. The Model c modelling output for non-loaded static condition is as shown in Figure 5.26 below.

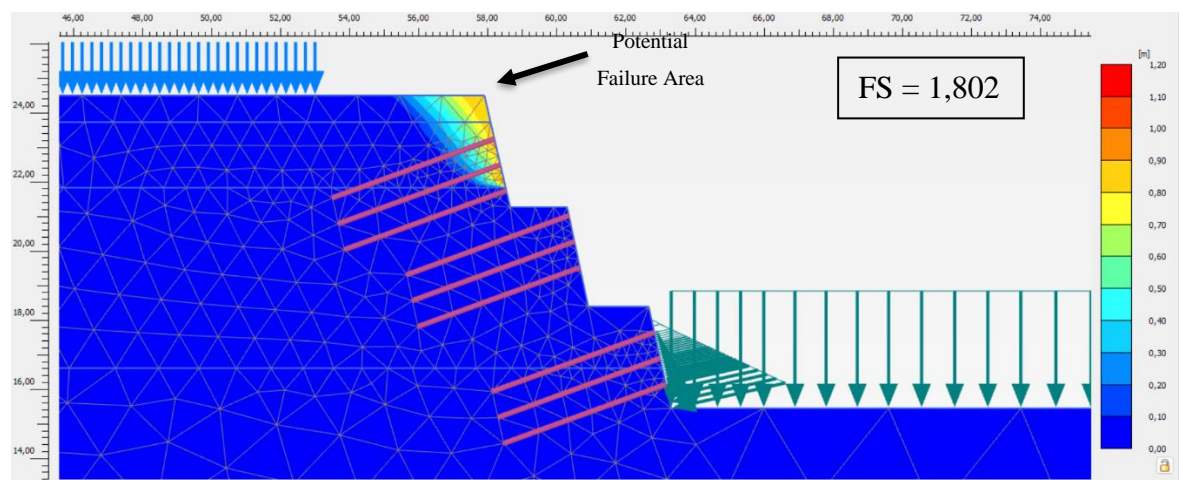


**Figure 5.26 Model c Non-Loaded Static Potential Failure Area Output**



The Model c modelling output for non-loaded dynamic condition is as shown in Figures 5.27 below.

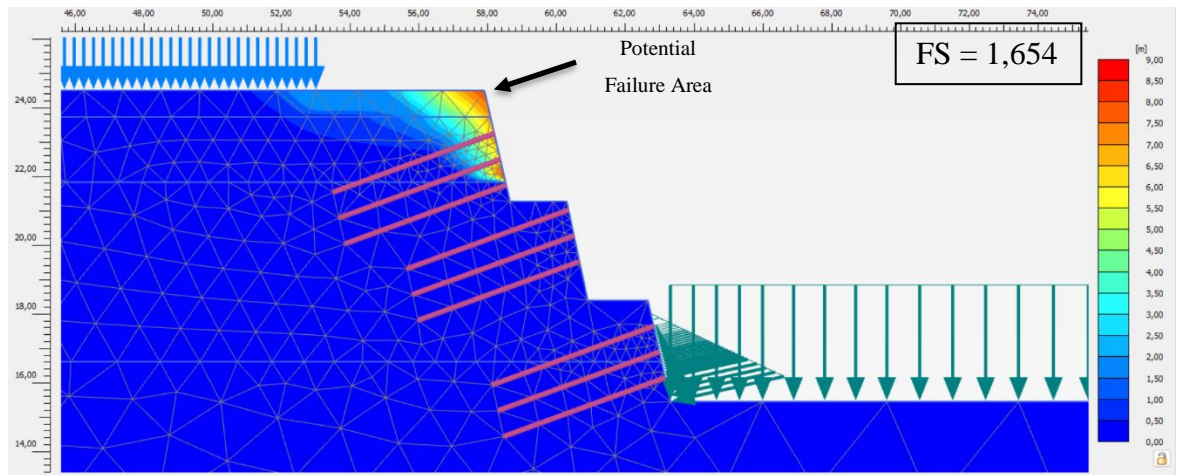


**Figure 5.27 Model c Non-Loaded Dynamic Potential Failure Area Output**

The Model c modelling output for loaded static condition is as shown in Figure 5.28 below.

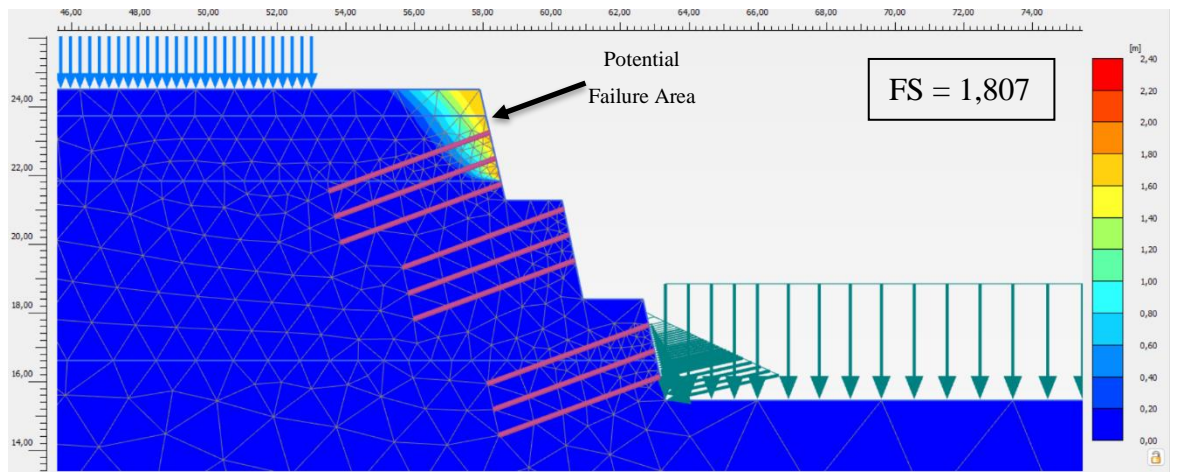


**Figure 5.28 Model c Loaded Static Potential Failure Area Output**

The Model c modelling output for loaded dynamic condition is as shown in Figure 5.29 below.

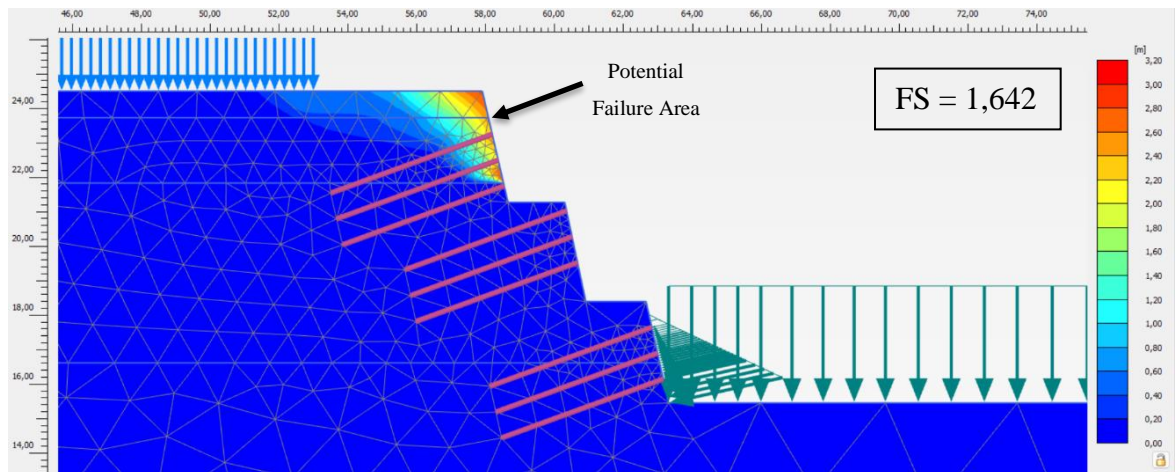


**Figure 5.29 Model c Loaded Dynamic Potential Failure Area Output**

The non-loaded static and non-loaded dynamic experience a drop in FS from 1,802 to 1,654, meaning the earthquake load impact is quite significant. Meanwhile, the drop of FS from loaded static to loaded dynamic is slightly bigger from 1,807 to 1,642, meaning the traffic load combined with earthquake load has bigger impact towards FS. The FS between non-loaded and loaded static increases by 0,005, a value that is not significant. Lastly, the FS drops from non-loaded to loaded dynamic.

#### 4) Model d

The third modification for slope reinforcement at STA 7+300 of Tawang-Ngalang Road and Bridge Project is soil nailing with the length of 5 meters, nail inclination of 20°, and vertical spacing of 1,5 meters. The FS for non-loaded condition is 1,917 in static condition and 1,610 in dynamic condition. Meanwhile, for loaded condition, the FS is 1,789 in static condition and 1,680 in dynamic condition. The displacements vary; for non-loaded static condition the displacement is  $2,167 \times 10^{-3}$  m, the non-loaded dynamic condition is 0,6586 m, the loaded static

condition is 0,01497 m, and the loaded dynamic condition is 0,6567 m. The Model d modelling output for non-loaded static condition is as shown in Figure 5.30 below.

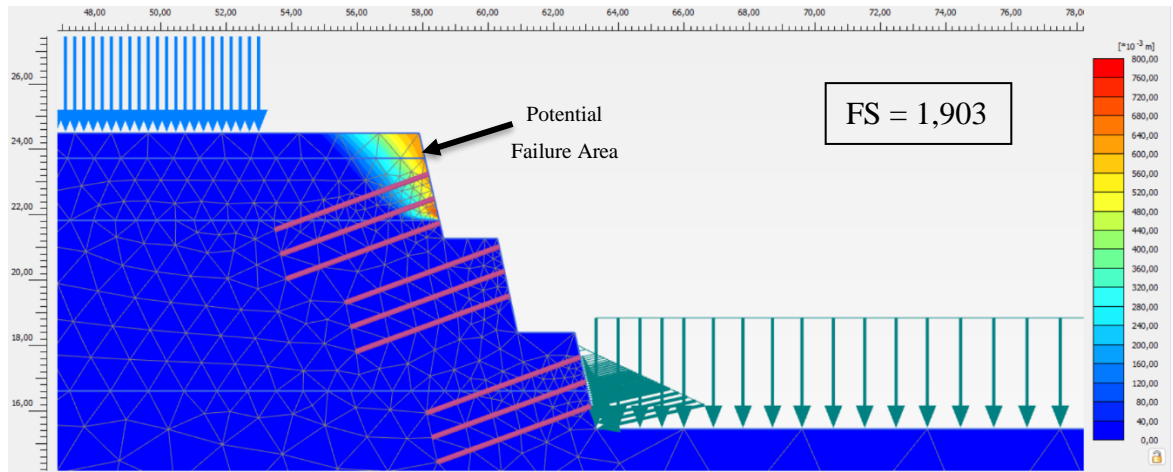


**Figure 5.30 Model d Non-Loaded Static Potential Failure Area Output**

The Model d modelling output for non-loaded dynamic condition is as shown in Figure 5.31 below.

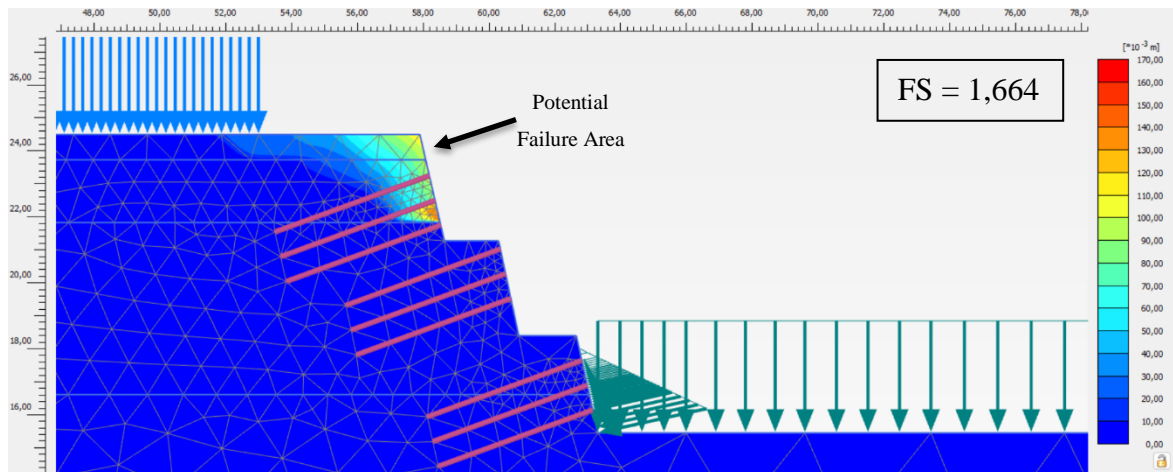


**Figure 5.31 Model d Non-Loaded Dynamic Potential Failure Area Output**

The Model d modelling output for loaded static condition is as shown in Figure 5.32 below.

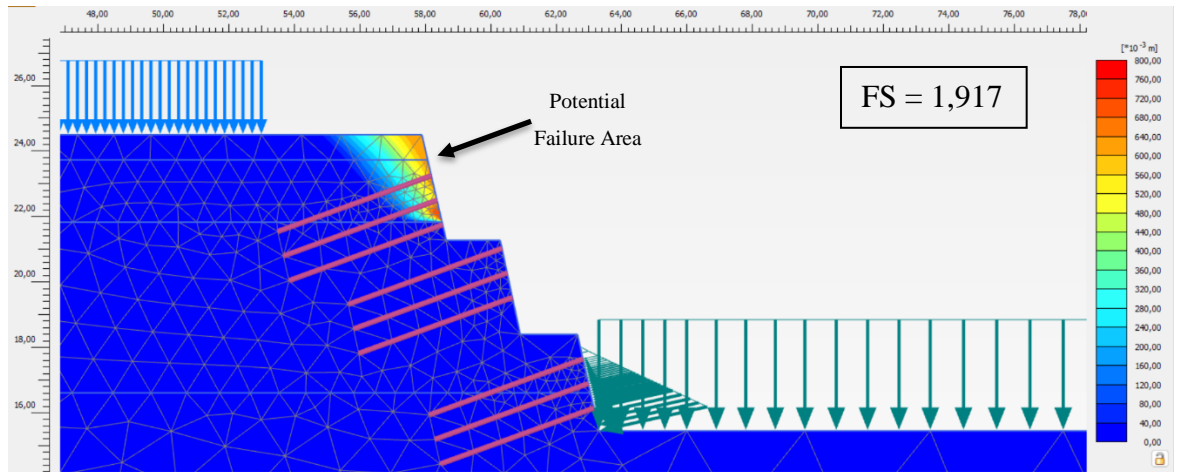


**Figure 5.32 Model d Loaded Static Potential Failure Area Output**

The Model d modelling output for loaded dynamic condition is as shown in Figures 5.33 below.

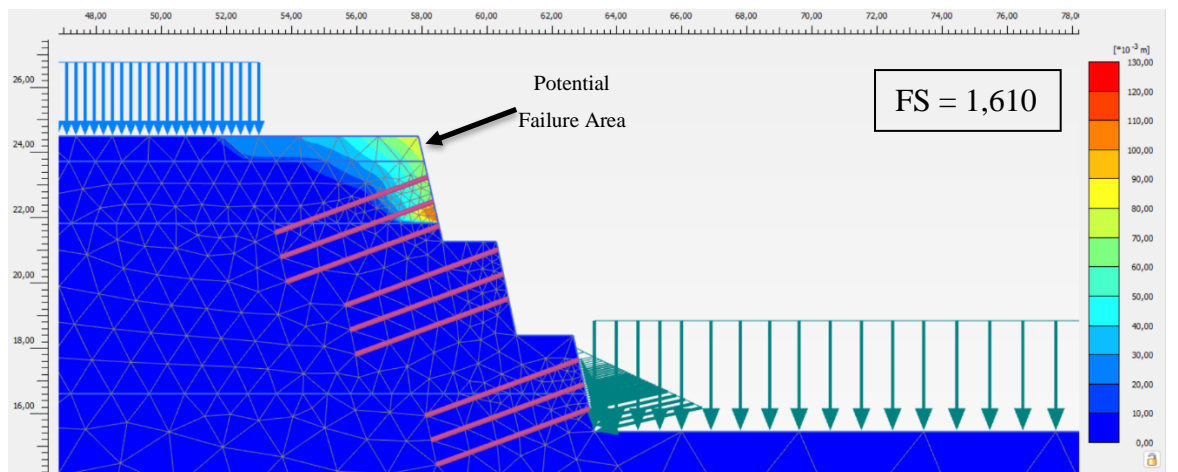


**Figure 5.33 Model d Loaded Dynamic Potential Failure Area Output**

The illustrations indicate a significant increase of FS across all phases compared to the former models. The non-loaded static and non-loaded dynamic experience slight drop in FS from 1,903 to 1,664, meaning the earthquake load impact of 0,2 g is significant. Meanwhile, the drop of FS from loaded static to

loaded dynamic is bigger from 1,917 to 1,610, meaning the traffic load combined with earthquake has significant impact towards FS. The FS between non-loaded and loaded static only increases by 0,014, a number that is not significant. The FS between non-loaded and loaded dynamic condition drops by 0,054, not very significant.

#### 5) Model e

The fourth modification for slope reinforcement at STA 7+300 of Tawang-Ngalang Road and Bridge Project is soil nailing with the length of 5 meters, nail inclination of  $50^\circ$ , and vertical spacing of 2,5 meters. The FS for non-loaded condition is 1,653 in static condition and 1,577 in dynamic condition. Meanwhile, for loaded condition, the FS is 1,660 in static condition and 1,576 in dynamic condition. The displacements vary; for non-loaded static condition the displacement is  $1,811 \times 10^{-3}$  m, the non-loaded dynamic condition is 0,6502 m, the loaded static condition is 0,01497 m, and the loaded dynamic condition is 0,6477 m. The Model e modelling output for non-loaded static condition is as shown in Figure 5.34 below.

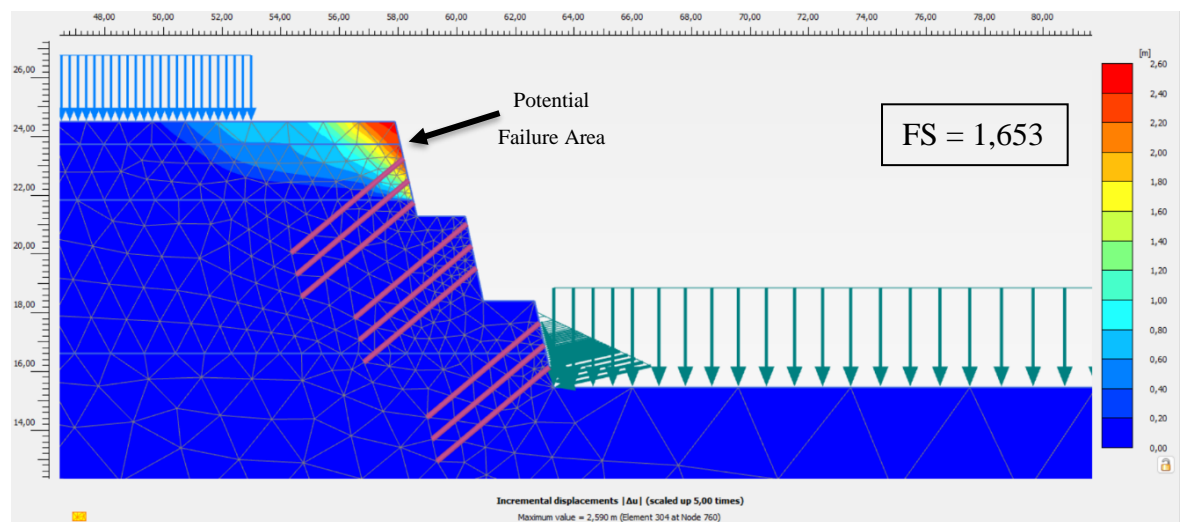


**Figure 5.34 Model e Non-Loaded Static Potential Failure Area Output**



The Model e modelling output for non-loaded dynamic condition is as shown in Figure 5.35 below.

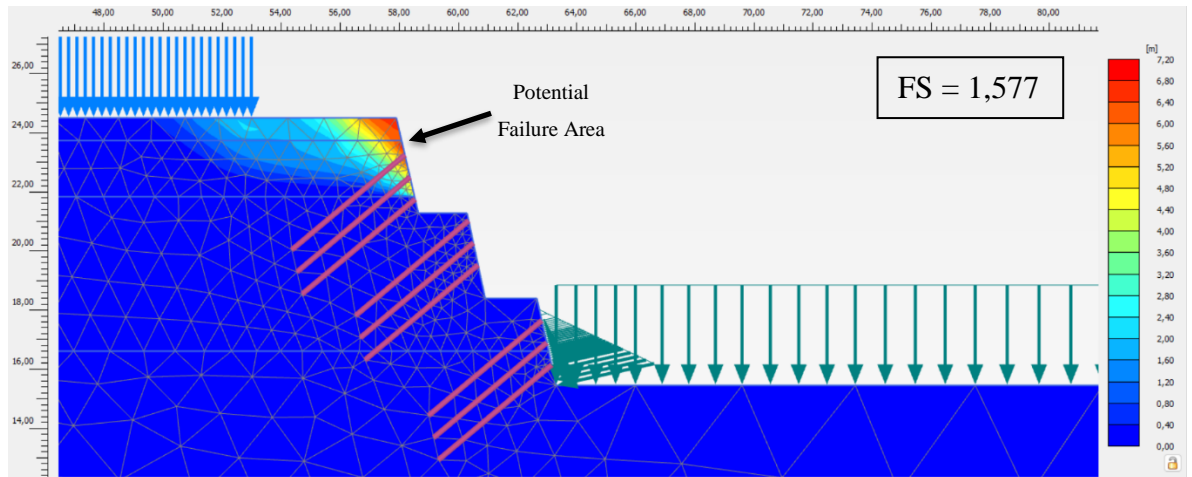


**Figure 5.35 Model e Non-Loaded Dynamic Potential Failure Area Output**

The Model e modelling output for loaded static condition is as shown in Figure 5.36 below.

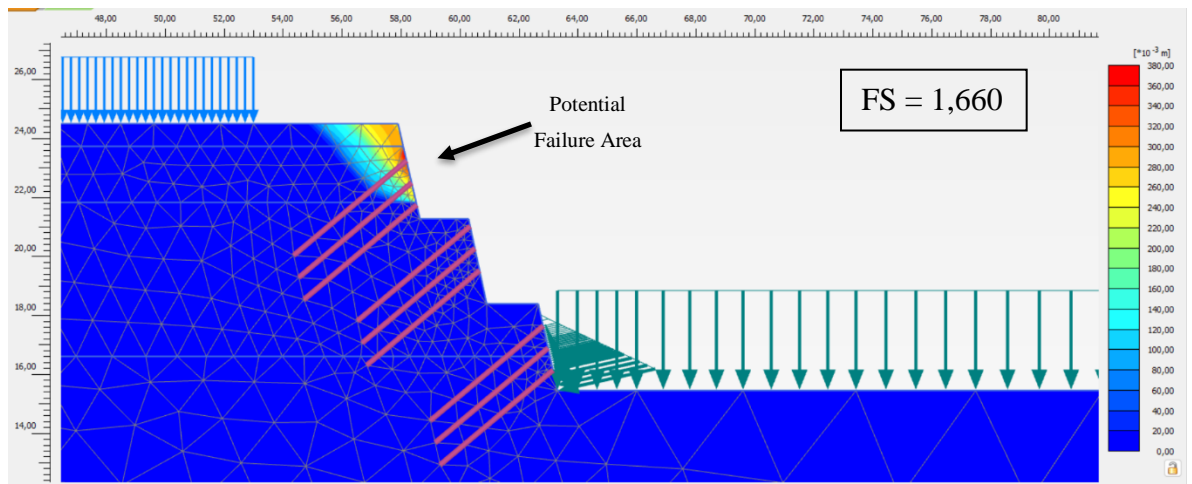


**Figure 5.36 Model e Loaded Static Potential Failure Area Output**

The Model e modelling output for loaded dynamic condition is as shown in Figure 5.37 below.

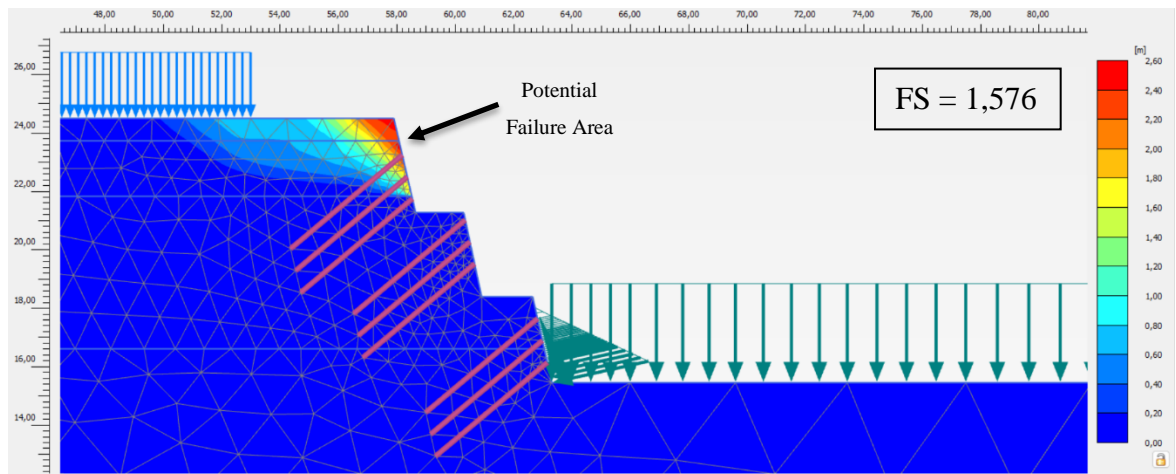


**Figure 5.37 Model e Loaded Dynamic Potential Failure Area Output**

The illustrations indicate a significant drop of FS across all phases compared to Model b, c, and d. The non-loaded static and non-loaded dynamic experience a slight drop in FS from 1,653 to 1,557, meaning the earthquake load impact is not significant. Meanwhile, the drop of FS from loaded static to loaded dynamic is slightly bigger from 1,660 to 1,576, meaning the traffic load combined with earthquake load has bigger impact towards FS. The FS between non-loaded and loaded static only increases by 0,007, indicating that traffic loading alone is not significant. However, the non-loaded and loaded dynamic FS drops by 0,084, quite significant.

6) Model f

The fifth modification for slope reinforcement at STA 7+300 of Tawang-Ngalang Road and Bridge Project is soil nailing with the length of 5 meters, nail inclination of  $50^\circ$ , and vertical spacing of 1,5 meters. The FS for non-loaded condition is 1,768 in static condition and 1,667 in dynamic condition. Meanwhile, for loaded condition, the FS is 1,740 in static condition and 1,679 in dynamic condition. The displacements vary; for non-loaded static condition the displacement

is  $1,765 \times 10^{-3}$  m, the non-loaded dynamic condition is 0,6487 m, the loaded static condition is 0,01497 m, and the loaded dynamic condition is 0,6462 m. The Model f modelling output for non-loaded static condition is as shown in Figure 5.38 below.

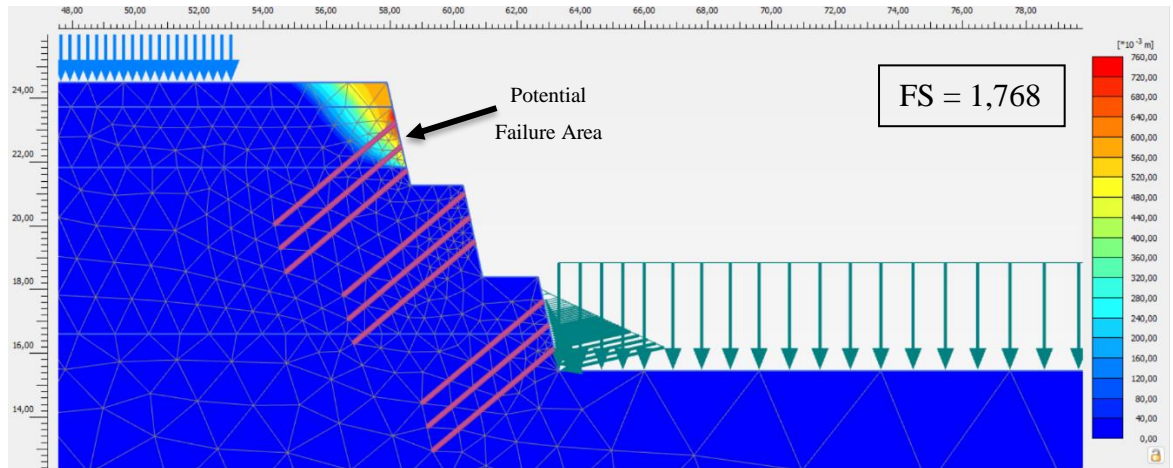


**Figure 5.38 Model f Non-Loaded Static Potential Failure Area Output**

The Model f modelling output for non-loaded dynamic condition is as shown in Figure 5.39 below.

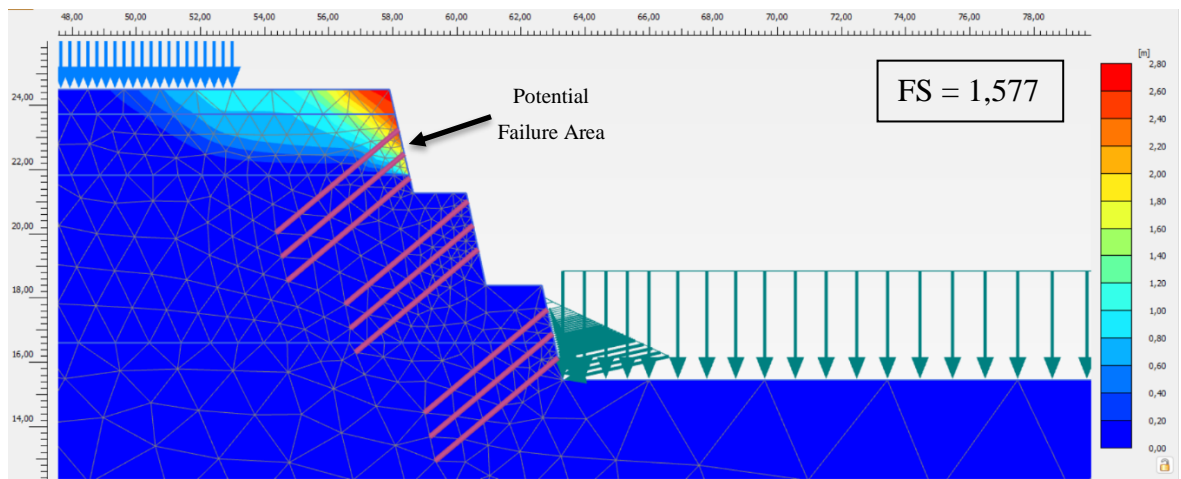


**Figure 5.39 Model f Non-Loaded Dynamic Potential Failure Area Output**



The Model f modelling output for loaded static condition is as shown in Figure 5.40 below.

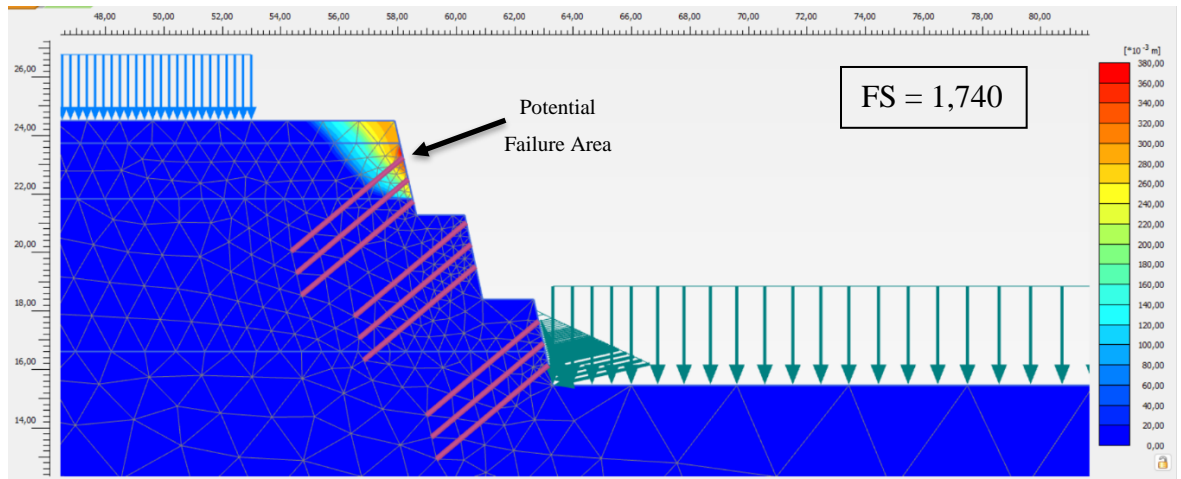


**Figure 5.40 Model f Loaded Static Potential Failure Area Output**

The Model f modelling output for loaded dynamic condition is as shown in Figure 5.41 below.

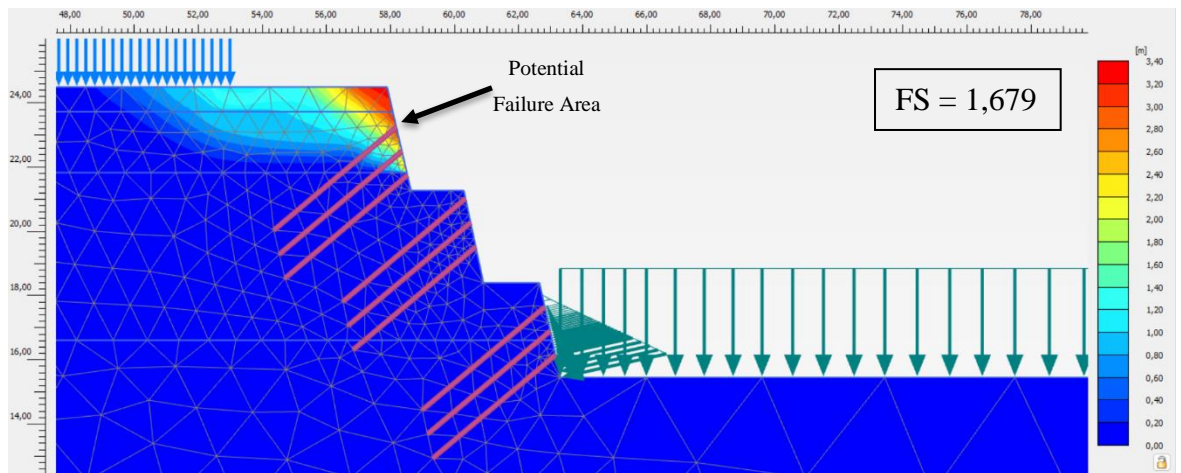


**Figure 5.41 Model f Loaded Dynamic Potential Failure Area Output**

The illustrations indicate a significant increase of FS from Model e. The non-loaded static and non-loaded dynamic experience a significant drop in FS from 1,768 to 1,577, meaning the earthquake load impact is quite significant. Meanwhile,

the FS from loaded static to loaded dynamic increases from 1,740 to 1,679, a number that is not significant, meaning in loaded condition, earthquake loading is not very impactful. The FS between non-loaded and loaded static only drops by 0,028, indicating that traffic loading alone is not significant. However, non-loaded and loaded dynamic FS increases, albeit insignificantly.

#### 7) Model g

The sixth modification for slope reinforcement at STA 7+300 of Tawang-Ngalang Road and Bridge Project is soil nailing with the length of 4,5 meters, nail inclination of  $20^\circ$ , and vertical spacing of 2,5 meters. The FS for non-loaded condition is 1,807 in static condition and 1,651 in dynamic condition. Meanwhile, for loaded condition, the FS is 1,812 in static condition and 1,649 in dynamic condition. The displacements vary; for non-loaded static condition the displacement is  $2,058 \times 10^{-3}$  m, the non-loaded dynamic condition is 0,6735 m, the loaded static condition is 0,01497 m, and the loaded dynamic condition is 0,6715 m. The Model g modelling output for non-loaded static condition is as shown in Figure 5.42 below.

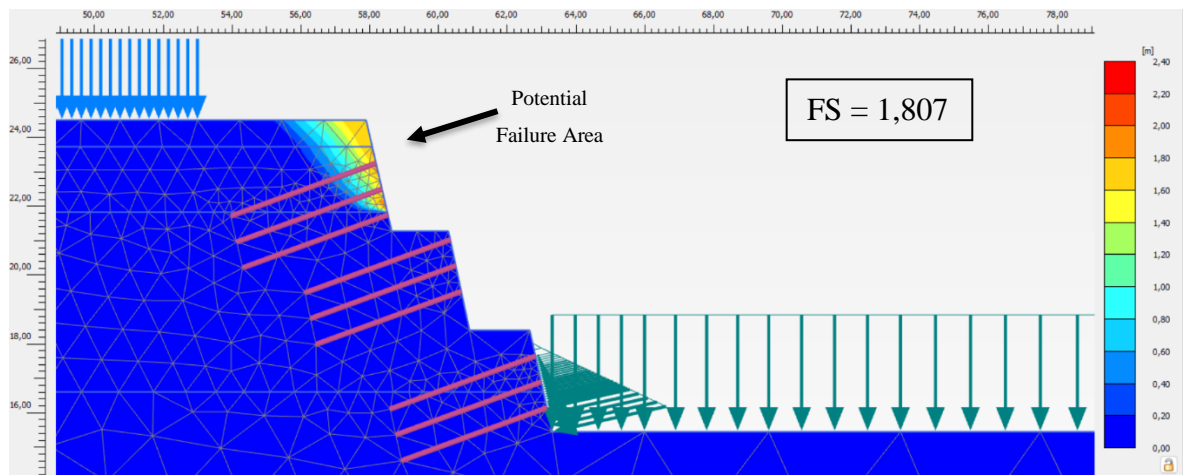


**Figure 5.42 Model g Non-Loaded Static Potential Failure Area Output**

The Model g modelling output for non-loaded dynamic condition is as shown in Figure 5.43 below.

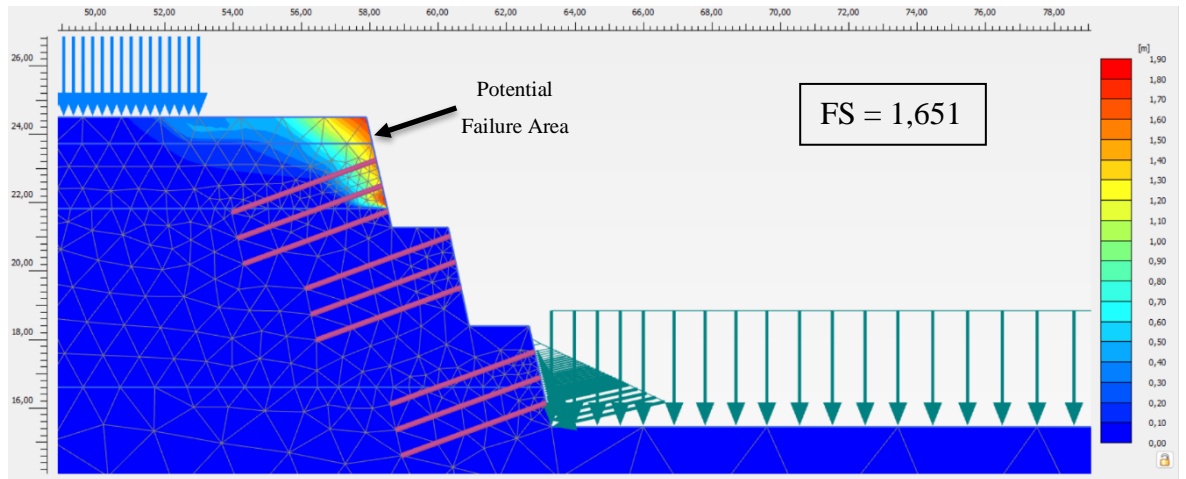


**Figure 5.43 Model g Non-Loaded Dynamic Potential Failure Area Output**

The Model g modelling output for loaded static condition is as shown in Figure 5.44 below.

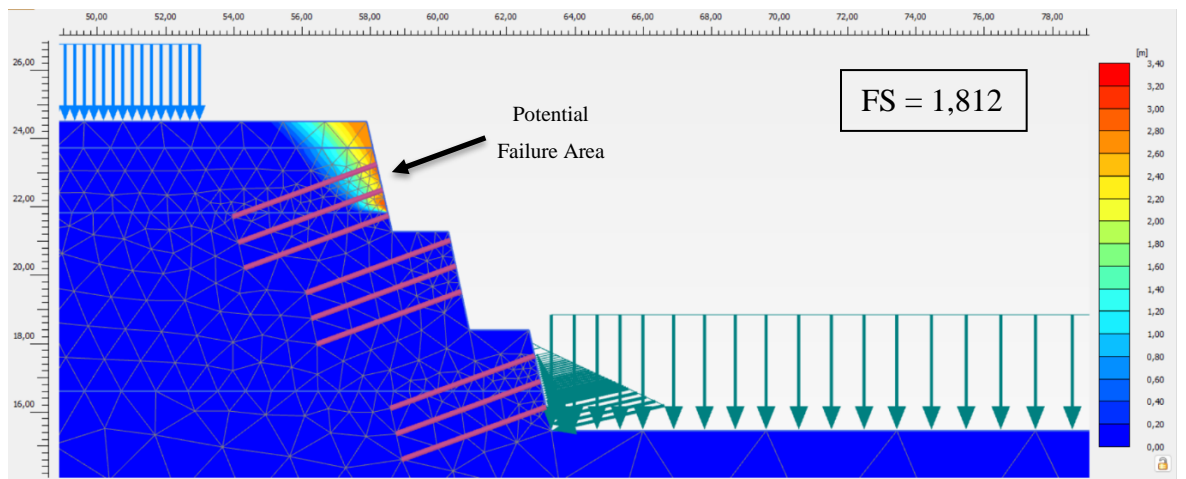


**Figure 5.44 Model g Loaded Static Potential Failure Area Output**

The Model g modelling output for loaded dynamic condition as shown in Figure 5.45 below.

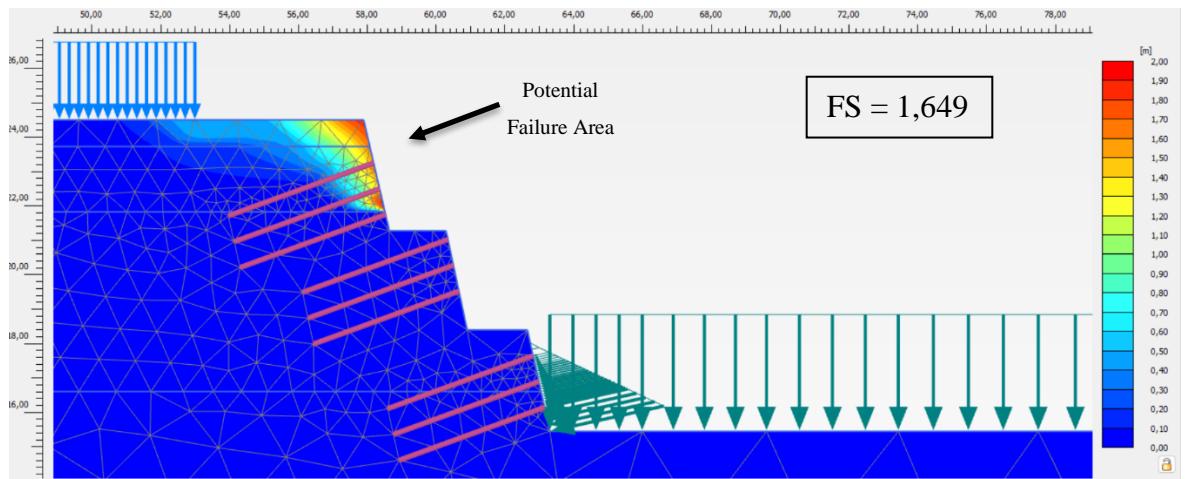


**Figure 5.45 Model g Loaded Dynamic Potential Failure Area Output**

The illustrations indicate a slight increase of FS compared to Model f. The non-loaded static and non-loaded dynamic experience a significant drop in FS from 1,807 to 1,651, meaning the earthquake load impact is significant. Meanwhile, the drop of FS from loaded static to loaded dynamic is similar from 1,812 to 1,649, meaning the traffic load combined with earthquake load has similar impact towards FS. The FS between non-loaded and loaded static only increases by 0,005, indicating that traffic loading alone is not significant. The non-loaded and loaded dynamic FS decreases very slightly.

#### 8) Model h

The seventh modification for slope reinforcement at STA 7+300 of Tawang-Ngalang Road and Bridge Project is soil nailing with the length of 4,5 meters, nail inclination of 20°, and vertical spacing of 1,5 meters. The FS for non-loaded condition is 1,924 in static condition and 1,557 in dynamic condition. Meanwhile, for loaded condition, the FS is 1,929 in static condition and 1,558 in dynamic condition. The displacements vary; for non-loaded static condition the displacement is  $2,014 \times 10^{-3}$  m, the non-loaded dynamic condition is 0,6594 m, the loaded static

condition is 0,01497 m, and the loaded dynamic condition is 0,6579 m. The Model h modelling output for non-loaded static condition is as shown in Figure 5.46 below.

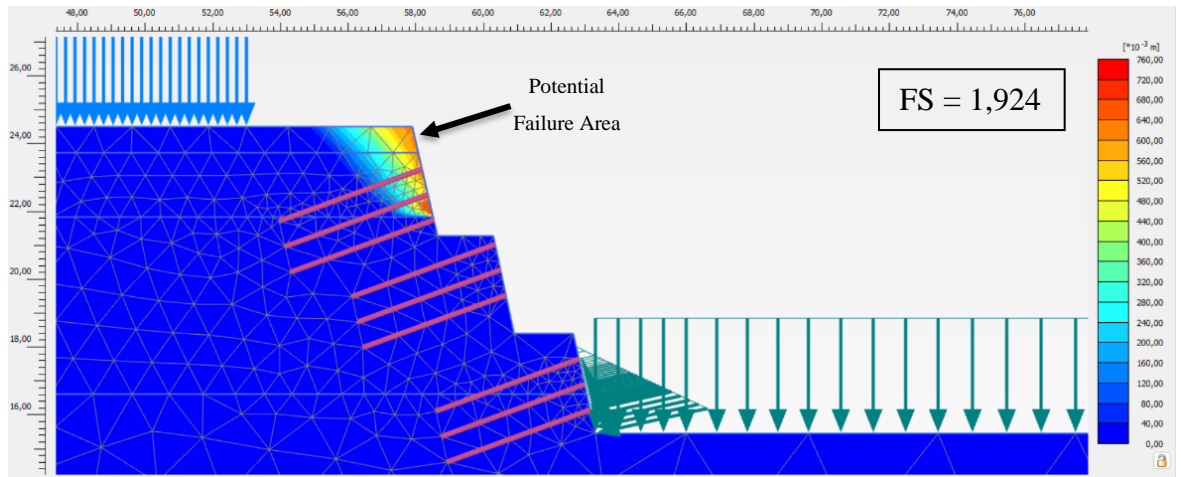


**Figure 5.46 Model h Non-Loaded Static Potential Failure Area Output**

The Model h modelling output for non-loaded dynamic condition is as shown in Figure 5.47 below.

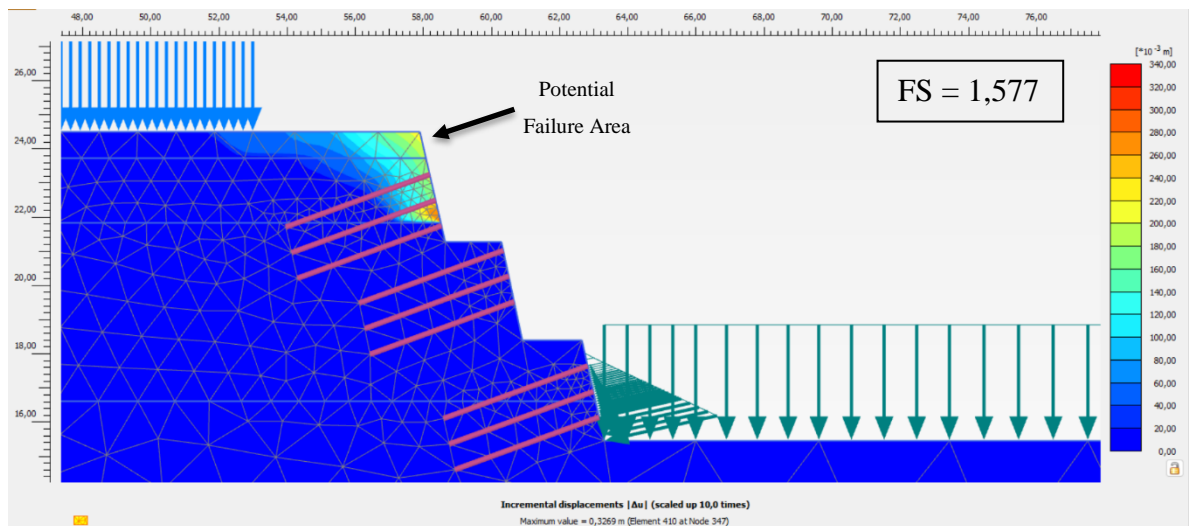


**Figure 5.47 Model h Non-Loaded Dynamic Potential Failure Area Output**

The Model h modelling output for loaded static condition is as shown in Figure 5.48 below.

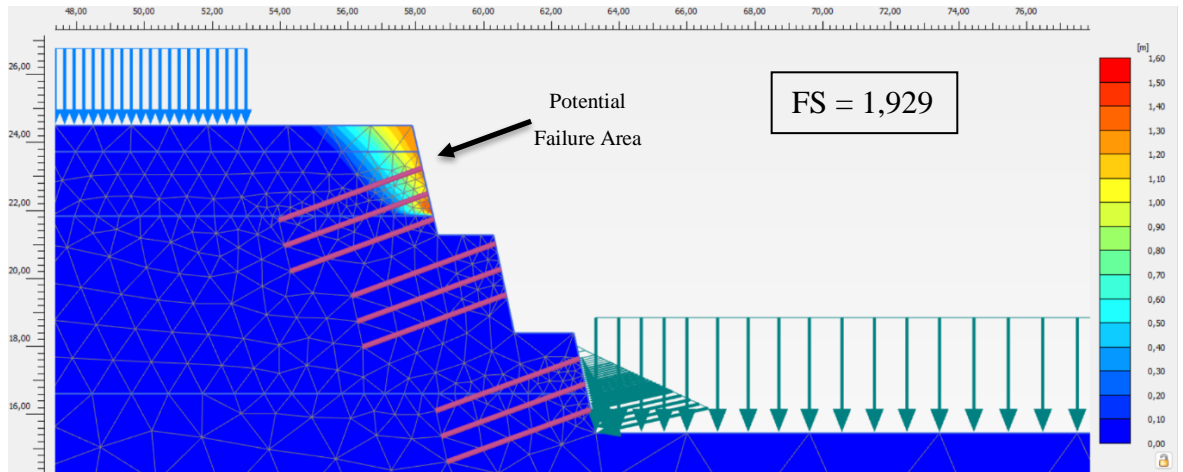


**Figure 5.48 Model h Loaded Static Potential Failure Area Output**

The Model h modelling output for loaded dynamic condition is as shown in Figure 5.49 below.

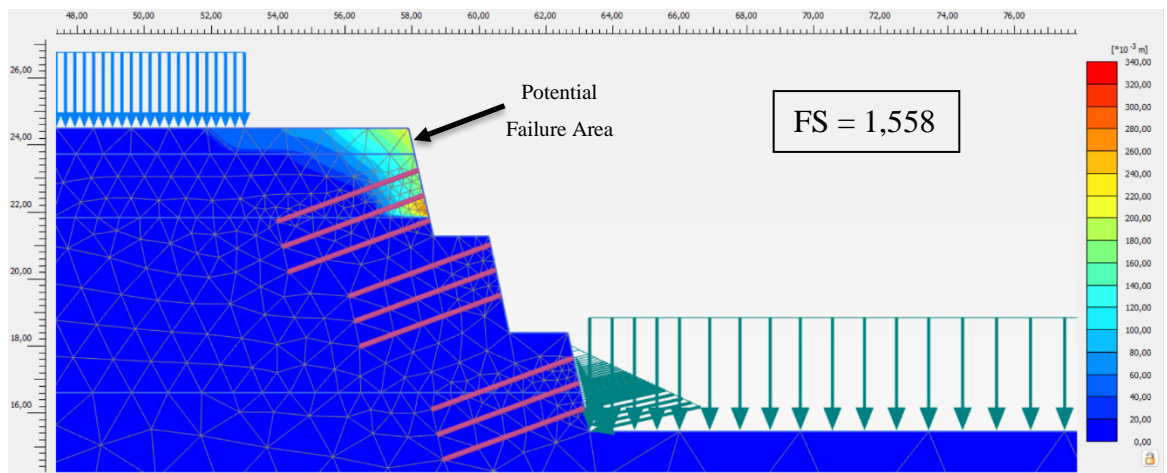


**Figure 5.49 Model h Loaded Dynamic Potential Failure Area Output**

The non-loaded static and non-loaded dynamic FS drops from 1,924 to 1,577. So does the loaded static to loaded dynamic FS. The FS from non-loaded and loaded static increases by 0,005, so traffic loading alone is not significant.



### 5.3.4 Recapitulation of Modelling Results using PLAXIS V20

Below is the recapitulation of the models above, specifically for Factor of Safety.

**Table 5.10 Recapitulation of Modelling Results for Factor of Safety using PLAXIS V20**

Factor of Safety Type	Non-reinforced Slope	Reinforced Slope							
		Model a	Model b	Model c	Model d	Model e	Model f	Model g	Model h
Non-Loaded Static	1,360	1,603	1,809	1,802	1,903	1,653	1,768	1,807	1,924
Loaded Static	1,360	1,600	1,789	1,807	1,917	1,660	1,740	1,812	1,929
Non-Loaded Dynamic	1,057	1,426	1,664	1,654	1,552	1,577	1,667	1,651	1,557
Loaded Dynamic	1,057	1,386	1,680	1,642	1,610	1,576	1,679	1,649	1,558

Below is the recapitulation of the models in subchapter 5.3.3, specifically for Displacement.

**Table 5.11 Recapitulation of Modelling Results for Displacement using PLAXIS V20**

Displacement Type	Non-reinforced Slope (m)	Reinforced Slope							
		Model a (m)	Model b (m)	Model c (m)	Model d (m)	Model e (m)	Model f (m)	Model g (m)	Model h (m)
Non-Loaded Static	$0,3010 \times 10^{-3}$	$2,078 \times 10^{-3}$	$1,965 \times 10^{-3}$	$2,215 \times 10^{-3}$	$2,167 \times 10^{-3}$	$1,811 \times 10^{-3}$	$1,765 \times 10^{-3}$	$2,058 \times 10^{-3}$	$2,014 \times 10^{-3}$
Loaded Static	0,01497	0,01496	0,01497	0,01497	0,01497	0,01497	0,01497	0,01497	0,01497
Non-Loaded Dynamic	0,6413	0,6742	0,6561	0,6680	0,6586	0,6502	0,6487	0,6735	0,6594
Loaded Dynamic	0,6402	0,6726	0,6540	0,6689	0,6567	0,6477	0,6462	0,6715	0,6579

### 5.3.5 Analysis of Variable Comparison

In subchapter 5.3.2 there are four groups of variable comparison. In this subchapter, based on the results in 5.3.4, the comparisons will be analyzed.

#### a) Group 1

Group 1 compares the inclination variable at 5 meters length and 2,5 meters vertical spacing. The Factor of Safety results for Group 1 are as follows in Table 5.12, and are charted into Figure 5.50.

**Table 5.12 Factor of Safety of Group 1**

Model Name	Soil Nail			Factor of Safety			
	Length (m)	Inclination (°)	Vertical Spacing (m)	Non-Loaded Static	Loaded Static	Non-Loaded Dynamic	Loaded Dynamic
a	5	35	2,5	1,603	1,600	1,426	1,386
c	5	20	2,5	1,802	1,807	1,654	1,642
e	5	50	2,5	1,653	1,660	1,577	1,576

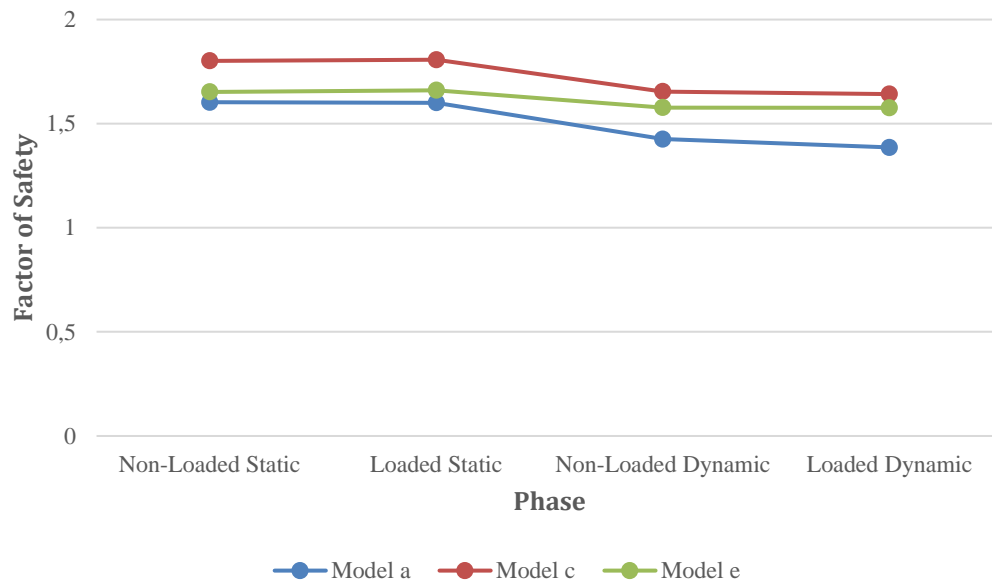


**Figure 5.50 Factor of Safety of Group 1**

The table and figure above show the difference in Factor of Safety for three inclination angles. As can be seen, in general, the Model a with 35° and Model e with 50° inclination have similar results, with 50° giving higher results across all phases. This is to be expected because based on Table 5.10, model a has the



lowest results compared to all the eight other models. The drop of FS from non-loaded static to dynamic and from loaded static to dynamic is less noticeable in 50° compared to 35° inclination. Lastly, the 20° inclination charts the highest FS with 0,1 to 0,2 difference compared to model a and c across all phases.

Then, the displacement results for Group 1 are as follows in Table 5.13 and Figure 5.51.

**Table 5.13 Displacement of Group 1**

Model Name	Soil Nail			Displacement			
	Length (m)	Inclination (°)	Vertical Spacing (m)	Non-Loaded Static (m)	Loaded Static (m)	Non-Loaded Dynamic (m)	Loaded Dynamic (m)
a	5	35	2,5	$2,078 \times 10^{-3}$	0,01497	0,6742	0,6726
c	5	20	2,5	$2,215 \times 10^{-3}$	0,01497	0,6680	0,6689
e	5	50	2,5	$1,811 \times 10^{-3}$	0,01497	0,6502	0,6477

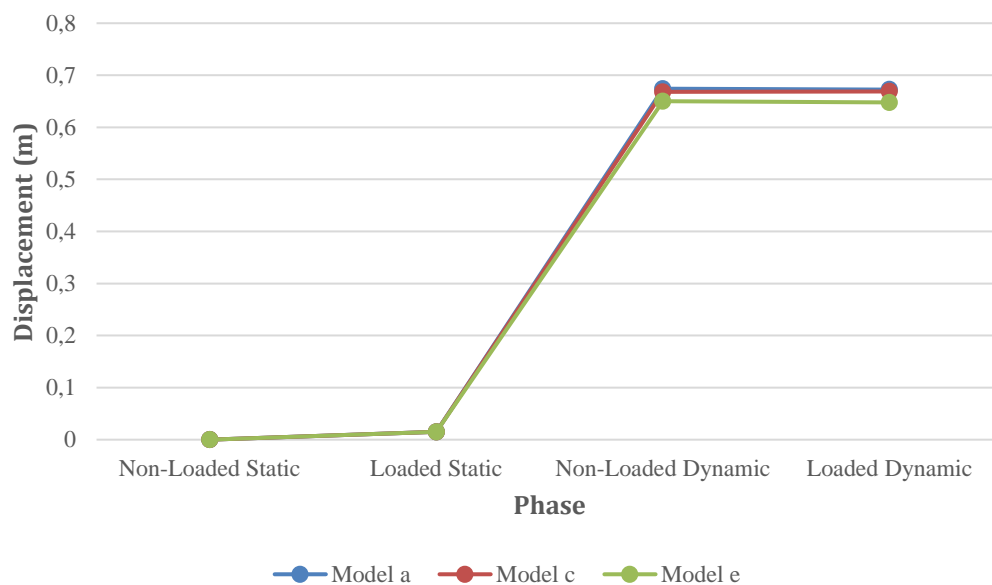


**Figure 5.51 Displacement of Group 1**

The table and figure above show the displacement for three inclination angles. Model e with 50° inclination has the lowest displacement, while Model c with 20° has the highest displacement across all phases. However, since the differences are at 0,025 or less, the comparison of displacement is not that

significant. This is reflected in the graph that shows barely any space between one line and the others.

b) Group 2

Group 2 compares the inclination variable at 5 meters nail length and 1,5 meters vertical spacing. The Factor of Safety results for Group 2 are as shown in Table 5.14 and Figure 5.52 below.

**Table 5.14 Factor of Safety of Group 2**

Model Name	Soil Nail			Factor of Safety			
	Length (m)	Inclination (°)	Vertical Spacing (m)	Non-Loaded Static	Loaded Static	Non-Loaded Dynamic	Loaded Dynamic
b	5	35	1,5	1,809	1,789	1,664	1,680
d	5	20	1,5	1,903	1,917	1,552	1,610
f	5	50	1,5	1,768	1,740	1,667	1,679

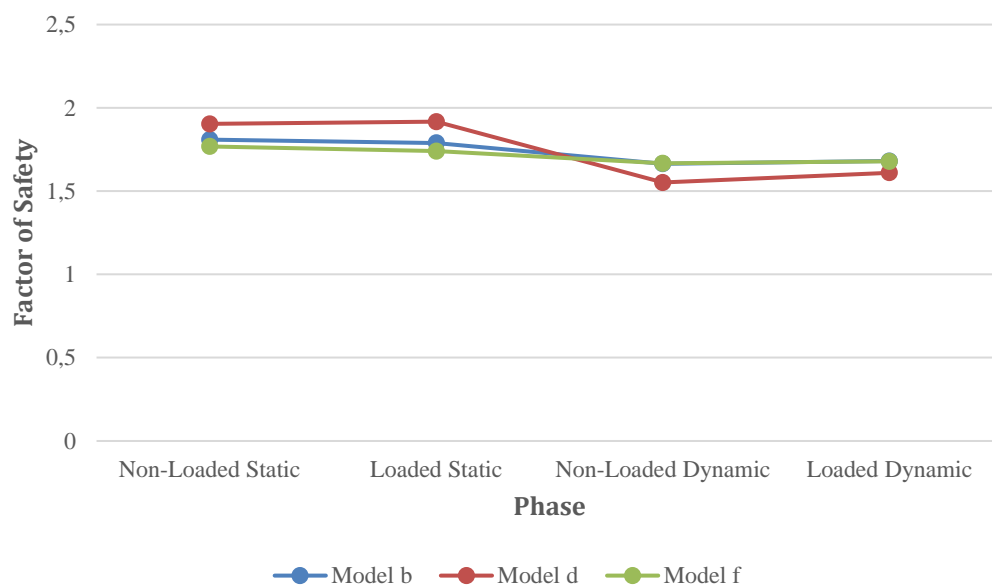


**Figure 5.52 Factor of Safety of Group 2**

The table and figure above show that for 1,5 meters vertical spacing, the 20° inclination achieves highest FS for static condition, but the dynamic FS under earthquake loading drops more than the 35° and 50°. However, since all vales are above the targeted FS of 1,5, the condition is not as significant. Once again,

the 50° inclination yields the lowest FS for static conditions, and average FS for dynamic conditions. This means that 20° achieves highest results yet is most affected by earthquake loading, while 35° and 50° are more stable albeit with lower FS.

The displacement results for Group 2 are as follows in Table 5.15.

**Table 5.15 Displacement of Group 2**

Model Name	Soil Nail			Displacement			
	Length (m)	Inclination (°)	Vertical Spacing (m)	Non-Loaded Static (m)	Non-Loaded Dynamic (m)	Loaded Static (m)	Loaded Dynamic (m)
b	5	35	1,5	$1,965 \times 10^{-3}$	0,01497	0,6561	0,6540
d	5	20	1,5	$2,167 \times 10^{-3}$	0,01497	0,6586	0,6567
f	5	50	1,5	$1,765 \times 10^{-3}$	0,01497	0,6487	0,6462

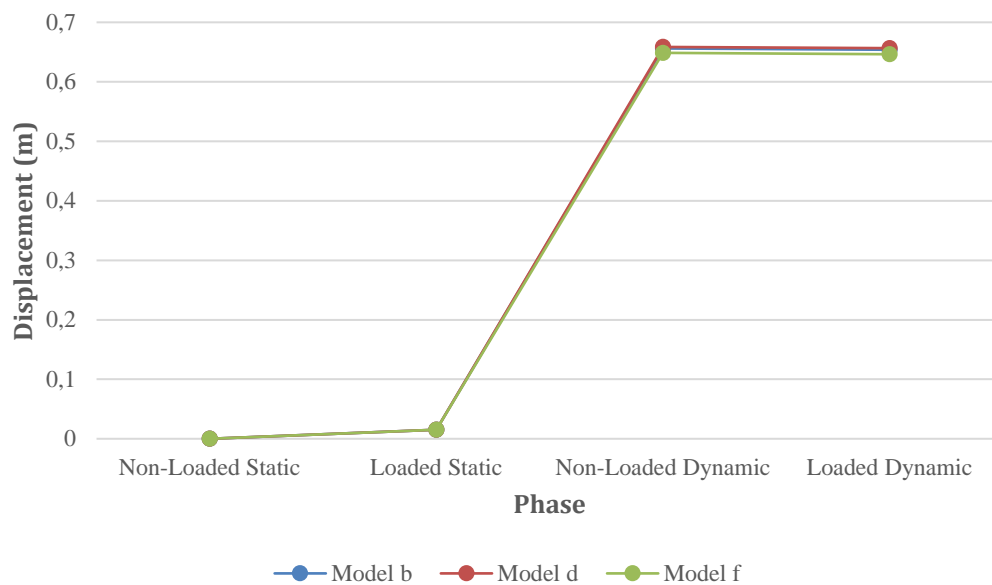


**Figure 5.53 Displacement of Group 2**

In terms of displacement, the 20° inclination once again has the highest displacement, but by small margin, while 50° inclination has the lowest displacement.

The comparison analysis for Factor of Safety of Group 1 and Group 2 is presented below.

**Table 5.16 Factor of Safety Comparison between Group 1 and Group 2**

Model Name	Soil Nail			Factor of Safety			
	Length (m)	Inclination (°)	Vertical Spacing (m)	Non-Loaded Static	Loaded Static	Non-Loaded Dynamic	Loaded Dynamic
Group 1							
a	5	35	2,5	1,603	1,600	1,426	1,386
c	5	20	2,5	1,802	1,807	1,654	1,642
e	5	50	2,5	1,653	1,660	1,577	1,576
Group 2							
b	5	35	1,5	1,809	1,789	1,664	1,680
d	5	20	1,5	1,903	1,917	1,552	1,610
f	5	50	1,5	1,768	1,740	1,667	1,679

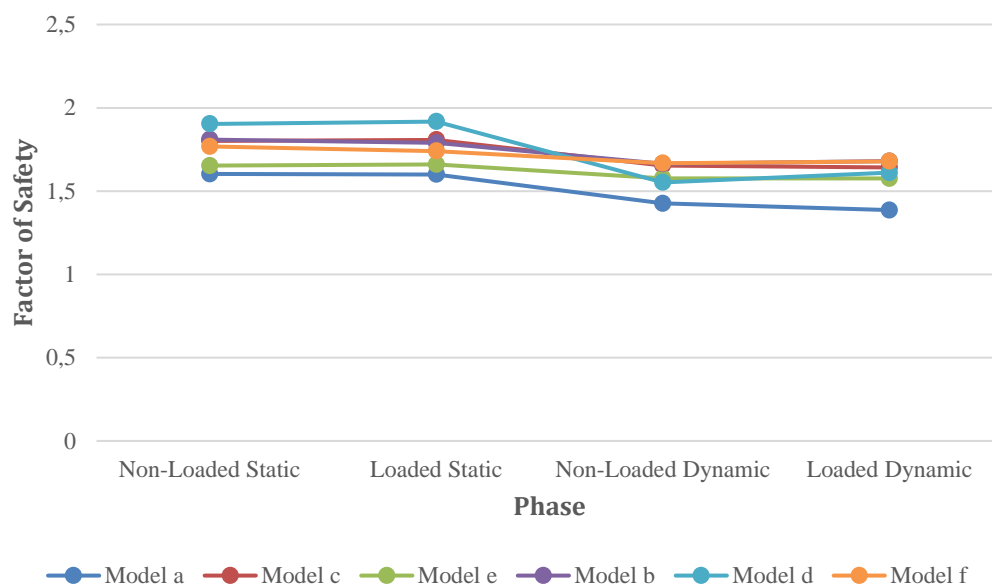


**Figure 5.54 Factor of Safety Comparison between Group 1 and Group 2**

The table and figure above show the 20° inclination yields the highest FS across all phases and spacing. The 50° inclination and the current 35° inclination charts in the middle. The table and figure above also show that for 1,5 meters vertical spacing, the FS is higher across all phases compared to the 2,5 meters as shown in previous section, except for the dynamic phases for Model d.

The comparison analysis for displacement of Group 1 and Group 2 is presented below.

**Table 5.17 Displacement Comparison between Group 1 and Group 2**

Model Name	Soil Nail			Displacement			
	Length (m)	Inclination (°)	Vertical Spacing (m)	Non-Loaded Static (m)	Loaded Static (m)	Non-Loaded Dynamic (m)	Loaded Dynamic (m)
Group 1							
a	5	35	2,5	$2,078 \times 10^{-3}$	0,01496	0,6742	0,6726
c	5	20	2,5	$2,215 \times 10^{-3}$	0,01497	0,6680	0,6689
e	5	50	2,5	$1,811 \times 10^{-3}$	0,01497	0,6502	0,6477
Group 2							
b	5	35	1,5	$1,965 \times 10^{-3}$	0,01497	0,6561	0,6540
d	5	20	1,5	$2,167 \times 10^{-3}$	0,01497	0,6586	0,6567
f	5	50	1,5	$1,765 \times 10^{-3}$	0,01497	0,6487	0,6462

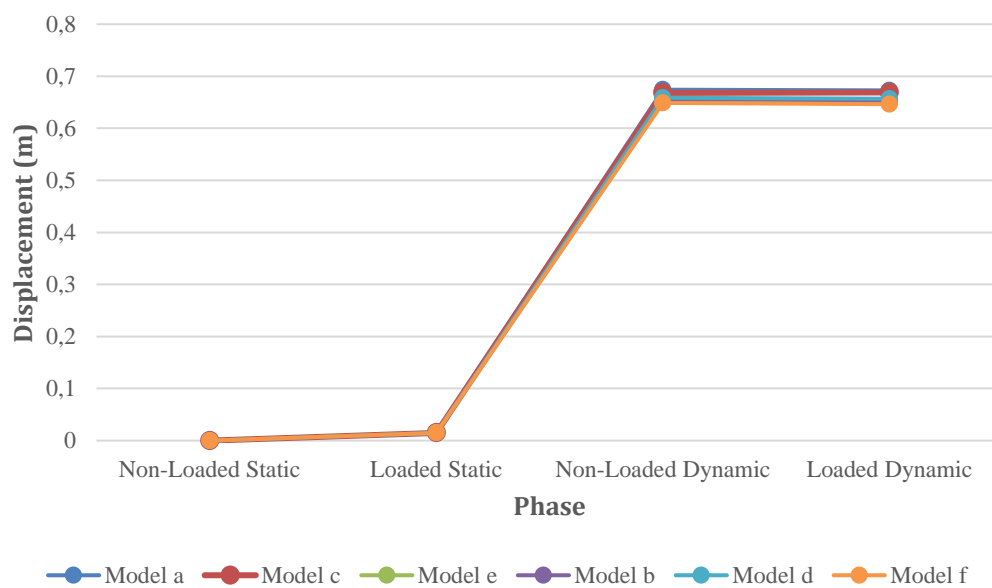


**Figure 5.55 Displacement Comparison between Group 1 and Group 2**

The table and figure show that the 20° inclination has slightly bigger displacement compared to the 35° and 50° inclinations across all phases, however, since the value differences are around 0,001 meters or less, this is not significant. The table and figure above also show that the displacement for 1,5 meter vertical spacing is lower across all phases than 2,5 meter as shown in previous section, this can be observed by comparing Model a displacement that

is bigger than Model b of the same nail length and inclination. This is true for the comparison of Model c to Model d and Model e to Model f.

c) Group 3

Group 3 compares the length variable at 20° inclination and 2,5 meters vertical spacing. The Factor of Safety results for Group 3 are as shown in table and figure below.

**Table 5.18 Factor of Safety of Group 3**

Model Name	Soil Nail			Factor of Safety			
	Length (m)	Inclination (°)	Vertical Spacing (m)	Non-Loaded Static	Loaded Static	Non-Loaded Dynamic	Loaded Dynamic
c	5	20	2,5	1,802	1,807	1,654	1,642
g	4,5	20	2,5	1,807	1,812	1,651	1,649

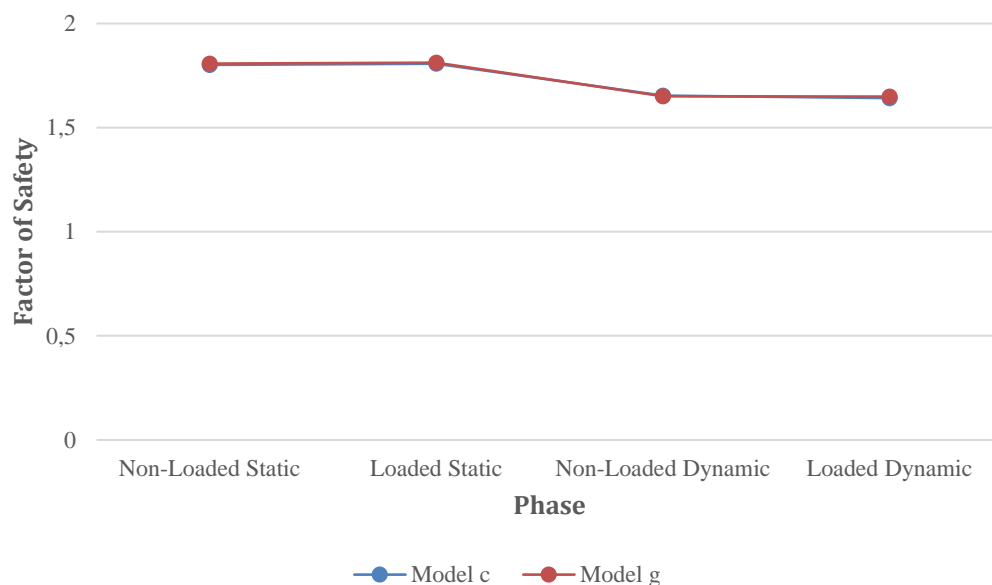


**Figure 5.56 Factor of Safety of Group 3**

Having gauged that the 20° inclination might be the most effective variation, this group compares the decrease of length based on the 20° inclination and 2,5 meters vertical spacing to see if the shorter nail will yield similar results. As can be seen from Table 5.16 and Figure 5.55, both lengths yield similar results. In some cases, the 4,5 meters nail yields higher results, albeit insignificantly.

This means that for 2,5 meters vertical spacing, the shorter nail is still as reliable as the original length of 5 meters, and is still characterized by being affected by earthquake loading for both non-loaded and loaded conditions.

The displacement results for Group 3 are as follows in Table 5.19 and Figure 5.57.

**Table 5.19 Displacement of Group 3**

Model Name	Soil Nail			Displacement			
	Length (m)	Inclination (°)	Vertical Spacing (m)	Non-Loaded Static (m)	Loaded Static (m)	Non-Loaded Dynamic (m)	Loaded Dynamic (m)
c	5	20	2,5	$2,215 \times 10^{-3}$	0,01497	0,6680	0,6689
g	4,5	20	2,5	$2,058 \times 10^{-3}$	0,01497	0,6735	0,6715

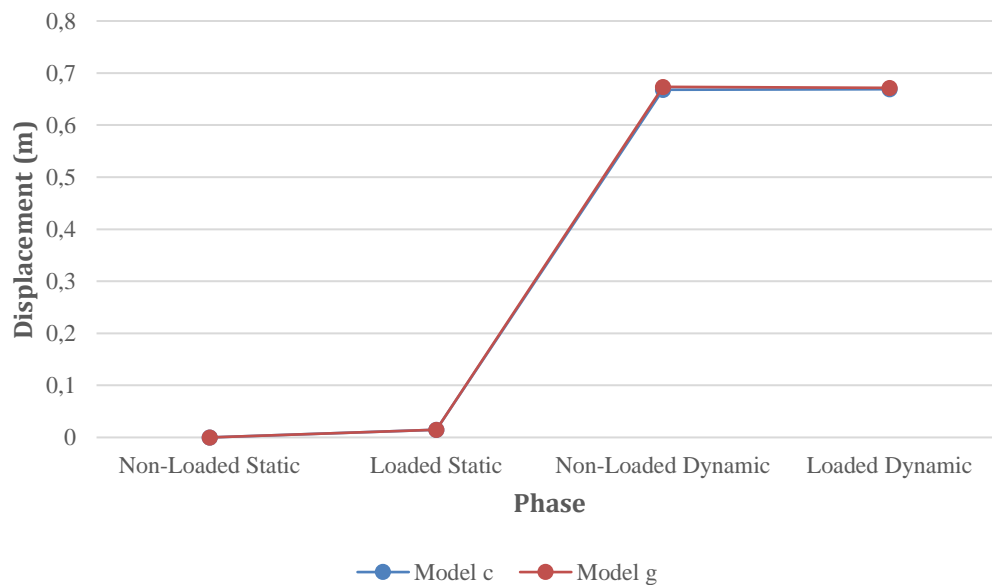


**Figure 5.57 Displacement of Group 3**

The table and figure above show that the displacement values for both models are also similar, with Model g having lower displacements for non-loaded conditions, albeit insignificantly. This means that the shorter nail doesn't equate bigger displacements at 2,5 meters vertical length.

## d) Group 4

Group 4 compares the length variable at 20° inclination and 1,5 meters vertical spacing. The Factor of Safety results for Group 4 are as shown in table and figure below.

**Table 5.20 Factor of Safety of Group 4**

Model Name	Soil Nail			Factor of Safety			
	Length (m)	Inclination (°)	Vertical Spacing (m)	Non-Loaded Static	Loaded Static	Non-Loaded Dynamic	Loaded Dynamic
d	5	20	1,5	1,903	1,917	1,552	1,610
h	4,5	20	1,5	1,924	1,929	1,557	1,558

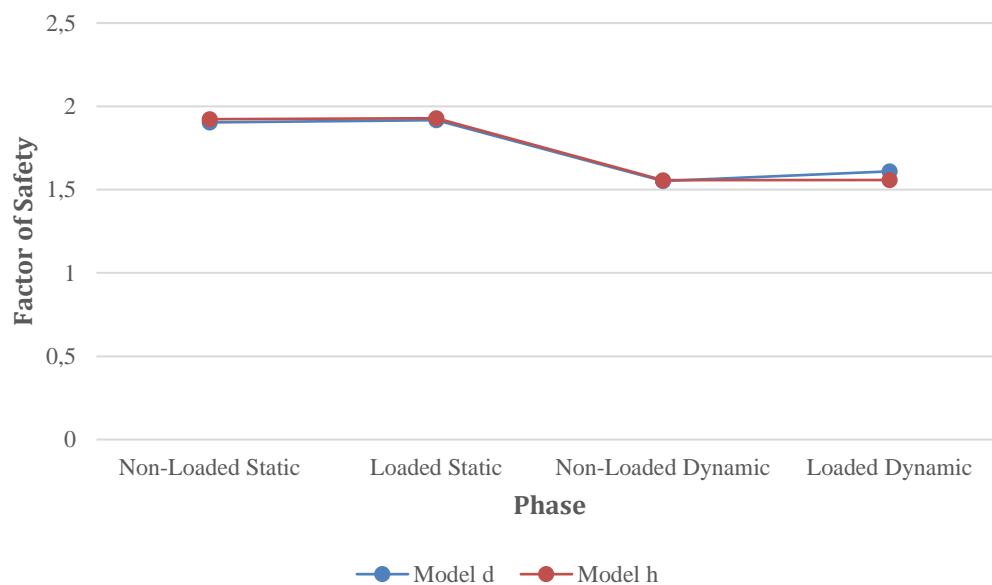


**Figure 5.58 Factor of Safety of Group 4**

The table and figure show, interestingly, that for the first three phases, the 4,5 meters nail yield higher FS compared to the original 5 meters. This doesn't apply to the last phase where earthquake loading is applied along with traffic loading. The drop of FS caused by earthquake loading is quite far, but it is not significant enough to cause any concern, and as such, the 20° inclination and 1,5 meters vertical spacing are justified to be implemented under static and dynamic conditions. This comparison points to 4,5 meters nail length being



more ideal as it costs less in material, and yet still preserves the desired FS to ensure protection from landslide.

The displacement results for Group 4 are as follows in Table 5.19 and Figure 5.58.

**Table 5.21 Displacement of Group 4**

Model Name	Soil Nail			Displacement			
	Length (m)	Inclination (°)	Vertical Spacing (m)	Non-Loaded Static (m)	Loaded Static (m)	Non-Loaded Dynamic (m)	Loaded Dynamic (m)
d	5	20	1,5	$2,167 \times 10^{-3}$	0,01497	0,6586	0,6567
h	4,5	20	1,5	$2,014 \times 10^{-3}$	0,01497	0,6594	0,6579

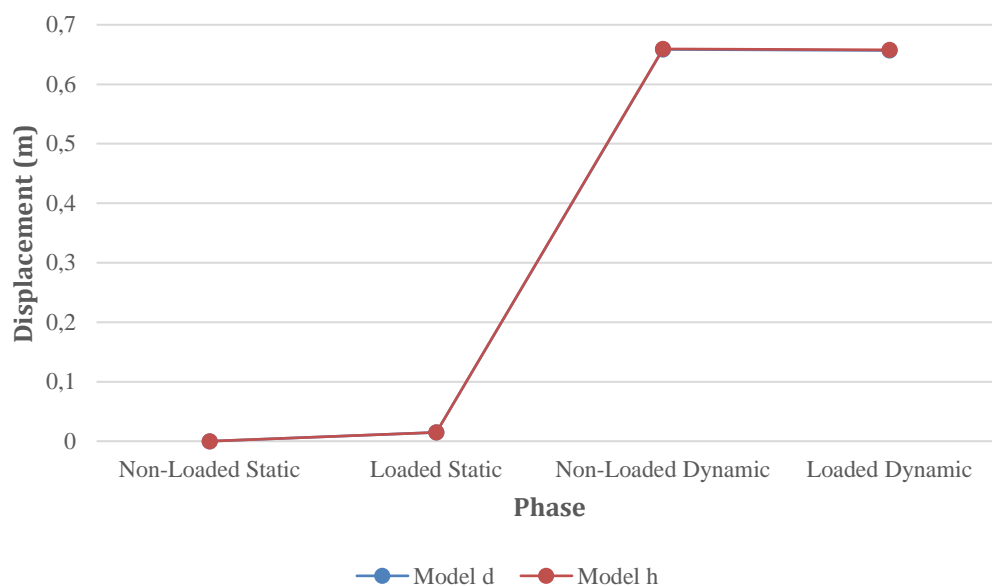


**Figure 5.59 Displacement of Group 4**

The table and figure above show that the 4,5 meters length yields higher displacement in dynamic condition, and very slightly lower displacement in non-loaded static condition. The loaded static displacement, as has been mentioned, refers to the biggest displacement caused by traffic loading at the bottom of the slope. This reinforces the idea that 4,5 meters nail length performs just as well as the 5 meters, ensuring only slightly higher values of

displacement of around 0,002 meter in dynamic conditions, and much less than that for static conditions.

The comparison analysis for Factor of Safety of Group 3 and Group 4 is presented below.

**Table 5.22 Factor of Safety Comparison between Group 3 and Group 4**

Model Name	Soil Nail			Factor of Safety			
	Length (m)	Inclination (°)	Vertical Spacing (m)	Non-Loaded Static	Loaded Static	Non-Loaded Dynamic	Loaded Dynamic
Group 3							
c	5	20	2,5	1,802	1,807	1,654	1,642
g	4,5	20	2,5	1,807	1,812	1,651	1,649
Group 4							
d	5	20	1,5	1,903	1,917	1,552	1,610
h	4,5	20	1,5	1,924	1,929	1,557	1,558

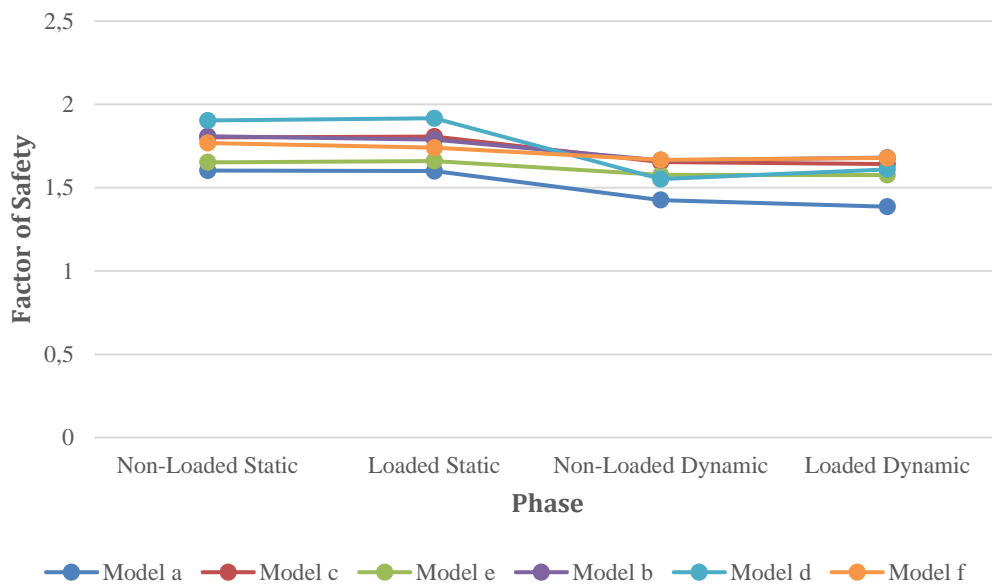


**Figure 5.60 Factor of Safety Comparison between Group 3 and Group 4**

The table and figure above show that the 1,5 meters vertical spacing actually reaches higher FS than 2,5 meters. However, this is accompanied by bigger drops under earthquake loading. The values, however, are not significant to be notable, and as such, 1,5 meters of vertical spacing can still ensure adequate FS across all phases, with or without earthquake and traffic loading.

The comparison analysis for displacement of Group 3 and Group 4 is presented below.

**Table 5.23 Displacement Comparison between Group 3 and Group 4**

Model Name	Soil Nail			Displacement			
	Length (m)	Inclination (°)	Vertical Spacing (m)	Non-Loaded Static (m)	Loaded Static (m)	Non-Loaded Dynamic (m)	Loaded Dynamic (m)
2,5 Meters Vertical Spacing							
c	5	20	2,5	$2,215 \times 10^{-3}$	0,01497	0,6680	0,6689
g	4,5	20	2,5	$2,058 \times 10^{-3}$	0,01497	0,6735	0,6715
1,5 Meters Vertical Spacing							
d	5	20	1,5	$2,167 \times 10^{-3}$	0,01497	0,6586	0,6567
h	4,5	20	1,5	$2,014 \times 10^{-3}$	0,01497	0,6594	0,6579

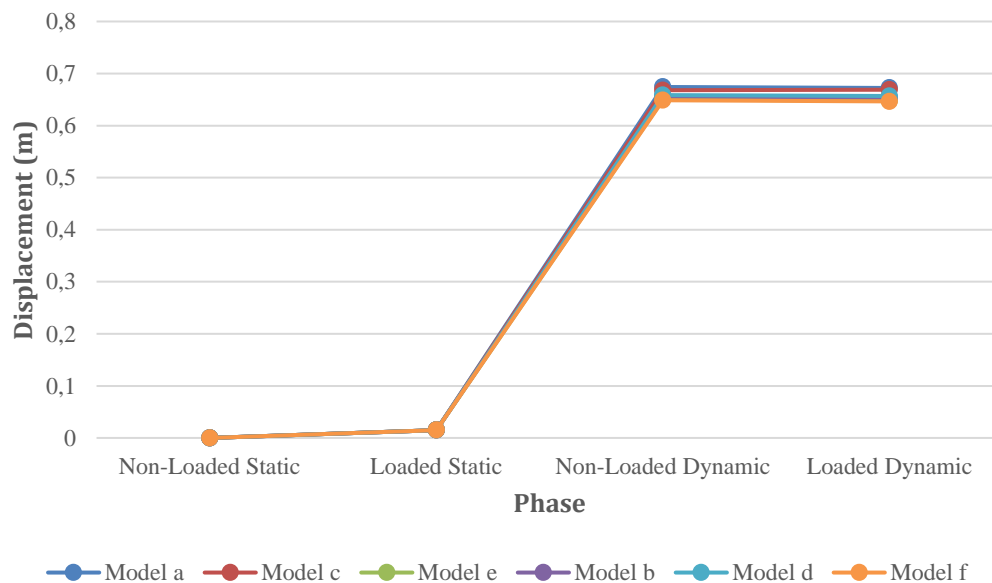


**Figure 5.61 Displacement Comparison between Group 3 and Group 4**

The table and figure show that the displacement for 2,5 meters vertical spacing is slightly bigger compared to the 1,5 meters. This indicates that the 1,5 meters vertical spacing is more effective. Overall, judging from high FS, middle range displacement, and cost-effectiveness, Model h with 4,5 meters nail length, 20° inclination, and 1,5 meters vertical spacing is the most effective compared to all the other models.

## CHAPTER VI

### CONCLUSIONS AND SUGGESTIONS

#### 6.1 CONCLUSIONS

Based on the case study and results provided in Chapter V, several conclusions that can be drawn are as such.

1. The existing slope which has been conditioned holds the Factor of Safety of 1,360 under static loading for non-loaded and loaded condition, as well as 1,057 under dynamic loading for non-loaded and loaded condition. These results indicate slope failure unless reinforced.
2. The current soil nailing-reinforced slope has the nail length of 5 meters, 35° inclination angle, and 2,5 meters vertical spacing. This configuration, called Model a, with Factor of Safety of 1,603 for the non-loaded static condition, 1,426 for non-loaded dynamic condition, 1,600 for the loaded static, and 1,386 for loaded dynamic condition. These results, while still above the standard FS of 1,5 for static condition and is adequate, can still be improved by changing the configuration of the nails. The displacement is  $0,3010 \times 10^{-3}$  meter for the non-loaded static condition, 0,6413 meter for non-loaded dynamic condition, 0,01497 meter for the loaded static, and 0,6402 meter for loaded dynamic condition. These values are not outstanding and may yet be improved still.
3. All the seven models that vary in nail length, inclination angle, and vertical spacing yield higher FS and reasonable displacement difference compared to Model a. The stability indicated by Factor of Safety (FS) in the static condition is the highest at 20° for both 5 meters and 4,5 meters nail length, as well as for 2,5 meters and 1,5 meters nail vertical spacing. The inclination that yields that lowest FS is 50° across all conditions as well. For both 5 meters and 4,5 meters nail length and 35°, 20°, as well as 50° inclination angle, the 1,5 meters vertical spacing yields the higher FS compared to the 2,5 meters. Then, comparing the most optimum 20° inclination with 2,5 meters and 1,5 meters vertical spacing, the 4,5 meters nail length yields slightly higher FS compared to the 5 meters,

still with the most optimum vertical spacing of 1,5 meters. The displacement of non-loaded static condition for 20° is slightly higher than the 35°, while the 50° yields the lowest displacement. The 1,5 meters vertical spacing yields smaller displacement across all models compared to the 2,5 meters. The 5 meters nail length yields bigger displacement compared to the 4,5 meters. Meanwhile, for the loaded static condition with the addition of traffic loading has the same displacement of 0,01497, this is caused by the traffic loading at the bottom of the slope that is identified by the application as bigger than the displacement around the slip surface atop the slope.

4. The earthquake loading decreases the FS across all models, this is also true for the existing slope. The drop in FS is most noticeable for the 20° inclination angle for non-loaded and loaded condition. It is least noticeable in 50° inclination due to lower FS in static condition and average FS for dynamic condition across all models. The 2,5 meters vertical spacing yields lower dynamic FS compared to the 1,5 meters for 35° and 50°, while the 20° yields the opposite result. The 4,5 meters nail length yields the same pattern of results compared to the 5 meters one, with the 20, the 1,5 meters vertical spacing yields lower FS than the 2,5 meters. The displacement for all dynamic conditions is noticeably higher than the static conditions, jumping up to 0,6 meters on average. The traffic loading combined with earthquake loading yield bigger displacement compared to the non-loaded condition, except for Model c with minor difference.

## 6.2 SUGGESTIONS

Based on the study case and modelling, several suggestions that can be given for future analyses are as follows.

1. The next research should model more configurations in terms of soil nail length, inclination, and vertical spacing, especially in terms of cost-effectiveness. Meaning, the model can explore shorter nails relative to the slope slip surface.

2. There needs to be more careful modelling to mitigate the possibilities of outliers, such as a big drop in FS under dynamic loading compared to static loading.
3. PLAXIS 3D may be employed to have a more comprehensive look at the condition for considerations of horizontal spacing, which relates to cost and time effectiveness, as well as safety.

## BIBLIOGRAPHY

- API. (1987). *Recommended Practice for Field Testing Water-based Drilling Fluids*. Washington, D.C.: American Petroleum Institute.
- Arvin, M. R., Ghavami, E., & Motamedi Azari, M. (2021, September 26). *Optimization of nail inclination angle in soil nail walls based on a prevalent limit equilibrium method - indian geotechnical journal*. SpringerLink. <https://link.springer.com/article/10.1007/s40098-021-00574-z>
- Badan Standardisasi Nasional. (2014). *Baja tulangan beton*. SNI 2052:2014. Jakarta.
- Benayoun, F., Boumezerane, D., Bekkouche, S. R., & Ismail, F. (2021, September 8). *Optimization of geometric parameters of soil nailing using response surface methodology - Arabian Journal of Geosciences*. SpringerLink. <https://link.springer.com/article/10.1007/s12517-021-08280-z>
- Bentley Communities. (2022) *Safety Analysis and undrained behaviour*. Safety analysis and undrained behaviour - GeoStudio | PLAXIS Wiki - GeoStudio | PLAXIS - Bentley Communities. <https://communities.bentley.com/products/geotech-analysis/w/wiki/45955/safety-analysis-and-undrained-behaviour#:~:text=Safety%20analysis%20in%20Plaxis%20uses,of%20calculation%20steps%20is%20reached.>
- Bowles, J. (1996). "Special Footings and Beams on Elastic Foundations." Chapter. In *Foundation Analysis and Design Fifth Edition*, 505–505. Singapore: The McGraw-Hill Companies, Inc.
- Budhu, M. (2011). *Soil Mechanics and foundations*. Wiley.
- Cruikshank, K. M. (2002). *Kenneth M. Cruikshank Slope Stability Programs*. Portland State University. <https://web.pdx.edu/~i1kc/programming/slopes/>
- Das, B. M. (1985). *Mekanika Tanah (Prinsip-Prinsip Rekayasa Geoteknis) Jilid I*. Jakarta: Penerbit Erlangga.
- Dazzi, C., & Papa, G. L. (2021, July 4). *A new definition of soil to promote soil awareness, sustainability, security and governance*. International Soil and Water Conservation Research. <https://www.sciencedirect.com/science/article/pii/S2095633921000708>

- Fauzi, A. N. (2012). Analisis Tegangan-Perpindahan dan Faktor Keamanan (FS) Pada Lereng Miring Dengan Perkuatan Soil Nailing Menggunakan Program PLAXIS 8.2. Digilib UNS. <https://digilib.uns.ac.id>
- Gunawan, I., Surjandari, N. S., & Purwana, Y. M. (2017). *The study on length and diameter ratio of nail as preliminary design for Slope Stabilization*. Journal of Physics: Conference Series, 909, 012073. <https://doi.org/10.1088/1742-6596/909/1/012073>
- Hanif, F. (2016, July 28). *Analisis Perkuatan Soil Nailing sebagai Metode Perbaikan Stabilitas Lereng (Soil Nailing Reinforcement Analysis as Slope Stability Improvement Method)*. Digilib UNS. <https://digilib.uns.ac.id>
- Hardiyatmo, H.C. (2012). *Mekanika Tanah II*. Edisi Kelima, Penerbit Gadjah Mada University Press, Yogyakarta
- Hermawan, R.B. (2016). *Analisis Stabilitas Lereng Dengan Perkuatan Soil Nailing Menggunakan Program Komputer (Studi Kasus: Desa Tambakmerang, Kecamatan Girimarto, Kabupaten Wonogiri)*. Digilib UNS. <https://digilib.uns.ac.id>
- Jacob, A., & Venkataramana, K. (2021). *Slope Stability Analysis Under Earthquake Load using Plaxis Software*. Journal of Advances in Geotechnical Engineering. <https://doi.org/10.5281/zenodo.4432296>
- Juran, I., & Elias, V. (1990). *Foundation Engineering Handbook*. Chapman & Hall.
- Khan, M. I., & Wang, S. (2020). *Comparing The Various Slope Stability Methods To Find The Optimum Method For Calculating Factor Of Slope Safety*. Northeastern University, China.
- Kumalasari. (2012), *Analisis Stabilitas Lereng Dengan Perkuatan Soil Nailing Menggunakan Program Geoslope (Studi Kasus Pada Lereng Desa Bantas, Kecamatan Selemadeg Timur, Kabupaten Tabanan, Provinsi Bali)*. Tugas Akhir, Universitas Sebelas Maret, Surakarta.
- Lambe, T. W. (2012). *Soil Mechanics*. Wiley.
- Lazarte, C. A., Robinson, H., Gomez, J. E., Baxter, A., Cadden, A., Berg, R. R., Ryan R. Berg & Associates, Inc., & Engineering, S. (2015, February 1). *Geotechnical Engineering Circular no. 7 soil nail walls - reference manual*. Federal Highway Administration (.gov). <https://rosap.nrl.bts.gov/view/dot/40556>
- Lazarte, C., Baecher, G., & Withiam, J. (2003, December 1). *New Directions in LRFD for soil nailing design and specifications*. Semantic Scholar.



<https://www.semanticscholar.org/paper/New-Directions-in-LRFD-for-Soil-Nailing-Design-and-Lazarte-Baecher/a1a0ec5d6ead0ca77bc15dbf023caefd7d267e72>

Nalgire, T., Dahale, P., Mehta, A., & Hiwase, P. (2020). *Slope Stability Analysis by GeoSlope*. HeLIX The Scientific Explorer. <https://helixscientific.pub/index.php/home/article/download/58/60>

Nowroozi, V., Hashemolhosseini, H., Afrazi, M., & Kasehchi, E. (2021). *Optimum Design for Soil Nailing to Stabilize Retaining Walls Using FLAC3D*. Journal of Advanced Engineering and Computation. <https://jaec.vn/index.php/JAEC/article/view/329>

Obrzud, R., & Truty, A. (2018). *The Hardening Soil Model – A Practical Guidebook*. Zsoil.com. [http://www.zsoil.com/zsoil\\_manual\\_2018/Rep-HS-model.pdf](http://www.zsoil.com/zsoil_manual_2018/Rep-HS-model.pdf)

Pham, T., Bing, P., & Nguyen, N. (2020). *Study on The Effect of some Parameters of Soil Nails on The Stability of Vertical Slopes*. Researchgate.net. [https://www.researchgate.net/profile/Nhan-Pham-18/publication/349922887\\_Study\\_on\\_the\\_effect\\_of\\_some\\_parameters\\_of\\_soil\\_nails\\_on\\_the\\_stability\\_of\\_vertical\\_slopes/links/63e394a3c002331f72625290/Study-on-the-effect-of-some-parameters-of-soil-nails-on-the-stability-of-vertical-slopes.pdf](https://www.researchgate.net/profile/Nhan-Pham-18/publication/349922887_Study_on_the_effect_of_some_parameters_of_soil_nails_on_the_stability_of_vertical_slopes/links/63e394a3c002331f72625290/Study-on-the-effect-of-some-parameters-of-soil-nails-on-the-stability-of-vertical-slopes.pdf).

PT. Geomine Bara Studio. (2022). *Final Report Soil Investigation Tawang-Ngalang Segment IV*.

PUPR. (2002) “*Timbunan Jalan Pada Tanah Lunak Salinan - Kementerian PUPR*.” Kementerian PUPR. <https://binamarga.pu.go.id/index.php/peraturan/dokumen/panduan-geoteknik-4-desain-dan-konstruksi>.

Putra, H., Yasuhara, H., Kinoshita, N., Erizal, & Sudiby. (2018). *Improving Shear Strength Parameters of Sandy Soil using Enzyme-Mediated Calcite Precipitation Technique*. Petra.ac.id. <https://ced.petra.ac.id/index.php/civ/article/download/21132/19504/28043>.

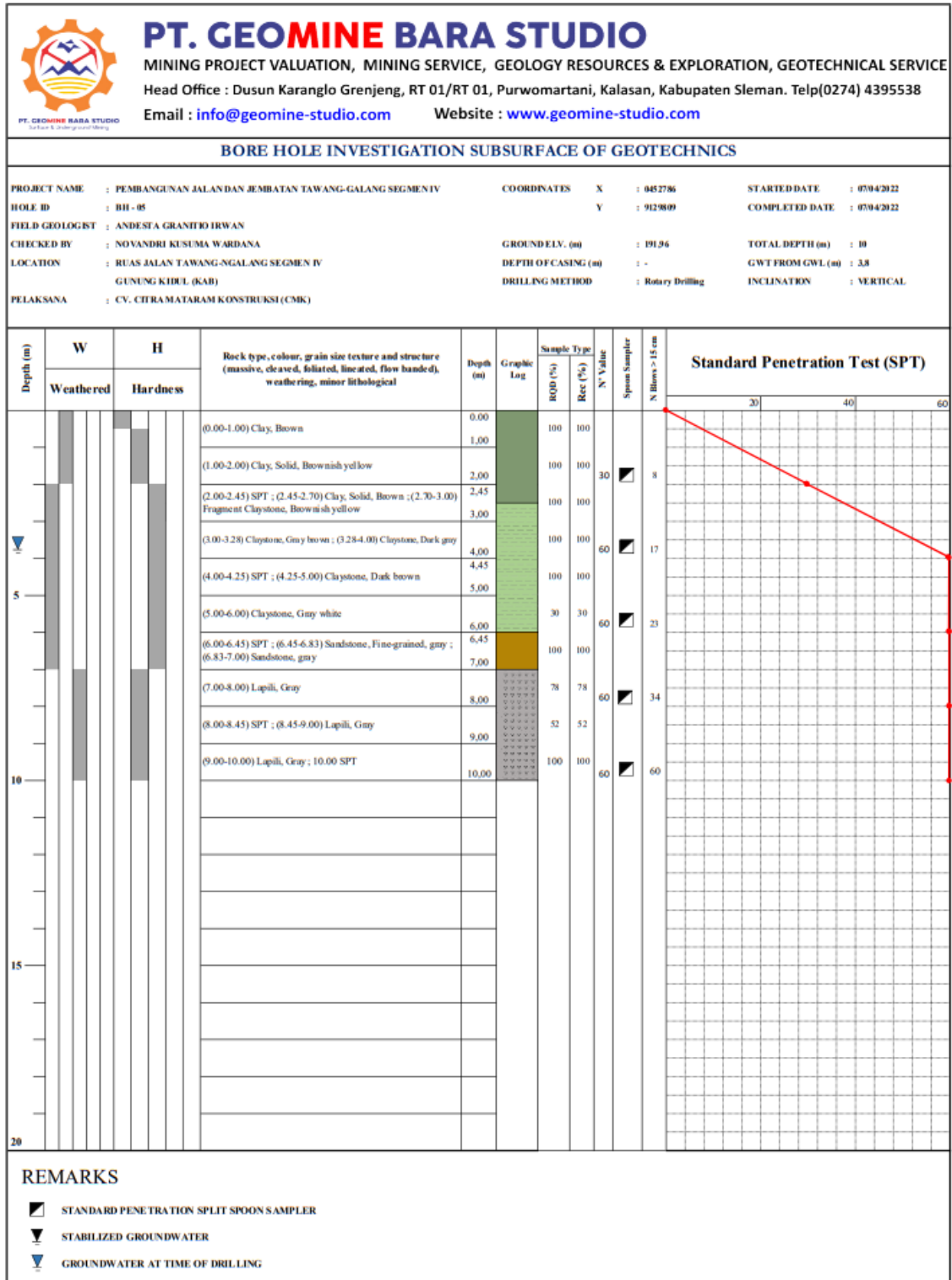
Qualsiasi. (2012). *Metode Fellenius*.

Rahmanta, L. M. (2018, June 5). *Analisis Stabilitas Lereng Dengan Perkuatan Soil Nailing Menggunakan Metode Perhitungan Fellenius Dan Taylor Serta Program GEOSLOPE (analysis of slope stability reinforced with soil nailing using fellenius and Taylor Methods and GEOSLOPE program) Studi Kasus Desa Srimartani, Kecamatan Piyungan, Kabupaten Bantul*. DSpace Home. <https://dspace.uui.ac.id/handle/123456789/7954>

- Sari, M. (2016). *Pemetaan Percepatan Getaran Tanah Maksimum dan Intensitas Gempa Bumi di Kawasan Jalur Sesar Sungai Oyo Yogyakarta*. Universitas Negeri Yogyakarta. <http://eprints.uny.ac.id/46135/1/Bab%20Lengkap.pdf>
- Styles, J., & Yuen, S. (2009, March) “*Geomechanics & Geotechnical Engineering (Electronic Text)*.” University of Melbourne, March 2009. [https://people.eng.unimelb.edu.au/stsy/geomechanics\\_text/content.htm](https://people.eng.unimelb.edu.au/stsy/geomechanics_text/content.htm).
- Tsytoovich, N. (1976). *Soil Mechanics*. Mir Publishers Moscow. <https://vulcanhammer.net/2021/06/17/soil-mechanics-textbook-by-tsytoovich-available/>
- U.S. Department of the Interior, & U.S. Geological Survey. (2004, July). *Landslide Types and Processes*. Landslide types and processes. [https://pubs.usgs.gov/fs/2004/3072/fs-2004-3072.html#:~:text=The%20two%20major%20types%20of,transverse%20across%20the%20slide%20\(fig.](https://pubs.usgs.gov/fs/2004/3072/fs-2004-3072.html#:~:text=The%20two%20major%20types%20of,transverse%20across%20the%20slide%20(fig.)
- United States Department of Agriculture. (1999). *Soil Taxonomy: A Basic System of Soil Classification for Making and Interpreting Soil Surveys*. USDA. <https://www.nrcs.usda.gov/sites/default/files/2022-06/Soil%20Taxonomy.pdf>
- Utomo, B. (2019, July 5). *Analisis Stabilitas Lereng Dengan Perkuatan Soil Nailing Dengan Menggunakan Program GEOSLOPE (analysis of slope stability reinforced with soil nailing using GEOSLOPE program)*. DSpace Home. <https://dspace.uui.ac.id/handle/123456789/15325>
- Villalobos, S. A., & Villalobos, F. A. (2020, October 10). *Effect of nail spacing on the global stability of soil nailed walls using limit equilibrium and finite element methods*. Transportation Geotechnics. <https://www.sciencedirect.com/science/article/abs/pii/S221439122030342>
- World Bank Group. (2023, June 27). *EIndonesia Economic Prospects (IEP) June 2023: The invisible toll of covid-19 on learning*. World Bank. <https://www.worldbank.org/en/country/indonesia/publication/indonesia-economic-prospects-iep-june-2023-the-invisible-toll-of-covid-19-on-learning>

# ATTACHMENT

## Attachment 1 Bore Log



# Attachment 2 Soil Laboratory Test Results

**LABORATORIUM MEKANIKA TANAH**
  
 Gedung 04 Muli Nalir
   
 Kampus Teknik Universitas Islam Indonesia
   
 Jl. Kusurwo KM 14,4 Yogyakarta 55084
   
 Telp. (0271) 890131
   
 F. (0271) 890133
   
 W. http://uii.ac.id

No : 022/Kabid.MT/01/Lab.MT.V/2022
   
 Lampiran : 1 bendel
   
 Hal : Hasil Uji Sampel

Kepada Yth:
   
 Pimpinan
   
 PT Geotek Bina Studio
   
 di Tempat

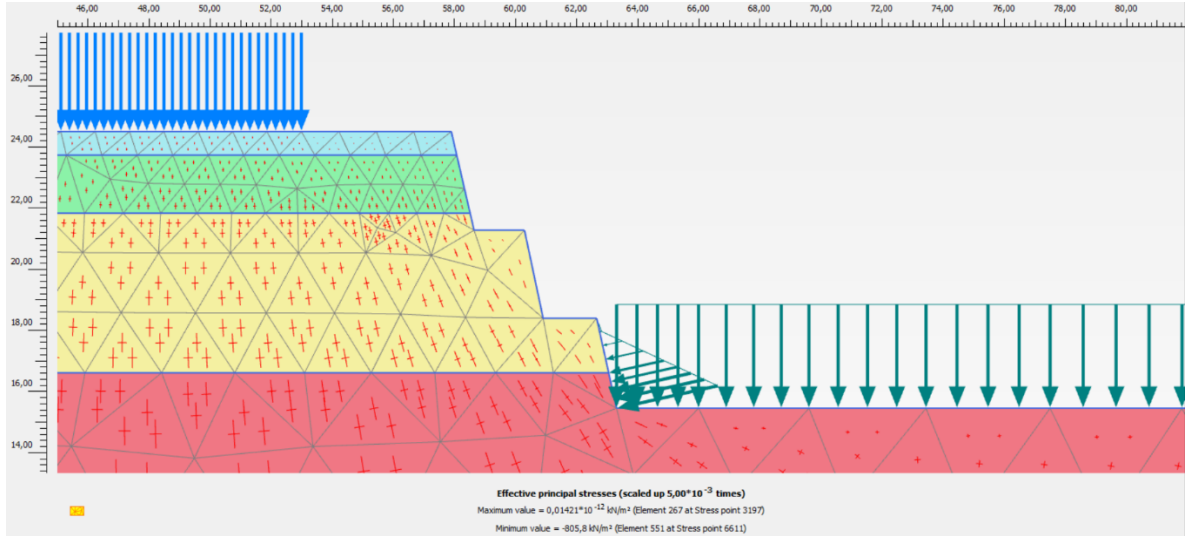
Dengan ini kami sampaikan Hasil Uji Sampel Tanah untuk Pekerjaan : Proyek Pembangunan Jalan Segmen IV Tawang-Nglang,
   
 sebagai berikut

No	Parameter Uji	Hasil Uji													
		DO1 GTTW08 BH 01	DO4 GTTW07 BH 04	DO1 GTTW03 BH 01	DO4 GTTW02 BH 04	DO1 GTTW05 BH 01	DO1 GTTW04 BH 01	DO1 GTTW01 BH 01	DO1 GTTW02 BH 01	DO1 GTTW09 BH 01	DO1 GTTW09 BH 01	DO1 GTTW06 BH 01	DO1 GTTW03 BH 01	DO1 GTTW01 BH 01	DO1 GTTW01 BH 01
Soil Properties	Kadar air (Moisture Content, w)	51.997	4.470	32.238	32.238	2.810	30.797	36.679	4.470	17.996	9.957	30.797	49.765	13.476	25.536
	Berat Jenis Tanah (Specific Gravity of Soil, G <sub>s</sub> )	2.601	2.994	2.558	2.594	2.724	2.672	2.599	2.601	2.675	2.558	2.631	2.724	2.538	2.724
	Berat volume tanah basah (s <sub>w</sub> )	1.668	2.180	1.628	1.652	2.289	1.651	1.698	1.620	2.023	2.101	1.815	2.104	1.916	1.668
	Berat volume tanah kering (s <sub>w</sub> )	1.097	2.087	1.231	1.249	2.226	1.242	1.251	1.242	1.714	1.911	1.388	1.405	1.689	1.328
	Angka pori, e	1.371	0.243	1.078	1.077	0.224	1.117	1.092	0.678	0.560	0.339	0.896	0.939	0.503	1.051
	Porositas, n	57.83	19.53	51.88	51.85	18.28	52.76	52.20	40.40	35.90	25.30	47.25	48.42	33.47	51.24
	Densitas kejut	98.65	47.76	76.51	77.66	34.23	73.68	87.30	17.16	85.95	75.21	90.44	144.41	68.00	66.20
	Kandungan lelele (liquid part)	0.00	42.57	42.57	42.57	0.00	0.00	0.00	0.00	0.00	0.00	0.00	0.00	0.00	0.00
	Kandungan Plast (plast part)	23.78	39.90	39.90	52.17	39.27	16.03	46.23	16.03	46.23	16.03	29.22	33.95	33.95	48.45
	Kandungan Lempung (clay part)	57.53	17.53	38.64	38.64	51.59	74.38	42.68	11.08	9.00	11.08	59.70	57.05	31.80	17.75
Grain size analysis	Densitas lempung (clay part)	18.69	0.00	9.20	9.15	8.98	11.08	9.00	0.0013	0.0026	0.0013	0.0026	0.0026	-	
	D <sub>10</sub> (mm)	-	0.0282	0.0023	0.0023	0.0023	0.0026	0.0016	0.0016	0.0016	0.0013	0.0026	0.0026	-	
	D <sub>30</sub> (mm)	0.0077	0.0047	0.0184	0.0184	0.0059	0.0087	0.0068	0.0100	0.0100	0.0100	0.0046	0.0046	0.0546	
	D <sub>60</sub> (mm)	0.0405	0.0346	0.0639	0.0639	0.0320	0.0397	0.0299	0.0320	0.0320	0.0320	0.0626	0.0626	0.0626	
	Uniformity Coefficient, C <sub>u</sub>	-	1.2266	27.8059	27.8059	13.7998	15.1484	15.7241	15.7241	15.7241	15.7241	39.9034	23.8492	-	
	cc	-	0.0224	2.2989	2.2989	0.4739	0.7233	1.0767	1.0767	1.0767	1.0767	1.5852	18.1700	-	
Engineering Properties	q <sub>ult</sub> (t/cm <sup>2</sup> )	0.27	166.47	1.42	2.22	168.39	0.52	0.31	0.18	174.71	193.51	0.28	0.87	206.18	4.85
	Friction angle (Triaxial test UU), φ	10.75	24.53	14.58	14.58	16.48	33.53	15.41	15.41	15.41	5.51	22.28	22.28	9.39	
	Cohesion, c (Triaxial test UU)	0.19	0.53	0.15	0.15	0.01	0.34	0.11	0.11	0.11	0.20	0.48	0.48	0.24	
	Koef. Permeabilitas, k (constant head permeameter)	-	2.14E-08	-	-	3.06E-08	-	-	-	-	2.22E-08	2.02E-08	-	1.57E-08	-
	Koef. Permeabilitas, k (falling head permeameter)	3.23E-04	-	4.49E-05	4.82E-04	5.51E-04	1.71E-05	3.13E-04	3.13E-04	3.13E-04	-	2.84E-05	4.27E-05	-	9.74E-05

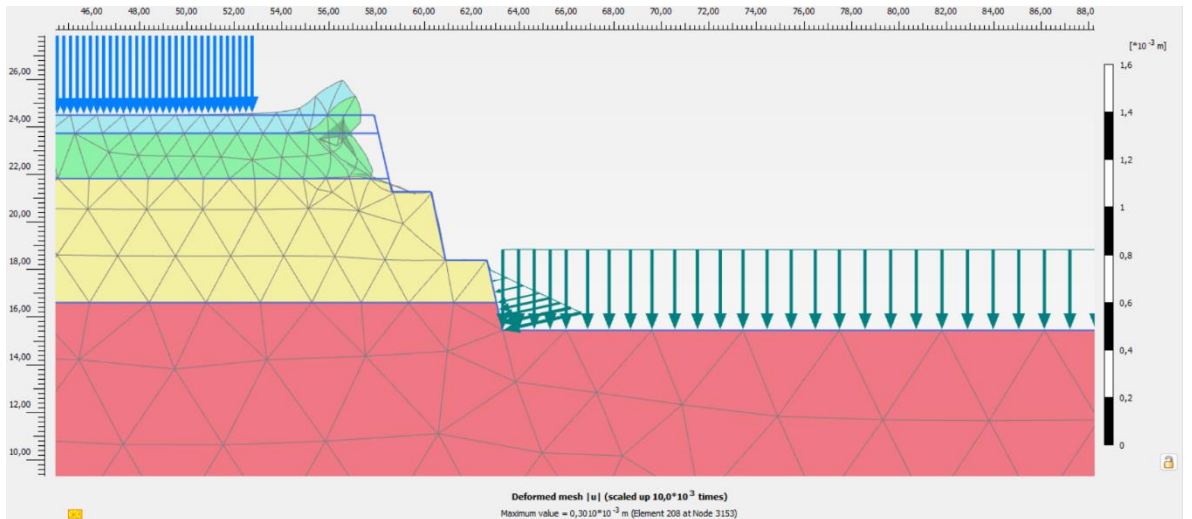
Atas kepercayaannya dan kejujurannya disampaikan terimakasih

MEWAJIBKAN  
 TANGGUNG  
 Jember, 14 Mei 2022  
 Kepala Laboratorium  
 Pelembagaan

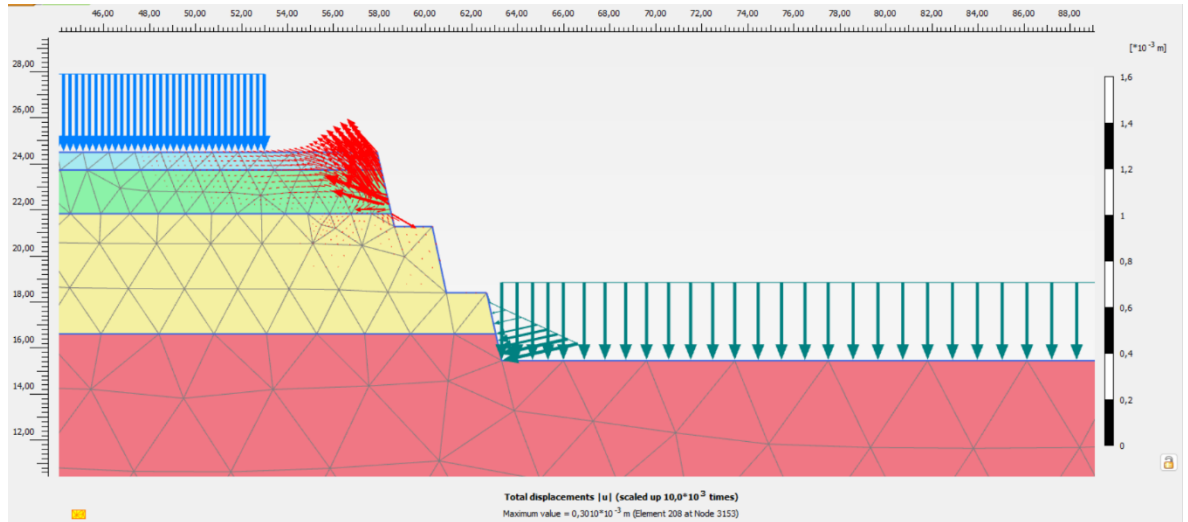
### Attachment 3 Non-Loaded Static Existing Slope Effective Stress Output



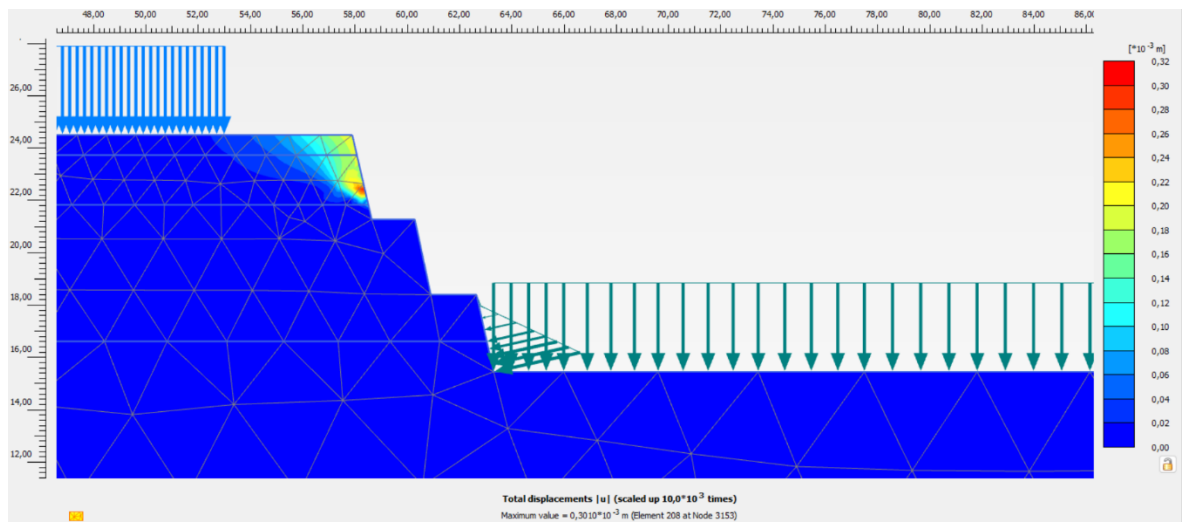
### Attachment 4 Non-Loaded Static Existing Slope Deformed Mesh Output



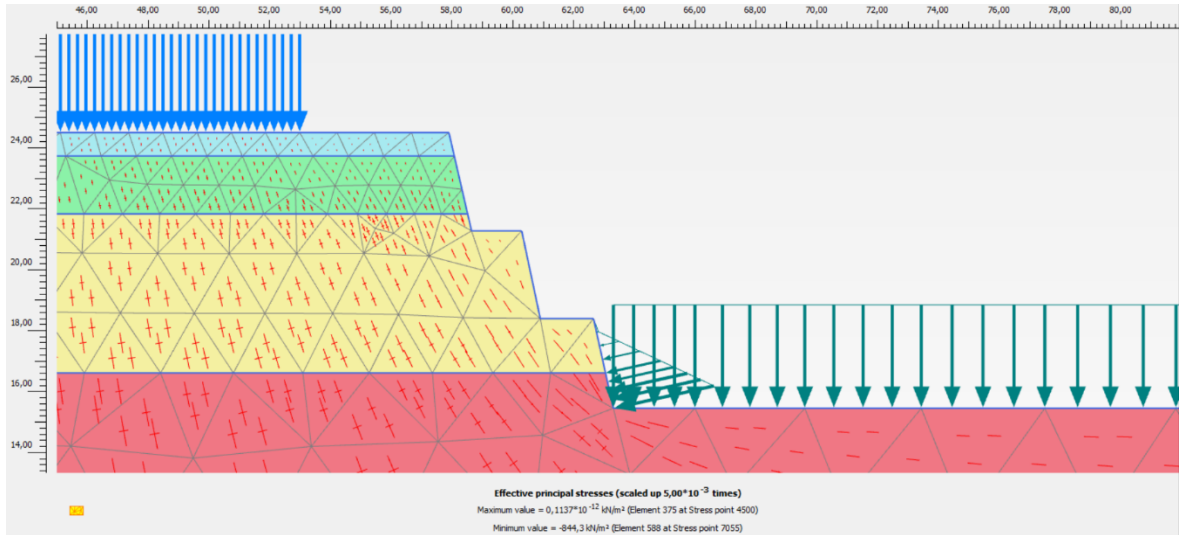
## Attachment 5 Non-Loaded Static Existing Slope Direction of Movement Output



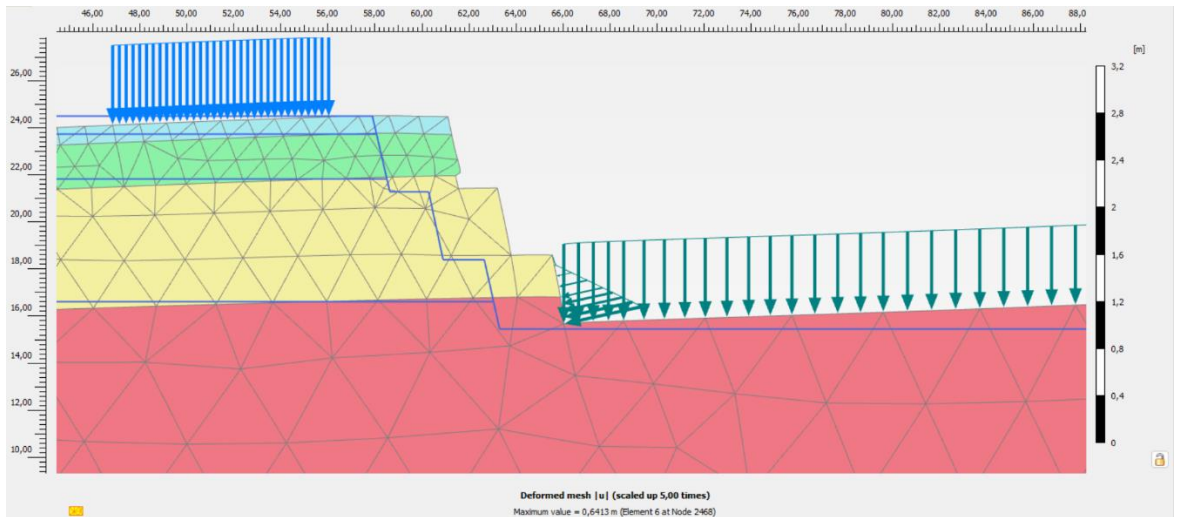
## Attachment 6 Non-Loaded Static Existing Slope Displacement Output



## Attachment 7 Non-Loaded Dynamic Existing Slope Effective Stress Output

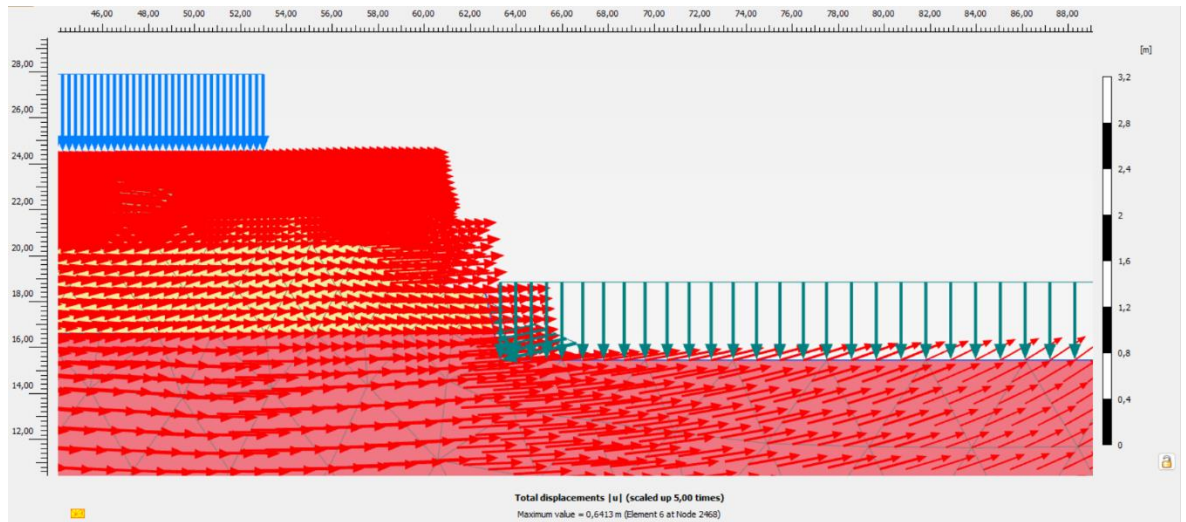


## Attachment 8 Non-Loaded Dynamic Existing Slope Deformed Mesh Output

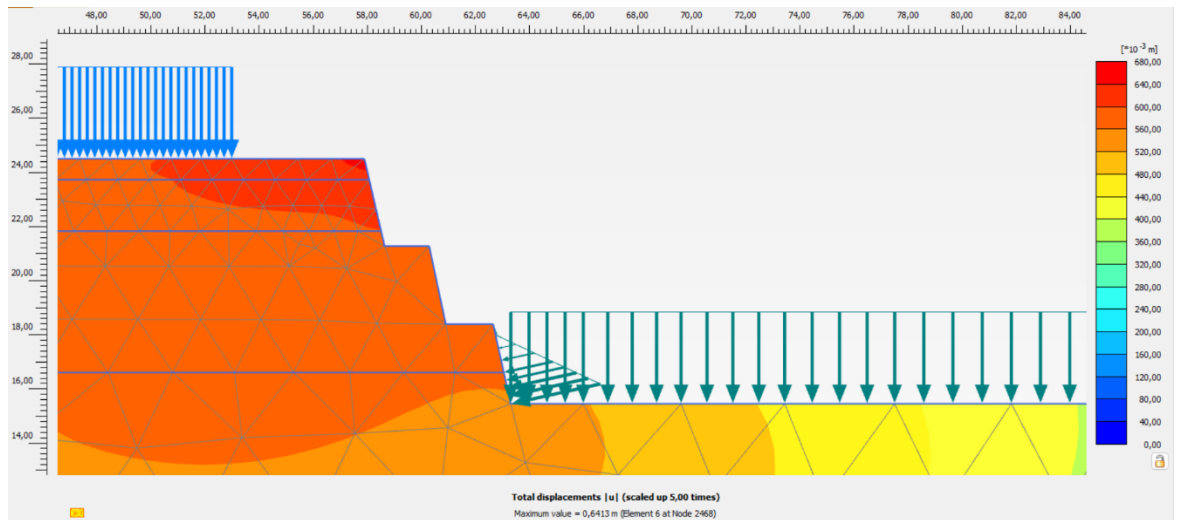




## Attachment 9 Non-Loaded Dynamic Existing Slope Direction of Movement Output

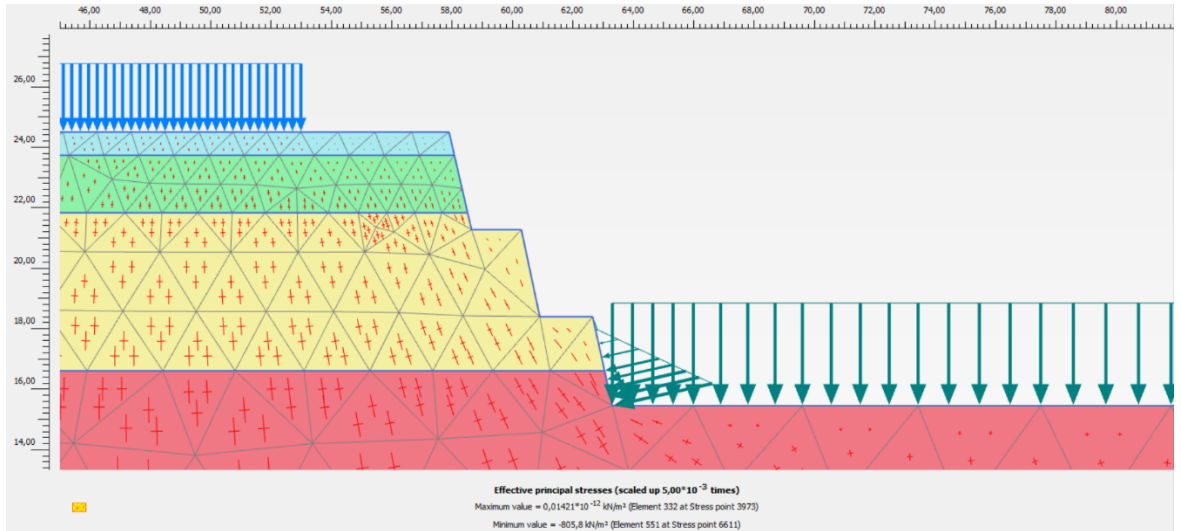


## Attachment 10 Non-Loaded Dynamic Existing Slope Displacement Output

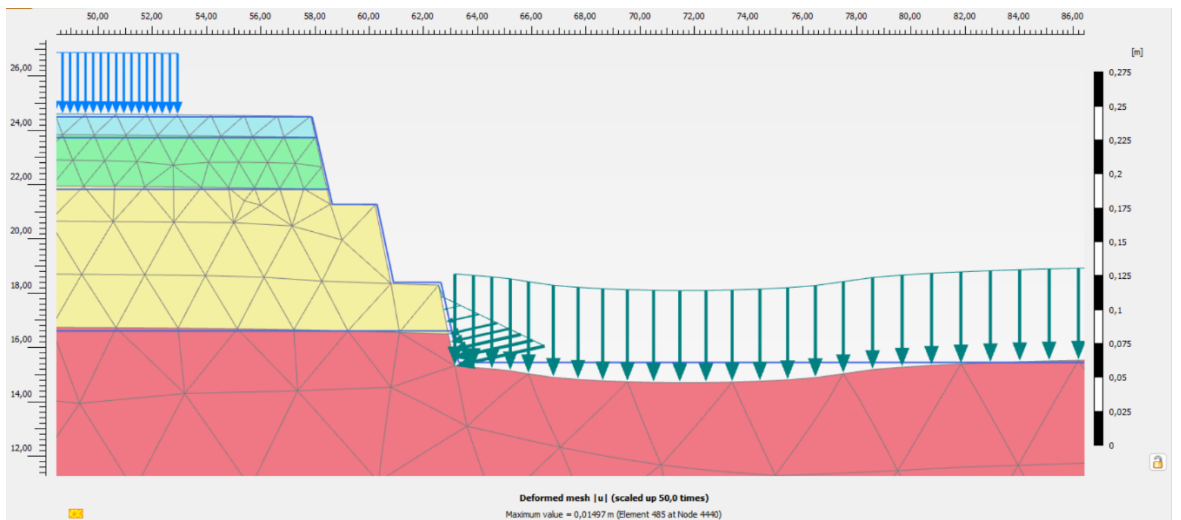




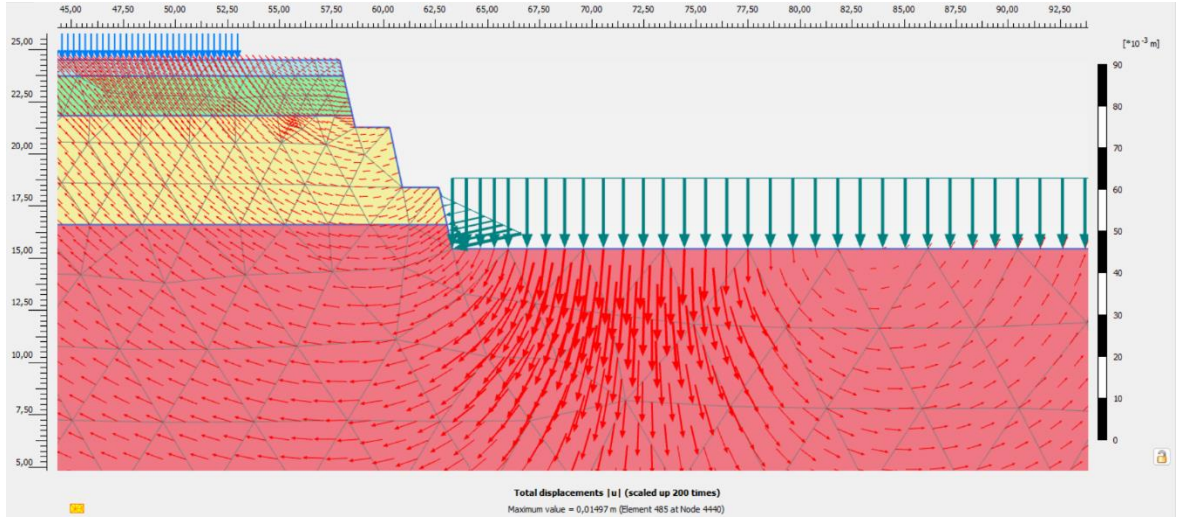
## Attachment 11 Loaded Static Existing Slope Effective Stress Output



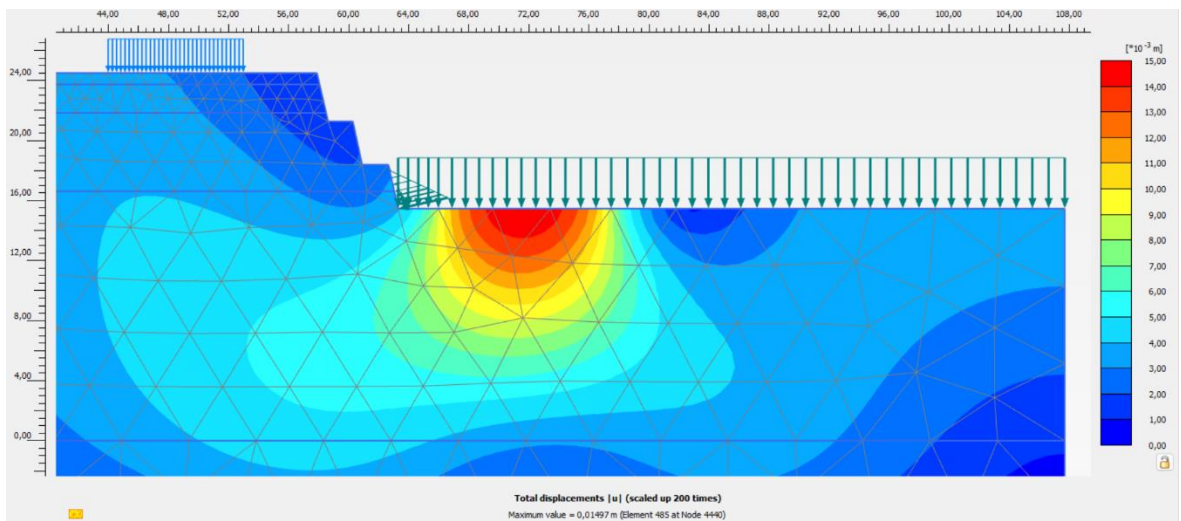
## Attachment 12 Loaded Static Existing Slope Deformed Mesh Output



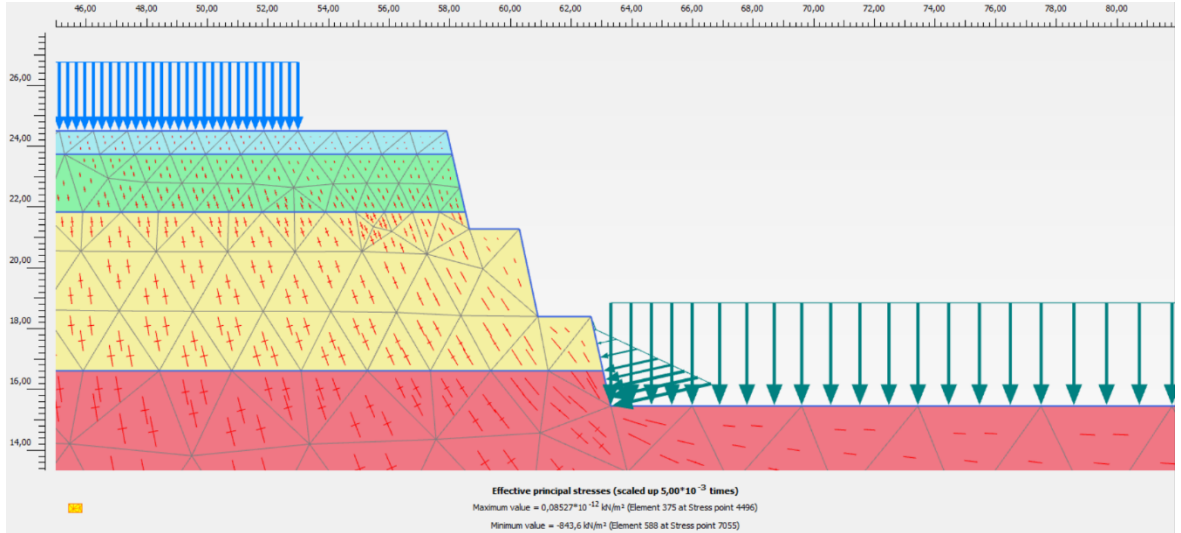
### Attachment 13 Loaded Static Existing Slope Direction of Movement Output



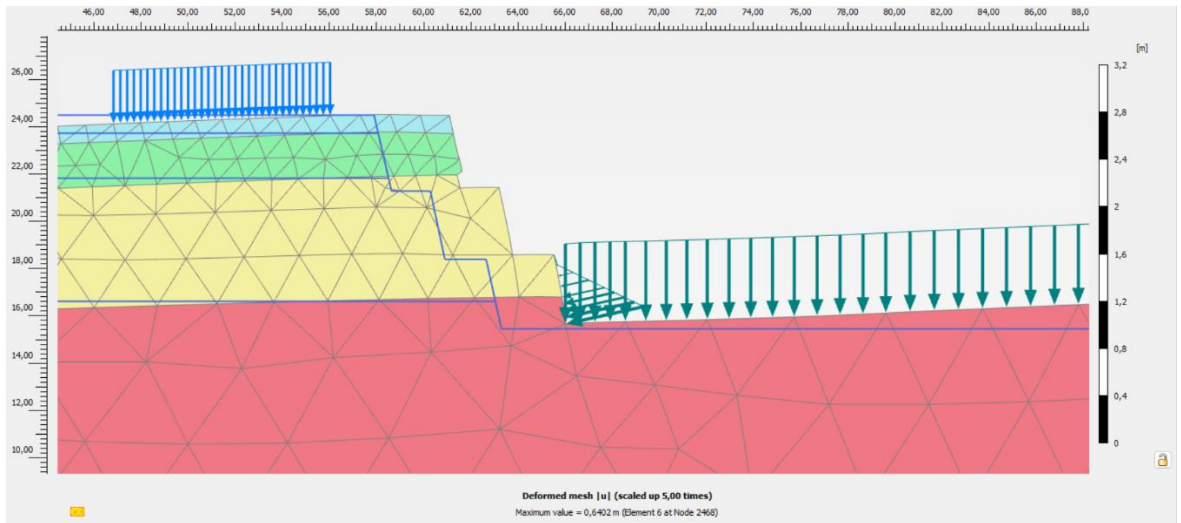
### Attachment 14 Loaded Static Existing Slope Displacement Output



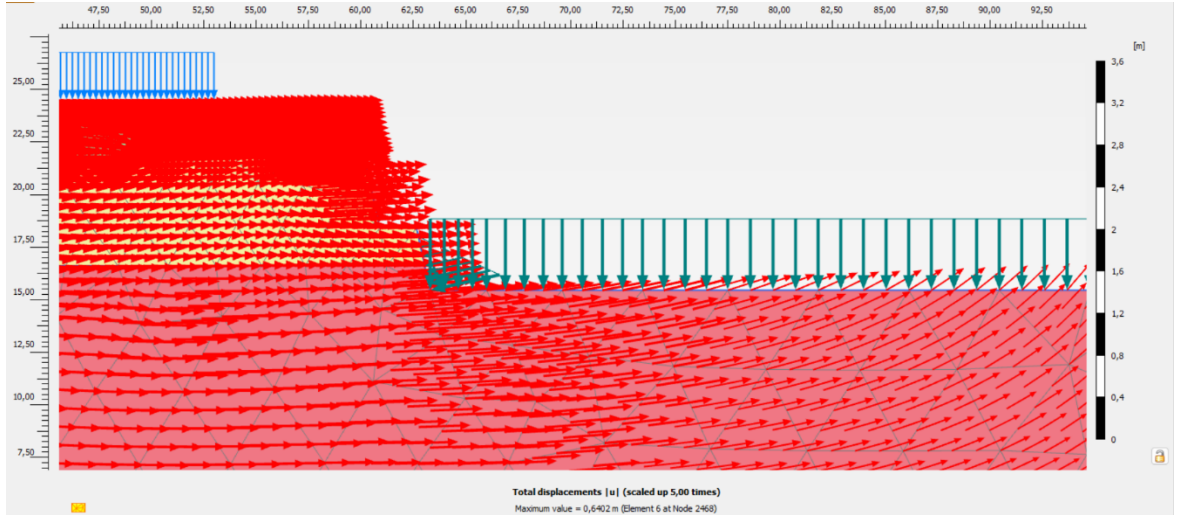
### Attachment 15 Loaded Dynamic Existing Slope Effective Stress Output



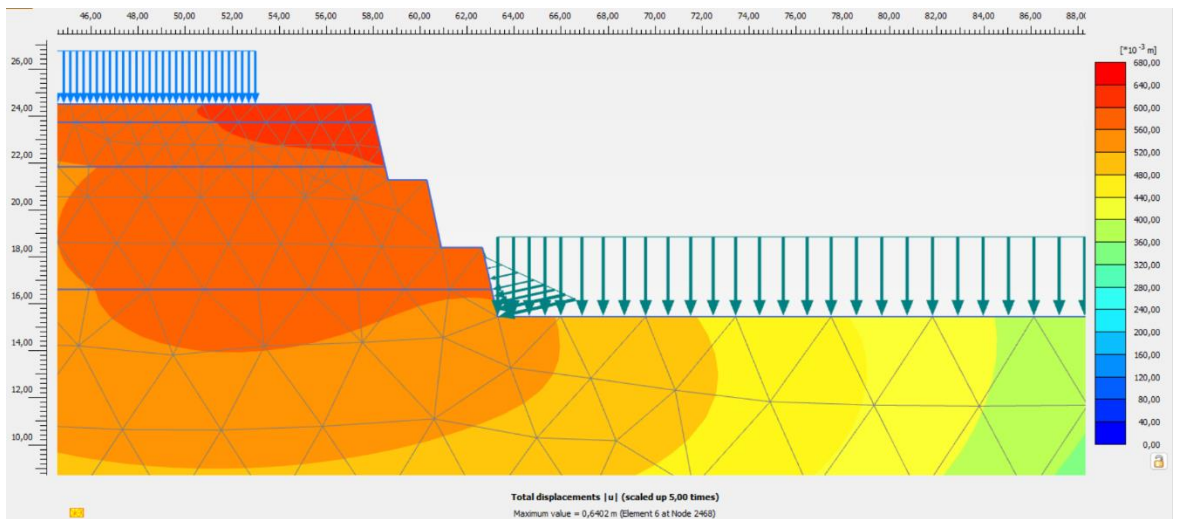
### Attachment 16 Loaded Dynamic Existing Slope Deformed Mesh Output



### Attachment 17 Loaded Dynamic Existing Slope Direction of Movement Output

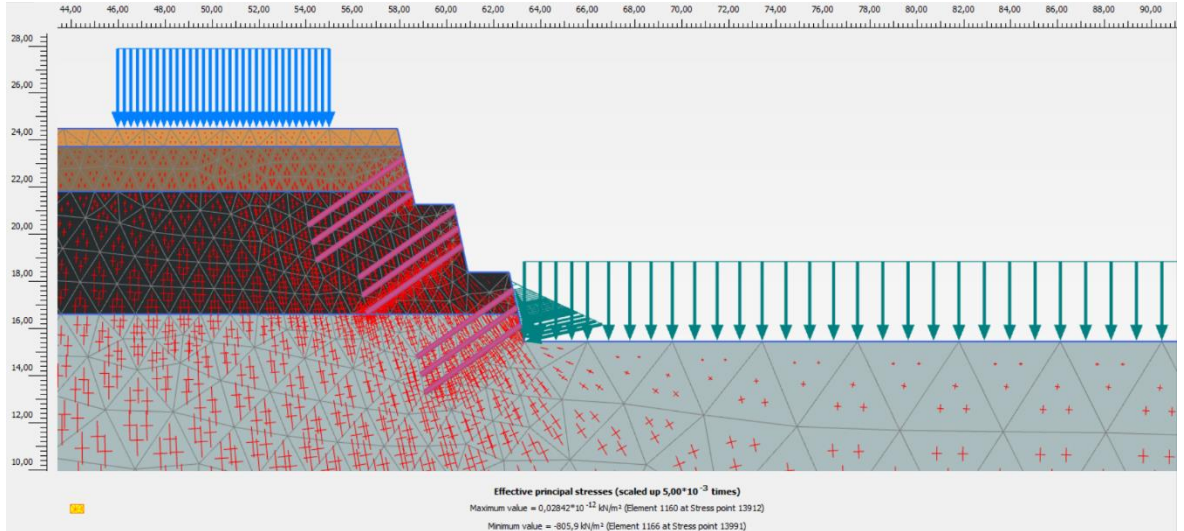


### Attachment 18 Loaded Dynamic Existing Slope Displacement Output

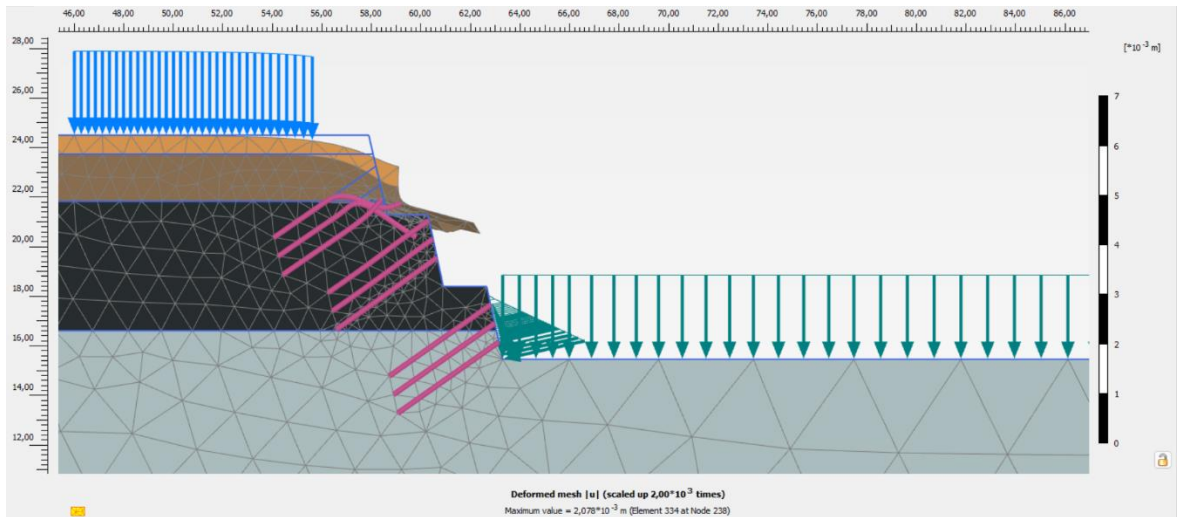




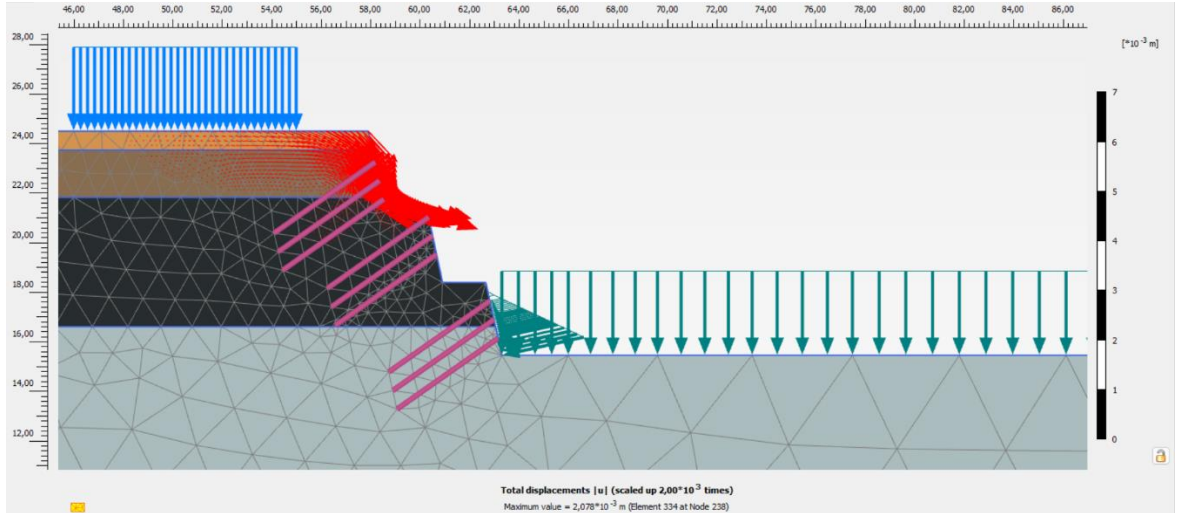
## Attachment 19 Model a Non-Loaded Static Effective Stress Output



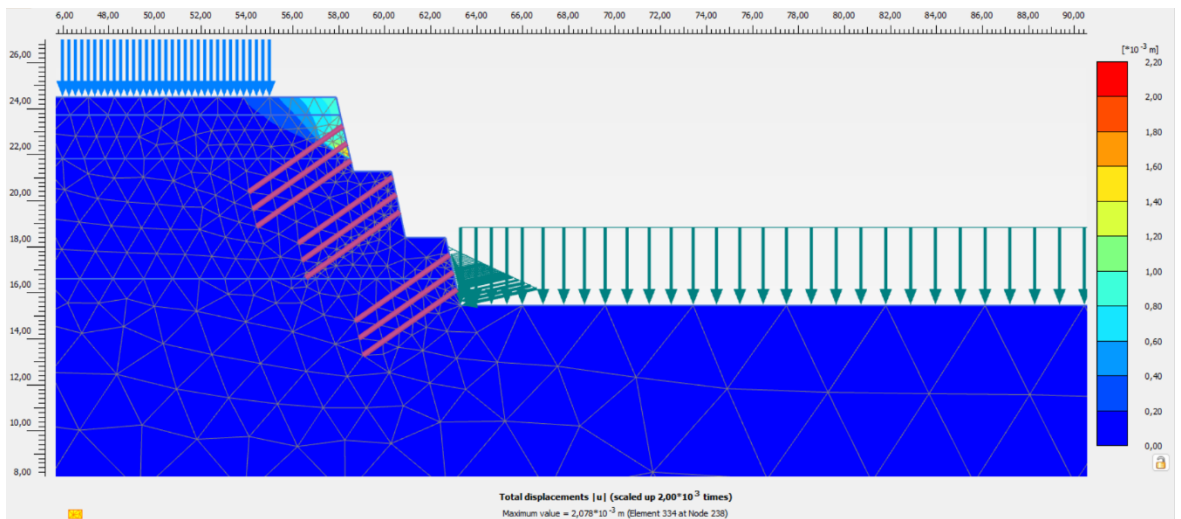
## Attachment 20 Model a Non-Loaded Static Deformed Mesh Output



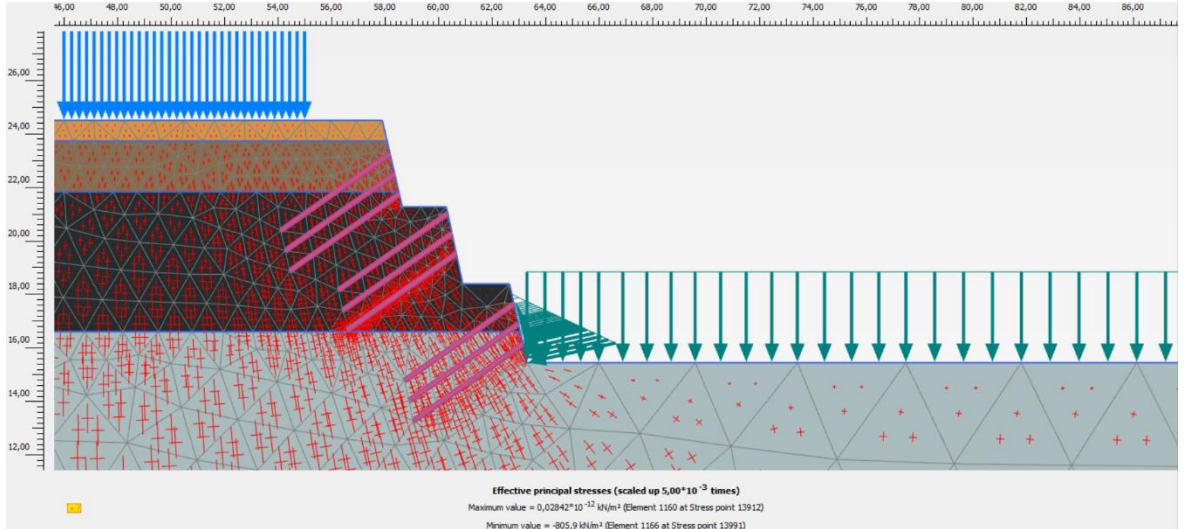
## Attachment 21 Model a Non-Loaded Static Direction of Movement Output



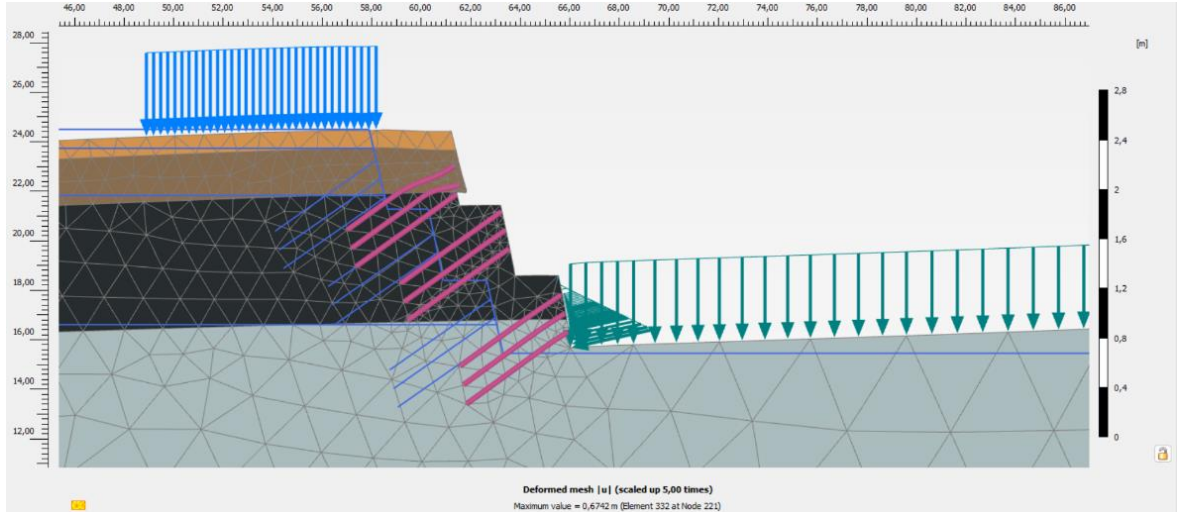
## Attachment 22 Model a Non-Loaded Static Displacement Output



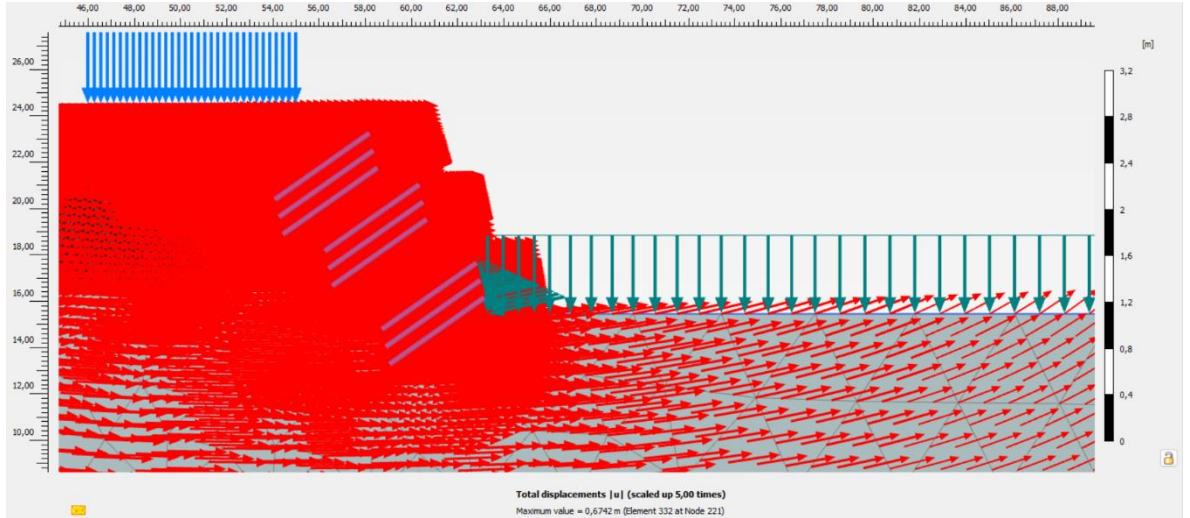
### Attachment 23 Model a Non-Loaded Dynamic Effective Stress Output



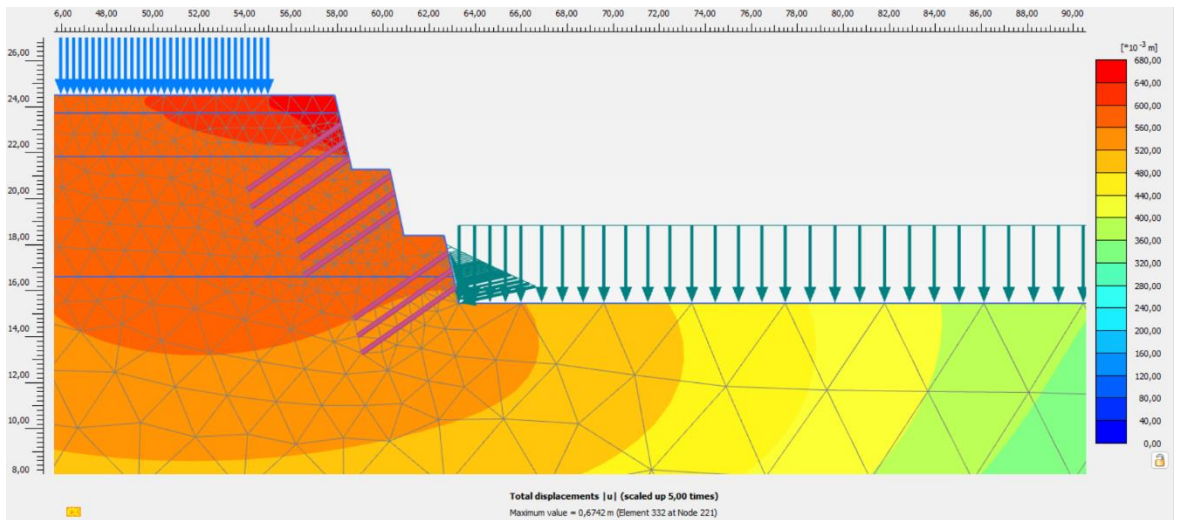
### Attachment 24 Model a Non-Loaded Dynamic Deformed Mesh Output



## Attachment 25 Model a Non-Loaded Dynamic Direction of Movement Output

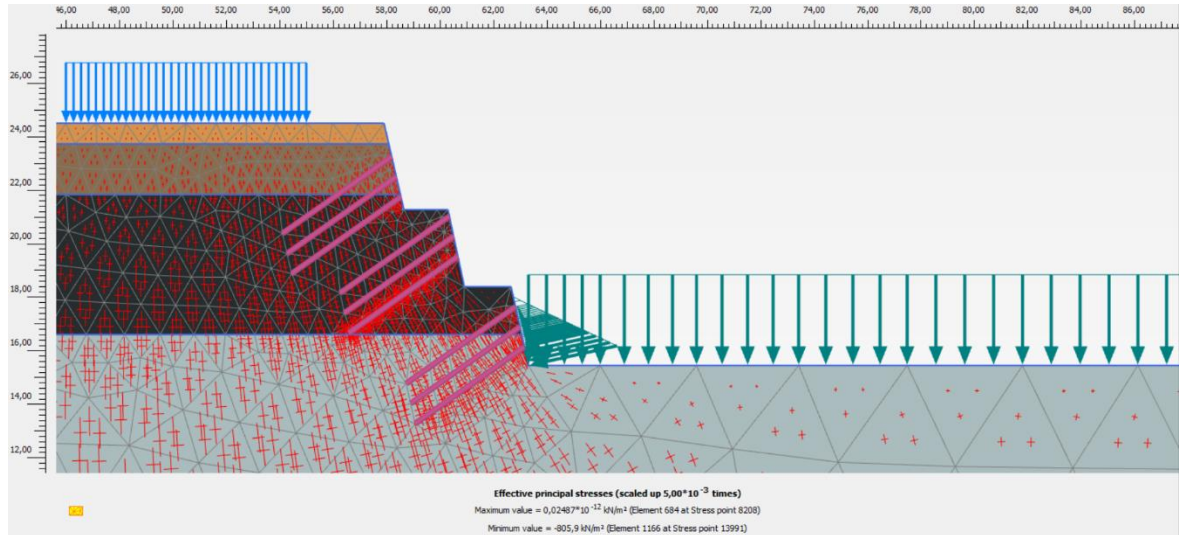


## Attachment 26 Model a Non-Loaded Dynamic Displacement Output

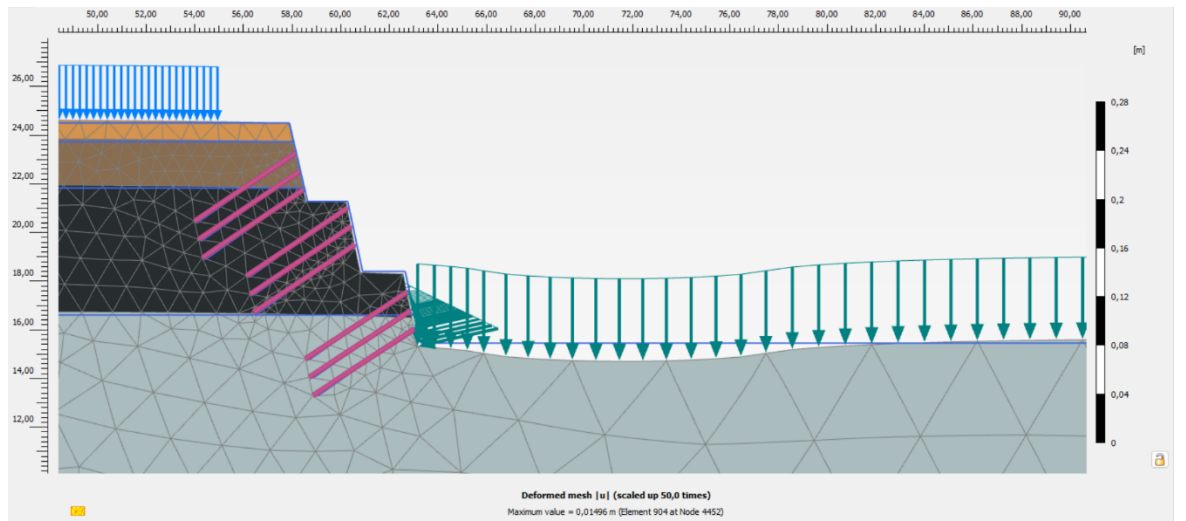




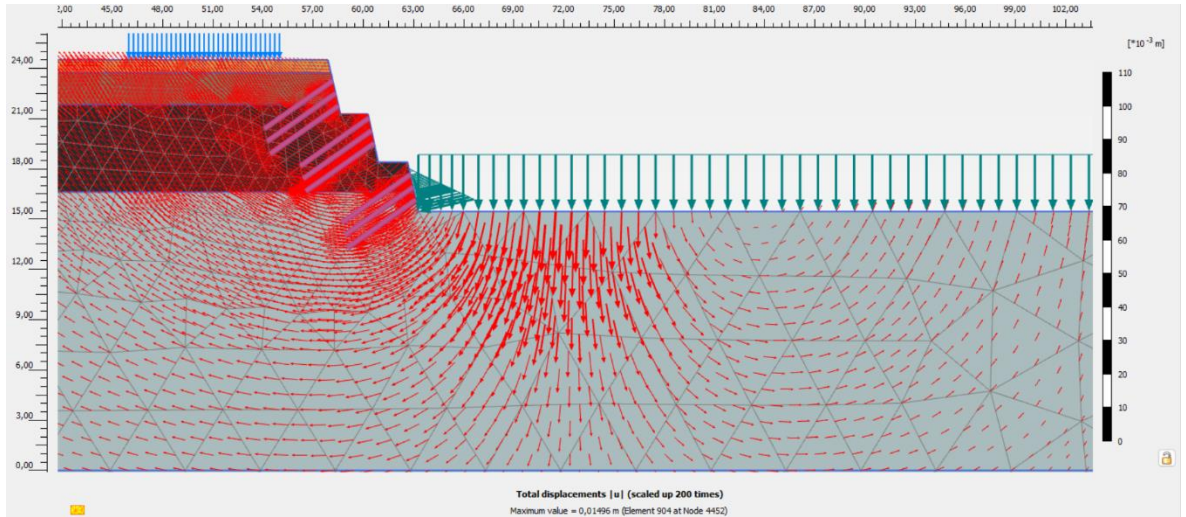
## Attachment 27 Model a Loaded Static Effective Stress Output



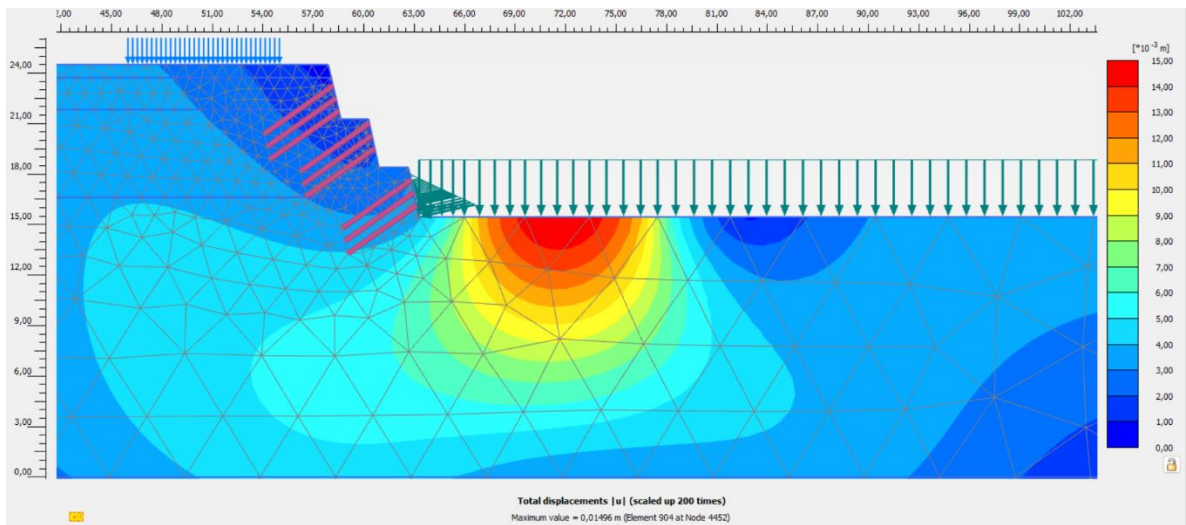
## Attachment 28 Model a Loaded Static Deformed Mesh Output



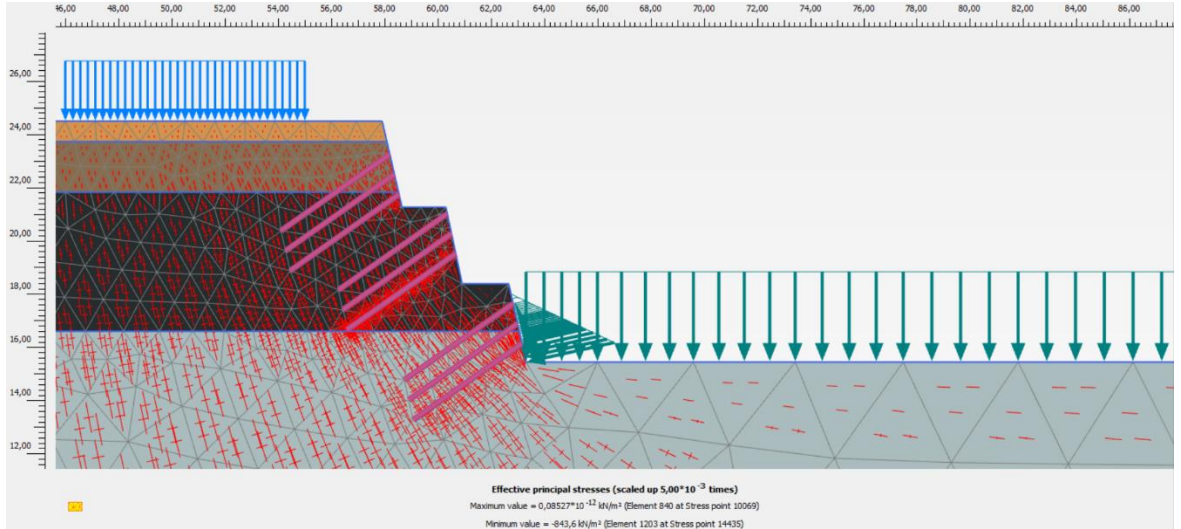
## Attachment 29 Model a Loaded Static Direction of Movement Output



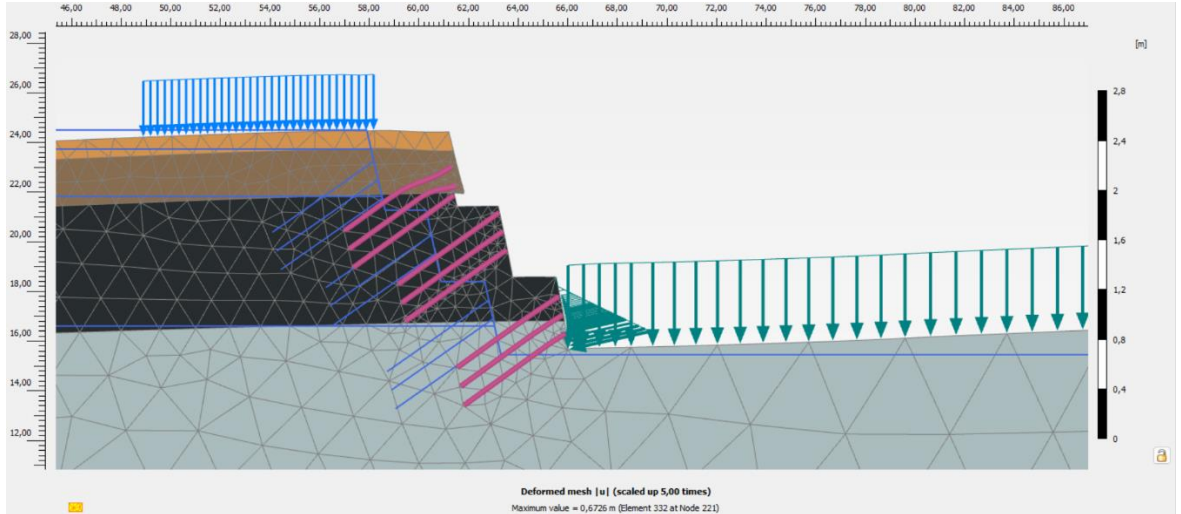
## Attachment 30 Model a Loaded Static Displacement Output



### Attachment 31 Model a Loaded Dynamic Effective Stress Output

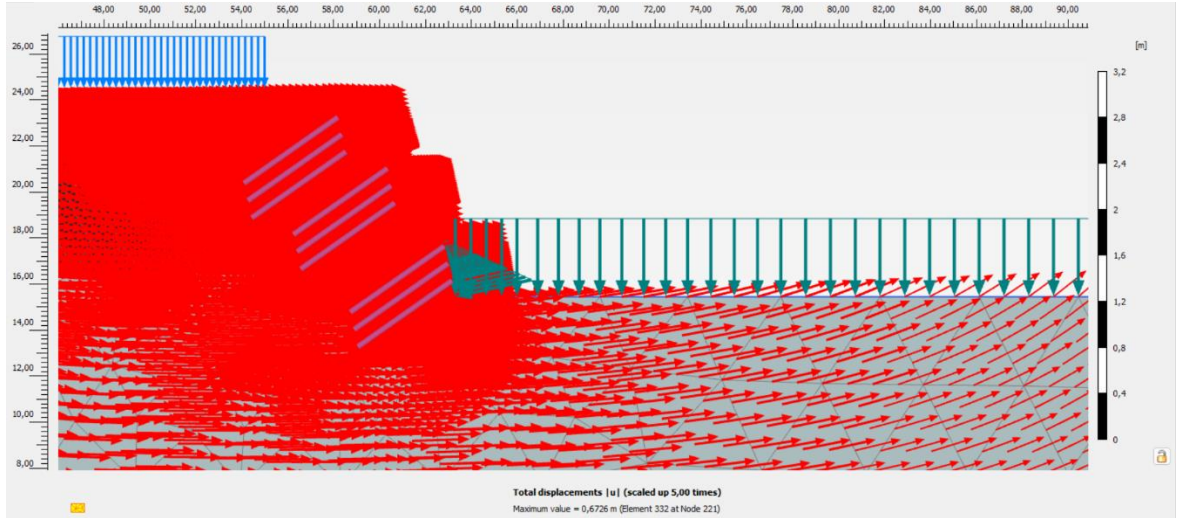


### Attachment 32 Model a Loaded Dynamic Deformed Mesh Output

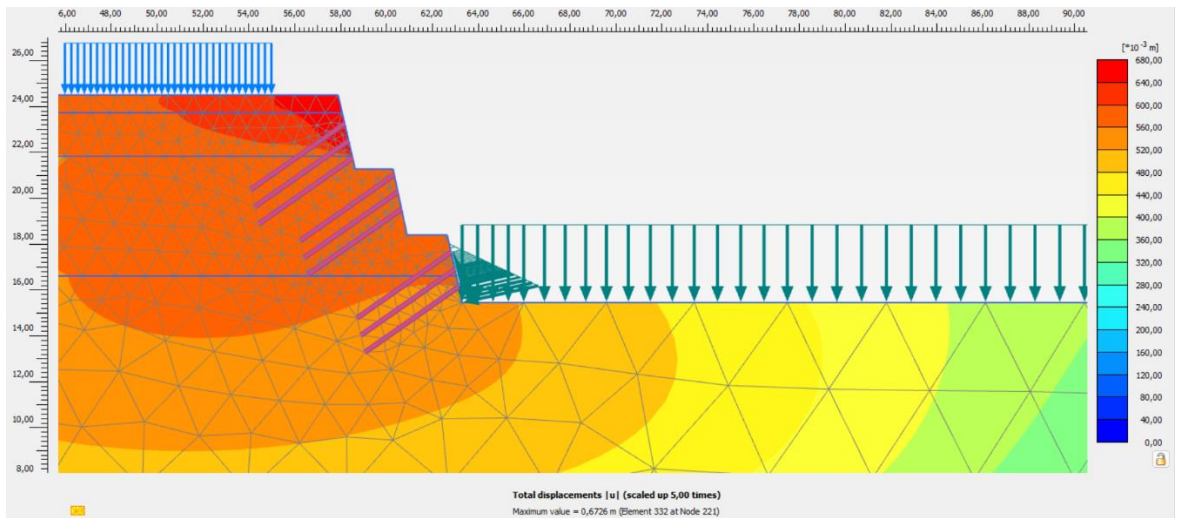




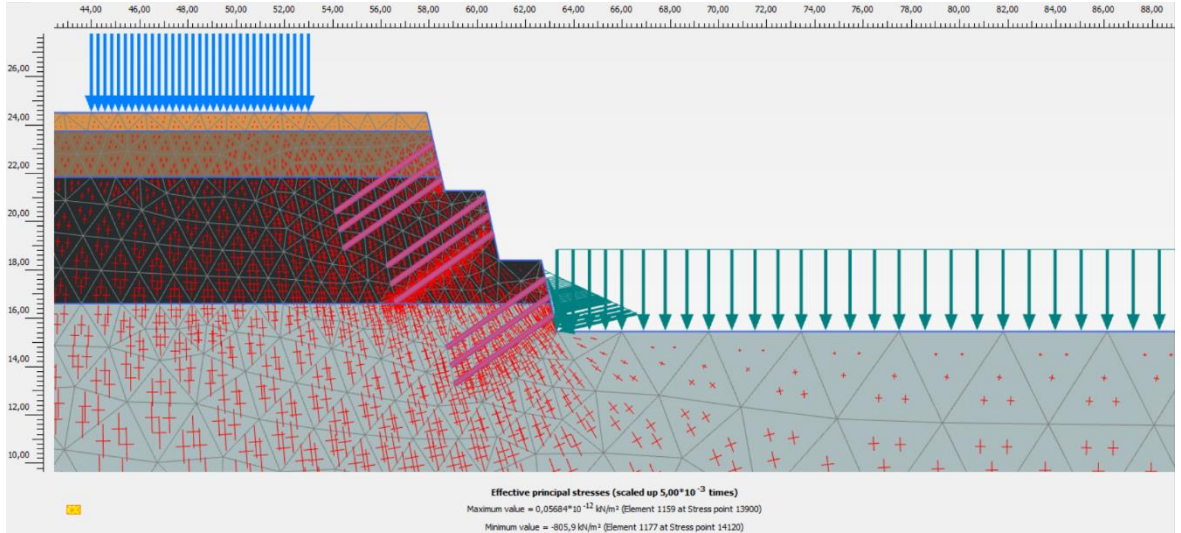
### Attachment 33 Model a Loaded Dynamic Direction of Movement Output



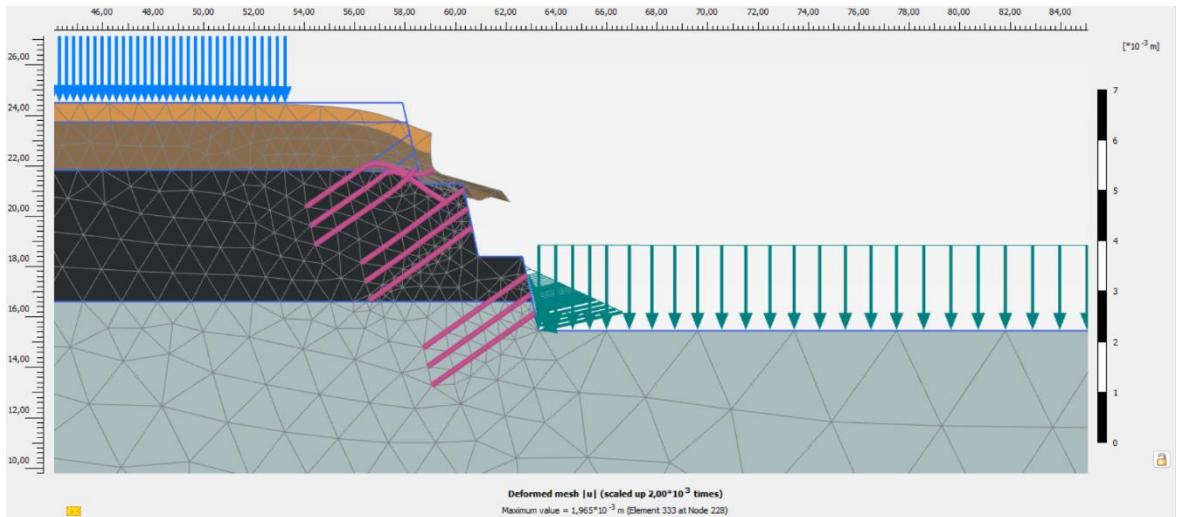
### Attachment 34 Model a Loaded Dynamic Displacement Output



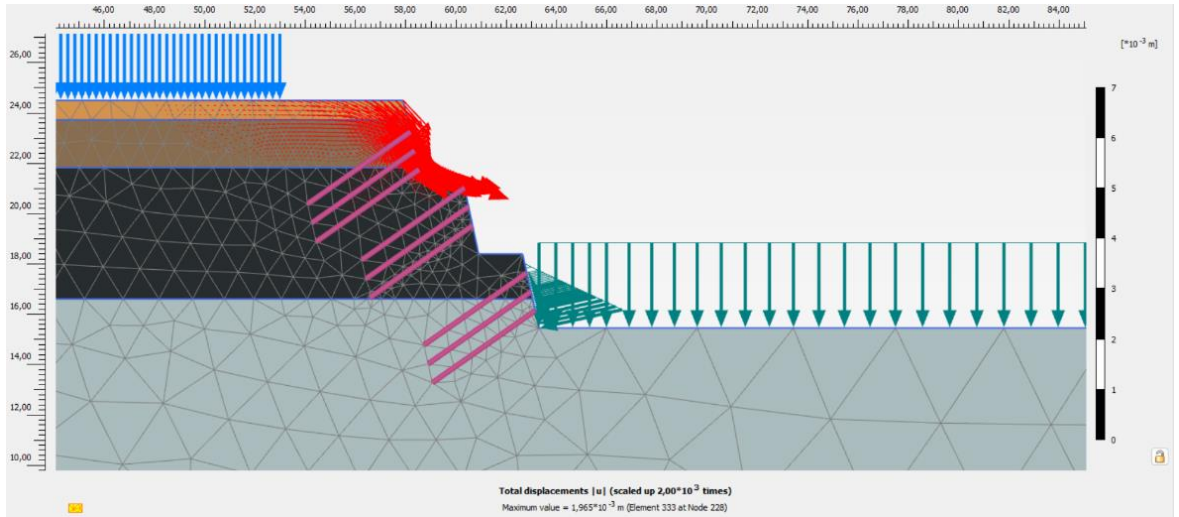
### Attachment 35 Model b Non-Loaded Static Effective Stress Output



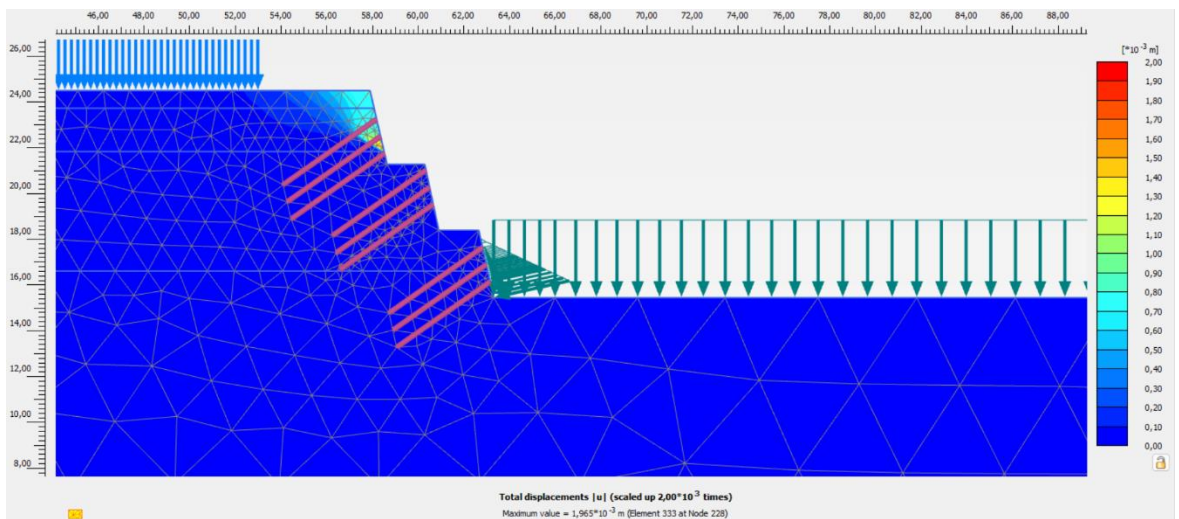
### Attachment 36 Model b Non-Loaded Static Deformed Mesh Output



### Attachment 37 Model b Non-Loaded Static Direction of Movement Output

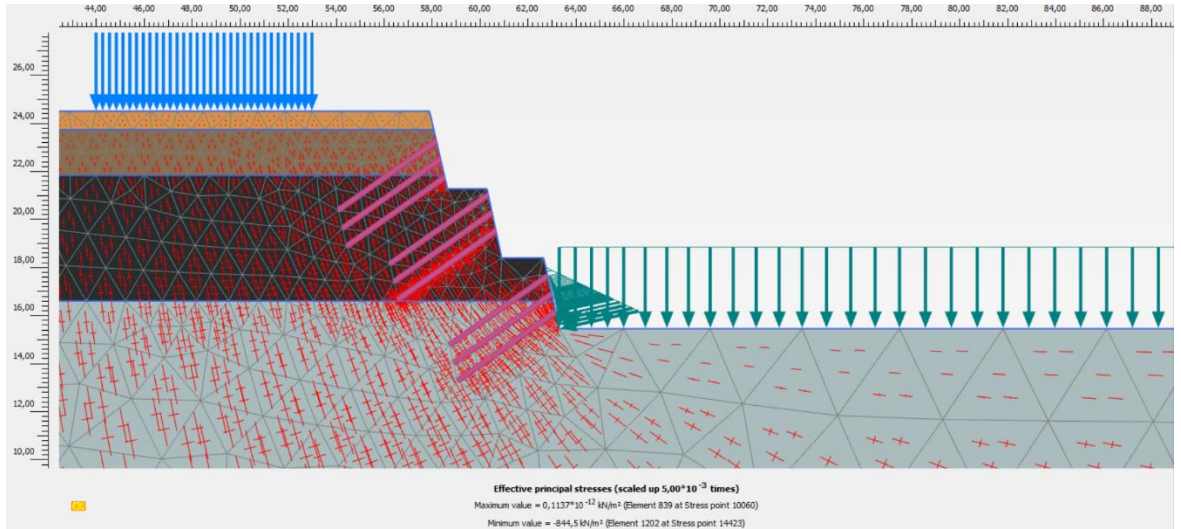


### Attachment 38 Model b Non-Loaded Static Displacement Output

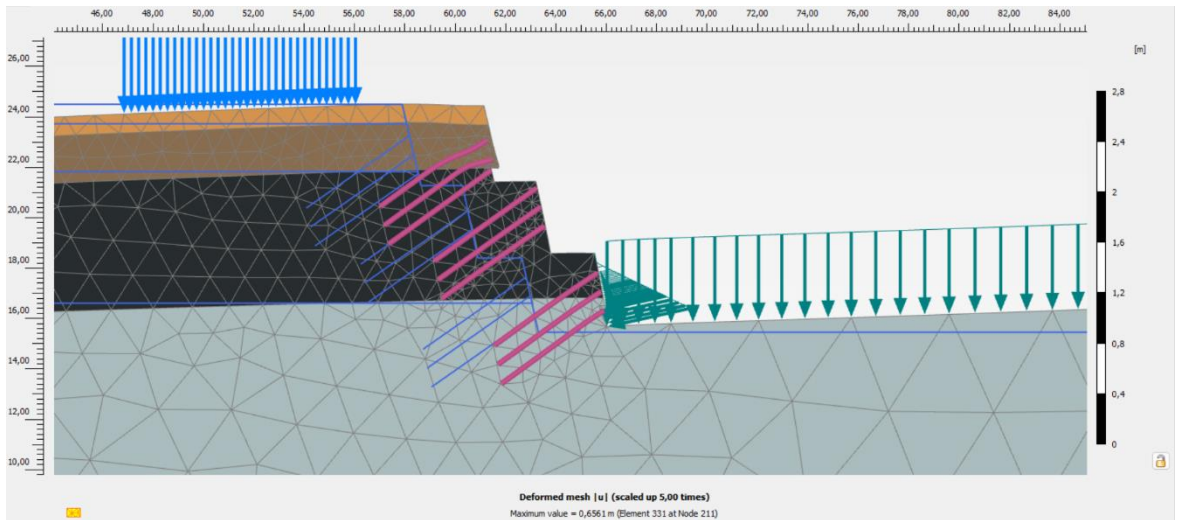




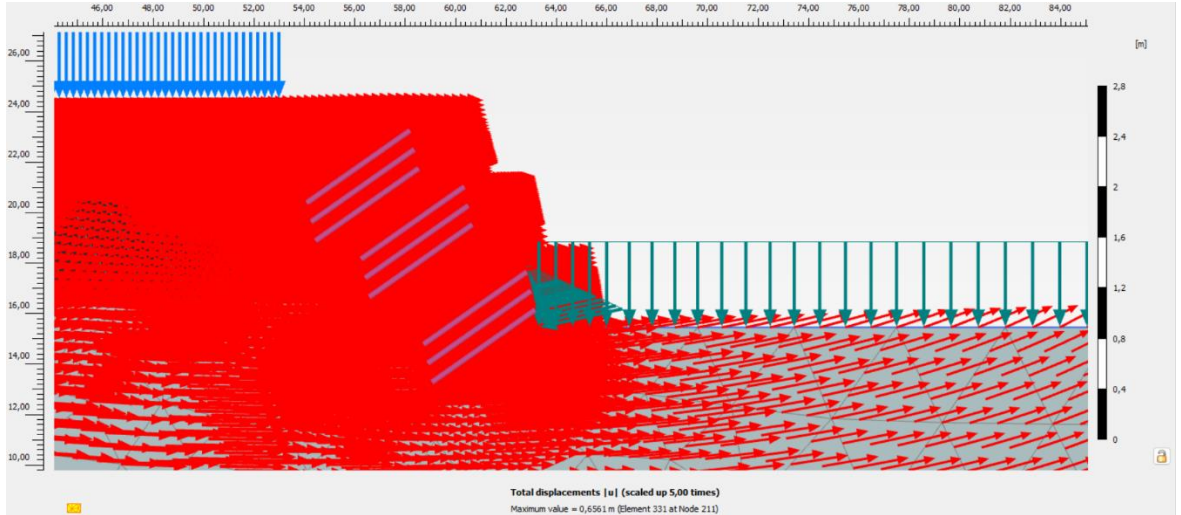
### Attachment 39 Model b Non-Loaded Dynamic Effective Stress Output



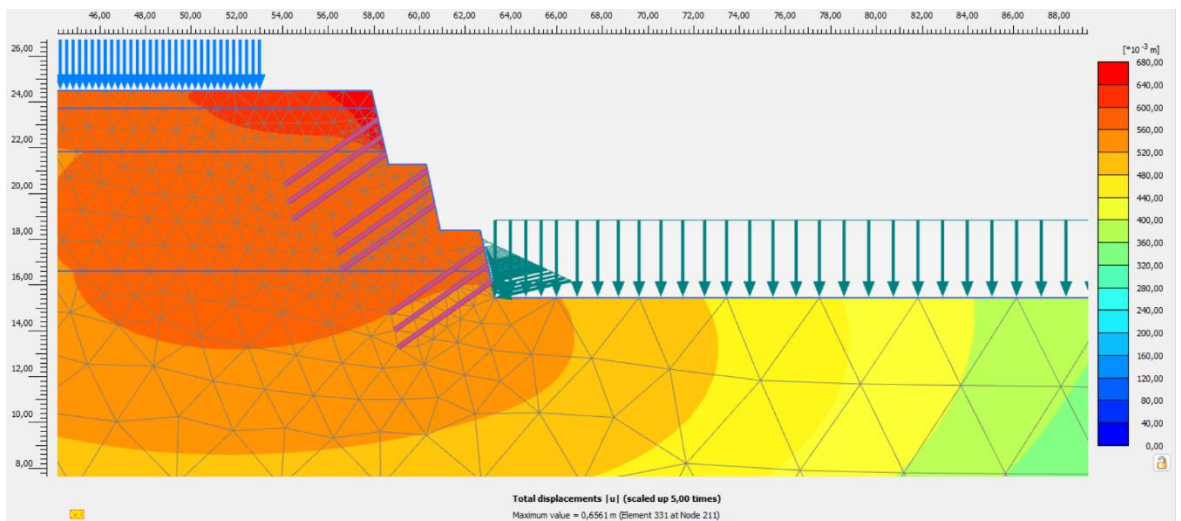
### Attachment 40 Model b Non-Loaded Dynamic Deformed Mesh Output



### Attachment 41 Model b Non-Loaded Dynamic Direction of Movement Output

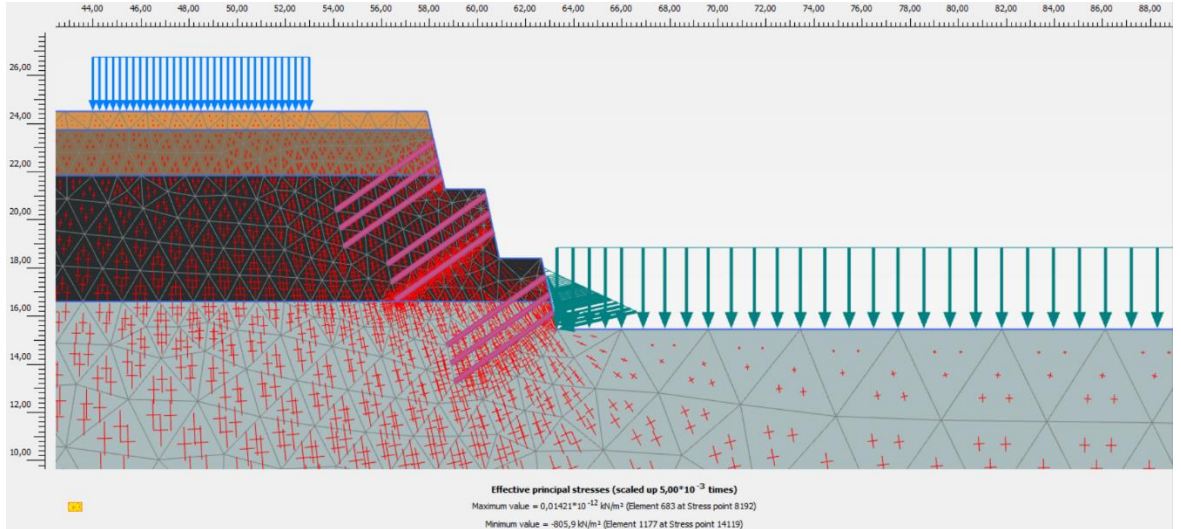


### Attachment 42 Model b Non-Loaded Dynamic Displacement Output

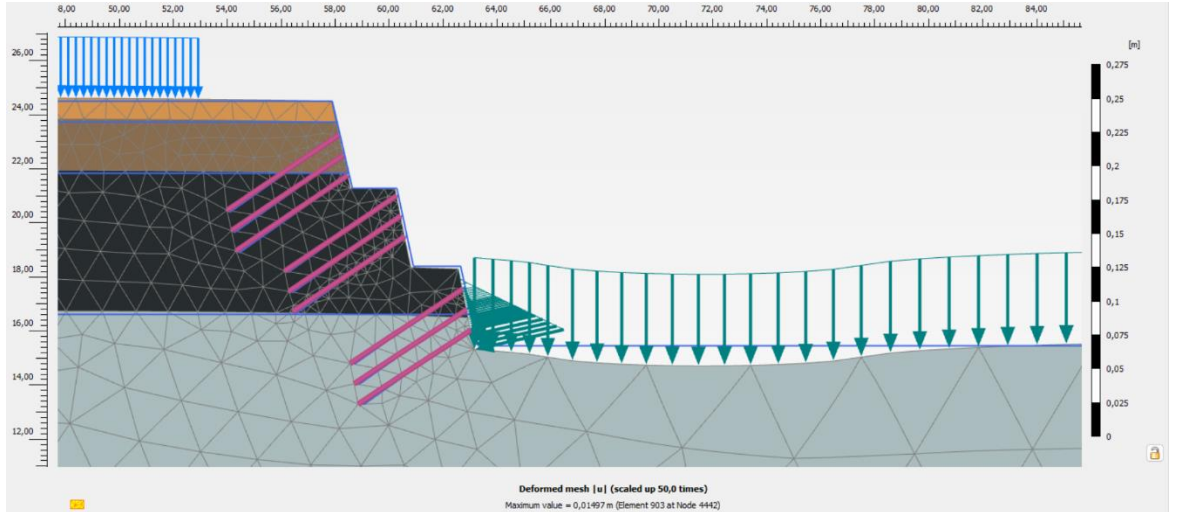




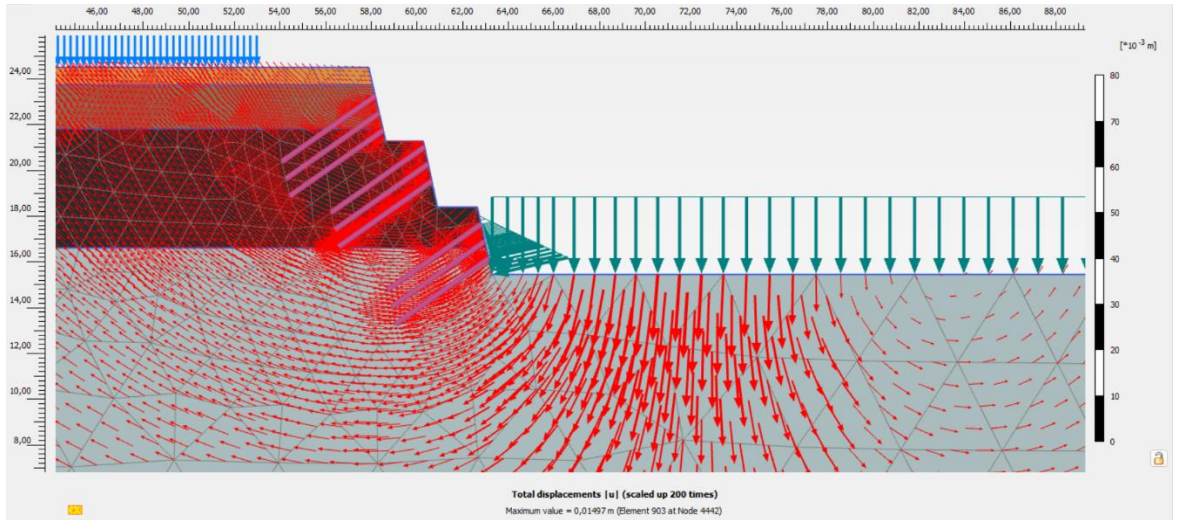
### Attachment 43 Model b Loaded Static Effective Stress Output



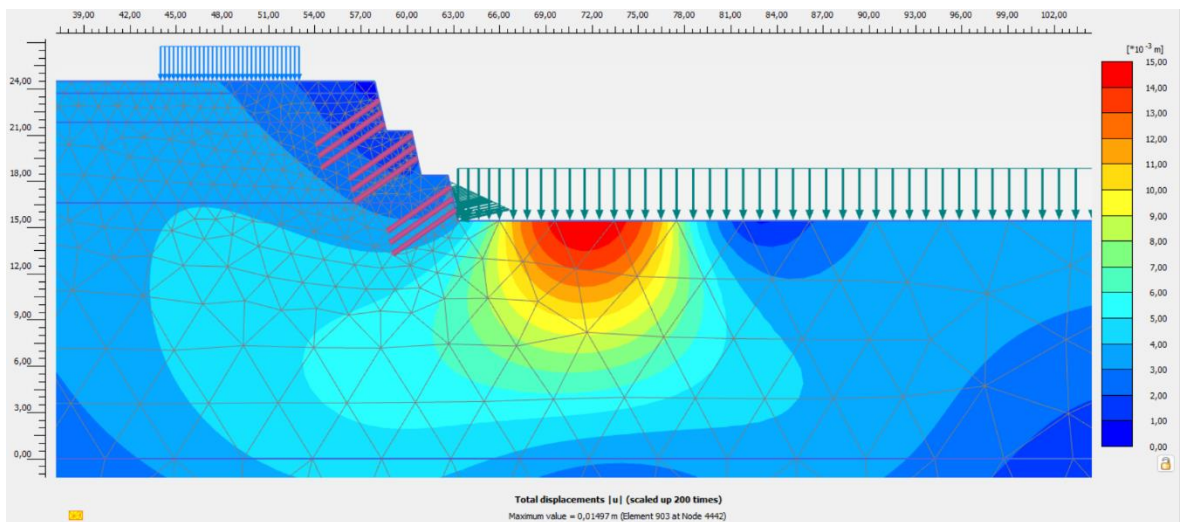
### Attachment 44 Model b Loaded Static Deformed Mesh Output



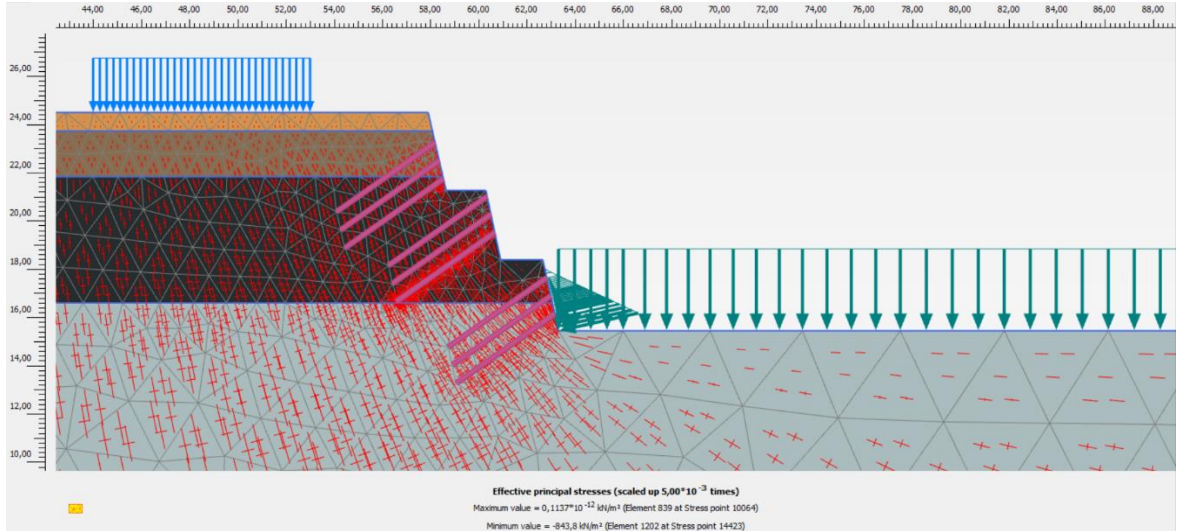
### Attachment 45 Model b Loaded Static Direction of Movement Output



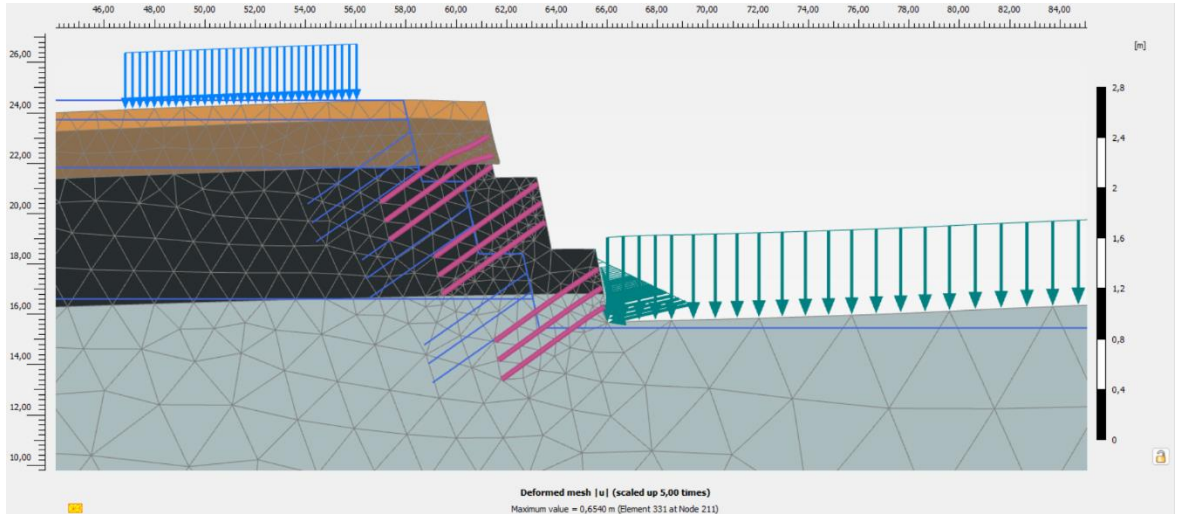
### Attachment 46 Model b Loaded Static Displacement Output



### Attachment 47 Model b Loaded Dynamic Effective Stress Output

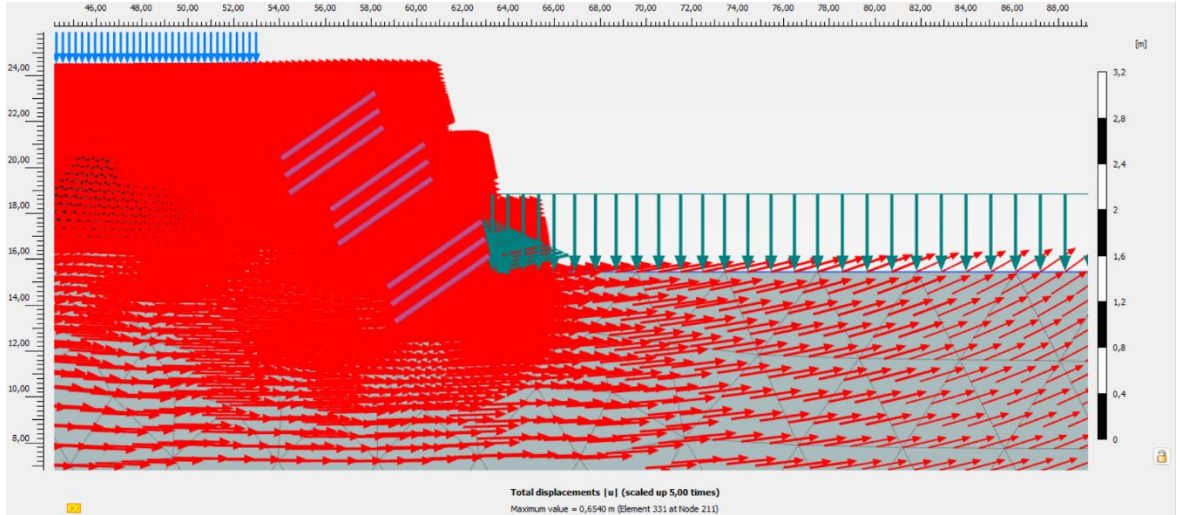


### Attachment 48 Model b Loaded Dynamic Deformed Mesh Output

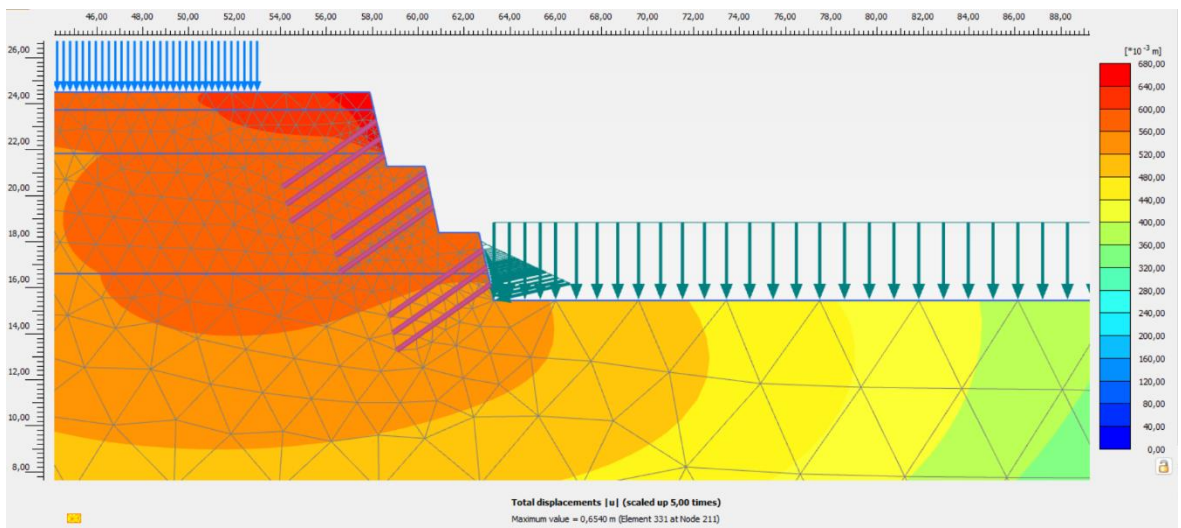




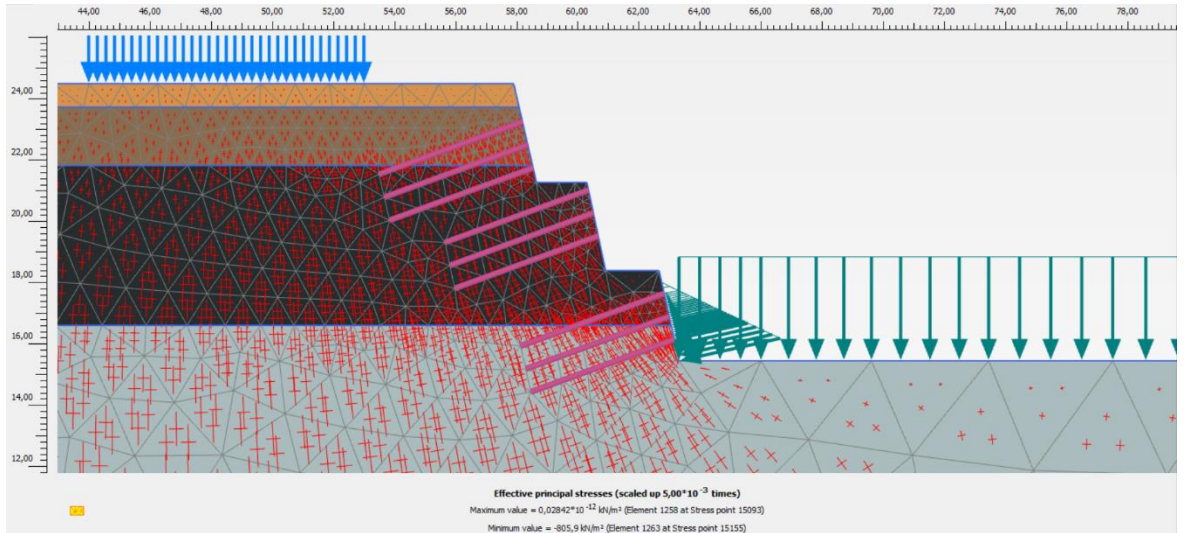
### Attachment 49 Model b Loaded Dynamic Direction of Movement Output



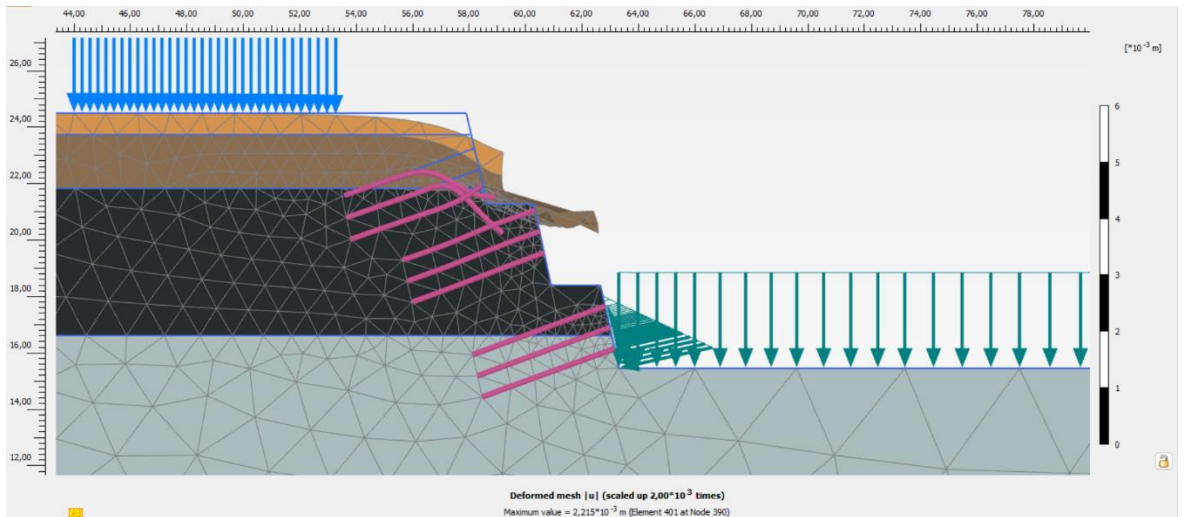
### Attachment 50 Model b Loaded Dynamic Displacement Output



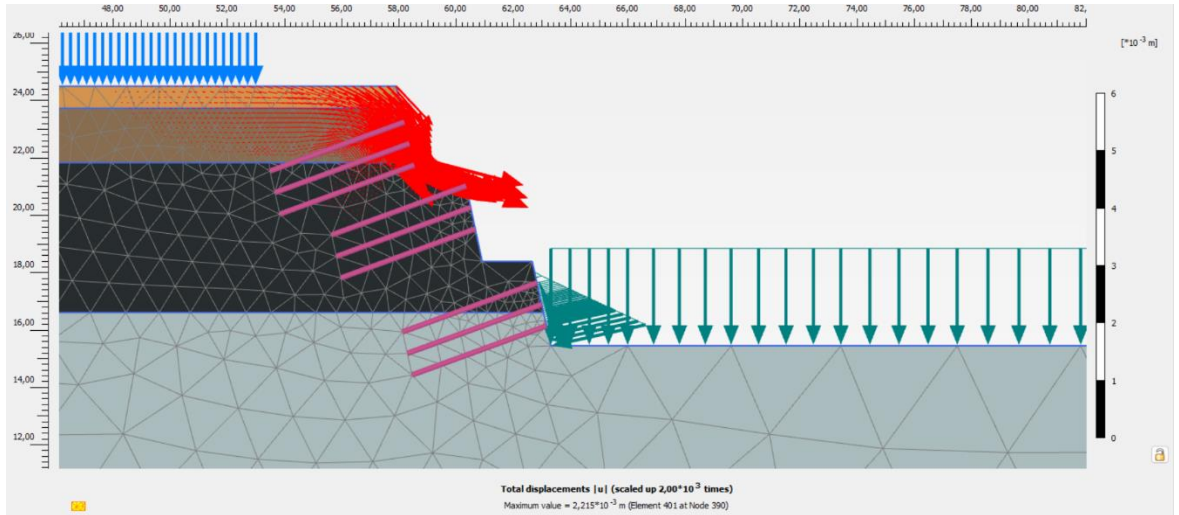
## Attachment 51 Model c Non-Loaded Static Effective Stress Output



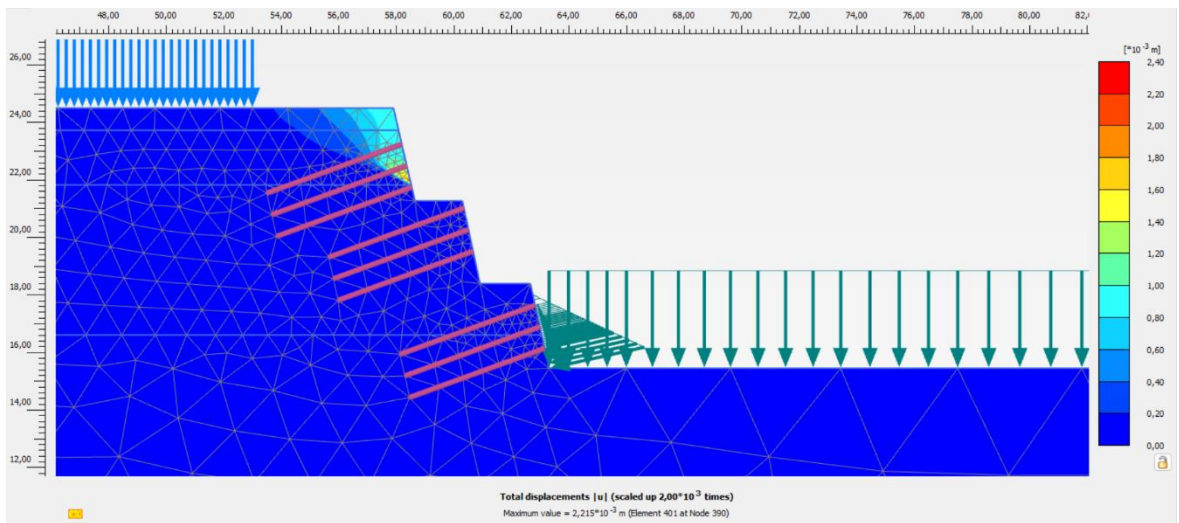
## Attachment 52 Model c Non-Loaded Static Deformed Mesh Output



### Attachment 53 Model c Non-Loaded Static Direction of Movement Output

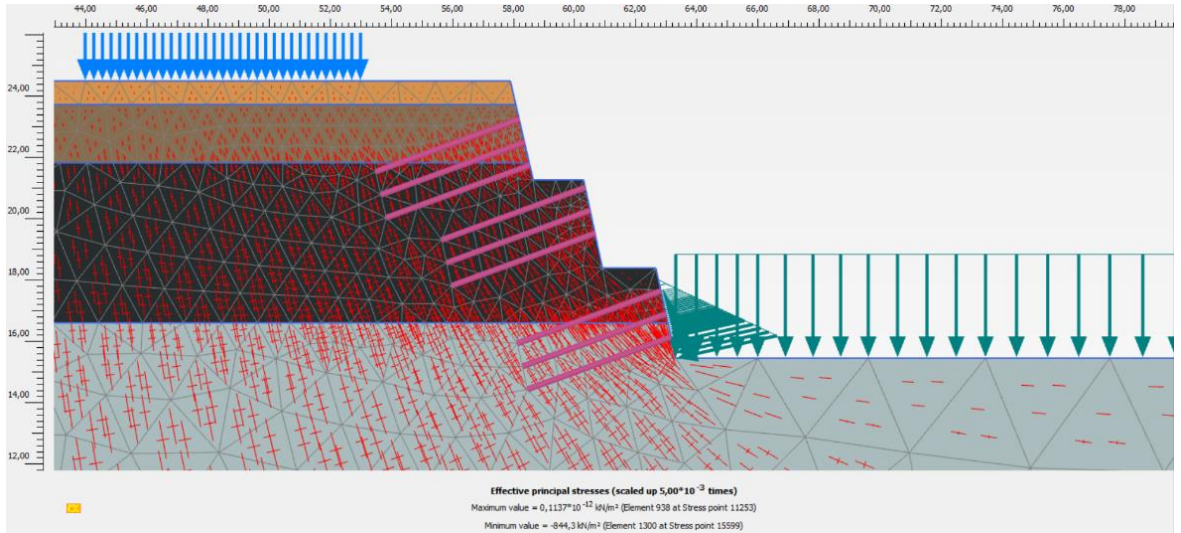


### Attachment 54 Model c Non-Loaded Static Displacement Output

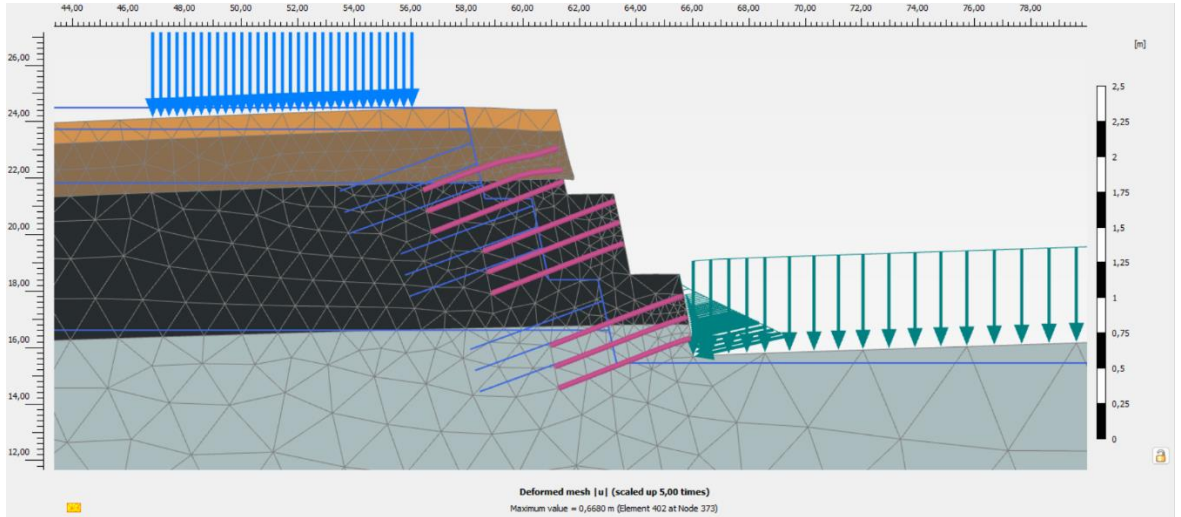




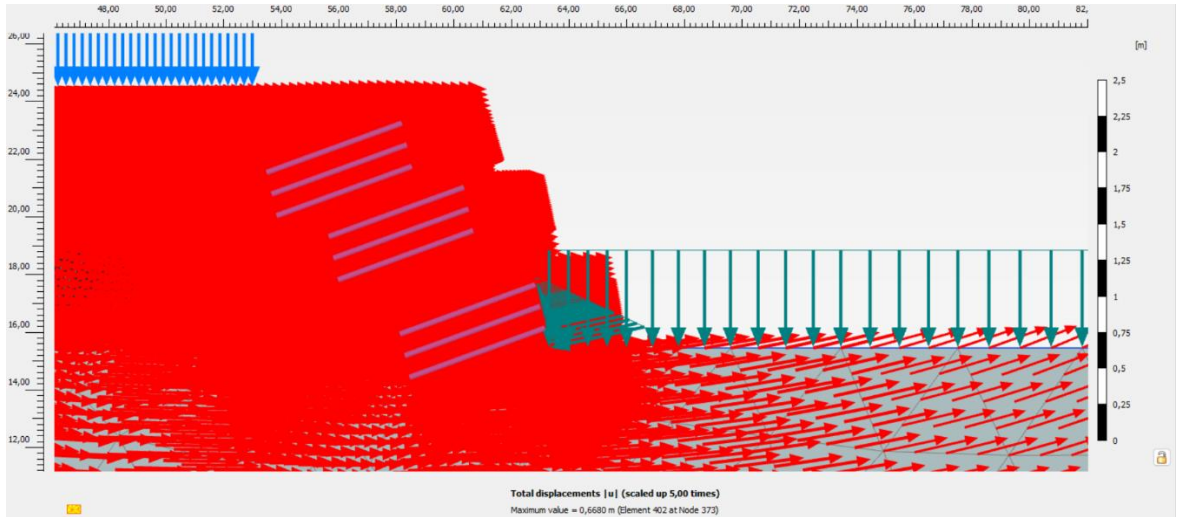
### Attachment 55 Model c Non-Loaded Dynamic Effective Stress Output



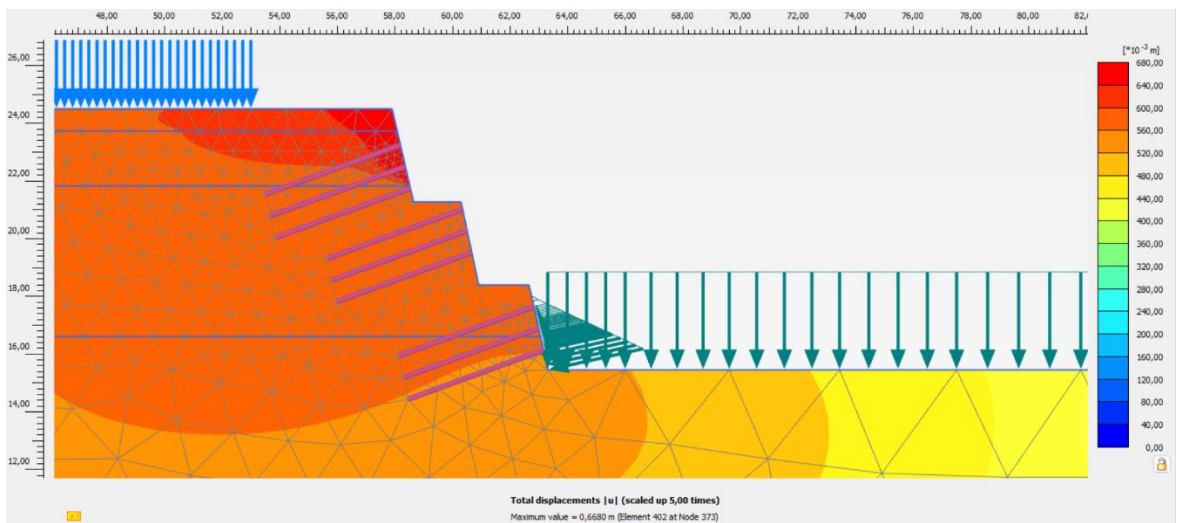
### Attachment 56 Model c Non-Loaded Dynamic Deformed Mesh Output



### Attachment 57 Model c Non-Loaded Dynamic Direction of Movement Output

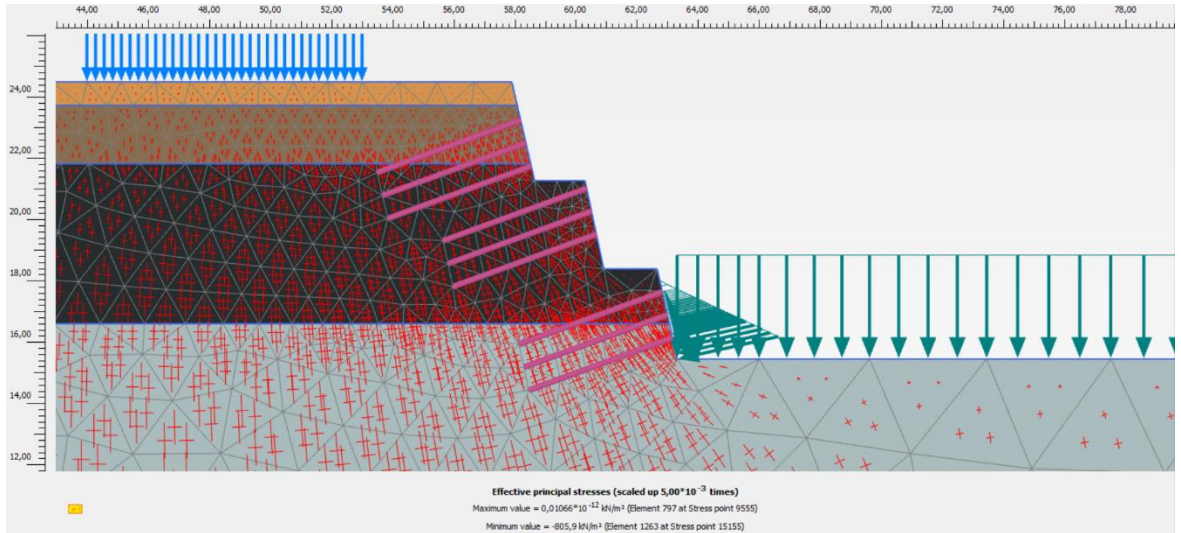


### Attachment 58 Model c Non-Loaded Dynamic Displacement Output

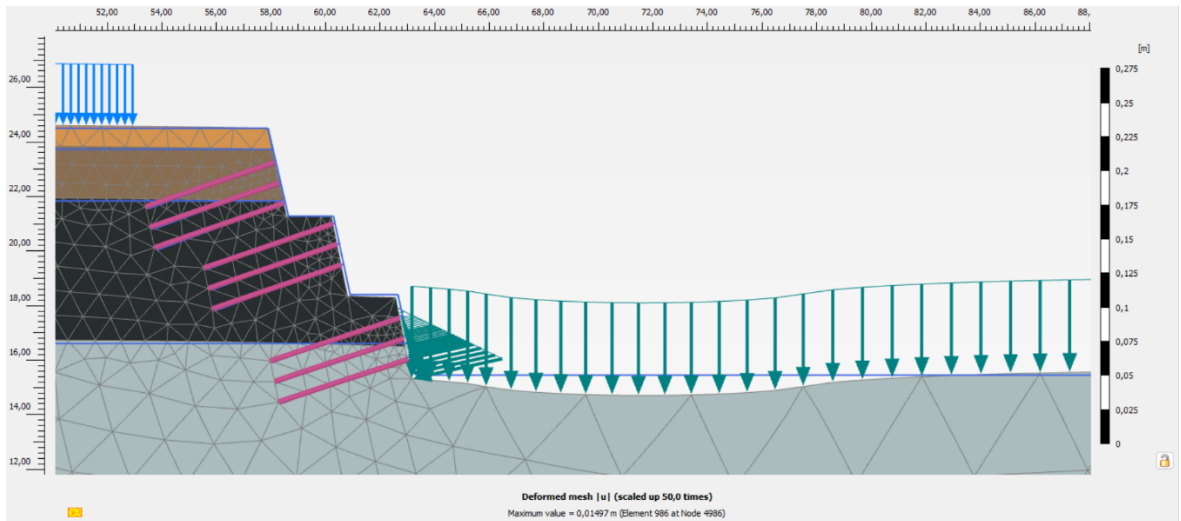




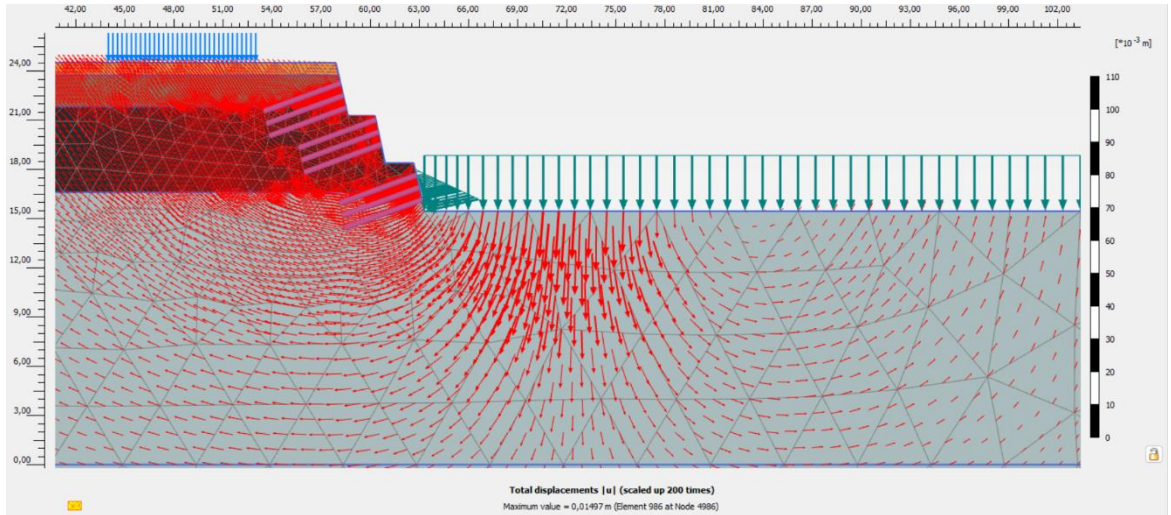
### Attachment 59 Model c Loaded Static Effective Stress Output



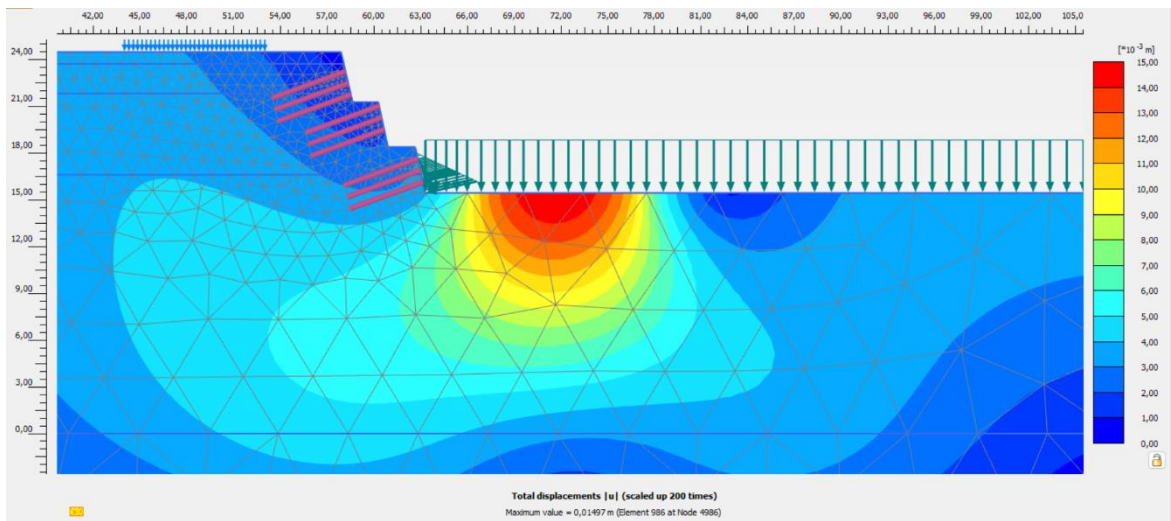
### Attachment 60 Model c Loaded Static Deformed Mesh Output



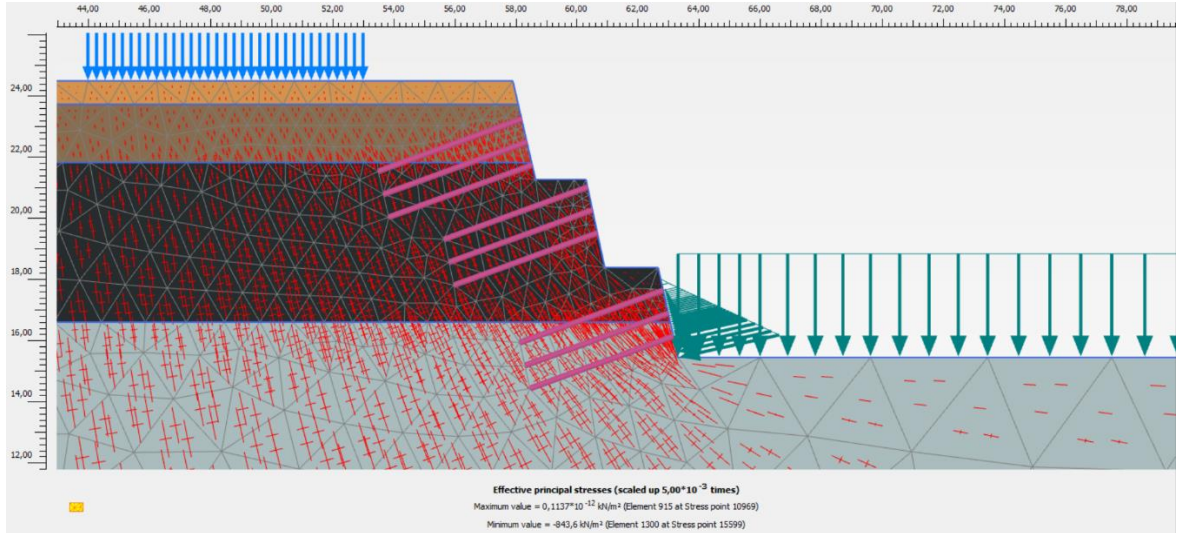
## Attachment 61 Model c Loaded Static Direction of Movement Output



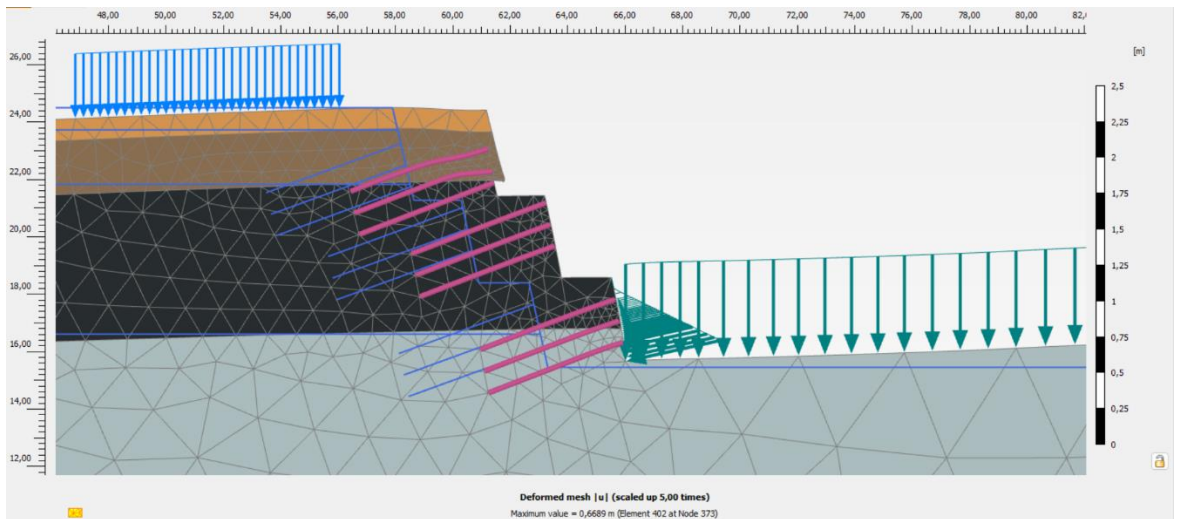
## Attachment 62 Model c Loaded Static Displacement Output



### Attachment 63 Model c Loaded Dynamic Effective Stress Output

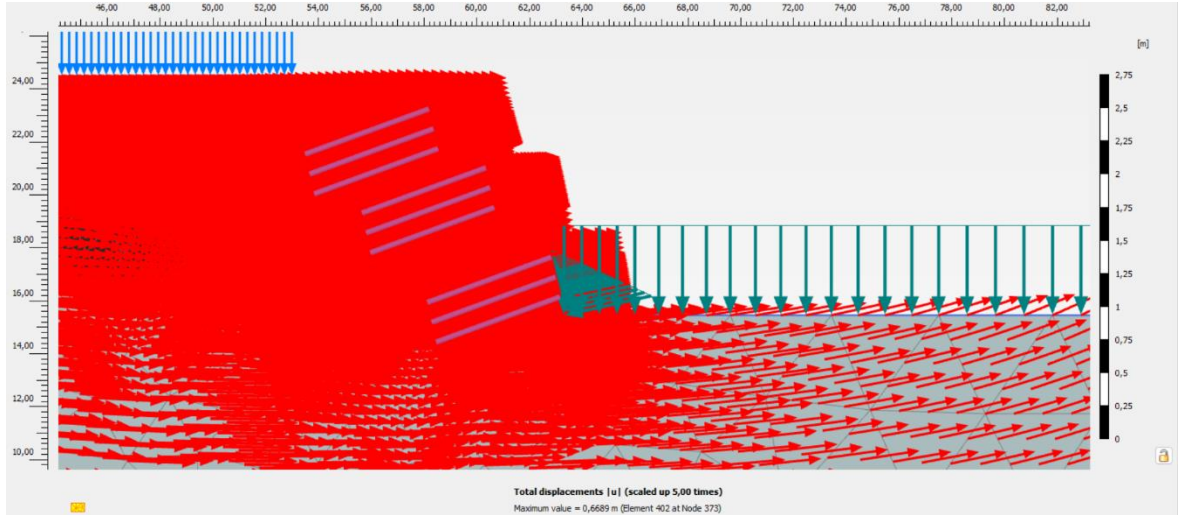


### Attachment 64 Model c Loaded Dynamic Deformed Mesh Output

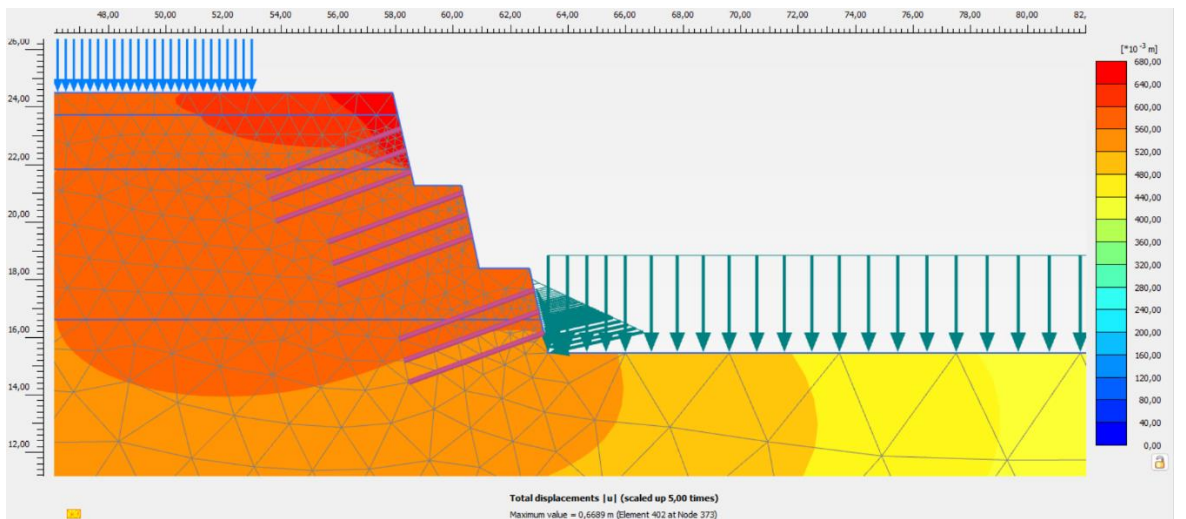




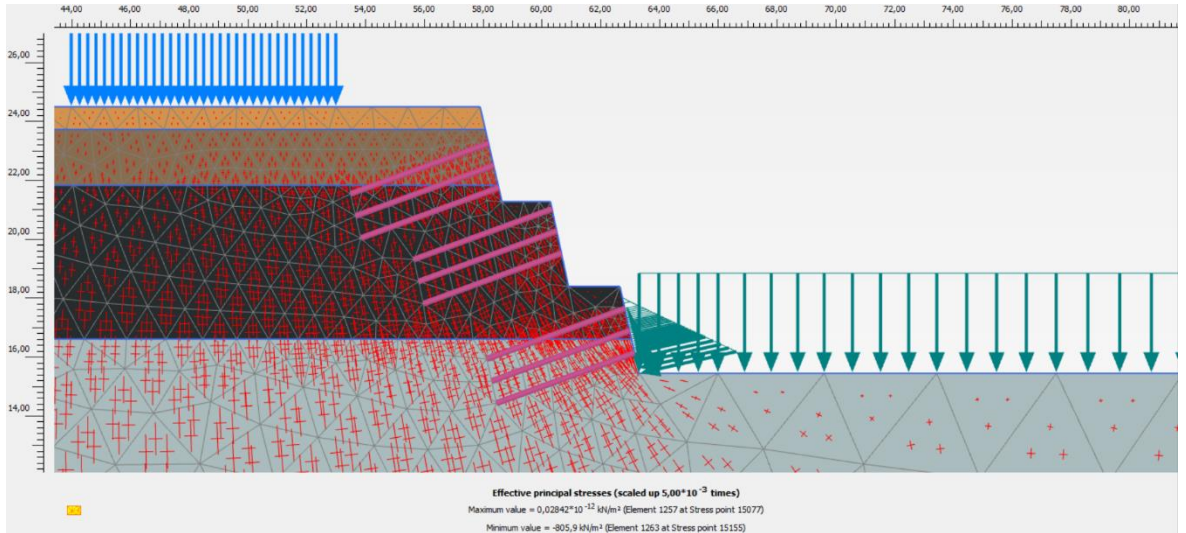
### Attachment 65 Model c Loaded Dynamic Direction of Movement Output



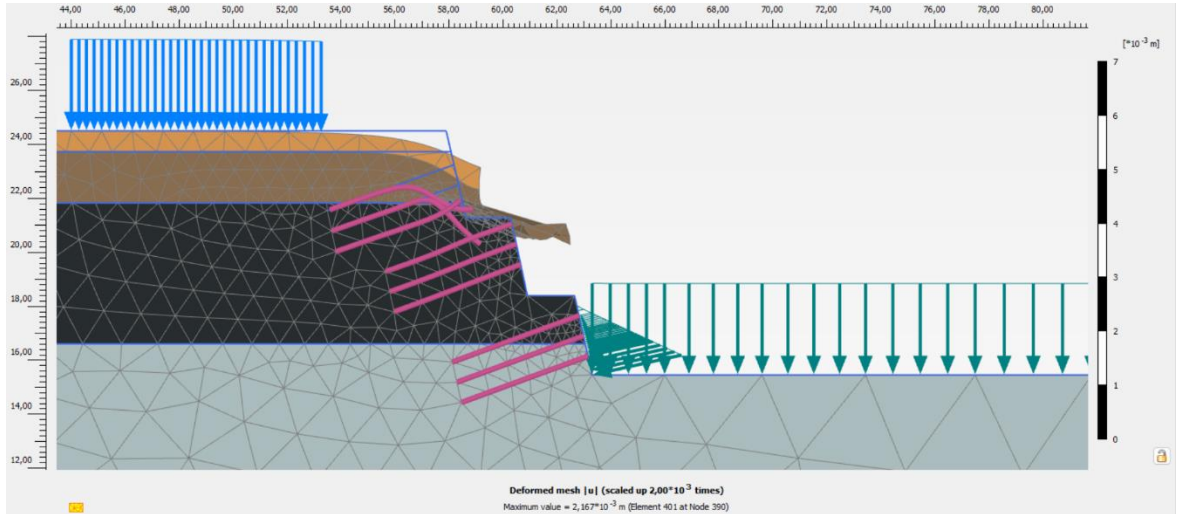
### Attachment 66 Model c Loaded Dynamic Displacement Output



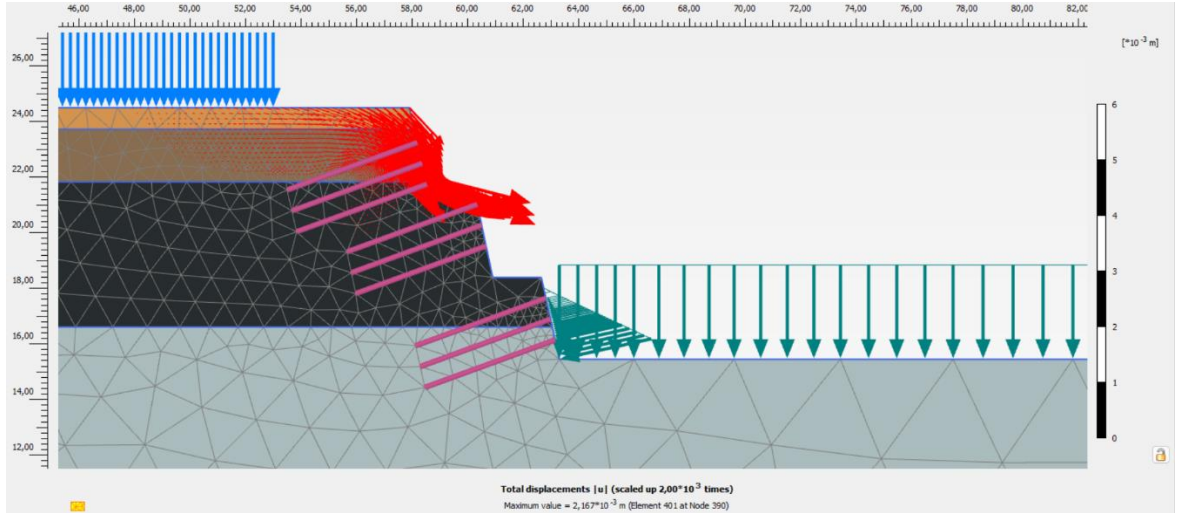
### Attachment 67 Model d Non-Loaded Static Effective Stress Output



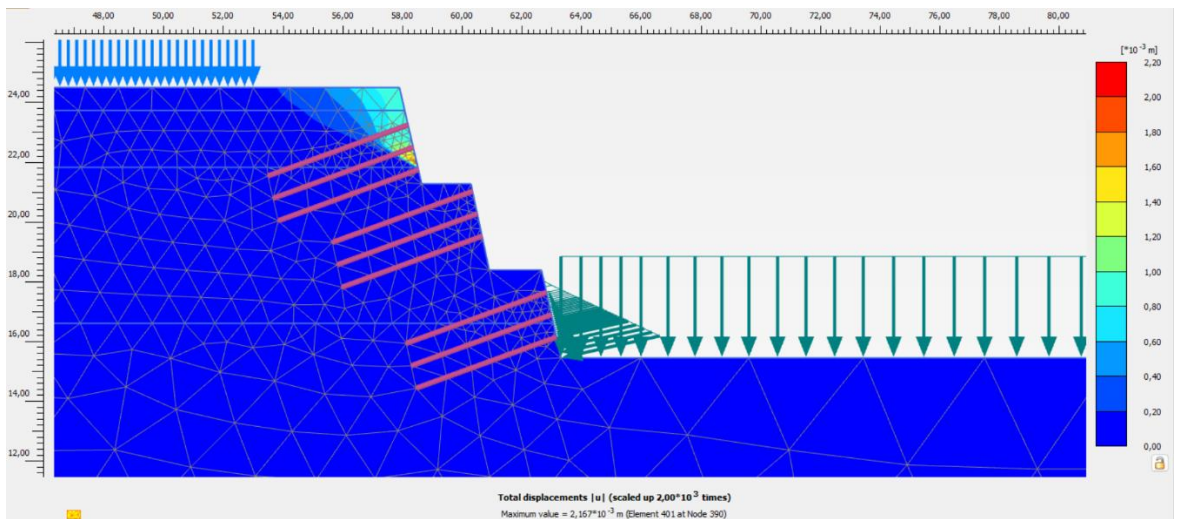
### Attachment 68 Model d Non-Loaded Static Deformed Mesh Output



### Attachment 69 Model d Non-Loaded Static Direction of Movement Output

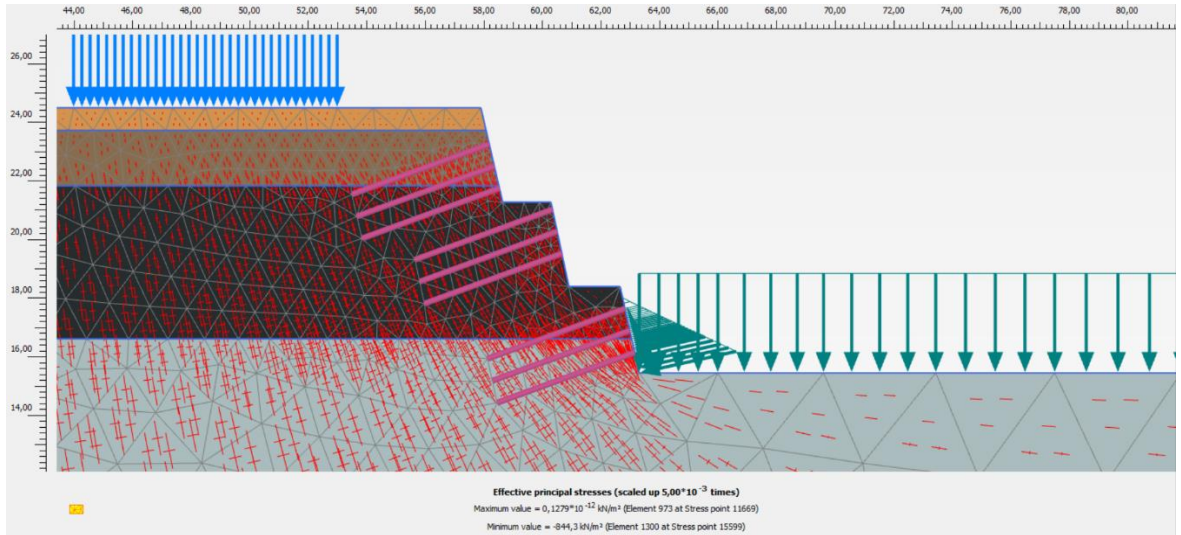


### Attachment 70 Model d Non-Loaded Static Displacement Output

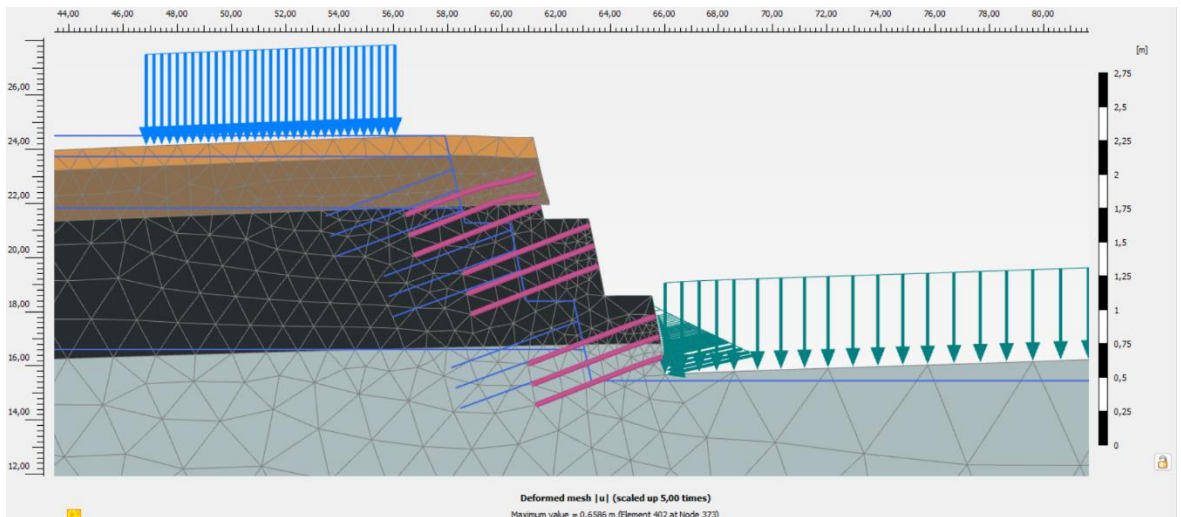




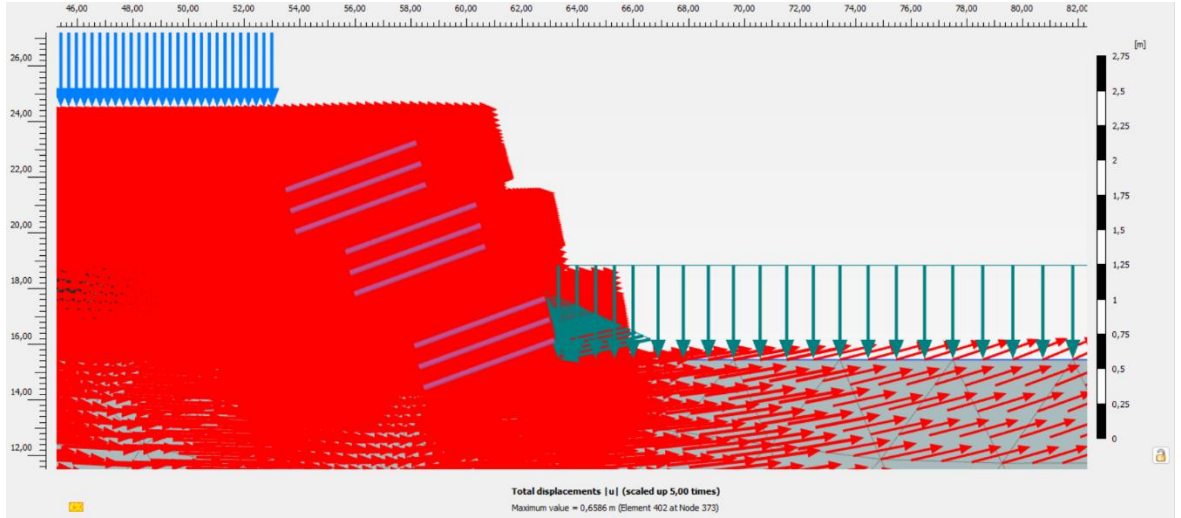
## Attachment 71 Model d Non-Loaded Dynamic Effective Stress Output



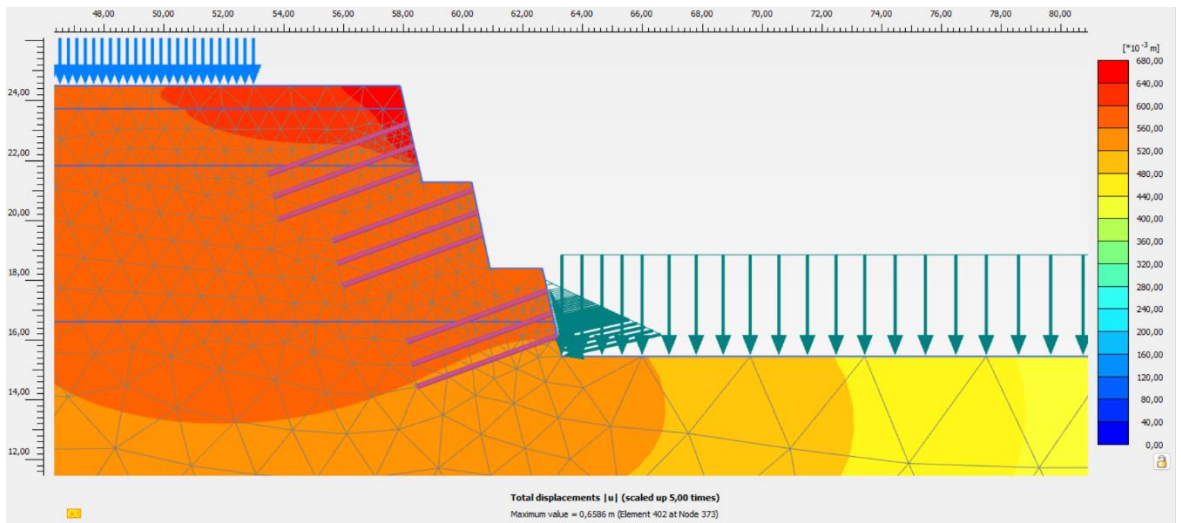
## Attachment 72 Model d Non-Loaded Dynamic Deformed Mesh Output



### Attachment 73 Model d Non-Loaded Dynamic Direction of Movement Output

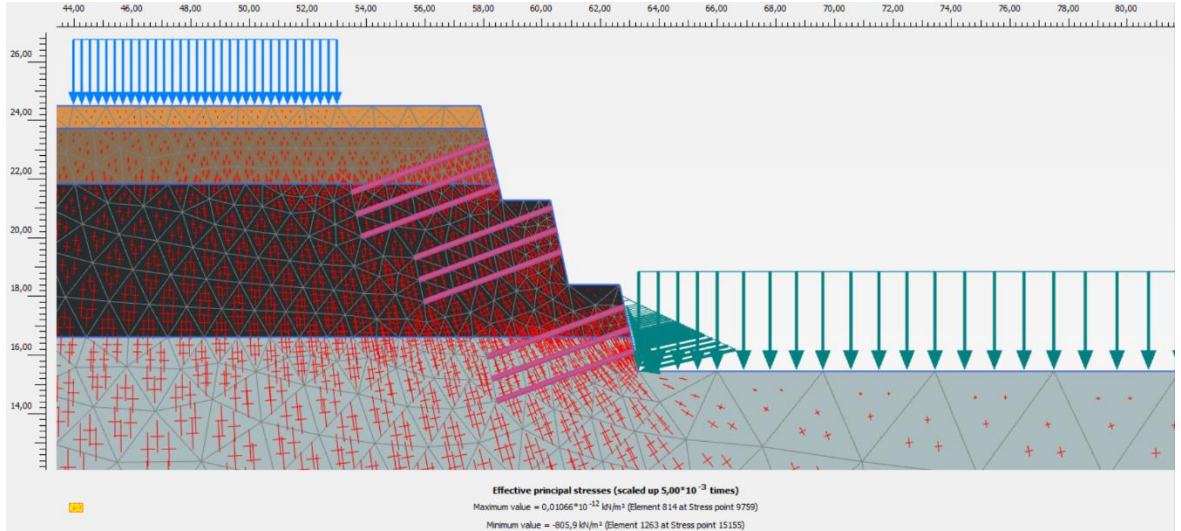


### Attachment 74 Model d Non-Loaded Dynamic Displacement Output

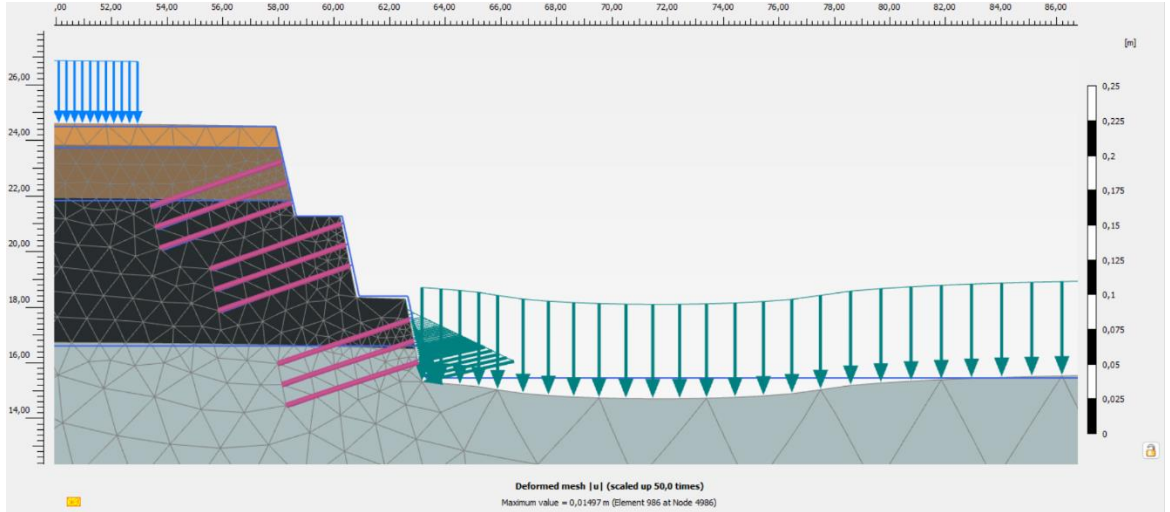




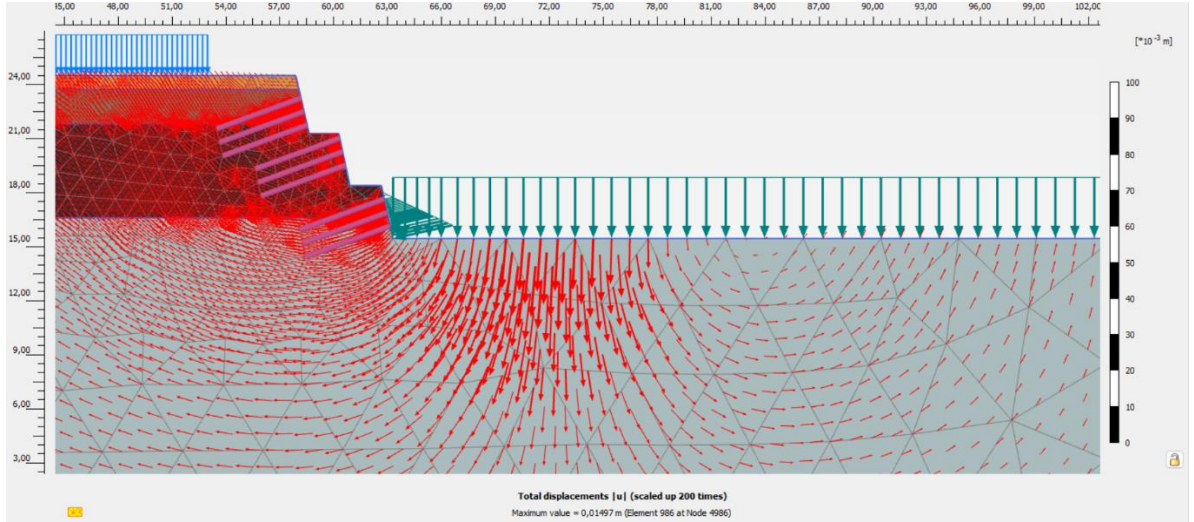
## Attachment 75 Model d Loaded Static Effective Stress Output



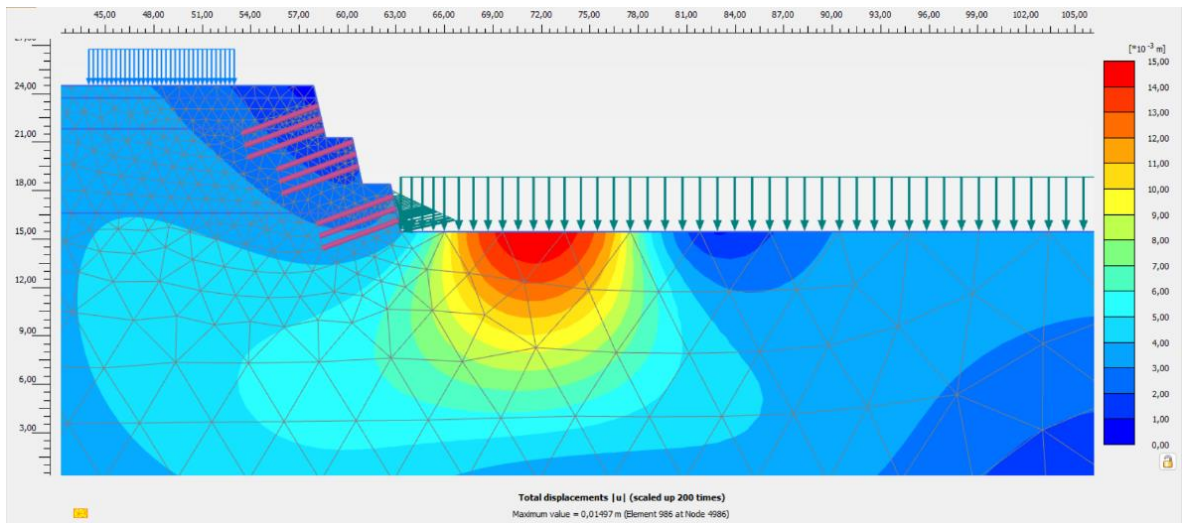
## Attachment 76 Model d Loaded Static Deformed Mesh Output



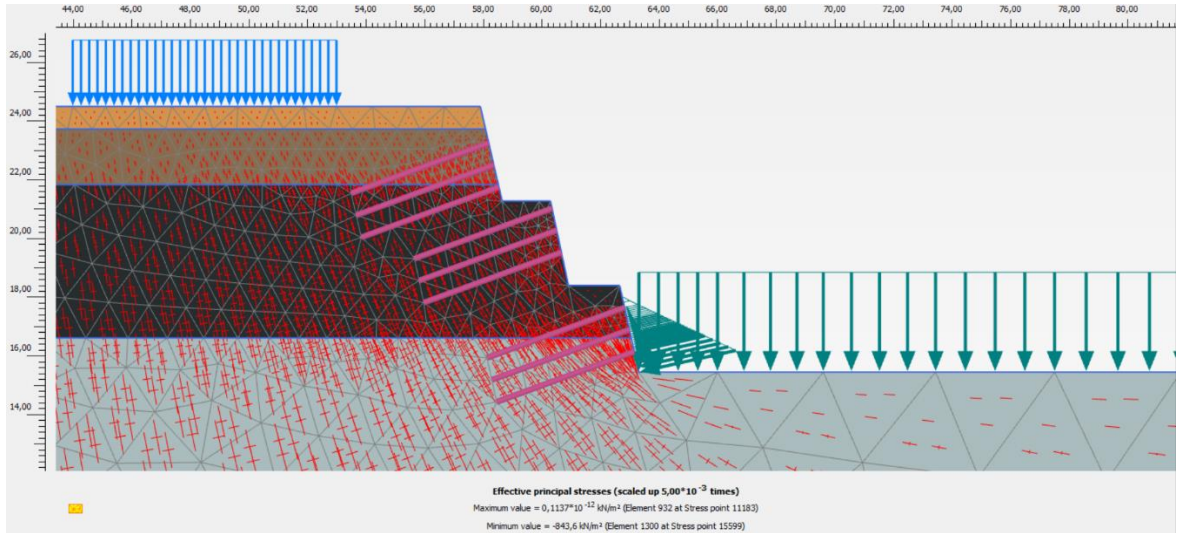
### Attachment 77 Model d Loaded Static Direction of Movement Output



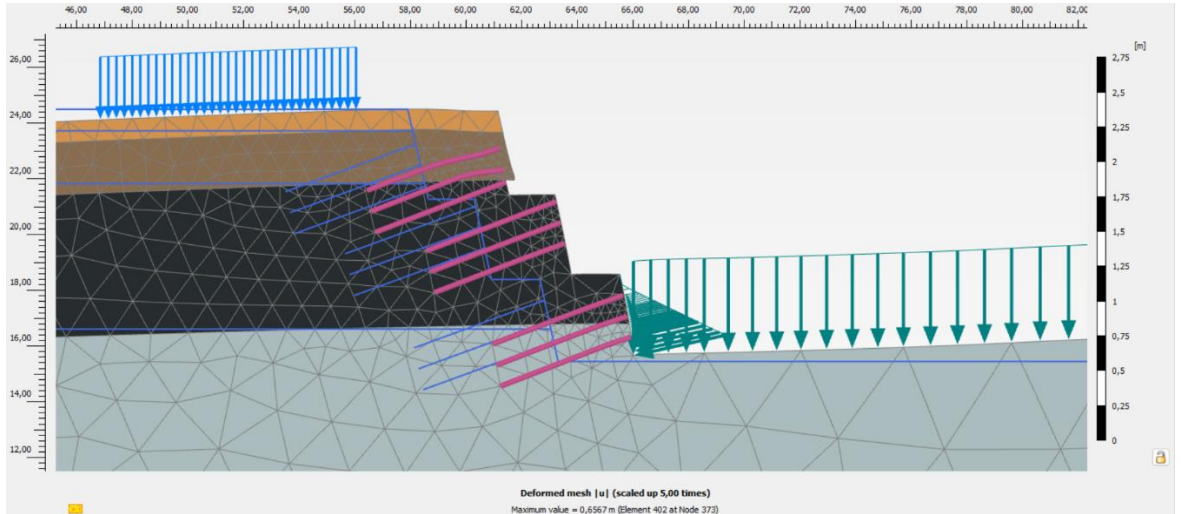
### Attachment 78 Model d Loaded Static Displacement Output



## Attachment 79 Model d Loaded Dynamic Effective Stress Output

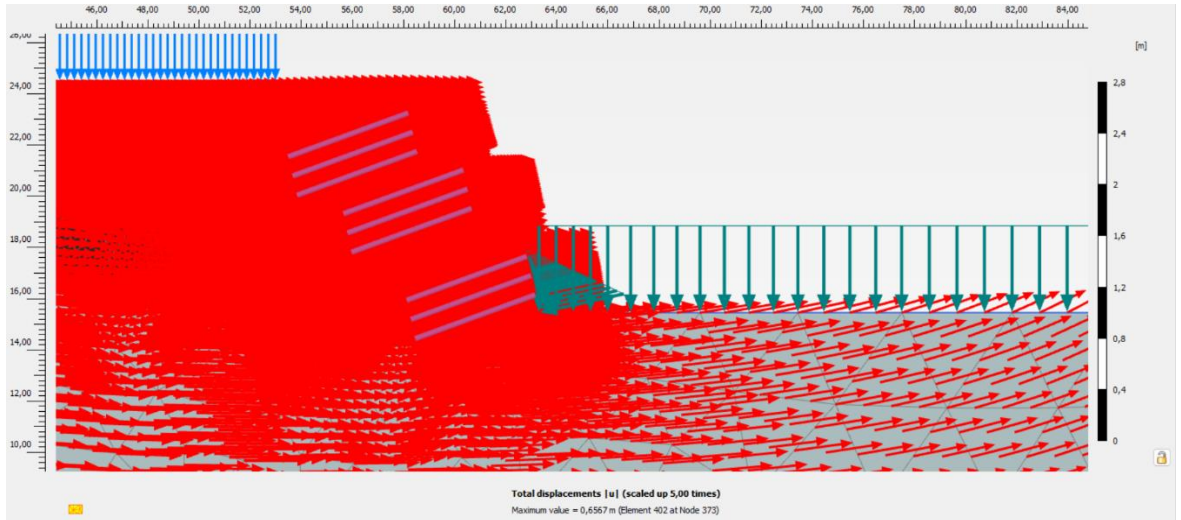


## Attachment 80 Model d Loaded Dynamic Deformed Mesh Output

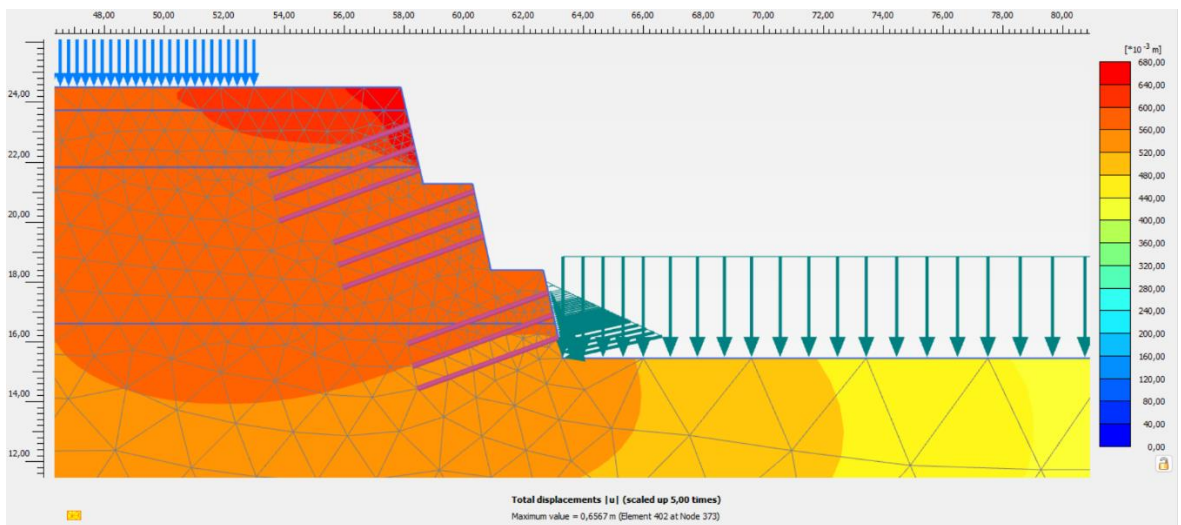




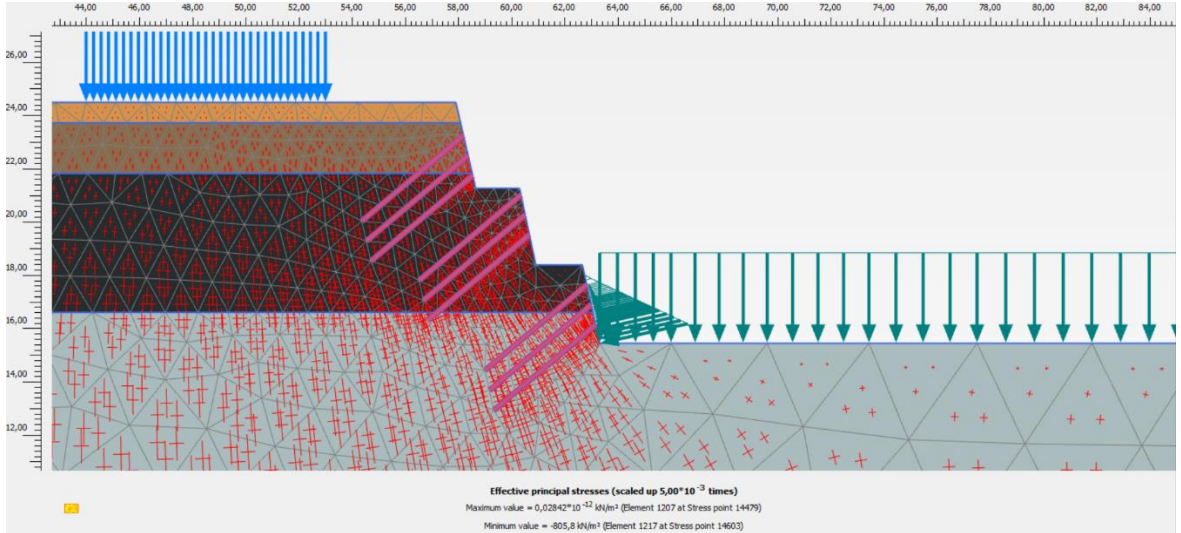
### Attachment 81 Model d Loaded Dynamic Direction of Movement Output



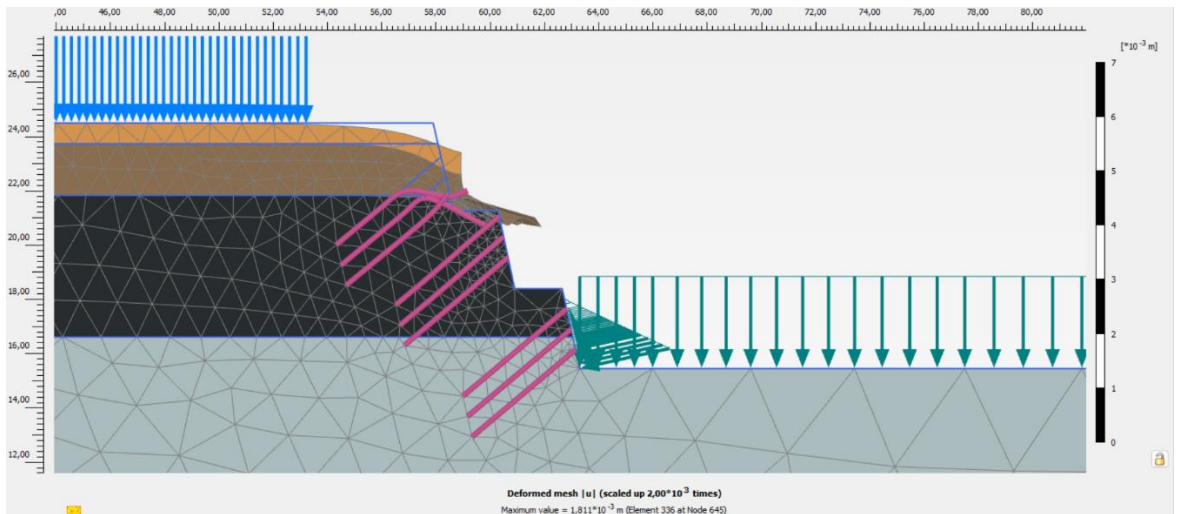
### Attachment 82 Model d Loaded Dynamic Displacement Output



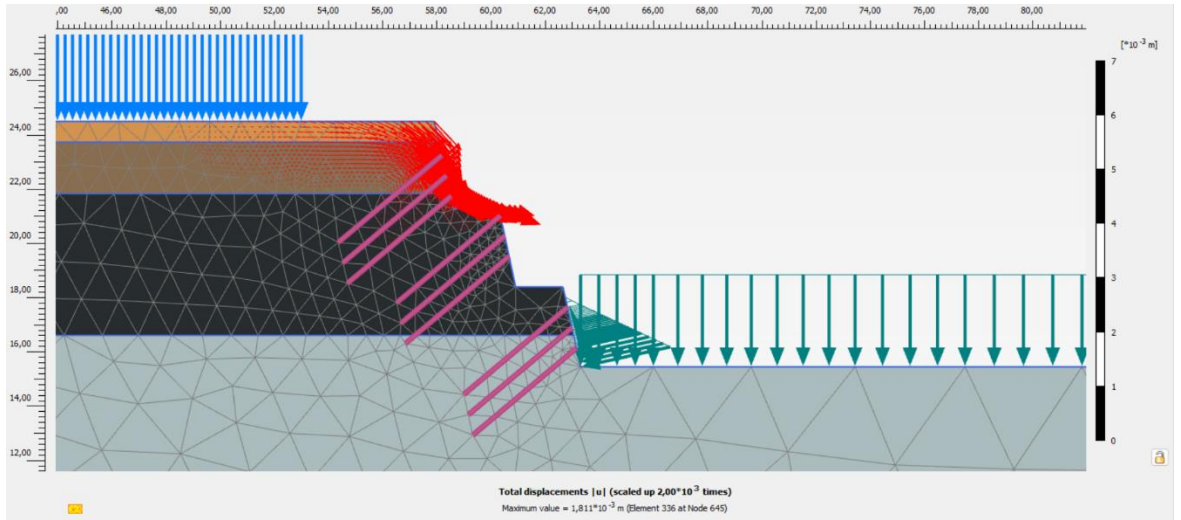
### Attachment 83 Model e Non-Loaded Static Effective Stress Output



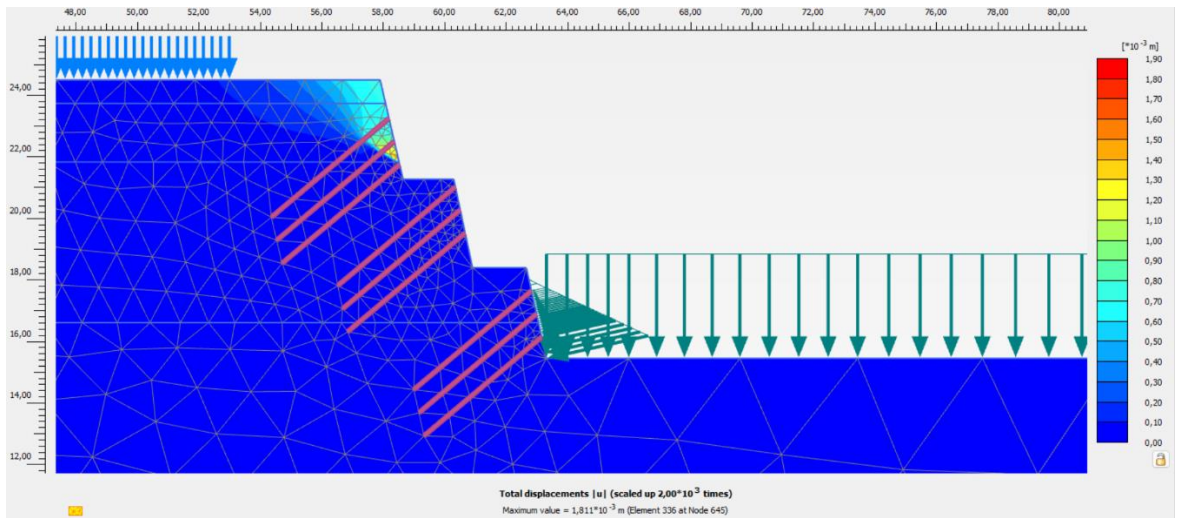
### Attachment 84 Model e Non-Loaded Static Deformed Mesh Output



### Attachment 85 Model e Non-Loaded Static Direction of Movement Output

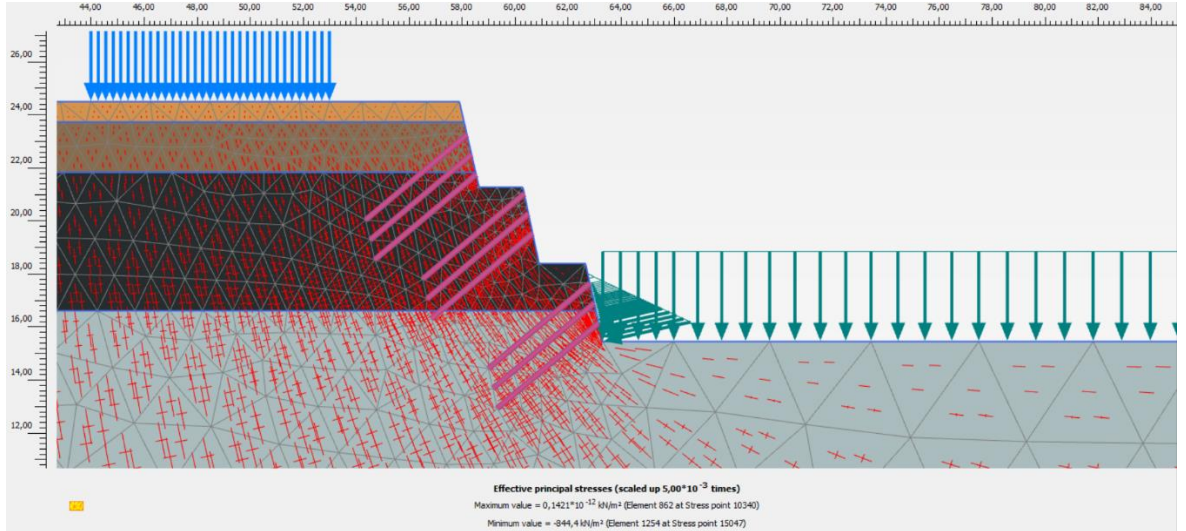


### Attachment 86 Model e Non-Loaded Static Displacement Output

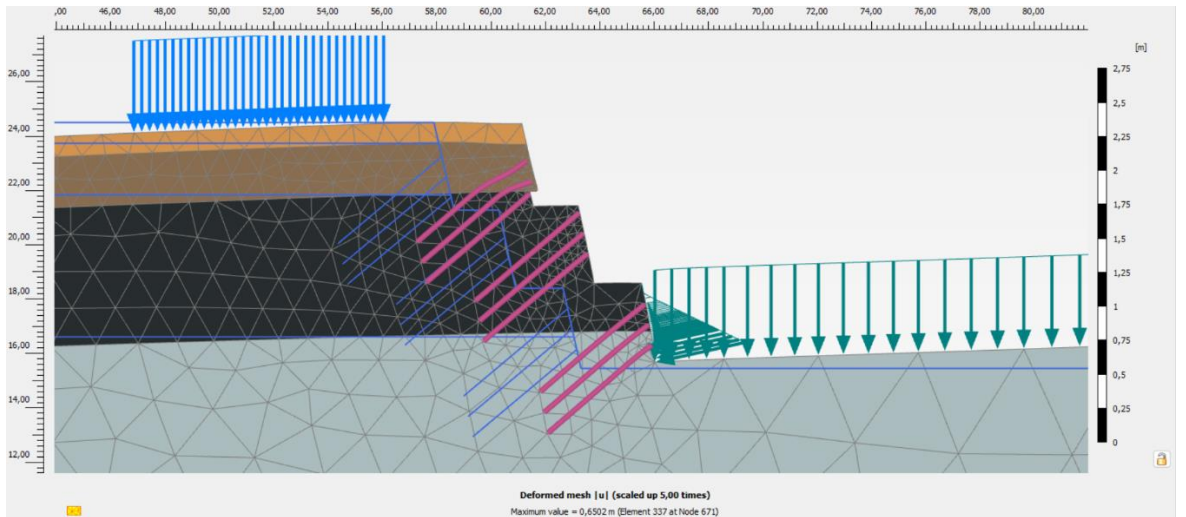




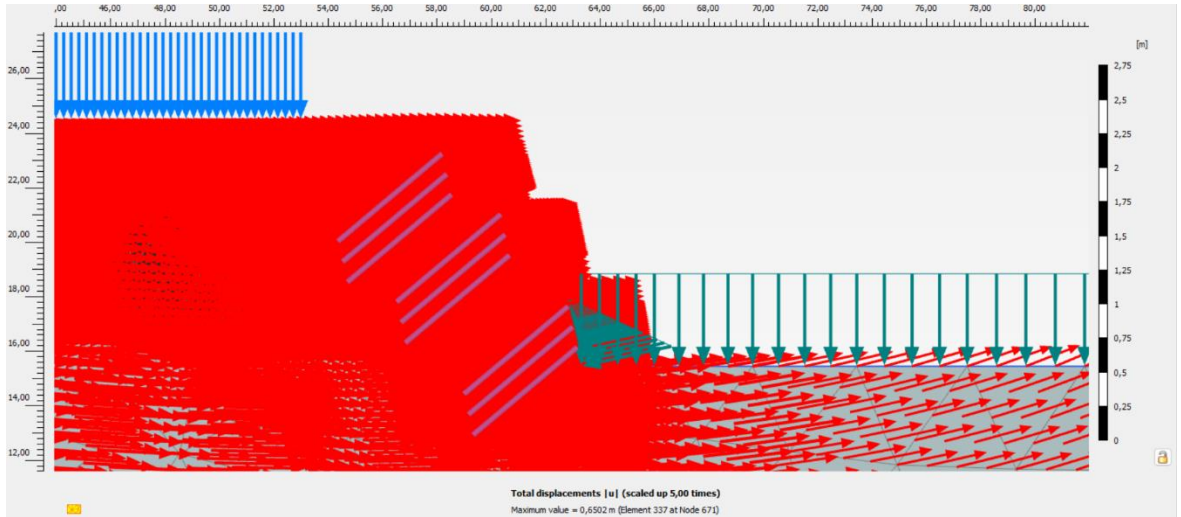
### Attachment 87 Model e Non-Loaded Dynamic Effective Stress Output



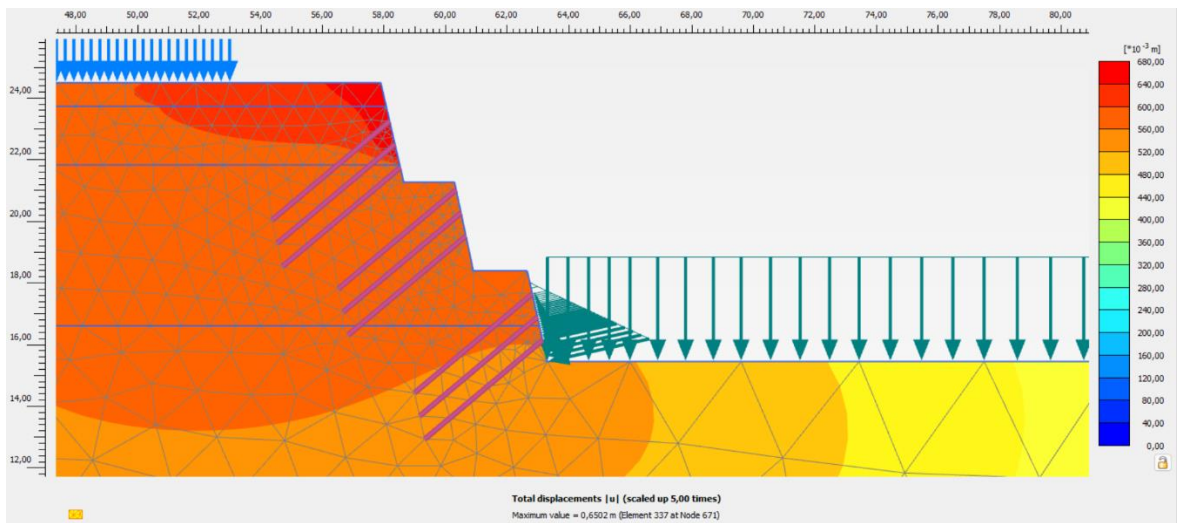
### Attachment 88 Model e Non-Loaded Dynamic Deformed Mesh Output



### Attachment 89 Model e Non-Loaded Dynamic Direction of Movement Output

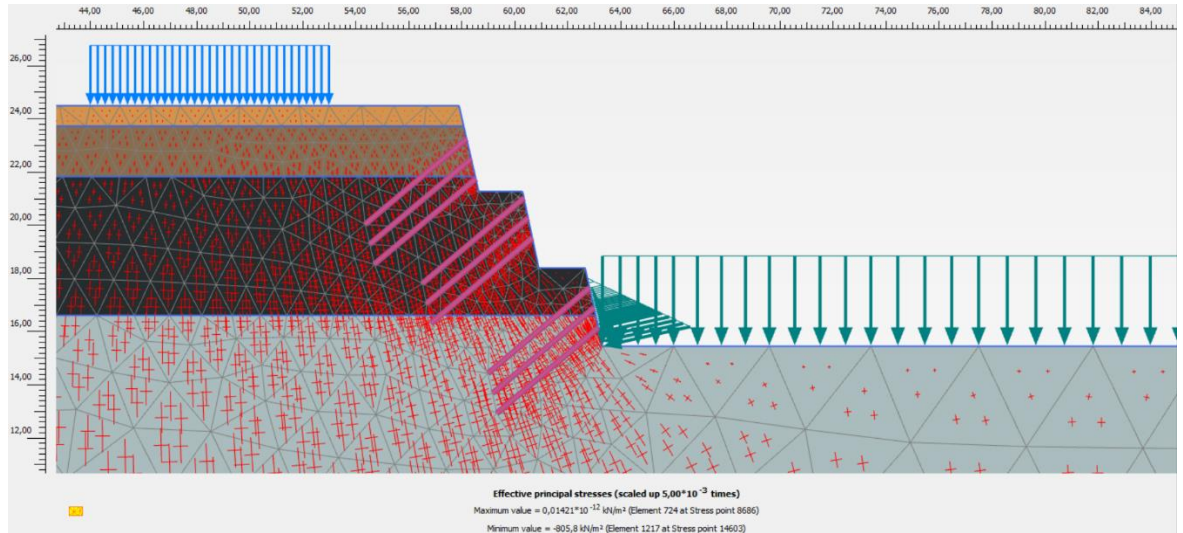


### Attachment 90 Model e Non-Loaded Dynamic Displacement Output

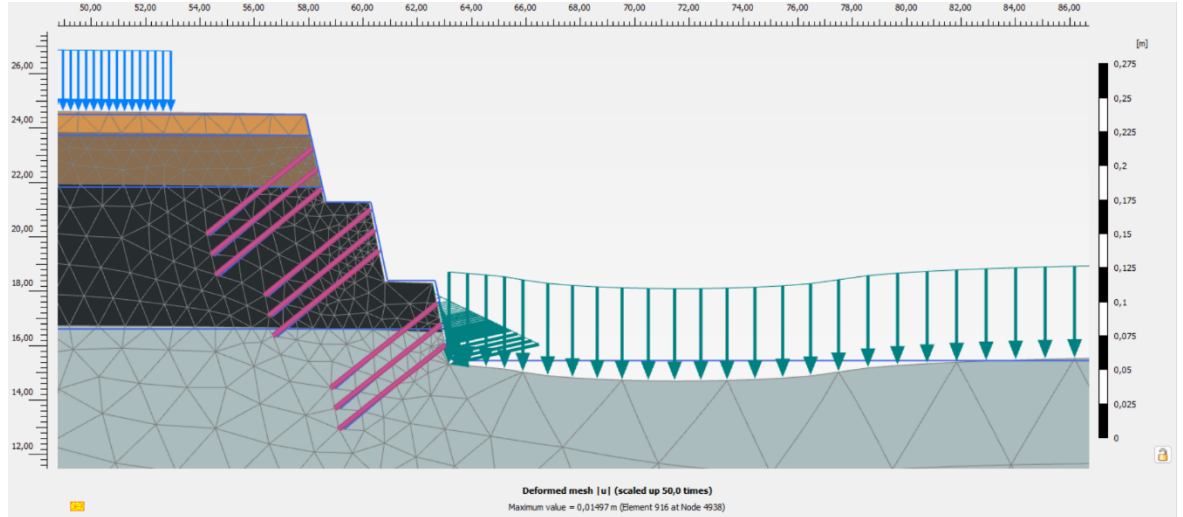




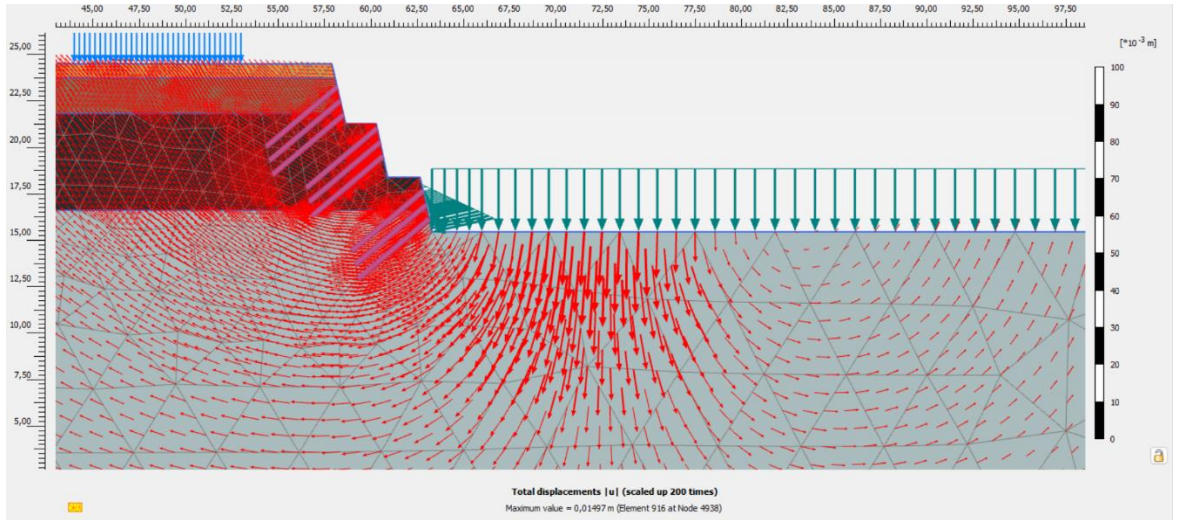
## Attachment 91 Model e Loaded Static Effective Stress Output



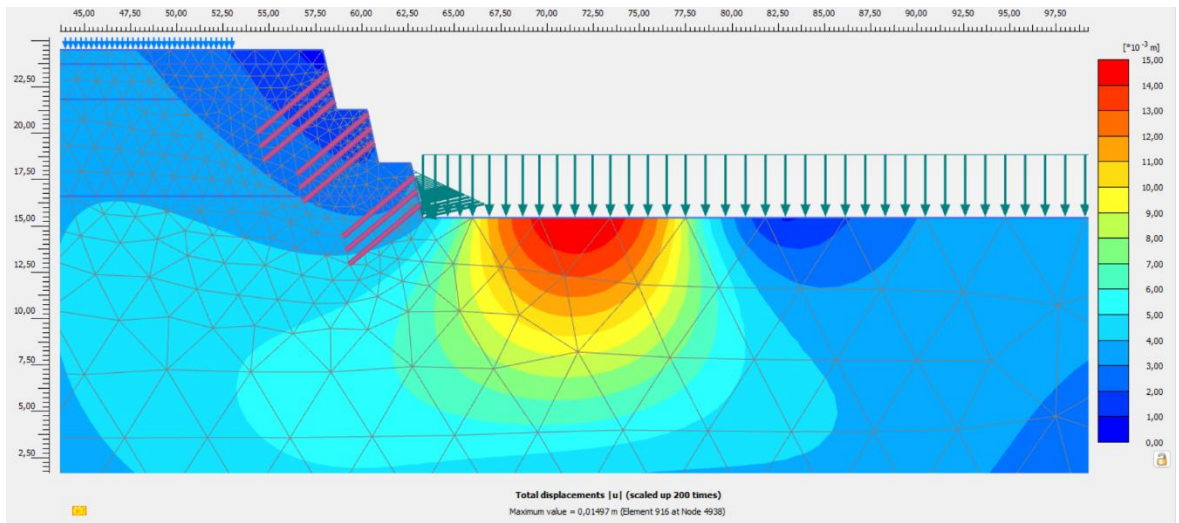
## Attachment 92 Model e Loaded Static Deformed Mesh Output



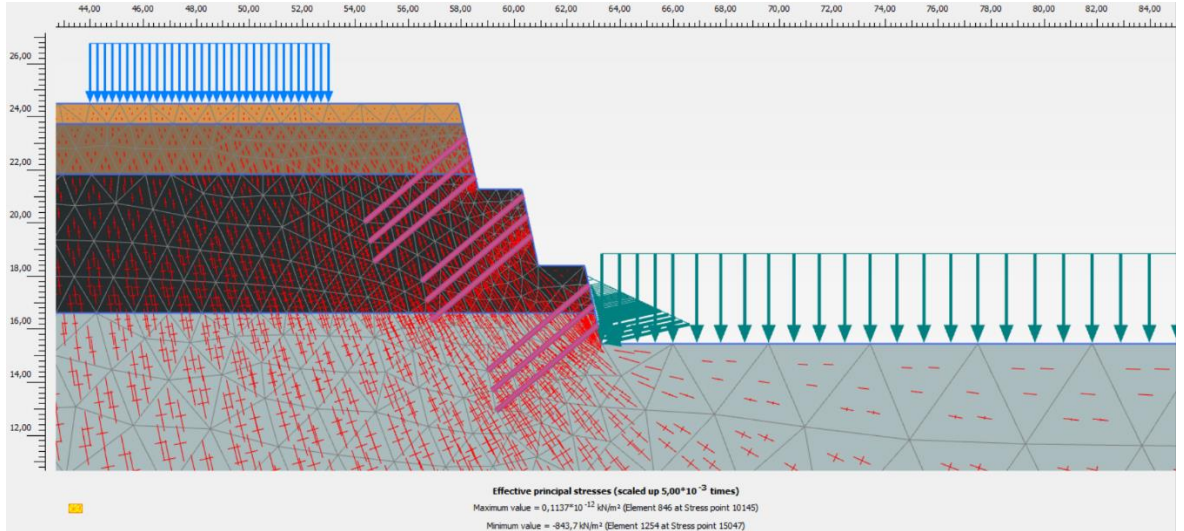
### Attachment 93 Model e Loaded Static Direction of Movement Output



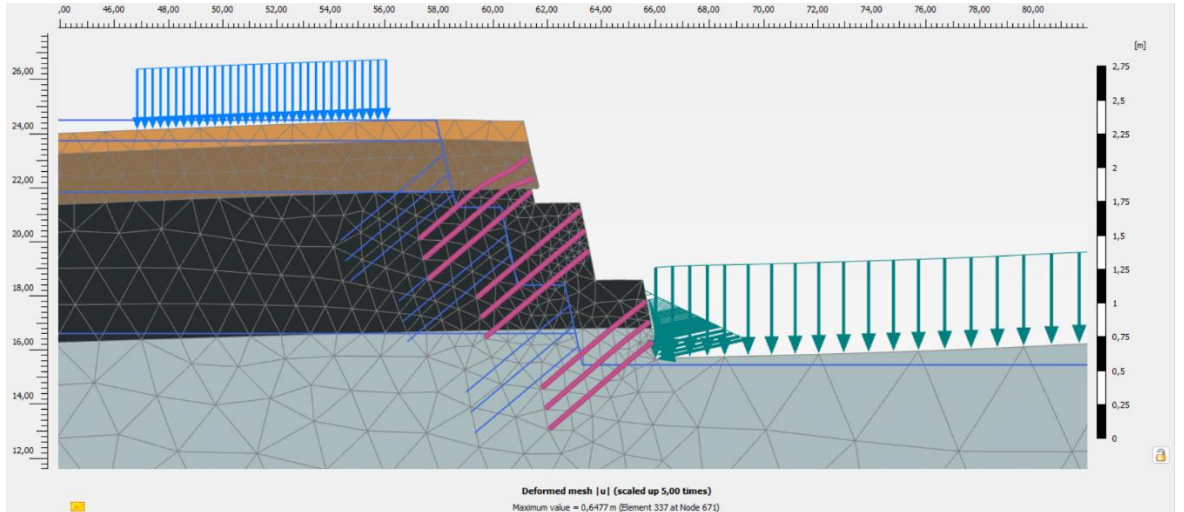
### Attachment 94 Model e Loaded Static Displacement Output



## Attachment 95 Model e Loaded Dynamic Effective Stress Output

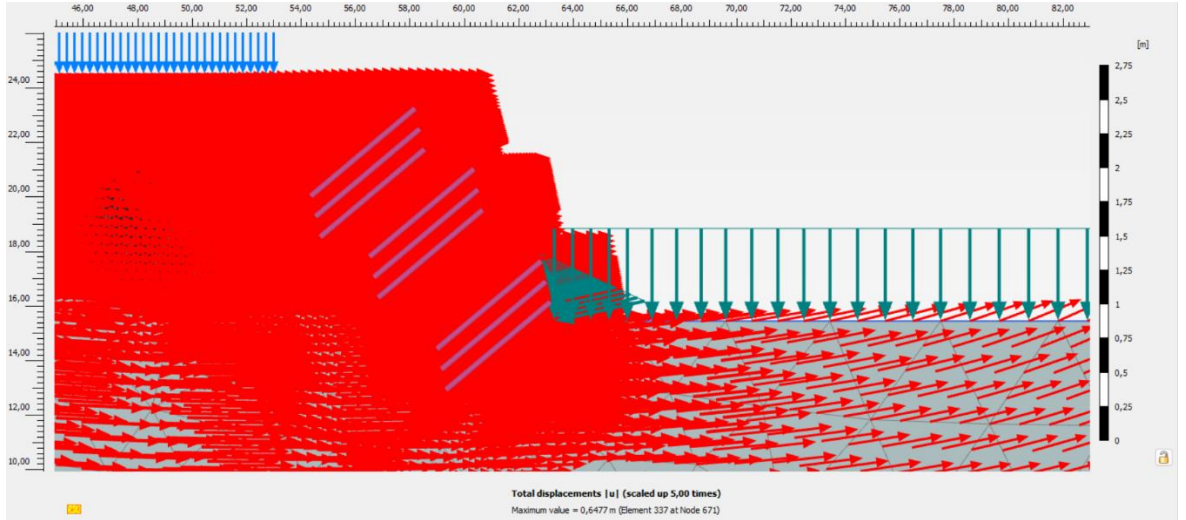


## Attachment 96 Model e Loaded Dynamic Deformed Mesh Output

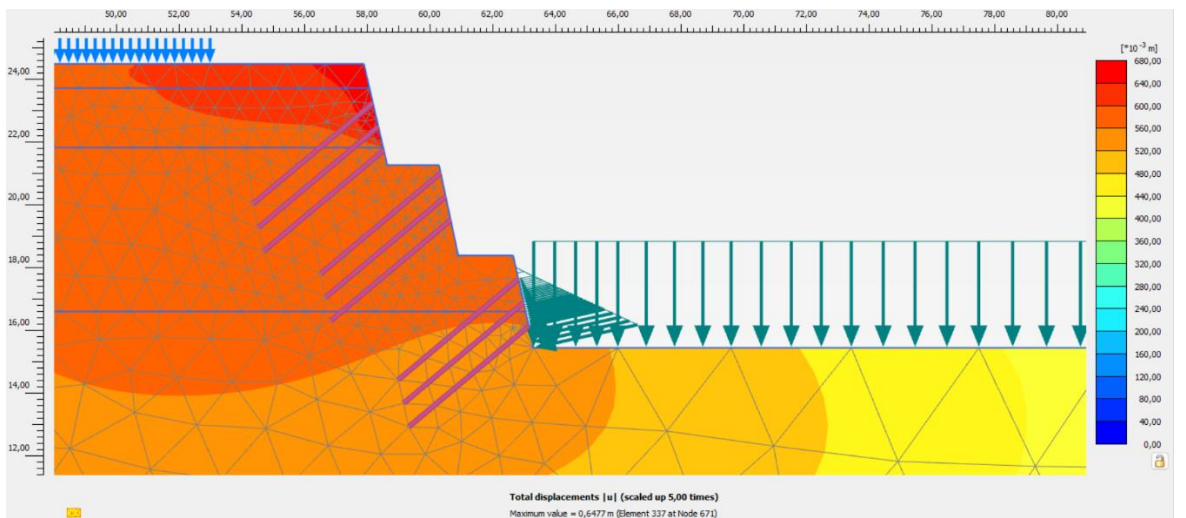




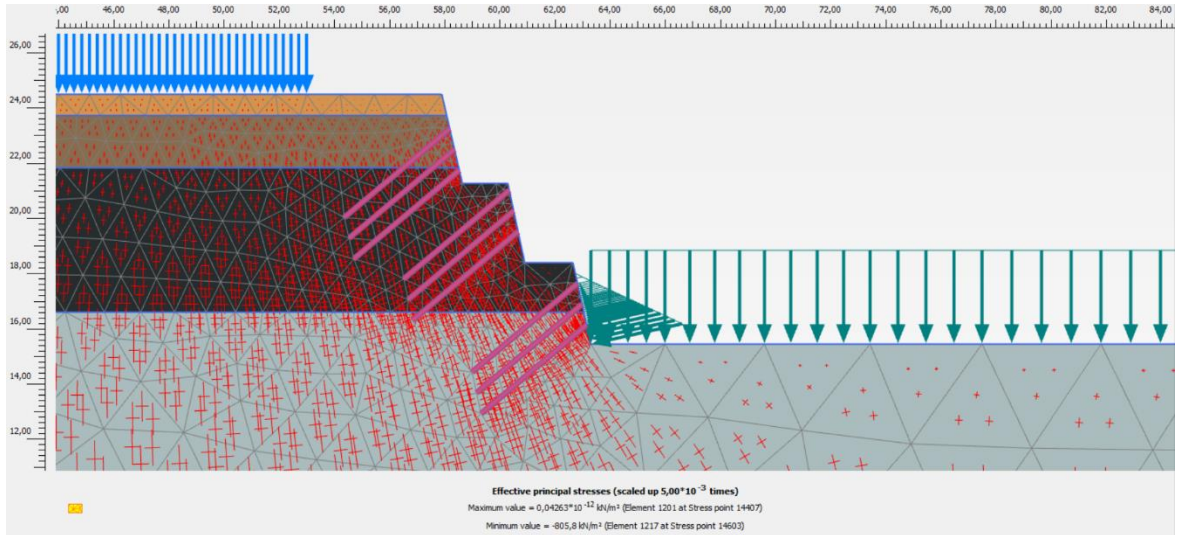
### Attachment 97 Model e Loaded Dynamic Direction of Movement Output



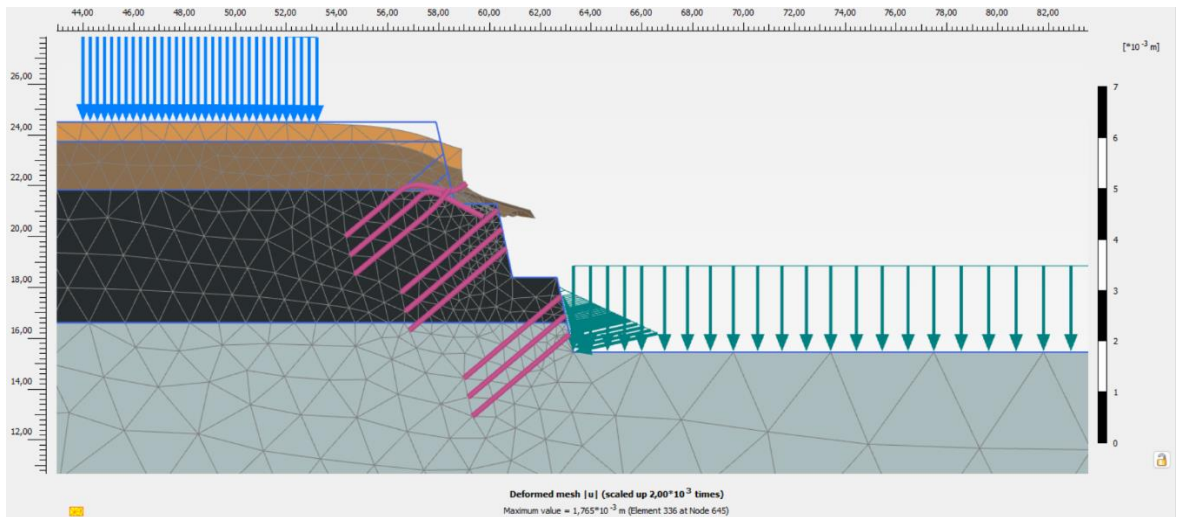
### Attachment 98 Model e Loaded Dynamic Displacement Output



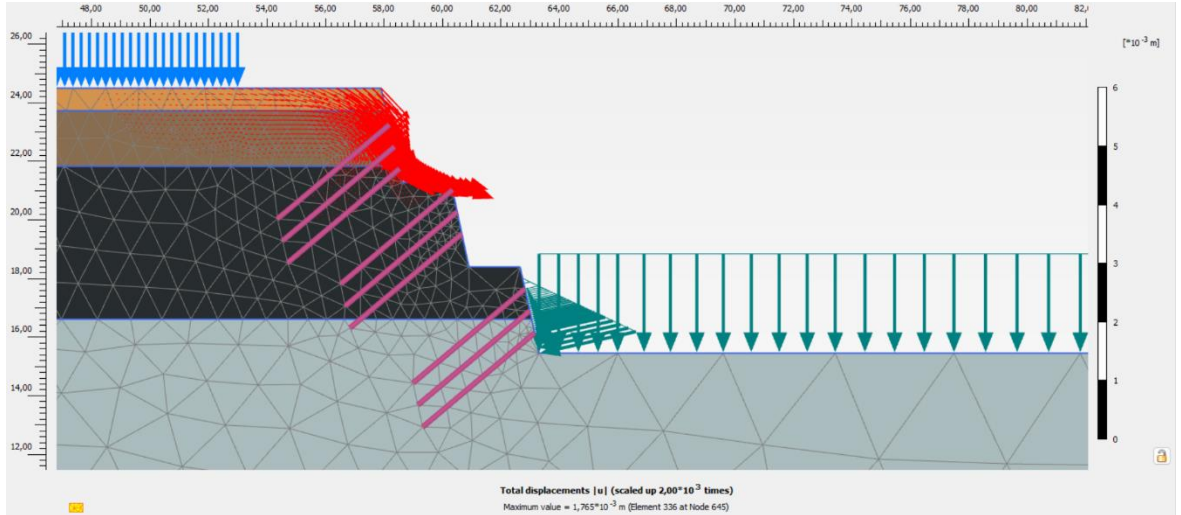
## Attachment 99 Model f Non-Loaded Static Effective Stress Output



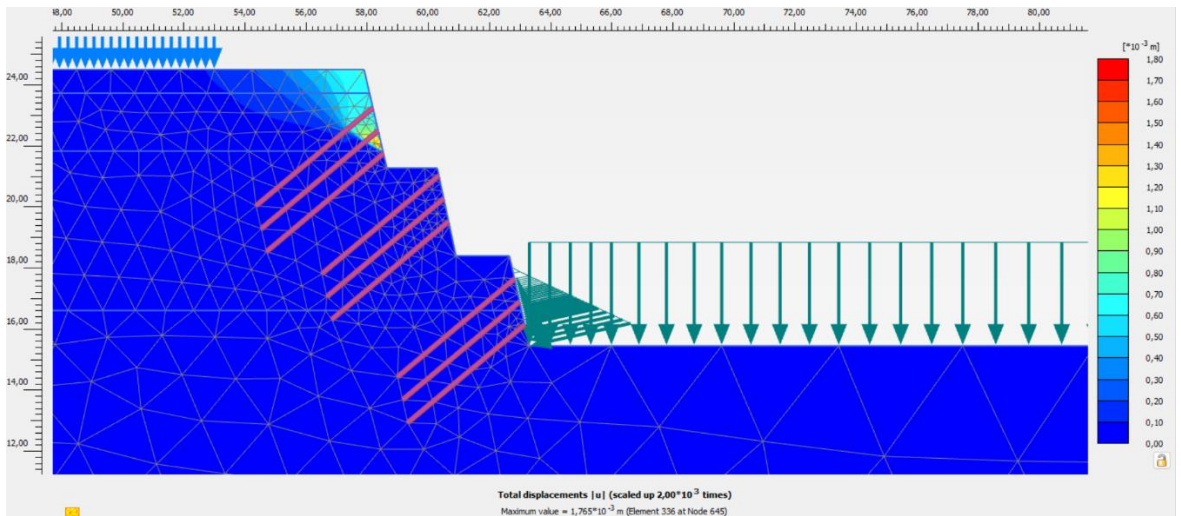
## Attachment 100 Model f Non-Loaded Static Deformed Mesh Output



## Attachment 101 Model f Non-Loaded Static Direction of Movement Output

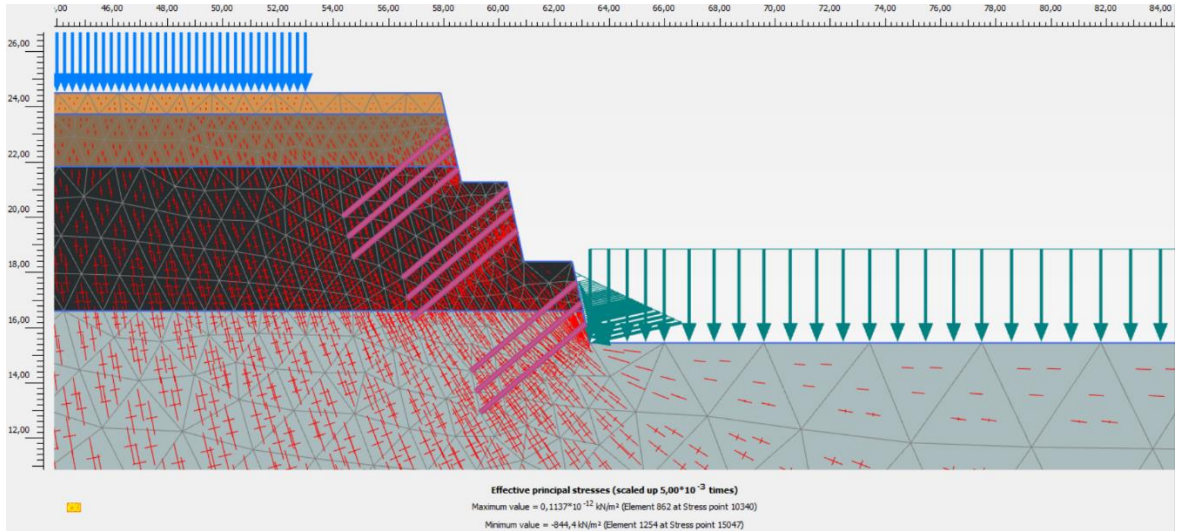


## Attachment 102 Model f Non-Loaded Static Displacement Output

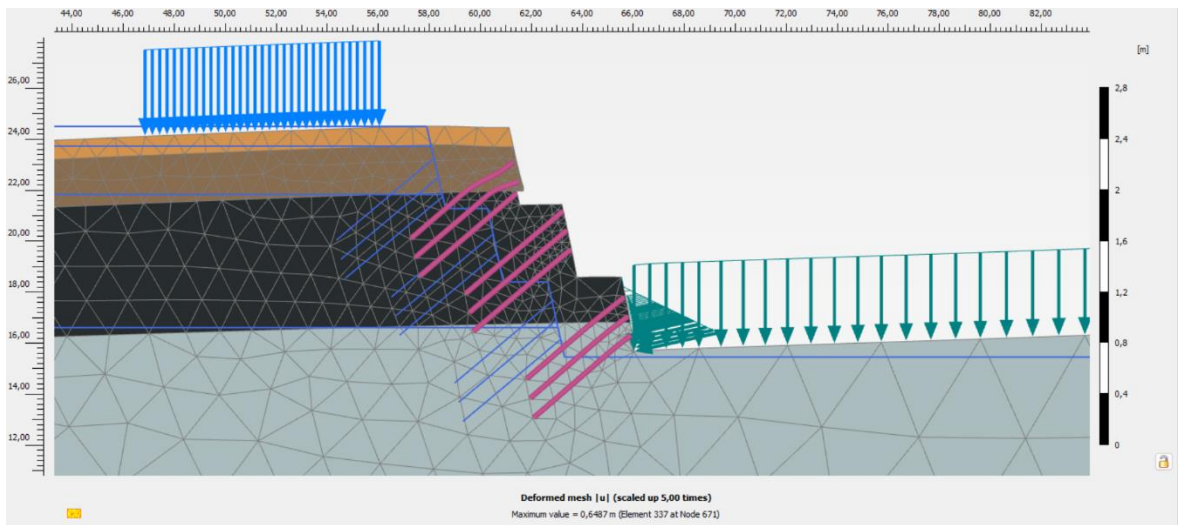




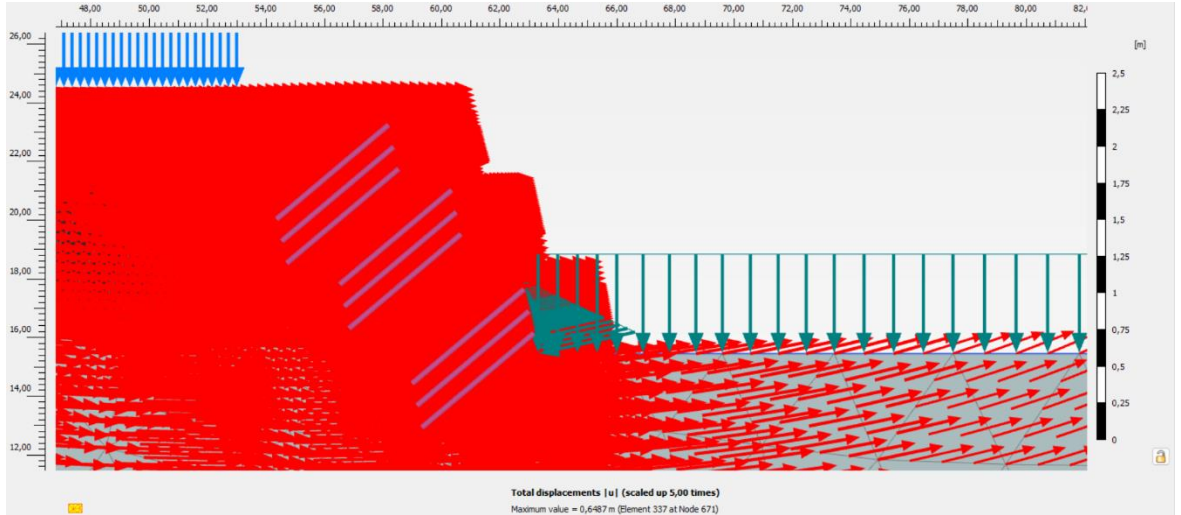
### Attachment 103 Model f Non-Loaded Dynamic Effective Stress Output



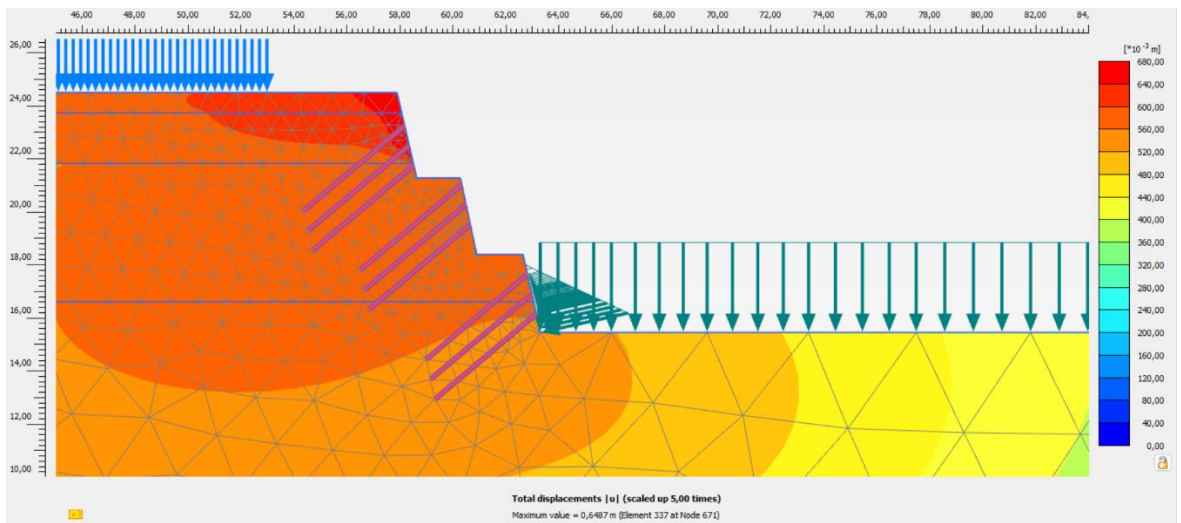
### Attachment 104 Model f Non-Loaded Dynamic Deformed Mesh Output



### Attachment 105 Model f Non-Loaded Dynamic Direction of Movement Output

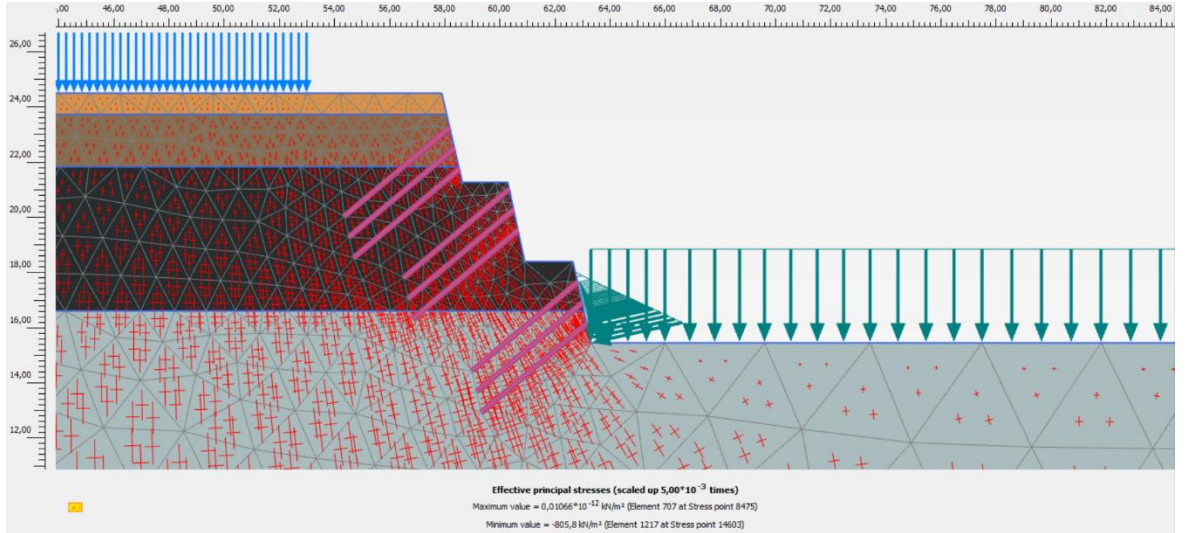


### Attachment 106 Model f Non-Loaded Dynamic Displacement Output

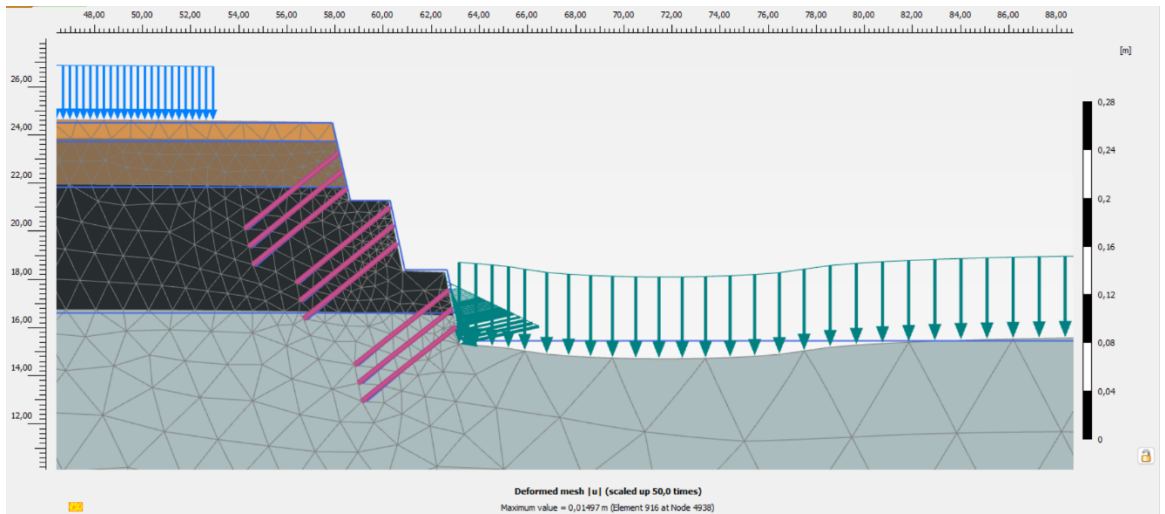




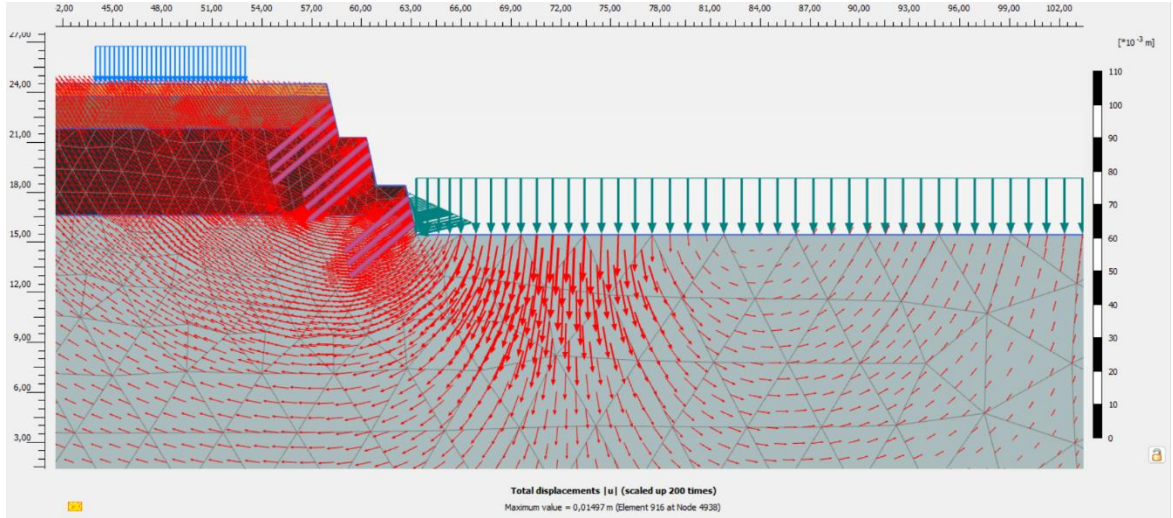
### Attachment 107 Model f Loaded Static Effective Stress Output



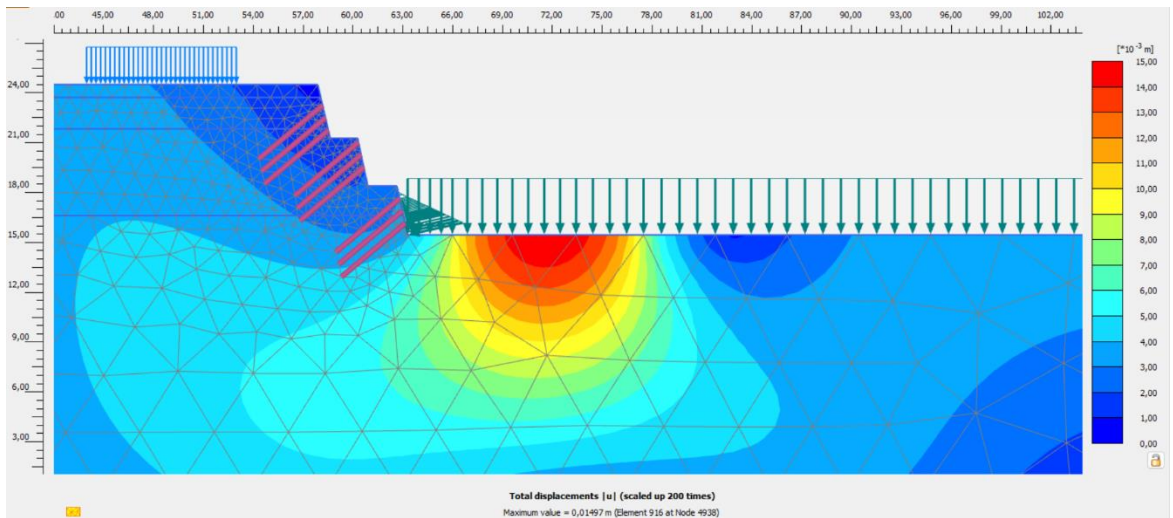
### Attachment 108 Model f Loaded Static Deformed Mesh Output



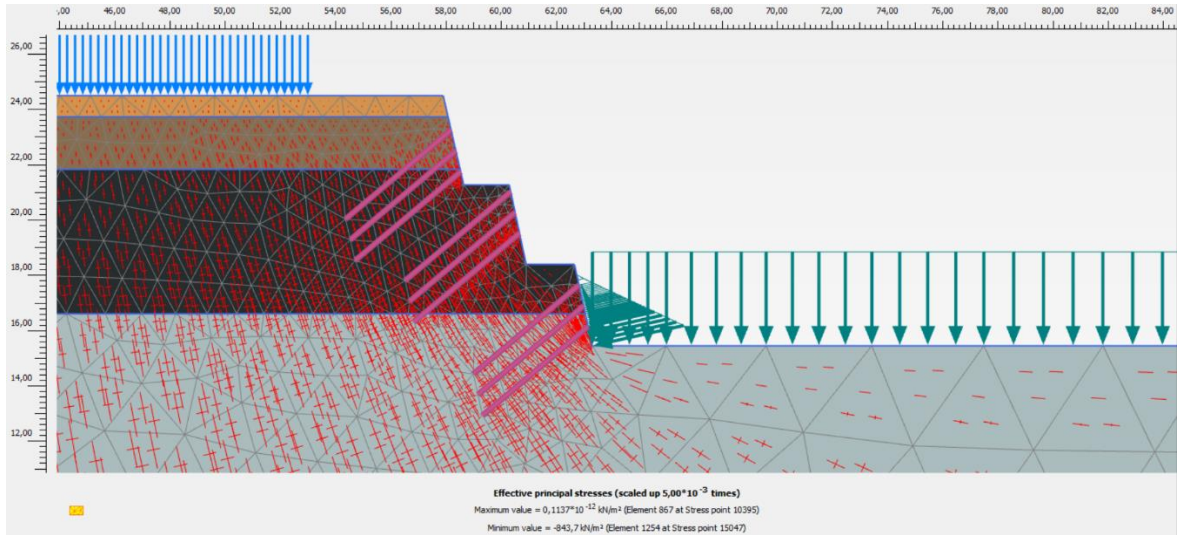
### Attachment 109 Model f Loaded Static Direction of Movement Output



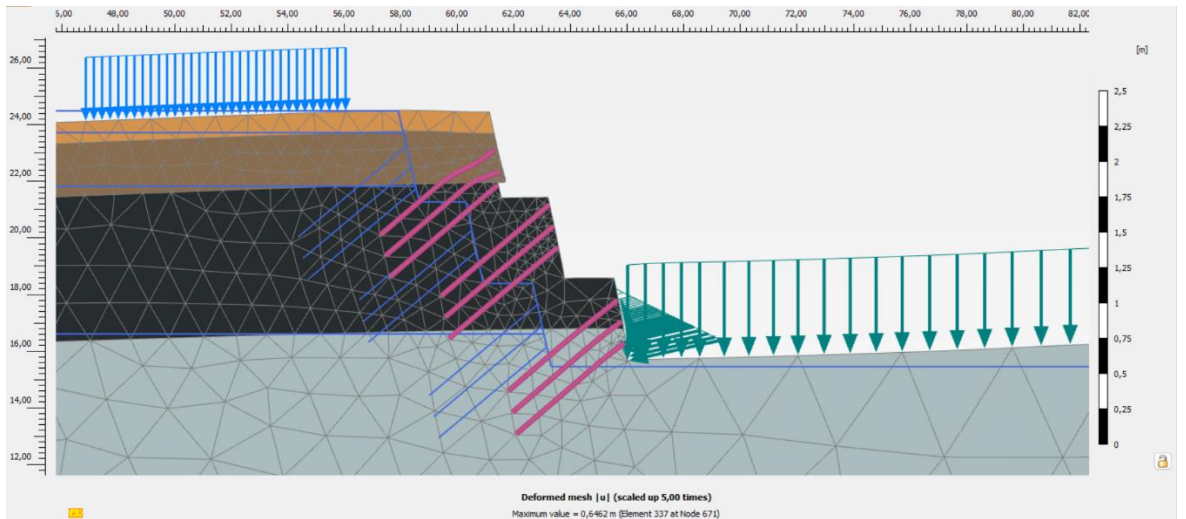
### Attachment 110 Model f Loaded Static Displacement Output



## Attachment 111 Model f Loaded Dynamic Effective Stress Output

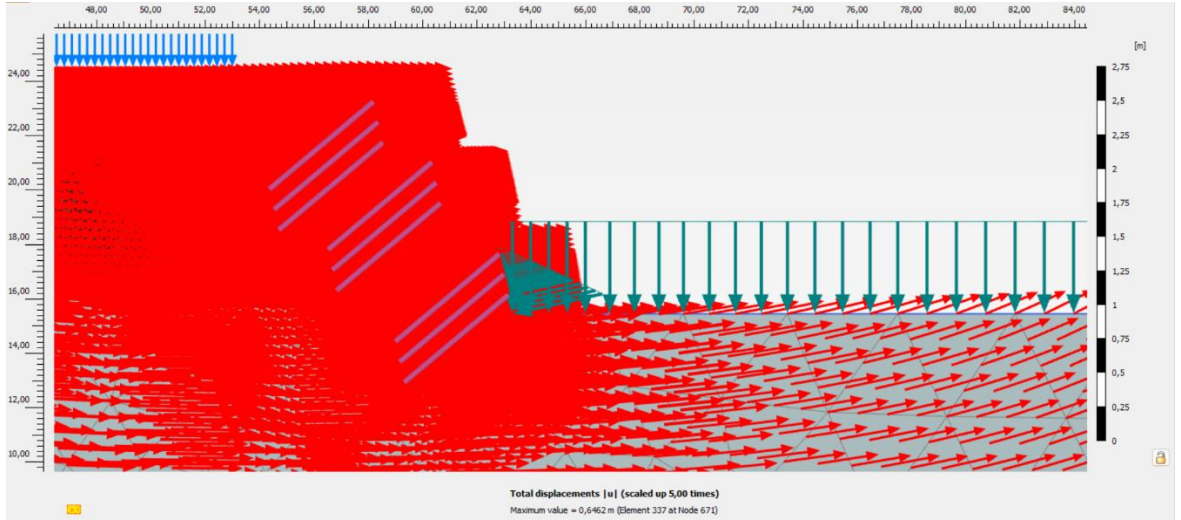


## Attachment 112 Model f Loaded Dynamic Deformed Mesh Output

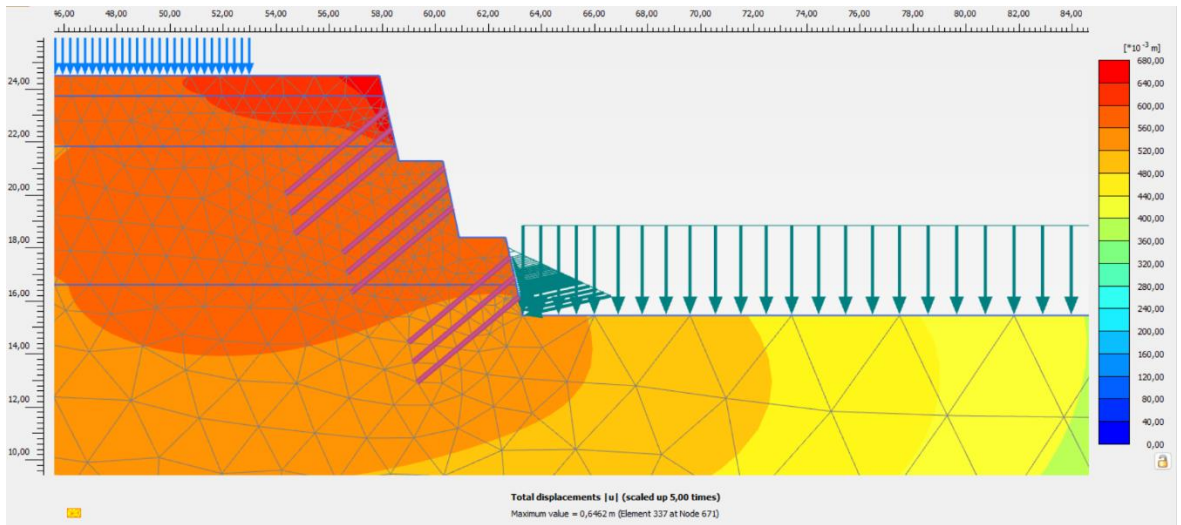




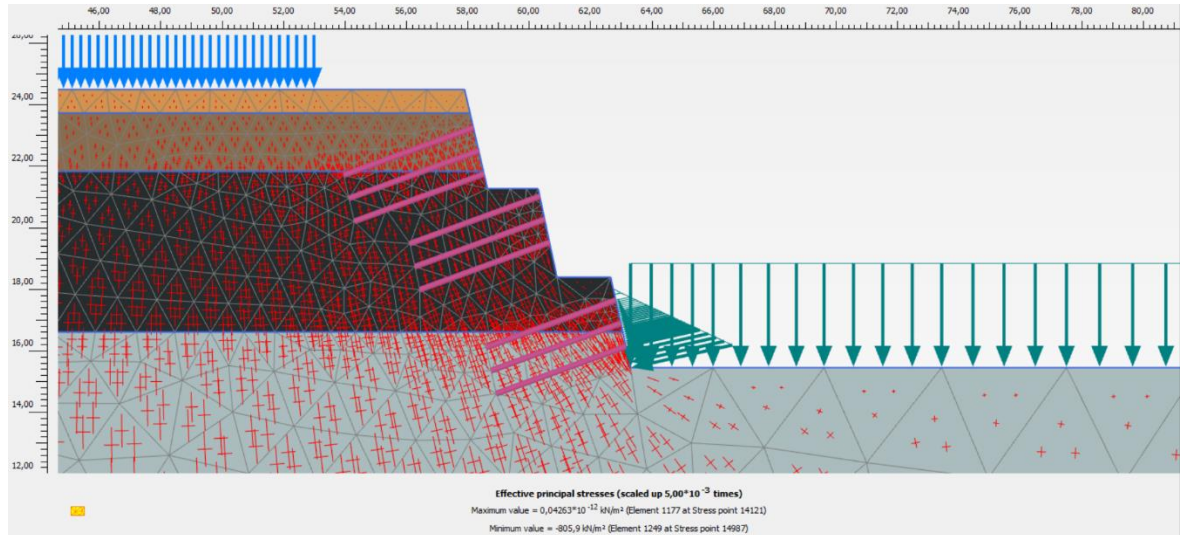
### Attachment 113 Model f Loaded Dynamic Direction of Movement Output



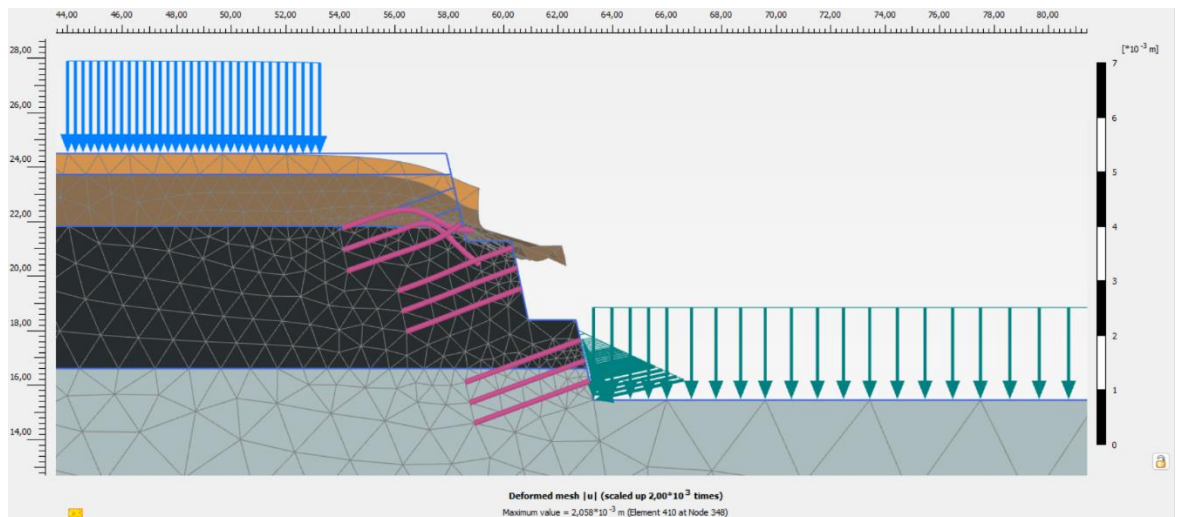
### Attachment 114 Model f Loaded Dynamic Displacement Output



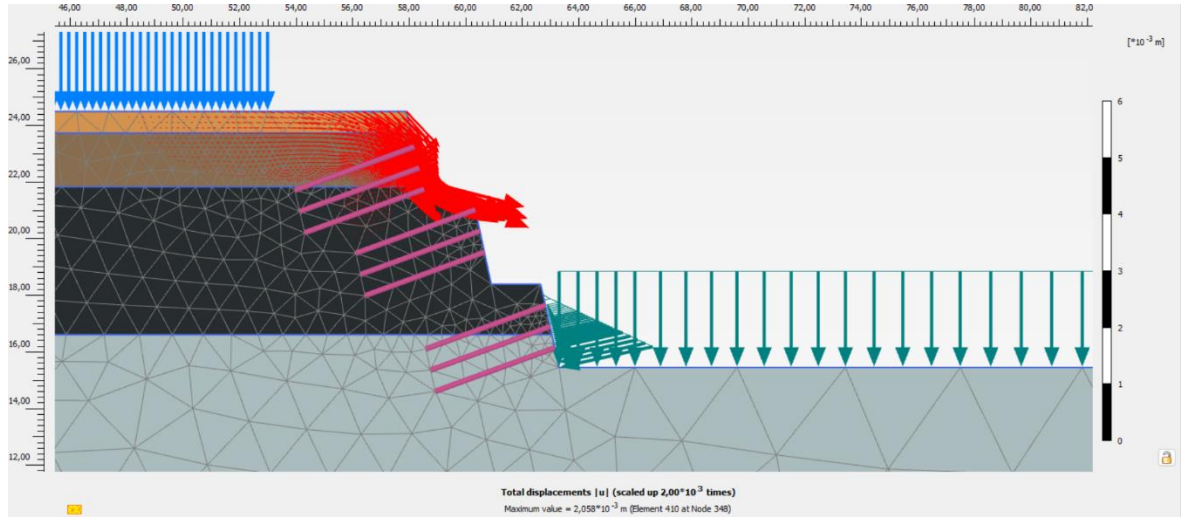
## Attachment 115 Model g Non-Loaded Static Effective Stress Output



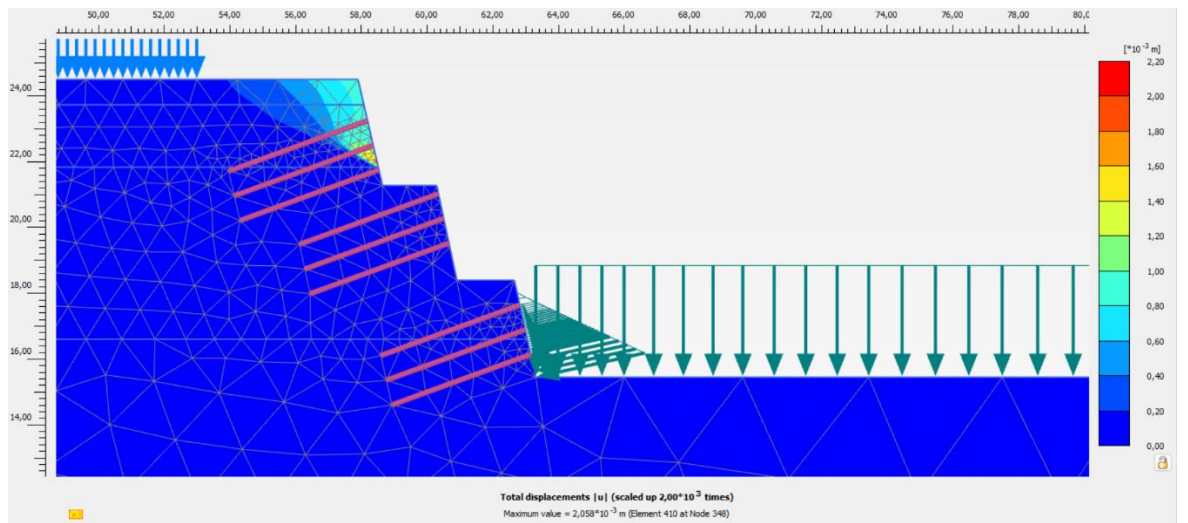
## Attachment 116 Model g Non-Loaded Static Deformed Mesh Output



### Attachment 117 Model g Non-Loaded Static Direction of Movement Output

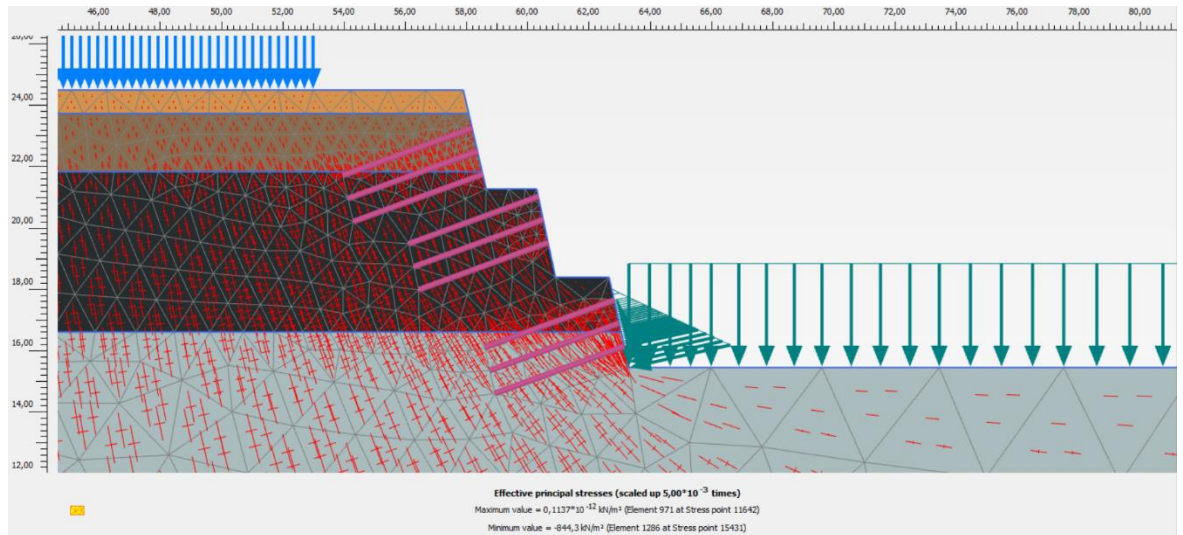


### Attachment 118 Model g Non-Loaded Static Displacement Output

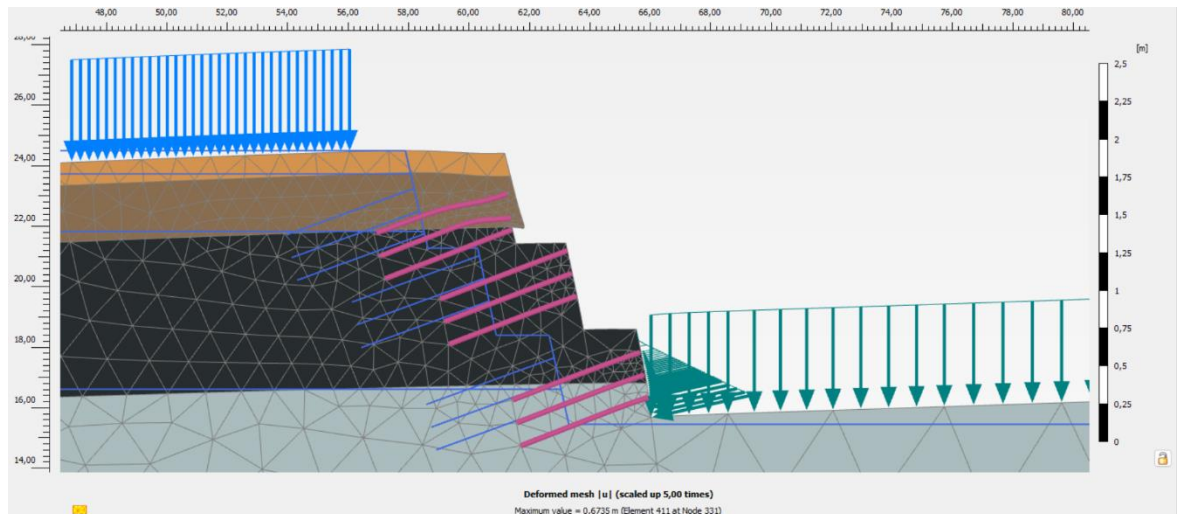




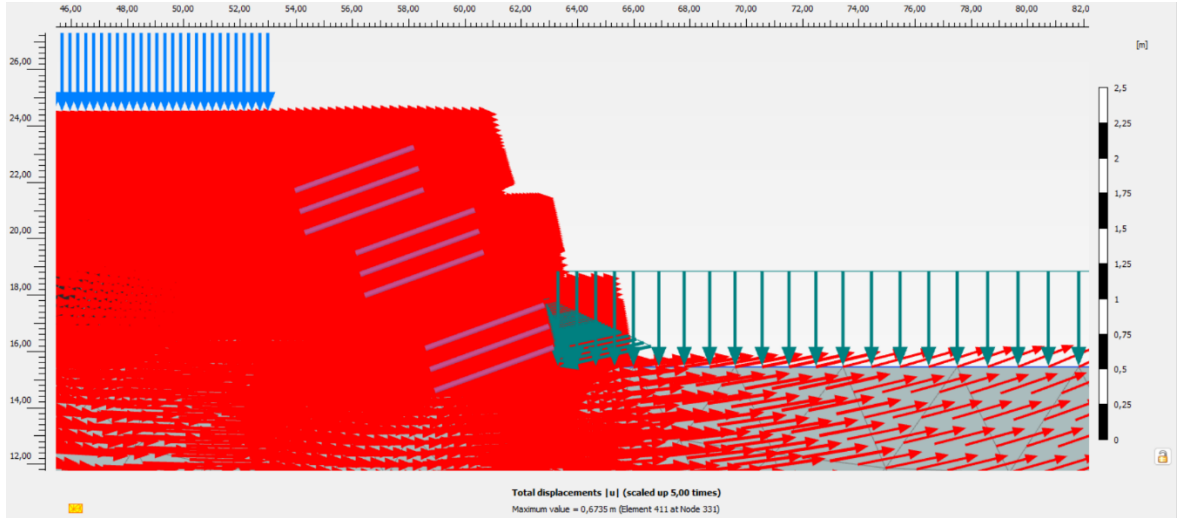
## Attachment 119 Model g Non-Loaded Dynamic Effective Stress Output



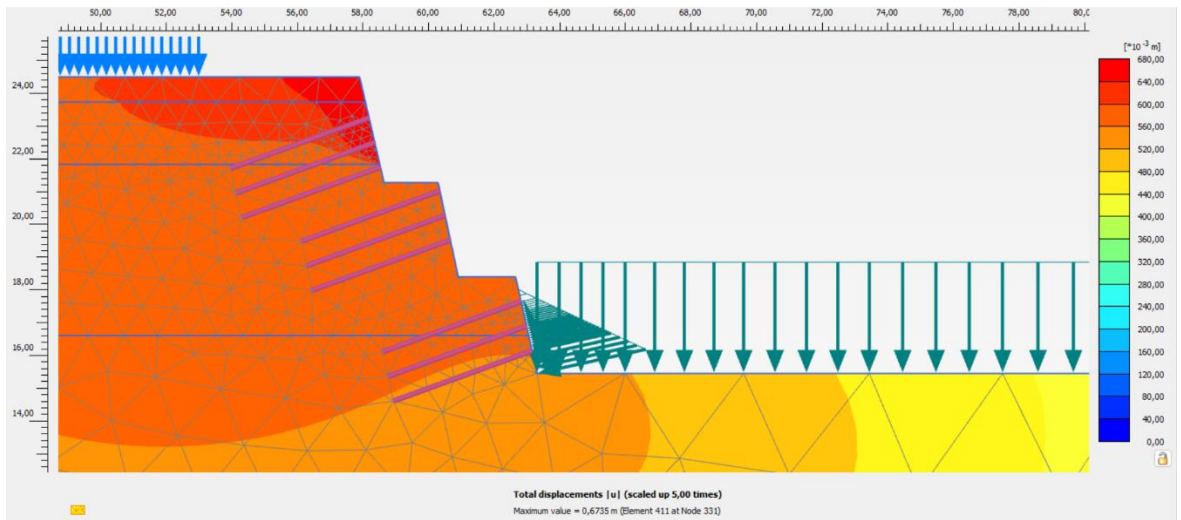
## Attachment 120 Model g Non-Loaded Dynamic Deformed Mesh Output



### Attachment 121 Model g Non-Loaded Dynamic Direction of Movement Output



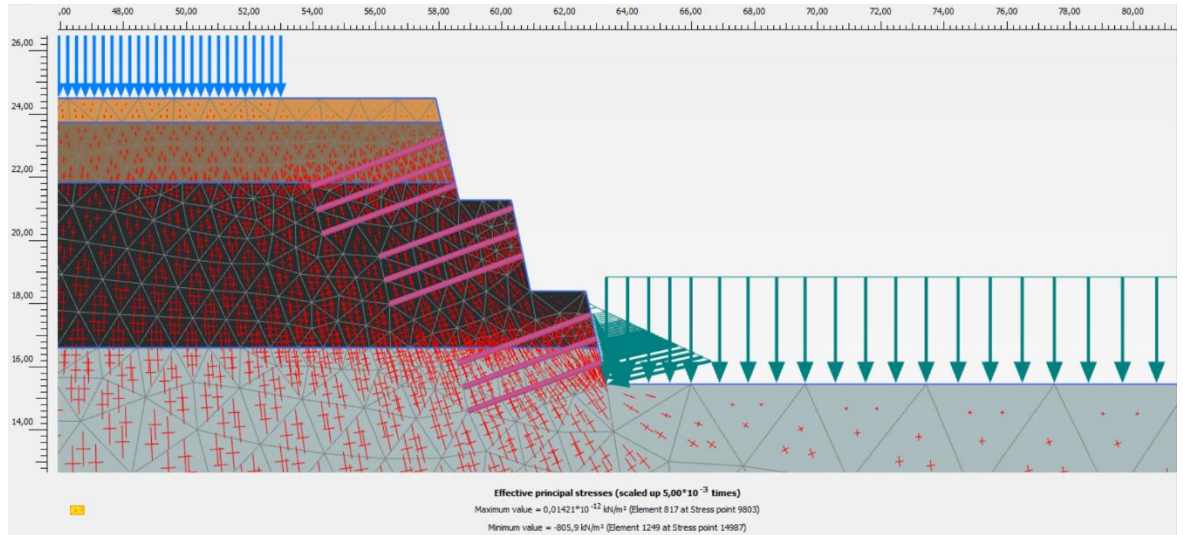
### Attachment 122 Model g Non-Loaded Dynamic Displacement Output



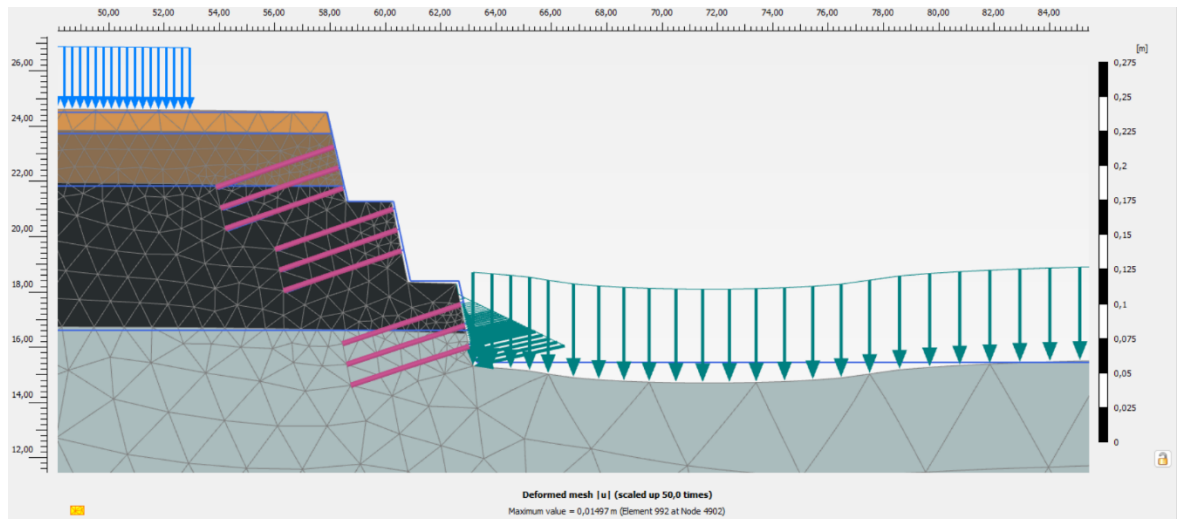
|



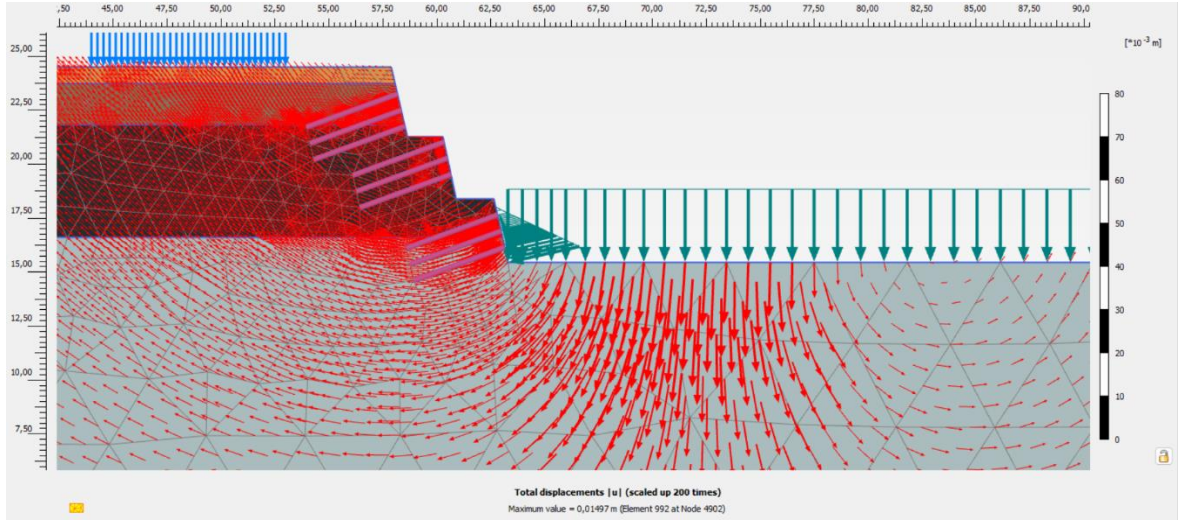
## Attachment 123 Model g Loaded Static Effective Stress Output



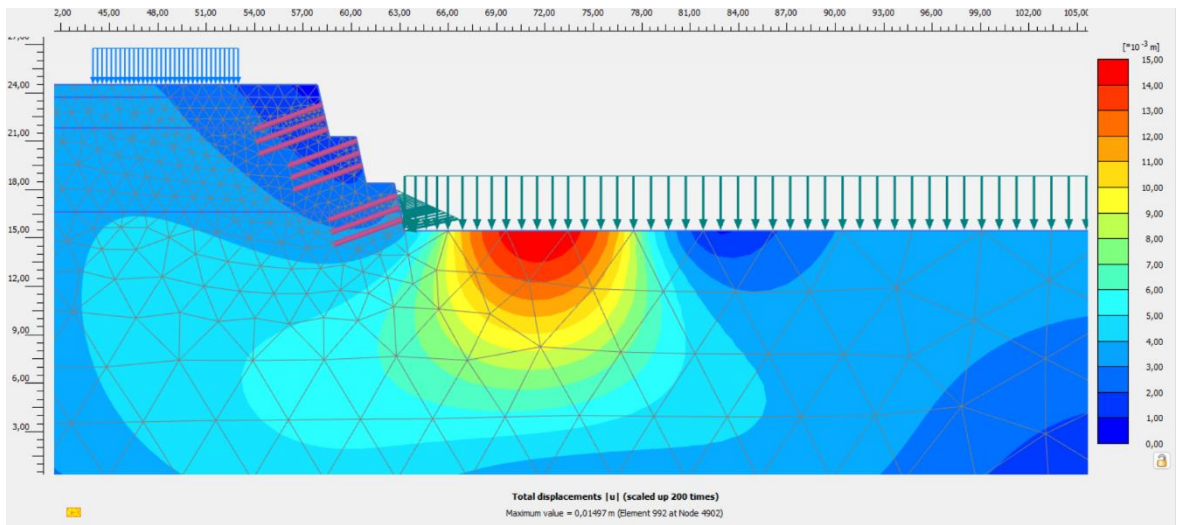
## Attachment 124 Model g Loaded Static Deformed Mesh Output



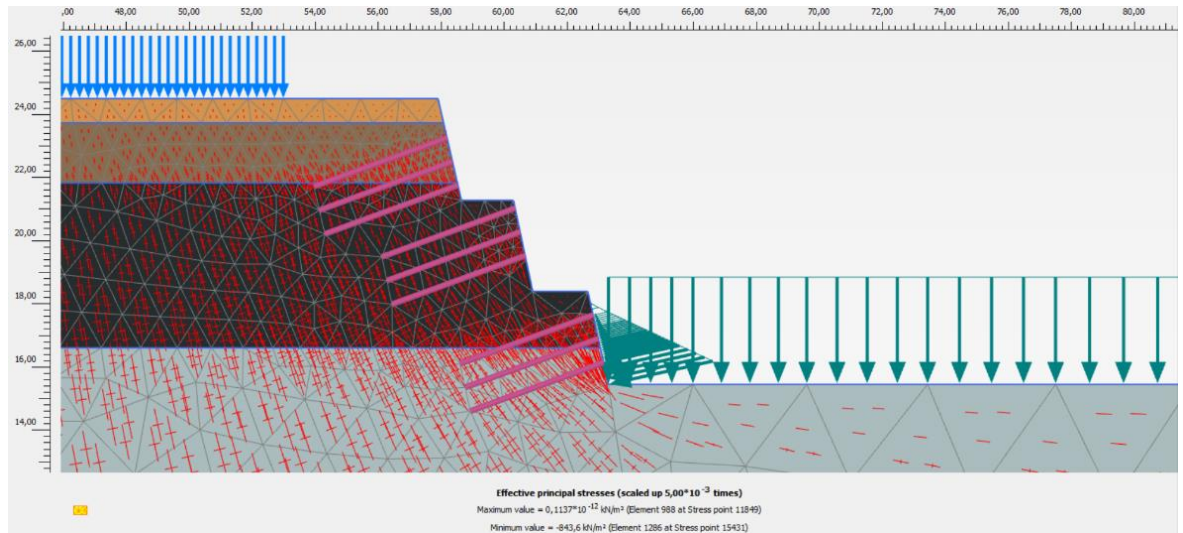
### Attachment 125 Model g Loaded Static Direction of Movement Output



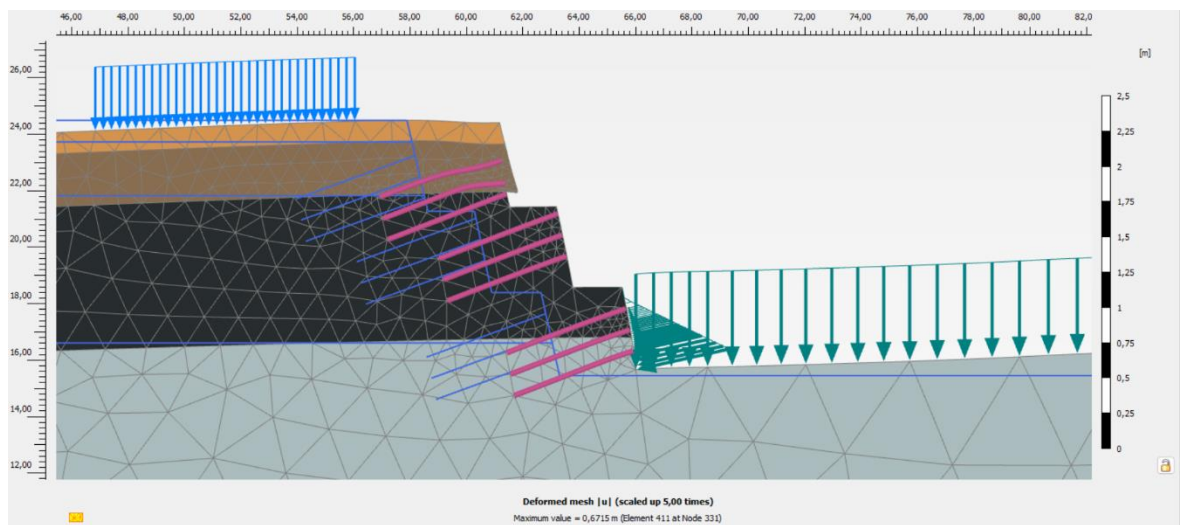
### Attachment 126 Model g Loaded Static Displacement Output



### Attachment 127 Model g Loaded Dynamic Effective Stress Output

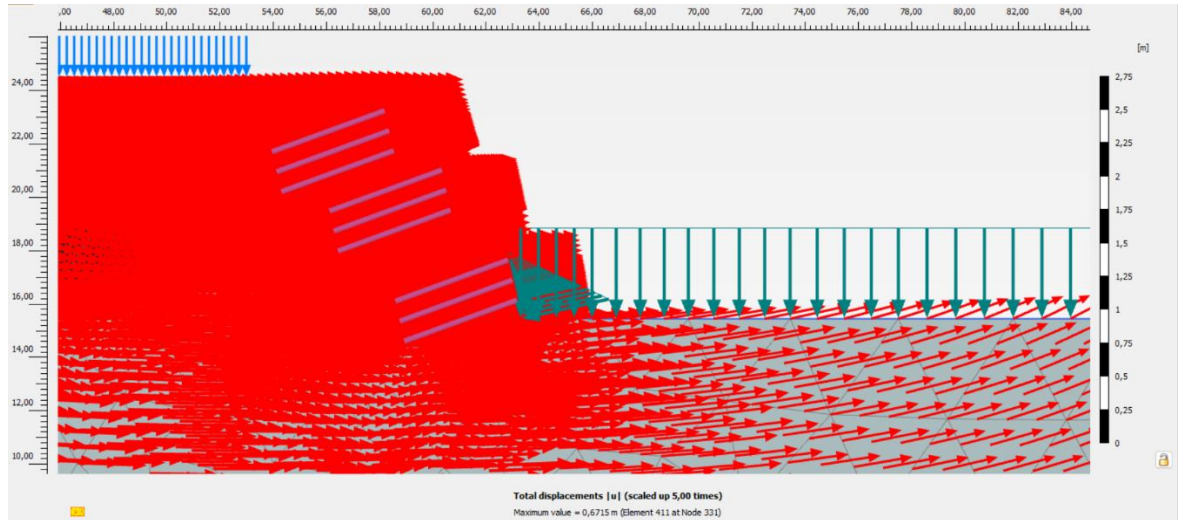


### Attachment 128 Model g Loaded Dynamic Deformed Mesh Output

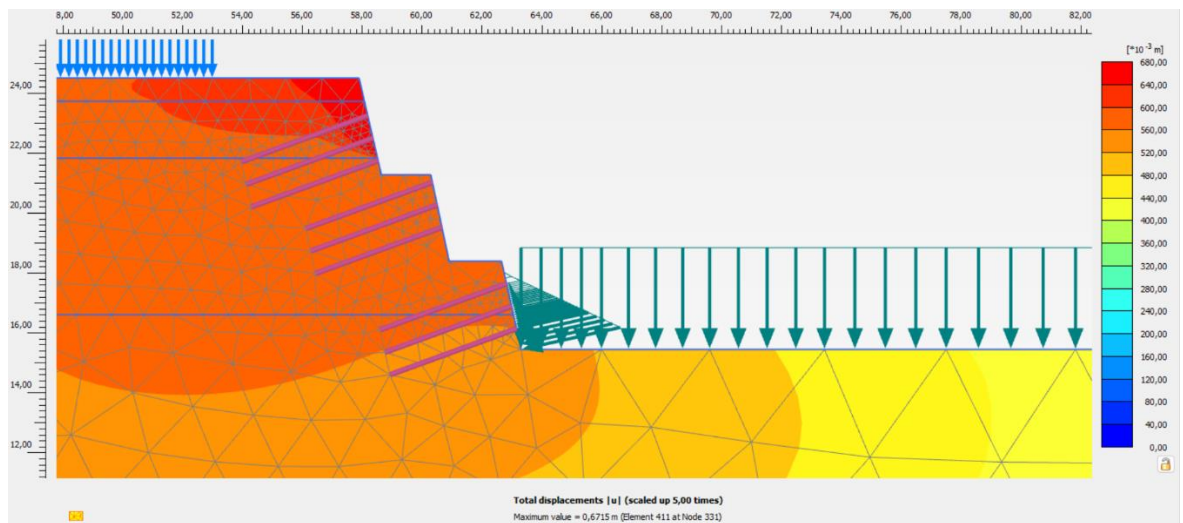




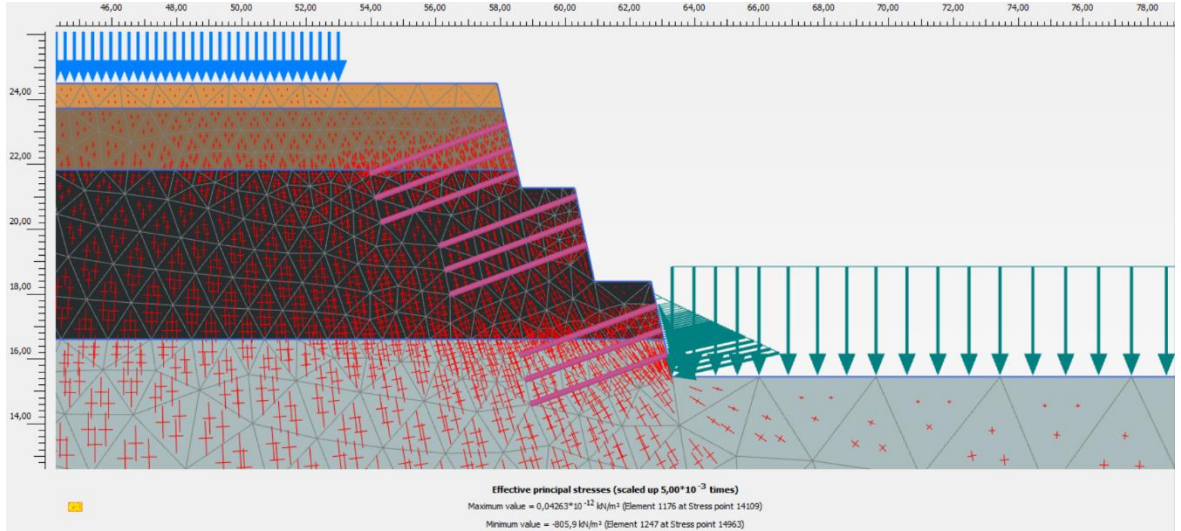
### Attachment 129 Model g Loaded Dynamic Direction of Movement Output



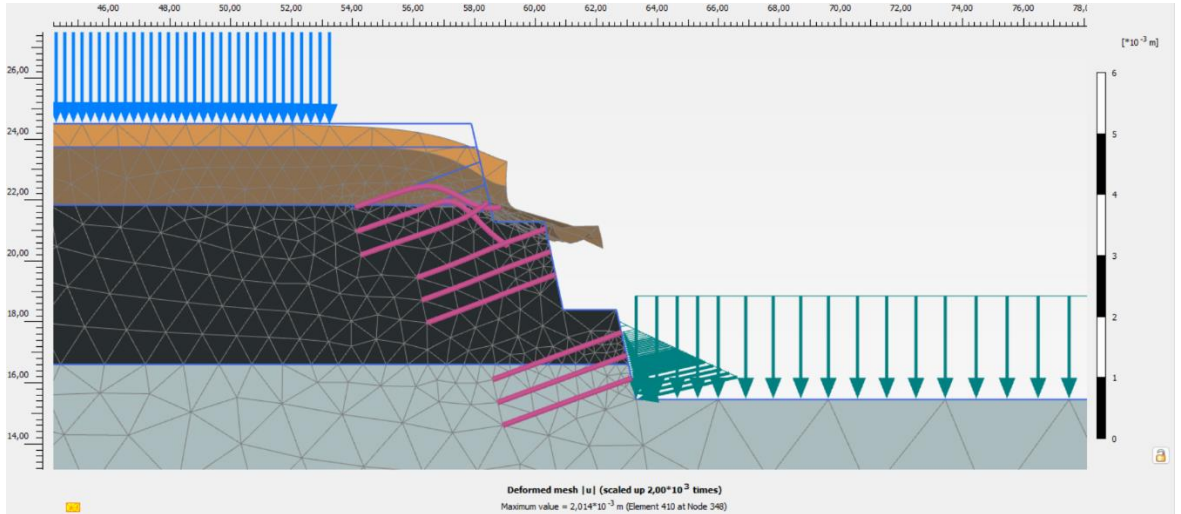
### Attachment 130 Model g Loaded Dynamic Displacement Output



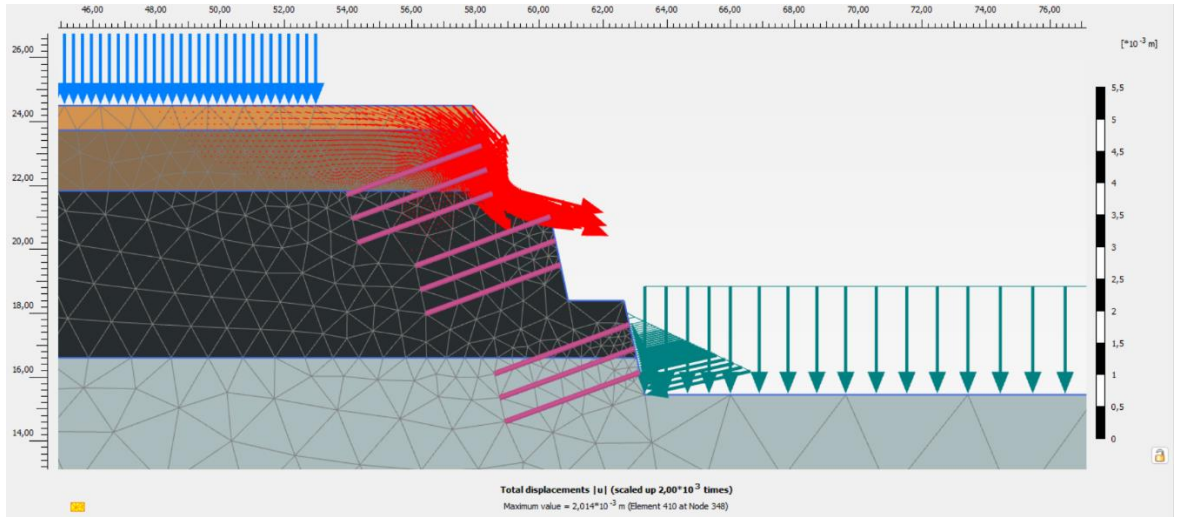
### Attachment 131 Model h Non-Loaded Static Effective Stress Output



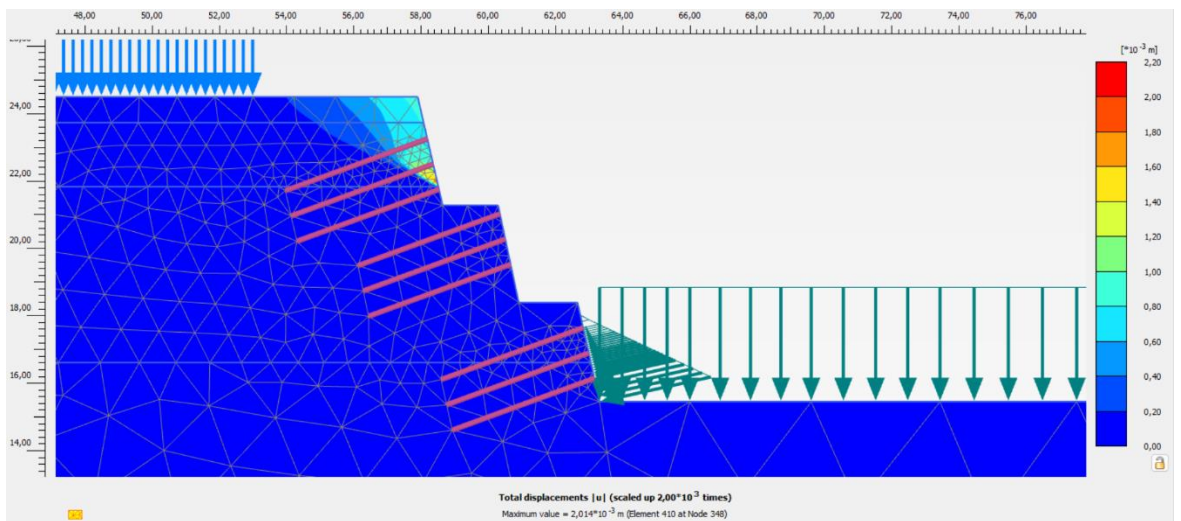
### Attachment 132 Model h Non-Loaded Static Deformed Mesh Output



### Attachment 133 Model h Non-Loaded Static Direction of Movement Output

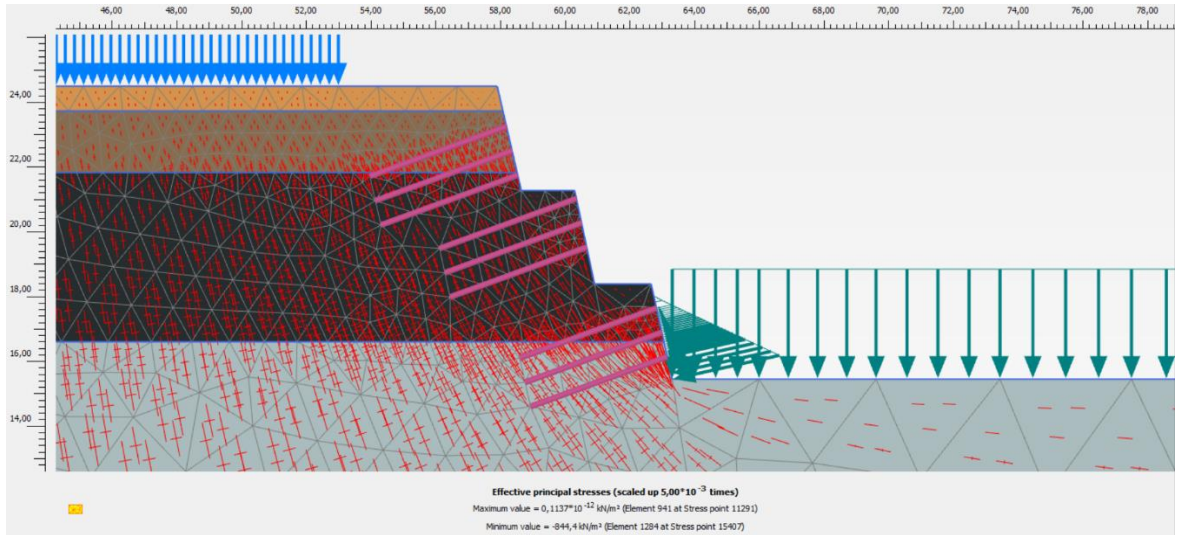


### Attachment 134 Model h Non-Loaded Static Displacement Output

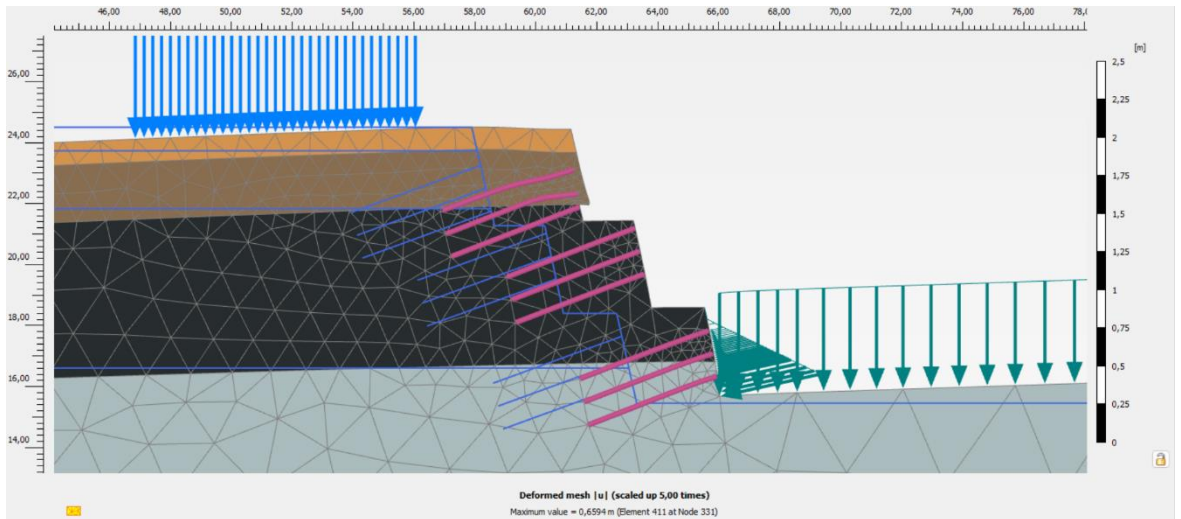




### Attachment 135 Model h Non-Loaded Dynamic Effective Stress Output

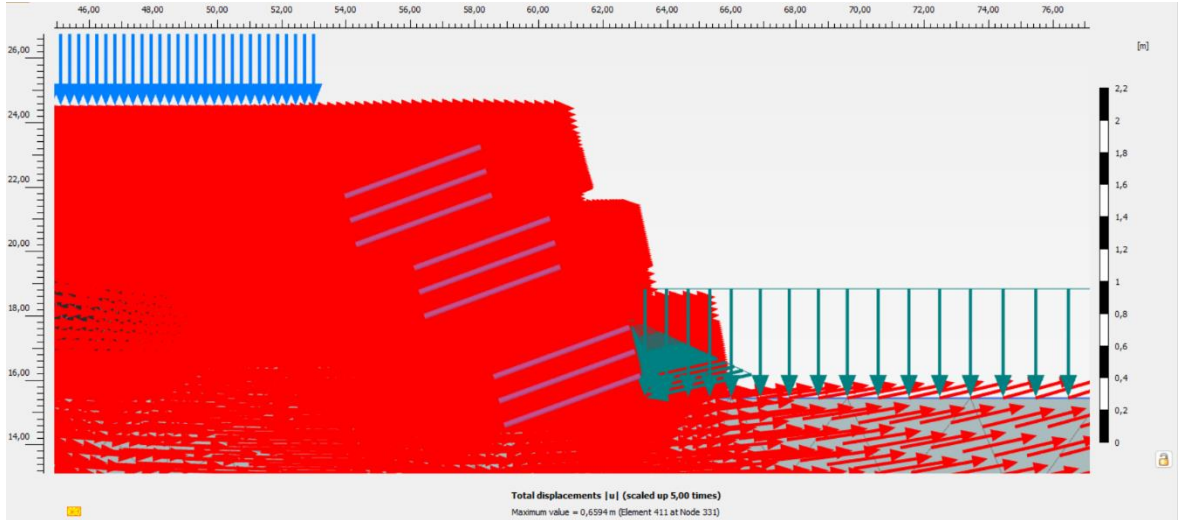


### Attachment 136 Model h Non-Loaded Dynamic Deformed Mesh Output

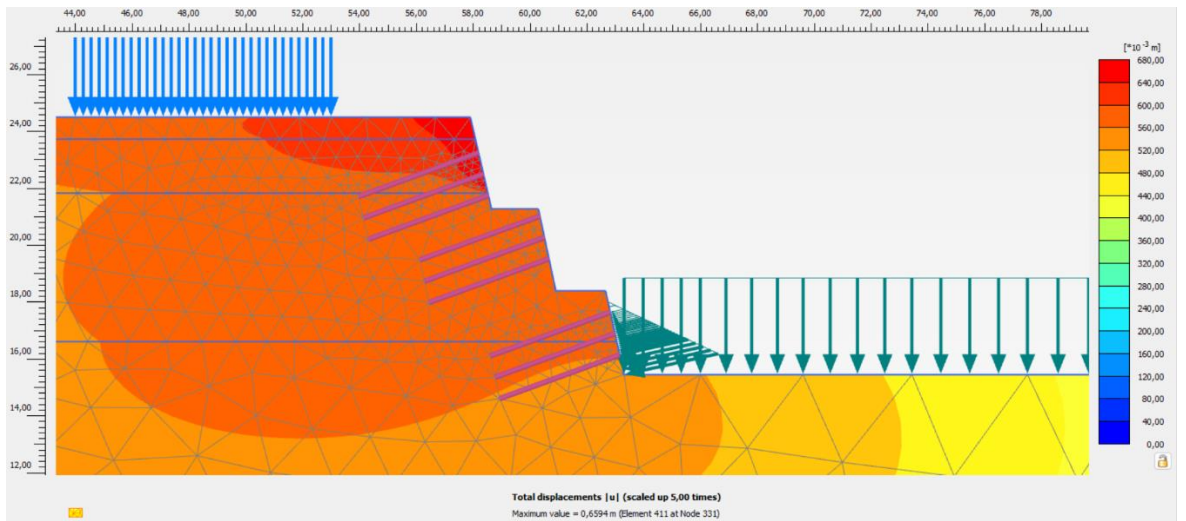




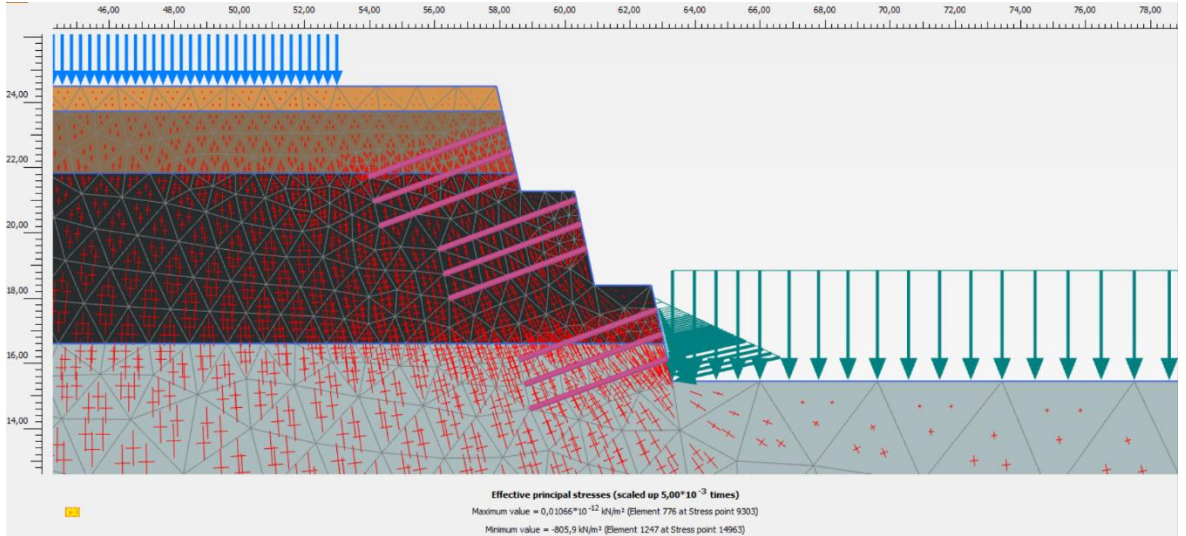
### Attachment 137 Model h Non-Loaded Dynamic Direction of Movement Output



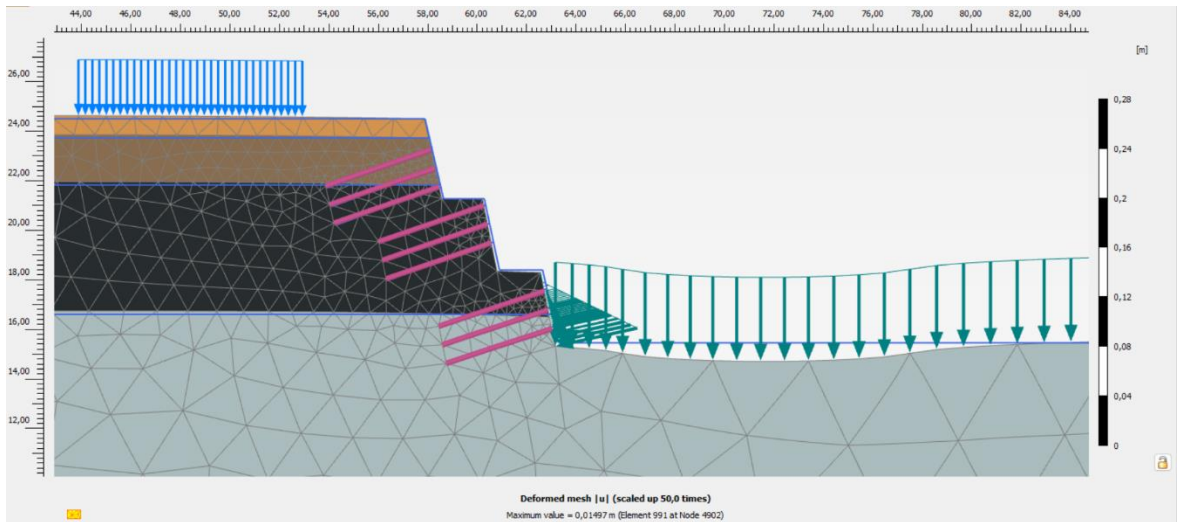
### Attachment 138 Model h Non-Loaded Dynamic Displacement Output



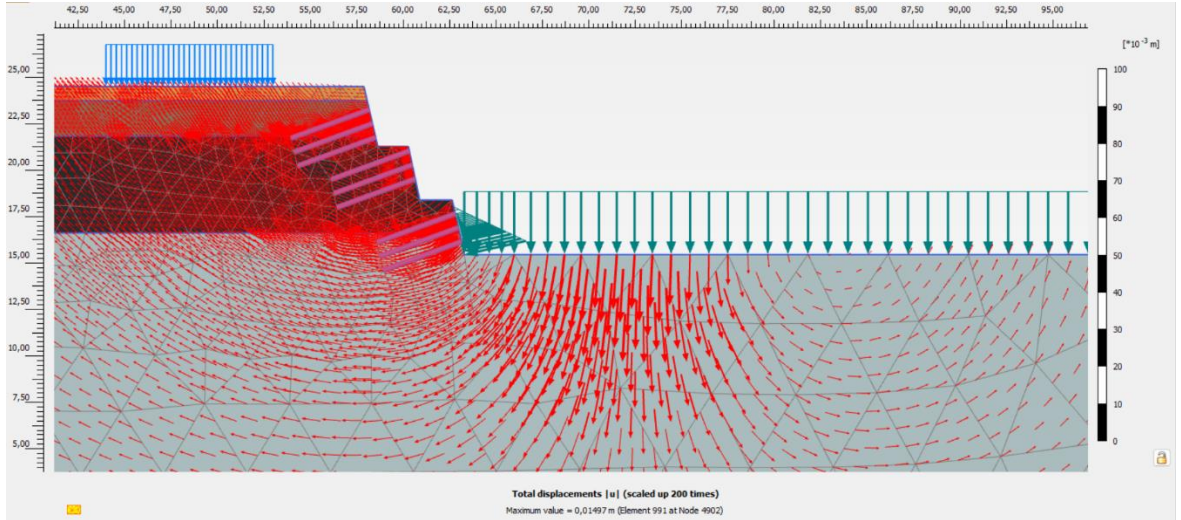
### Attachment 139 Model h Loaded Static Effective Stress Output



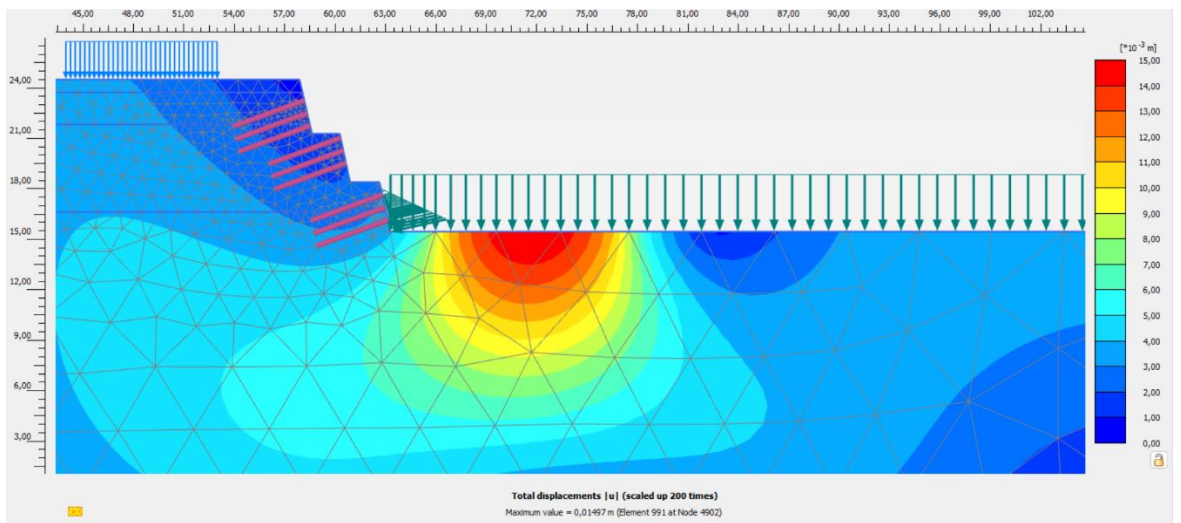
### Attachment 140 Model h Loaded Static Deformed Mesh Output



### Attachment 141 Model h Loaded Static Direction of Movement Output

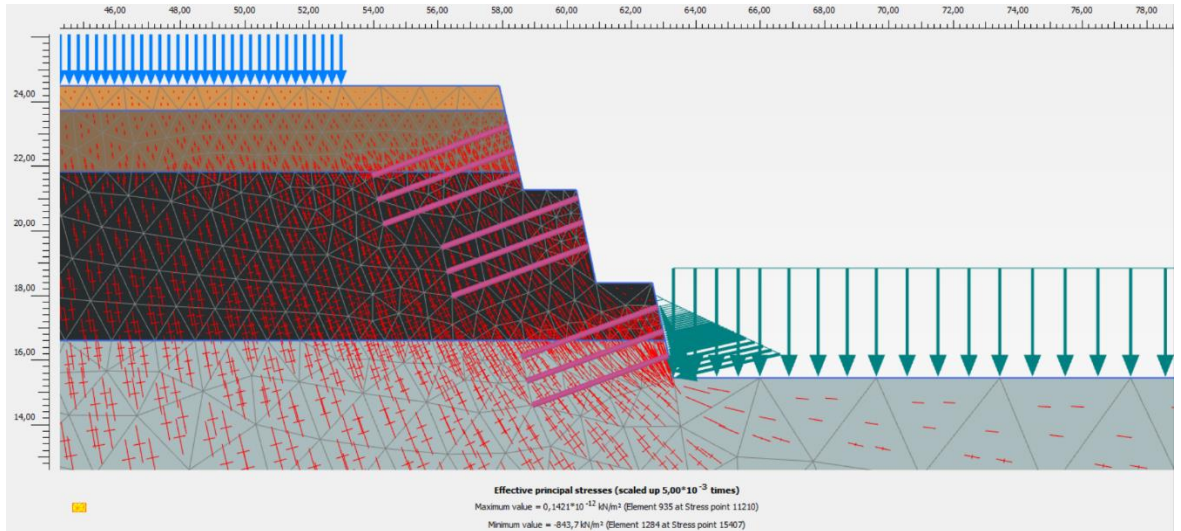


### Attachment 142 Model h Loaded Static Displacement Output

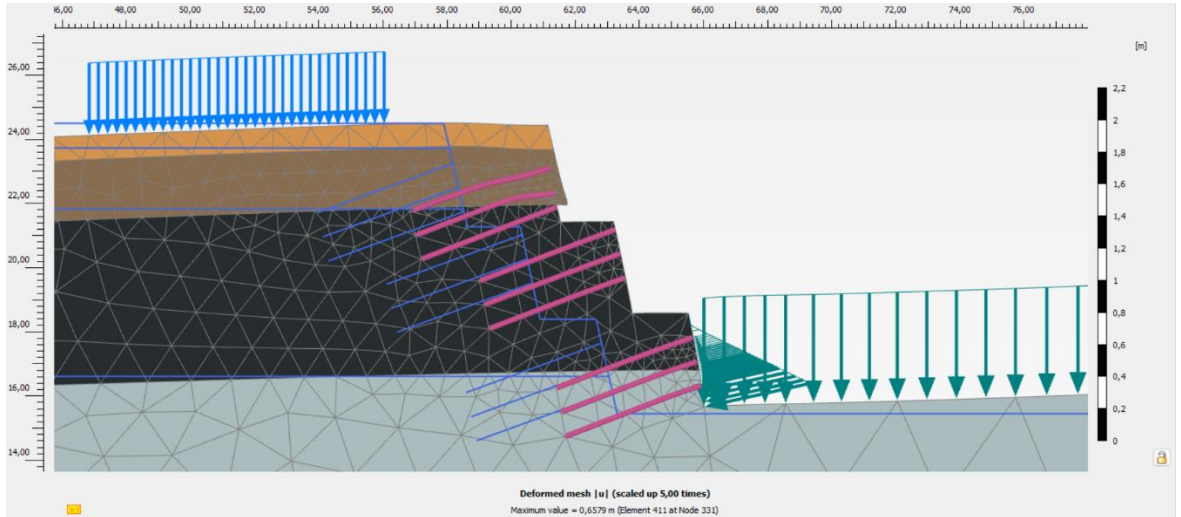




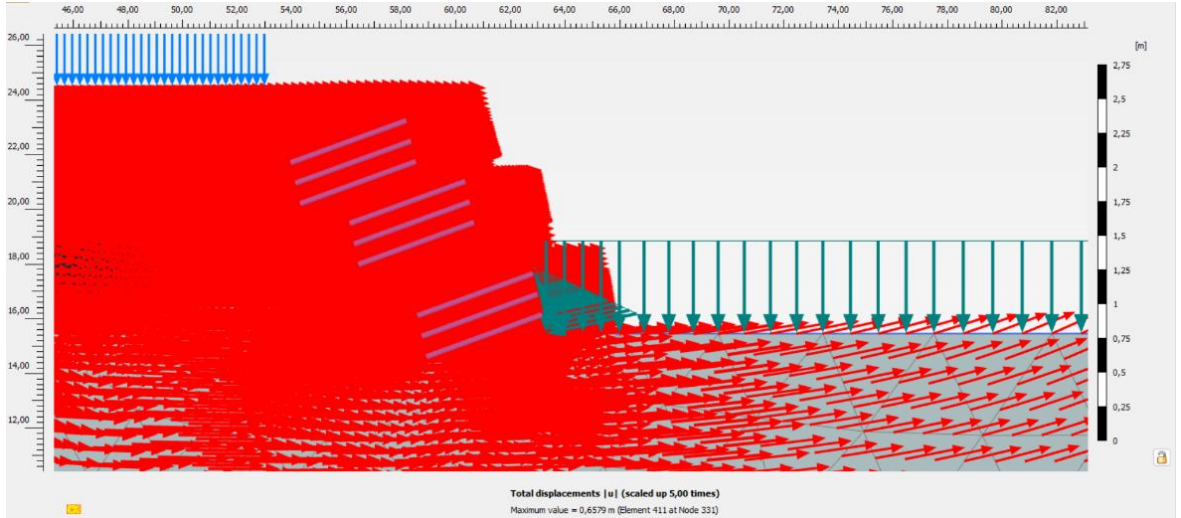
### Attachment 143 Model h Loaded Dynamic Effective Stress Output



### Attachment 144 Model h Loaded Dynamic Deformed Mesh Output



### Attachment 145 Model h Loaded Dynamic Direction of Movement Output



### Attachment 146 Model h Loaded Dynamic Displacement Output

